Modelling Motor Neuron Disease using Induced Pluripotent Stem Cells

Shum, Carole Yick Lam

Awarding institution:
King's College London

Modelling Motor Neuron Disease using Induced Pluripotent Stem Cells

By: Carole Shum

Thesis submitted for the degree of Doctor of Philosophy

Department of Clinical Neuroscience, Institute of Psychiatry

King's College London

ACKNOWLEDGMENTS

This thesis could not have been written on my own, and I am so grateful for all those who have supported this work. First, I would like to thank the individuals and organizations that funded this work. I am grateful to Dr. Robert Goodfellow and the Goodfellow family for creating this studentship and to the Psychiatry Research Trust and Motor Neurone Disease Association for funding this work.

I am hugely indebted to my supervisors, Professor Chris Shaw for giving me this opportunity to work in his amazing lab, his continual encouragement, his unjustified confidence in me and his tremendous work ethic and scientific knowledge. I am eternally grateful to Dr Agnes Nishimura, for being a wonderful teacher, giving me strength and hope when everything was going wrong, trusting me to be independent, and encouraging me to learn and develop. I couldn't ask for better supervisors. I would also like to thank Jose and Akira for giving me some (lots) of Agnes' valuable time.

I must thank the Shaw lab family for creating such a friendly and wonderful work environment. I'm grateful for my Shaw lab girls, Athina Soraya Gkazi and Valentina Sardone, thank you for the incredible friendship and for sharing adventures, laughs, tears, and everything else. Jack Miller, Jorge Gomez Deza, Remy Constable, Wejdan Kattuah, as well as new additions Simona Darovic, Martina De Majo and Chun Hao Wong, I cannot thank them enough for their wonderful company, "funny" pranks, and the creative and mostly out-of-control conversations and laughter. Super thanks to Han-Jou Chen for being my "FACS technician" and our lovely walks and chats. Special thanks to Emma Scotter for the many hours of image analysis tutorials and for her cheerful presence. I must thank Younbok Lee for his brilliant ideas and interesting scientific and philosophical discussions. Special thanks to Caroline Vance for allowing me to briefly adopt her as a supervisor and for being such a calm and steady leader. I must also thank Bradley Smith, Jacqueline Mitchell, Claire Troakes, Eva So, Simon Topp, Ryan Graves, and Lizzie Stevens for their guidance, ideas and help throughout my PhD. I am grateful for Vicky Strelzcyk for her

tireless work in keeping our labs functional. Thanks to Jamie Wright for the tissue culture support.

I must also thank the members of the Department of Clinical Neuroscience, especially Sophie Morris, Kate Tymms and Mulenga Duodu for their administrative support. I am grateful to our stem cell collaborators Siddarthan Chandran and Bilada Bilican for their help, advice and expertise. Special thanks to Gerald Finnerty and Catherine Smith for carrying out the electrophysiology experiments.

To my friends in Toronto, thank you for your visits, skype dates, care packages, words of love and encouragement. To my basketball team and friends, thank you for sharing my obsession and keeping me fit and sane. To my friends from the UK and abroad, thank you for your support and company during these years.

Most of all, I must thank my family for their love and support, for always having faith in me, and for letting me go to chase my dreams in a foreign place. Lastly and most importantly, I must thank the one who made all of this possible. Patrick Kwan, words can't express how grateful I am for you. Thank you for putting me first and helping me to achieve my goals.

DECLARATION

I hereby declare that, as the author of this thesis, the work reported here was performed by me. Assistance provided by others has been acknowledged and all previously published work has been identified and acknowledged. This work is original and has not been submitted for any other degree.

ABSTRACT

Amyotrophic Lateral Sclerosis (ALS) is the most common adult motor neuron disease. The majority of ALS cases are sporadic (SALS), but 10% of patients have a familial form of ALS (FALS). Mutations in Fused in Sarcoma (FUS) occur in approximately 4% of FALS and less than 1% of SALS. A hallmark feature of ALS is the degeneration of upper and lower motor neurons in the brain and spinal cord; however, the mechanism underlying this loss is not known. Studies of degenerative mechanisms have been impeded by the inaccessibility of human neural tissue. A possible solution is to use induced pluripotent stem cells (iPSCs) derived from patients, which may be differentiated into the cell types affected by disease.

To test whether patient-specific stem cells can be used to model aspects of ALS pathogenesis, iPSC lines were generated from a patient carrying the pathogenic FUS R521C mutation. FUS iPSCs derived from patient fibroblasts and WT iPSCs derived from fibroblasts from two healthy controls were differentiated into neural progenitors and motor neurons. FUS iPSC-derived neuronal cells recapitulate key aspects of FUS-associated ALS, including mislocalisation of FUS protein, the redistribution of FUS protein into cytoplasmic stress granules, and increased apoptotic cell death.

The second study uses this iPSC model to investigate the effects of mutant FUS on dendritic morphology and synaptic regulation. FUS iPSC-derived neurons display abnormal dendritic morphology, such as reduced neurite outgrowth and reduced density of dendritic protrusions. FUS iPSC-derived neurons also show differences in the localisation of synaptic proteins. This study suggests that physiological levels of mutant FUS protein affect the morphology and synaptic structure of human neurons.

These studies validate the stem cell approach to disease modelling and provide support for the use of patient-specific stem cells for the study of disease mechanisms.

ABBREVIATIONS

7AAD	7-aminoactinomycin D
ALS	Amyotrophic lateral sclerosis
ALSoD	Amyotrophic lateral sclerosis online genetics database
APC	Adenomatous polyposis coli
APC-RNP	Adenomatous polyposis coli ribonucleoprotein
ASO	Antisense morpholino oligonucleotide
ATCC	American Type Culture Collection
ATG	Adenine-thymine-guanine
ATXN2	Ataxin-2
β3-tubulin	Beta III tubulin
BDNF	Brain-derived neurotrophic factor
bFGF	Basic fibroblast growth factor
bp	Base pair
BSA	Bovine serum albumin
C-terminal	Carboxy terminal
C9ORF72	Chromosome 9 open reading frame 72
CAG	Cytosine-adenine-guanine
Caz	Cabeza
CDM	Chemically defined medium
cDNA	Complementary DNA
ChAT	Choline acetyltransferase
CHMP2B	Chromatin-modifying protein 2B
CNS	Central nervous system
CO_2	Carbon dioxide
CREST	Calcium-responsive transactivator

DAPI	4’,6-diamidino-2-phenylindole
DGCR8	Microprocessor complex subunit 2
DHP	DNA homologous pairing
DMEM	Dulbecco’s Modified Eagle Medium
DMSO	Dimethyl sulfoxide
DNA	Deoxyribonucleic acid
EB	Embryoid body
EDTA	Ethylenediaminetetra-acetic acid
EGFP	Enhanced green fluorescent protein
EGTA	Ethylene glycol tetraacetic acid
ELP3	Elongator protein 3
ER	Endoplasmic reticulum
ESC	Embryonic stem cell
EWS	Ewing sarcoma breakpoint region 1 protein
FACS	Fluorescence activated cell sorting
FALS	Familial amyotrophic lateral sclerosis
FBS	Fetal bovine serum
FIG4	Polyphosphoinsotide phosphatase
FTD	Frontotemporal dementia
FUS	Fused in sarcoma
GA	Glycine-alanine
GP	Glycine-proline
GR	Glycine-arginine
GDNF	Glial cell line-derived neurotrophic factor
GTP	Guanosine triphosphate
HA	Hemagglutinin
HB9	Homeobox transcription factor

HDAC1	Histone deacetylase 1
hESC	Human embryonic stem cell
HGPS	Hutchinson-Gilford progeria syndrome
HIV	Human immunodeficiency virus
hnRNP	Heterogeneous nuclear ribonucleoprotein
HNRNPA1	Heterogeneous nuclear ribonucleoprotein A1
HNRNPA2B1	Heterogeneous nuclear ribonucleoprotein A2/B1
iPSC	Induced pluripotent stem cell
kDa	kilodalton
KIFAP3	Kinesin-associated protein 3
KLF4	Kruppel-like factor 4
LB	Luria-Bertani
LMNA	Lamin A
MAP2	Microtubule-associated protein 2
MATR3	Matrin3
MEF	Mouse embryonic fibroblast
$MgCl_2$	Magnesium chloride
MN	Motor neuron
MOPS	4Morpholinepropanesulfonic acid
mRNA	Messenger ribonucleic acid
N-terminal	Amino terminal
NCI	Nuclear cytoplasmic inclusions
NES	Nuclear export signal
NF-κB	Nuclear factor kappa B
NLS	Nuclear localization signal
NMJ	Neuromuscular junction
NPC	Neural progenitor cell

OCT4	Octamer-binding transcription factor 4
OPTN	Optineurin
PA	Proline-arginine
PABP1	Poly(A)-binding protein
PBS	Phosphate buffered saline
PCR	Polymerase chain reaction
PE	Phycoerythrin
PFN1	Profilin 1
Poly-HEMA	Poly(2-hydroxyethylmethacrylate)
PR	Proline-arginine
PS	Phosphatidylserine
PSD95	Postsynaptic density protein 95
PY	Proline-tyrosine
RA	Retinoic acid
RAN	Repeat associated non-ATG
RGG	Arginine-glycine-glycine
RIPA	Radio immunoprecipitation assay
RNA	Ribonucleic acid
RNP	Ribonucleoprotein
ROCK	Rho-associated kinase
ROS	Reactive oxygen species
rpm	Revolutions per minute
RRM	RNA-recognition motif
RT-PCR	Reverse transcription-polymerase chain reaction
SC35	Serine/arginine-rich splicing factor 2
SCID	Severe combined immunodeficient
SDS	Sodium dodecyl sulfate

SETX	Senataxin
SF1	Splicing factor 1
Shh	Sonic hedgehog
SMA	Spinal muscular atrophy
SMN	Survival of motor neurons
snRNP	Small nuclear ribonucleoprotein
SOX2	Sex determining region-box 2
SPG11	Spastic paraplegia 11
SQSTM1	Sequestosome 1
SR	Serine-arginine
SRp75	Serine/arginine-rich protein 75
TAF15	TATA box binding protein-associated factor
TARDBP/TDP-43	TAR DNA-binding protein 43
TBS	Tris-buffered saline
TBST	Tris-buffered saline with Tween 20
TFIID	Transcription factor II D
UBQLN2	Ubiquilin 2
UPS	Ubiquitin-proteasome system
UV	Ultraviolet
VAPB	Vesicle-associated membrane protein-associated protein B/C
VCP	Valosin-containing protein
VGLUT1	Vesicular glutamate transporter 1
V_m	Membrane potential
w/v	Weight/volume
WT	Wild-type
ZnF	Zinc finger motif

LIST OF TABLES

LIST OF FIGURES

CONTENTS

CHAPTER 1

INTRODUCTION

1.1 MOTOR NEURONE DISEASE

1.1.1 ALS

Amyotrophic lateral sclerosis (ALS) is a neurodegenerative condition characterised by the selective loss of upper and lower motor neurons. Muscle weakness usually begins in one limb, or the throat, but gradually spreads to affect all skeletal muscles such that patients are unable to walk, talk, dress or toilet themselves. Death, usually due to respiratory failure, typically occurs 2-5 years from symptom onset. The relentless accumulation of disabilities and progressive loss of autonomy engenders a feeling of hopelessness. ALS is the most common reason that people seek Euthanasia, where the physician acts directly to end the patient's life. In the Netherlands where "physician assisted suicide" is legal, 20% of ALS patients choose to die this way, where the physician provides the means for death, most often with a prescription, but the patient ultimately administers the lethal medication (Veldink et al. 2002).

ALS has a prevalence of 3 to 6 per 100.000 and an incidence of 1 to 3 per 100,000 (Chiò et al. 2013). The onset of the disease usually occurs in late-adulthood, although juvenile onset (< 25 years) and early-onset ALS (< 45 years)occurs in about 10% of all cases (Turner et al. 2012). The clinical symptoms include fasciculations, muscle wasting and/or spasticity leading to progressive paralysis. There is currently no cure, and the sole disease-modifying treatment, riluzole, has only a modest effect on survival.

ALS is now recognised as being a part of a disease spectrum that is linked to frontotemporal dementia (FTD) due to overlap in the pathology and common genetic origins for these two neurodegenerative conditions. FTD is the second most common form of early-onset dementia, after Alzheimer's disease. It is characterised by the loss of neurons in the frontal and temporal cortices. This results in behaviour and personality changes, and the loss of language skills. Some ALS cases demonstrate cognitive impairment, and some FTD cases are diagnosed with ALS.

1.1.2 Diagnosis

There is no definitive test to diagnosis ALS. Instead, the diagnosis is made through a clinical examination and a series of tests to rule out diseases that have the same symptoms as ALS, according to the El Escorial criteria (Brooks et al. 2000). The diagnostic tests include electromyography, nerve conduction velocity, magnetic resonance imaging and muscle or nerve biopsy. Post mortem pathological examination may be done to confirm the clinical diagnosis of ALS.

1.1.3 Genetics

Most ALS cases are sporadic, but approximately 5-10% have a family history (Byrne et al. 2011; Chiò et al. 2013). Although sporadic cases are classically defined as those with a lack of clear genetic association, mutations in *C9ORF72, TARDBP* and *SOD1* have also been observed in sporadic cases (Chio et al., 2008; DeJesus-Hernandez et al., 2011; Kabashi et al., 2008; Renton et al., 2011; . In addition, *de novo* mutations have recently been reported in sporadic ALS patients (Chesi et al., 2013). This may arise from a lack of clinical information from the patient's family, as increased risk has been reported in relatives of people with SALS (Hanby et al., 2011).

Familial ALS (FALS) cases mainly exhibit autosomal dominant inheritance with incomplete penetrance, but autosomal recessive (where both copies of the gene in each cell have mutations; Andersen et al., 1996) and X-linked inheritance (where the gene is located on the X chromosome; Deng et al., 2011) have previously been reported. For instance, incomplete penetrance has been reported for the *C9ORF72* expansion, where the expansion has been observed in controls (Smith et al., 2013).

50% of familial ALS cases are associated with mutations in four genes, *SOD1, C9ORF72, FUS* and *TARDBP* in descending order of frequency of occurrence (Fig. 1.1) (Ling et al. 2013). *TARDBP* and *FUS* mutations are rarely observed in FTD, whereas the most common mutation in ALS and FTD is a massive expansion of a hexanucleotide repeat in

the first intron of *C9ORF72* (DeJesus-Hernandez et al. 2011; Renton et al. 2011). A summary of the genes linked to ALS is shown in Table 1.1. Some of the recent genetic discoveries will be discussed below.

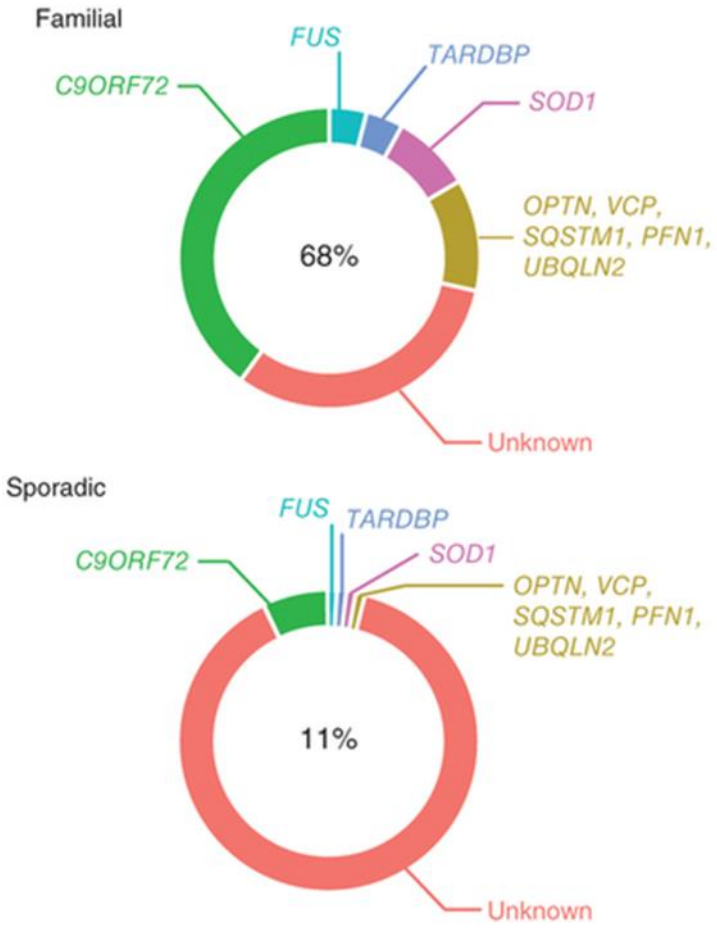

Figure 1.1 Proportion of ALS explained by each gene in European populations. (Figure adapted from (Renton et al. 2014)

Table 1.1 Genes implicated in the pathogenesis of ALS (genes in bold delineate causative genes, other genes delineate risk factors).

Function	Gene	Name	Location	Reference
Oxidative stress	***SOD1***	Superoxide dismutase 1	21q22	(Rosen et al. 1993)
	PON1-3	Paraoxonase 1-3	7q21	(Saeed et al. 2006; Slowik et al. 2006)
	DAO	D-amino-acid oxidase	12q24	(Mitchell et al. 2010)

RNA metabolism	***ANG***	Angiogenin	14q11	(Greenway et al. 2004)
	SETX	Senataxin	9q34	(Chen et al. 2004)
	TARDBP	TAR DNA binding protein	1p36	(Kabashi et al. 2008; Sreedharan et al. 2008)
	FUS	Fused in sarcoma	16p11	(Kwiatkowski et al. 2009; Vance et al. 2009)
	ELP3	Elongation protein 3 homolog	8p21	(Simpson et al. 2009)
	ATXN2	Ataxin 2	12q24	(Elden et al. 2010)
	TAF15	TATA box binding protein (TBP)-associated factor	17q11	(Couthouis et al. 2011)
	C9ORF72	Chromosome 9 open reading frame 72	9p21	(DeJesus-Hernandez et al. 2011; Renton et al. 2011)
	HNRNPA2B1	Heterogeneous nuclear ribonucleoprotein A2/B1	7p15	(Kim et al. 2013)
	HNRNPA1	Heterogeneous nuclear ribonucleoprotein A1	12q13	(Kim et al. 2013)
	MATR3	Matrin 3	5q31	(Johnson et al. 2014)
Protein homeostasis	***VAPB***	Vesicle-associated membrane protein-associated protein B and C	20q13	(Nishimura et al. 2004)
	CHMP2B	Chromatin modifying	3p11	(Parkinson et al. 2006)

		protein 2B		
	FIG4	SAC domain-containing protein gene family	6q21	(Chow et al. 2009)
	OPTN	Optineurin	10p13	(Maruyama et al. 2010)
	VCP	Valosin-containing protein	9p13	(Johnson et al. 2010)
	SQSTM1	Sequestosome 1	5q35	(Fecto et al. 2011)
	UBQLN2	Ubiquilin 2	Xp11	(Deng et al. 2011)
Cytoskeleton and axonal transport	*NEFH*	Neurofilament heavy polypeptide	22q12	(Figlewicz et al. 1994)
	DCTN1	Dynactin 1	2p13	(Münch et al. 2004)
	NTE	Neuropathy target esterase	19p13	(Rainier et al. 2008)
	KIFAP3	Kinesin-associated protein 3	1q24	(Landers et al. 2009)
	PFN1	Profilin 1	17p13	(Wu et al. 2012)
Other or unknown	***ALS2***	Alsin	2q33	(Hadano et al. 2001)
	SPG11	Spatacsin	15q14	(Orlacchio et al. 2010)
	SIGMAR1	Sigma non-opioid intracellular receptor 1	9p13	(Al-Saif et al. 2011)

1.1.3.1 Principal genes

SOD1

The first locus associated with ALS was identified on Chromosome 21 by linkage analysis (Siddique et al., 1991). The mutated gene was subsequently identified as the gene encoding the antioxidant enzyme copper-zinc superoxide dismutase (SOD1) (Rosen et al.

1993). Rosen et al. (1993) originally identified 11 missense mutations in FALS. 177 missense and nonsense mutations have since been reported (ALS Online database, ALSoD; (Abel et al. 2012).

Most *SOD1* mutations result in single amino acid substitutions and occur throughout the entire protein, with some clustering in exons four and five (Shaw et al. 1998). Mutations in *SOD1* occur in 20% of FALS and 1% of SALS (Shaw et al. 1998; Renton et al. 2014). SOD1 cases generally have a lower age of onset compared with the familial ALS cases without *SOD1* mutations (Cudkowicz et al. 1997). SOD1 cases demonstrate heterogeneous phenotypes, with some mutations, such as Ala4Val, giving rise to an aggressive phenotype, while others are associated with a milder phenotype, such as Asp90Val. SOD1 cases have predominantly lower motor neuron features, without cognitive impairment (Wicks et al. 2009). The pathology of SOD1-associated ALS appears to be distinct from other types of ALS. While protein aggregates containing SOD1 may be seen in FALS patients with *SOD1* mutations (Watanabe et al. 2001), this feature is not always present (Shaw et al. 1997) and is rarely observed in most sporadic cases.

Observations from cellular and animal models suggest that mutant SOD1 causes ALS by a toxic gain of function. SOD1 functions as an enzyme to catalyse the dismutation of superoxide anions and the production of free radicals with hydrogen peroxide as a substrate. Different ALS mutant forms of SOD1 have a wide range of dismutation activity (from nil to normal) and enhanced radical-generating function compared to WT SOD1 (Yim et al. 1996), suggesting that mutant SOD1 may play a modifying role in ALS (Saccon et al., 2013), but does not cause ALS by a loss of function. Rather, mutant SOD1 and oxidised WT SOD1 are misfolded and aggregate, potentially causing dysfunction of many cellular processes, including axonal transport (Bosco et al. 2010), suggesting a gain of toxic function may arise from both mutant and oxidised WT SOD1. Injection of mutant SOD1 in motor neuron cultures induces aggregation of SOD1 and motor neuron death mediated by glutamate stimulation (Roy et al. 1998). There is a strong link between mutant SOD1 and excitotoxicity as a pathogenic mechanism underlying motor neuron degeneration. Spinal

motor neurons from mutant SOD1 mice are characterised by persistent Na^+ current and enhanced neuronal excitability, which could be reduced by riluzole, the sole available treatment for ALS (Kuo et al. 2005).

TARDBP

In 2006, TDP-43 was identified as the major protein of pathological inclusions of postmortem tissue in 90% of ALS patients, 60% of FTD patients, as well as other neurodegenerative diseases (Neumann et al. 2006). Subsequently, three independent candidate gene studies reported the mutations in the gene encoding TDP-43, (TAR DNA-binding protein, *TARDBP*), in familial and sporadic ALS patients (Gitcho et al. 2008; Kabashi et al. 2008; Sreedharan et al. 2008). Sreedharan et al. (2008) showed that mutant TDP-43 protein underwent fragmentation and was neurotoxic *in vivo.* 50 mutations in *TARDBP* have now been observed (ALSoD), accounting for 4% of familial and 1% of sporadic cases (Renton et al. 2014).

All mutations identified reside in the carboxylate terminal (C-terminal) of the protein, with the exception of the D169G mutation. FALS cases with *TARDBP* mutations have pathology that is indistinguishable from SALS cases; the majority of cases are characterised by TDP-43-positive ubiquitinated inclusions in affected neurons and glia of the motor system (Van Deerlin et al. 2008). Most TDP-43 cases are associated with classical ALS symptoms and signs but have a lower age of onset and a slower disease course compared to non-familial cases (Corcia et al. 2012), whereas others are concomitant with dementia and Parkinsonism (Lattante et al. 2013). TDP-43 inclusions have also been observed in a number of other diseases, including FTD, Alzheimer's disease, Down syndrome and Parkinson's disease (Lagier-Tourenne et al. 2010).

TDP-43 is a 43-kDa protein that is ubiquitously expressed in various human tissues, including the brain and spinal cord. It was originally discovered in 1995 as a transcriptional repressor of the transactive response DNA binding element of the HIV1 virus (Ou et al. 1995). TDP-43 shuttles between the nucleus and cytoplasm, interacting

with other hnRNPs to bind RNA and function as a translational activator and repressor (Ayala et al. 2008; D'Ambrogio et al. 2009).

It remains unclear whether mutant TDP-43 causes ALS via a gain or loss of function. Nuclear clearing of TDP-43, accompanied by the accumulation of TDP-43 in the cytoplasm, is often observed in surviving neurons in patients with *TARDBP* mutations (Van Deerlin et al. 2008), suggesting that loss of nuclear function of TDP-43 as a component of the disease process. The loss of TDP-43 in mice results in embryonic lethality, whereas heterozygous *TARDBP* mice exhibit motor defects despite a lack of neurodegeneration or motor atrophy (Kraemer et al. 2010) . The selective removal of TDP-43 from motor neurons leads to progressive weight loss and motor impairment in mice, along with degeneration of motor axons and skeletal muscle and denervation in the neuromuscular junction (NMJ) (Iguchi et al. 2013). However, the mortality of these mice were not different from control mice (Iguchi et al. 2013). Therefore, loss of TDP-43 function may contribute to the development and progression of disease, but it does not appear to be sufficient to lead to fatal motor neuron disease.

The expression of WT TDP-43 in *C. elegans* results in neurodegeneration, locomotor deficits, and reduced lifespan (Ash et al. 2010). This study showed that the locomotor deficit correlated with the levels of endogenous protein, suggesting that neurotoxicity may result from excess TDP-43 function (Ash et al. 2010). The expression of either human WT or mutant TDP-43 in mice has also been shown to cause degeneration of motor neurons and the development of ALS-related motor dysfunction (Wils et al. 2010; Igaz et al. 2011; Arnold et al. 2013). However, the overexpression of human TDP-43 in mice is accompanied by a reduction in endogenous TDP-43 (Arnold et al. 2013), making it difficult to differentiate between a gain or loss of function mechanism in TDP-43 transgenic mice. Similarly, both overexpression of human TDP-43 and knockdown of endogenous *tardbp* in zebrafish causes a motor phenotype and motor neuron toxicity (Kabashi et al. 2010) . Thus, there is evidence to suggest that both mechanisms may be

involved in the molecular cascade through which mutant TDP-43 contributes to motor neuron degeneration.

FUS

Shortly after the identification of *TARDBP* mutations in ALS, mutations in *FUS*, another gene encoding a DNA/RNA-binding protein, were reported by two independent groups in 2009 (Kwiatkowski et al. 2009; Vance et al. 2009). This locus on Chromosome 16q had previously been linked to ALS (Abalkhail et al. 2003; Ruddy et al. 2003; Sapp et al. 2003). Vance et al. (2009) demonstrated in transfected cells that the mutations reduced the nuclear import of FUS leading to cytoplasmic accumulation. They also detected large FUS-immunoreactive inclusions in spinal cord and motor neurons.

The prevalence of *FUS* mutations is ~4% in FALS and 1% in SALS and so far, 77 FUS mutations have been identified (ALSoD). Most *FUS* mutations are missense mutations; however two nonsense mutations have also been reported, in addition to insertion and deletion mutations. Similar to the *TARDBP* mutation spectrum, most mutations are clustered within the 12 amino acids of the C-terminal that contains the nuclear localizing signal (Lagier-Tourenne et al. 2010). Unlike *TARDBP*, a number of amino terminal (N-terminal) mutations have also been identified. Whereas the C-terminal mutations are mostly associated with familial cases, the N-terminal mutations are more commonly sporadic. The finding that mutations identified in sporadic cases are localized in the glycine-rich region suggests several possibilities, that SALS patients with *FUS* patients may represent sporadic cases due to the lack of information about affected relatives or that N-terminal *FUS* mutations may represent low penetrance *FUS* variations (Corrado et al., 2010). Missense variants in the N-terminus of FUS have also been reported in controls (Corrado et al., 2010; Merner et al., 2012); therefore, further studies using functional assays are required to determine the involvement of these mutations in ALS pathogenesis.

A different set of mutations in *FUS* has been reported in essential tremor, which is a fairly benign slowly progressive and non-fatal movement disorder (Rajput et al. 2013).

Some *FUS* mutations are associated with an earlier onset and aggressive disease progression (Conte et al. 2012; Sproviero et al. 2012). FUS cases often present with signs of lower motor neuron degeneration and display limited upper motor neuron involvement (Blair et al. 2010). The only biochemical feature of FUS inclusions to date is decreased solubility (Kwiatkowski et al. 2009), in contrast to other proteins implicated in neurodegenerative diseases, such as Amyloid-beta (Aβ), TDP-43 and α-synuclein, which show abnormal cleavage and/or phosphorylation (Baba et al. 1998; Neumann et al. 2006).

FUS-immunoreactive inclusions are also a common feature of rare and atypical forms of FTD, such as neuronal intermediate filament inclusion disease and basophilic inclusion body disease (Munoz et al. 2009; Urwin et al. 2010). However, *FUS* mutations are rarely observed in FTD patients, and dementia is rare in FUS-mediated ALS (Lagier-Tourenne and Cleveland 2009; Blair et al. 2010; Groen et al. 2013). FUS inclusions have also been reported in polyglutamine disease, such as Huntington's disease, spinocerebellar ataxia and dentatorubral-pallidoluysian atrophy (Lagier-Tourenne et al. 2010). The functions this protein and the implications of mutations in this gene will be discussed further in Section 1.2.

C9ORF72

Another major breakthrough in ALS and FTD research came in 2011 with the identification of a large GGGGCC hexanucleotide repeat expansion in a noncoding region of the *C9ORF72* gene (DeJesus-Hernandez et al. 2011; Renton et al. 2011). This repeat expansion is the most common cause of ALS and FTD, accounting for up to 80% of familial ALS-FTD, 20-50% of familial ALS and 10-30% of FTD (Ling et al. 2013; Smith et al. 2013). In healthy individuals, this hexanucleotide is repeated 2-5 times. In ALS patients, the length of the expansion may contain hundreds or thousands of repeats.

C9ORF72 cases show combined upper and lower motor neuron degeneration and classical ALS pathology with TDP-43 inclusions in spinal motor neurons (Cooper-Knock et al. 2012). In addition, p62- and ubiquitin-positive, TDP-43 negative neuronal and glial

cytoplasmic inclusions containing dipeptide-repeat proteins are prevalent in non-motor regions of C9ORF72 cases (Mackenzie et al. 2014). Another unique feature of C9ORF72 cases is the formation of nuclear RNA foci in the frontal cortex, hippocampus and cerebellum (DeJesus-Hernandez et al. 2011; Mackenzie et al. 2014).

Symptoms and signs of FTD or mild cognitive impairment are often present in C9ORF72 ALS cases (Cooper-Knock et al. 2012). In addition, these cases often have a family history of other neurodegenerative diseases being diagnosed, such as Parkinson's disease, Huntington's disease and Charcot-Marie-Tooth disease (Cooper-Knock et al. 2012), which may be coincidental or due to phenotypic variation. The molecular mechanism by which the repeat expansion causes ALS or FTD is highly controversial. Three different pathogenic mechanisms have been proposed. Loss of function (haploinsufficiency) arising from failure of the mutant transcript to be translated into C9ORF72 protein seems unlikely as no other mutations in the gene have been identified and homozygosity of the mutant does not cause a more severe phenotype (Fratta et al. 2013). Gain of function may either be due to direct toxicity from the accumulation of sense (GGGGCC)- and antisense (GGCCCC)- containing RNA forming RNAse resistant foci that sequester RNA binding proteins (Lee et al. 2013; Mori et al. 2013; Xu et al. 2013; Zu et al., 2013) or repeat RNA-mediated toxicity or protein-mediated toxicity due to repeat-associated non-ATG translation of dipeptides from forward (GP, GA, GR) and antisense (PR and PA) RNA strands (Ash et al. 2013; Mori et al. 2013).

1.1.3.2 Genes involved in protein homeostasis

Ubiquilin 2 (UBQLN2)

In 2011, mutations in *UBQLN2* were shown to cause X-linked ALS and ALS-FTD (Deng et al. 2011). *UBQLN2* mutations are rarely observed in FALS and SALS, likely accounting for less than 1% of both (Daoud and Rouleau 2011). ALS patients carrying *UBQLN2* mutations are associated with an early age of onset, especially in male patients with disease progression ranging from 6 months to 5 years (Deng et al. 2011; Gellera et al.

2013). *UBQLN2* cases are characterised by widespread upper motor neuron signs, and often also present with dementia (Deng et al. 2011; Gellera et al. 2013). The pathology of FALS patients with *UBQLN2* mutations and SALS patients are typified by the presence of ubiquilin-2 and ubiquitin-positive inclusions, which also contain TDP-43, FUS and optineurin (Deng et al. 2011; Williams et al. 2012). This suggests that mutations in *UBQLN2* lead to an impairment of protein degradation via the ubiquitin proteasome system (UPS) (Deng et al. 2011).

Sequestosome 1 (SQSTM1)

Mutations in *SQSTM1* were identified in FALS and SALS in a candidate gene study (Fecto et al. 2011). These mutations occur throughout the protein and correspond to about 1.1% in FALS and 4% in SALS (Fecto et al. 2011; Teyssou et al. 2013). *SQSTM1* encodes the ubiquitin-binding adaptor protein p62, which enhances the formation and degradation of polyubiquitin-containing bodies by autophagy and the UPS. *SQSTM1* patients have p62- and TDP-43-positive inclusions and increased levels of p62 and TDP-43 protein in the spinal cord (Teyssou et al. 2013). The mean age at onset of *SQSTM1* patients was similar to those with *SOD1, FUS* or *TARDBP* mutations, whereas the duration of disease was relatively longer (Fecto et al. 2011).

Optineurin (OPTN)

OPTN mutations were first identified in Japanese FALS and SALS patients (Maruyama et al. 2010). Mutations in this gene had been previously linked to adult-onset open-angle glaucoma (Rezaie et al. 2002). Optineurin is involved in maintaining the Golgi complex, membrane and vesicle trafficking. *OPTN* mutations account for about 1% of both FALS and SALS patients (Del Bo et al. 2011). The spinal cord of *OPTN* patients shows cytoplasmic inclusions immunopositive for OPTN, ubiquitin and TDP-43 (Maruyama et al. 2010). Interestingly, Maruyama et al. (2010) also found that SOD1-positive inclusions

from *SOD1* FALS cases also label positively for OPTN, suggesting that OPTN may be involved in the pathogenesis of ALS arising from several different origins.

Valosin-containing protein (VCP)

Mutations in the valosin containing protein (*VCP*) were identified in ALS using exome sequencing of two members of an Italian family (Johnson et al. 2010). *VCP* mutations are also causative of inclusion body myopathy, which may also be associated with Paget's disease of bone and FTD (IBMFTD) (Watts et al. 2004). VCP is a protein that is involved in ubiquitin-dependent proteasome degradation and the pathology of ALS patients with *VCP* mutations includes cytoplasmic neuronal inclusions in the spinal cord and frontal cortex. *VCP* patients have a classical ALS phenotype along with some degree of cognitive impairment and mutations account for 1-2% of FALS (Johnson et al. 2010). *VCP* mutations are associated with a more rapidly progressive disease course and age of onset similar to *SOD1, FUS* or *TARDBP* mutations (Johnson et al. 2010; Koppers et al. 2012).

Chromatin-modifying protein 2B (CHMP2B)

CHMP2B mutations were first identified in a large Danish kindred with FTD (Skibinski et al. 2005), and later found in ALS (Parkinson et al. 2006). *CHMP2B* mutations may account for about 1% of FALS cases (Cox et al. 2010). This gene encodes a protein involved in endosome-lysosome-autophagy function. *CHMP2B* patients show neuropathology consistent with ALS/FTD, such as p62- and TDP-43-positive inclusions in oligodendroglia, as well as upper motor neuron degeneration typical of primary lateral sclerosis (Parkinson et al. 2006; Cox et al. 2010). *CHMP2B* patients with ALS show a variable age of onset and a typical disease progression (Cox et al. 2010).

Polyphosphoinsoitide phosphatase (FIG4)

Mutations in *FIG4* were reported in about 2% of ALS and primary lateral sclerosis patients with a typical age of onset but a longer disease duration of 9 years (Chow et al.

2009). *FIG4* mutations are also found in Charcot-Marie-Tooth disease (Chow et al. 2007). FIG4 is involved in the trafficking of endosomal vesicles to the Golgi network. Kon et al. (2014) reported that FIG4 is not localised in TDP-43 inclusions in SALS or FTD, but is observed in inclusions in other neurodegenerative diseases, such as Pick's disease, Parkinson's disease and dementia with Lewy bodies (Kon et al. 2014).

Vesicle-associated membrane protein-associated protein B/C (VAPB)

In 2004, a missense mutation in *VAPB* was found in a large kindred with adult spinal muscular atrophy (SMA) where two individuals had an ALS phenotype (Nishimura et al. 2004). Symptom onset occurs from 25-55 years and the disease course ranges from 2-60 years. *VAPB* encodes a membrane protein involved in the unfolded protein response and vesicle trafficking. Mutations in *VAPB* were shown to disrupt its subcellular distribution, leading to intracellular aggregation of the protein (Nishimura et al. 2004; Landers et al. 2008).

1.1.3.3 Genes involved in RNA metabolism

Elongator protein 3 (ELP3)

ELP3 variants were observed in ALS in an association study of UK, USA and Belgian populations (Simpson et al. 2009). ELP3 is implicated in axonal biology and synaptic development in animal models. Simpson et al. (2009) showed that the expression of ELP3 was decreased in ALS patients carrying risk-associated alleles. The mechanism through which ELP3 leads to motor neuron degeneration remains unknown, but it appears that variants in this gene modulates risk for susceptibility to SALS.

Senataxin (SETX)

Autosomal dominant mutations in *SETX* (ALS4) are found in a juvenile-onset, slowly progressive non-fatal form of spastic paraplegia with some lower motor neuron degeneration causing distal muscle weakness with absence of bulbar and respiratory

symptoms (Chen et al. 2004). Symptom onset occurs before 25 years and individuals with ALS4 have a normal life span (Chen et al. 2004). *SETX* likely encodes a DNA/RNA helicase that functions in DNA repair and the production of RNA. *SETX* mutations are also associated with ataxia with oculomotor apraxia (Moreira et al. 2004).

Ataxin-2 (ATXN2)

Ataxin-2 is a polyglutamine protein that is mutated in spinocerebellar ataxia type 2 (SCA2). A CAG trinucleotide repeat is expanded to >33 repeats in patients with SCA2 (Pulst et al. 1996). Elden et al. (2010) showed that ataxin-2 interacts with TDP-43 and is a modifier of TDP-43 toxicity in yeast and animal models. These findings led to an investigation of CAG repeat length in ALS. Elden et al. (2010) found Intermediate-length expansions of 27-33 in ataxin-2 occur in 4.7% of ALS cases and are significantly associated with susceptibility to ALS. ALS patients with intermediate-length ataxin-2 repeats have an earlier age of onset, and ataxin-2 accumulates in the cytoplasm in the spinal cord of ALS patients (Elden et al. 2010).

HNRNPA2B1 and HNRNPA1

Mutations in *HNRNPA2B1* and *HNRNPA1* were found in families with IBMPFD and ALS (Kim et al. 2013). Muscle biopsies from patients with these mutations show hnRNPA2B1/hnRNPA1-positive cytoplasmic inclusions and TDP-43 pathology (Kim et al. 2013). This study showed that disease mutations are centred within prion-like domains and enhance the fibrillisation of the protein and its incorporation into stress granules and cytoplasmic inclusions (Kim et al. 2013).

TAF15

Several variants were found in a screening of *TAF15* and *EWS*, two proteins structurally related to FUS, in FALS patients (Ticozzi et al. 2011). The pathogenicity of these variants is unclear. They appear to occur at a low frequency or may represent rare,

benign single nucleotide polymorphisms. Further studies are needed to determine whether mutations in *TAF15* are indeed a rare cause of ALS.

Matrin3 (MATR3)

Mutations in *MATR3* were recently found in FALS and SALS in an exome sequencing study and are likely a rare cause of FALS (Johnson et al. 2014). MATR3 cases demonstrate heterogeneous phenotypes including myopathic features; one mutation is associated with slowly progressive ALS, while another presented with typical, rapidly progressive ALS. *MATR3* encodes a nuclear matrix DNA/RNA-binding protein that interacts with TDP-43. MATR3 is localised in the nuclei of motor neurons in control subjects, but is occasionally in the cytoplasm in ALS patients, and rarely observed in cytoplasmic inclusions (Johnson et al. 2014).

1.1.3.4 Other genetic factors

Profilin 1 (PFN1)

Mutations in *PFN1* were reported in FALS in 2012 in an exome sequencing study and account for 1-2% of familial cases (Wu et al. 2012). PFN1 regulates the polymerisation of actin filaments and cells transfected with PFN1 mutants develop abnormal actin levels and axon outgrowth which may contribute to ALS pathogenesis by affecting the cytoskeleton. ALS cases with *PFN1* mutations have classical ALS pathology including ubiquintinated, insoluble TDP-43 aggregates (Wu et al. 2012). *PFN1* patients have a younger age at onset, slower disease progression with a predominantly limb onset phenotype.

SPG11

SPG11 mutations were also identified in an exome sequencing study (Daoud et al. 2012). *SPG11* mutations are associated with juvenile onset ALS and long-term survival (Orlacchio et al. 2010; Daoud et al. 2012). Individuals with *SPG11* mutations show upper

and lower motor neuron symptoms (Orlacchio et al. 2010). SPG11 encodes spatacsin, a predicted transmembrane protein involved in DNA damage. Mutations in *SPG11* are a common cause of autosomal recessive hereditary spastic paraplegia (Stevanin et al. 2007).

ALS2

Mutations in *ALS2* are observed in a juvenile-onset autosomal recessive form of ALS (Hadano et al. 2001). This form of ALS (ALS2) is rare and is characterised by slowly progressive spasticity of limbs and facial muscles. Symptom onset occurs in the first or second decade of life. *ALS2* encodes a guanine nucleotide exchange factor, which activates GTPases to regulate endosomal trafficking (Otomo et al. 2003). *ALS2* mutations are predicted to cause ALS through a loss of protein function.

1.1.4 Mechanisms of ALS pathogenesis

The study of the genetic aetiology of ALS has enabled the generation of animal and cellular models. This has provided some insight into the processes underlying ALS pathogenesis. It is believed that ALS is a complex disease that manifests as a result of defects in a multitude of cellular processes (Fig. 1.2). Some of the putative mechanisms will be discussed below.

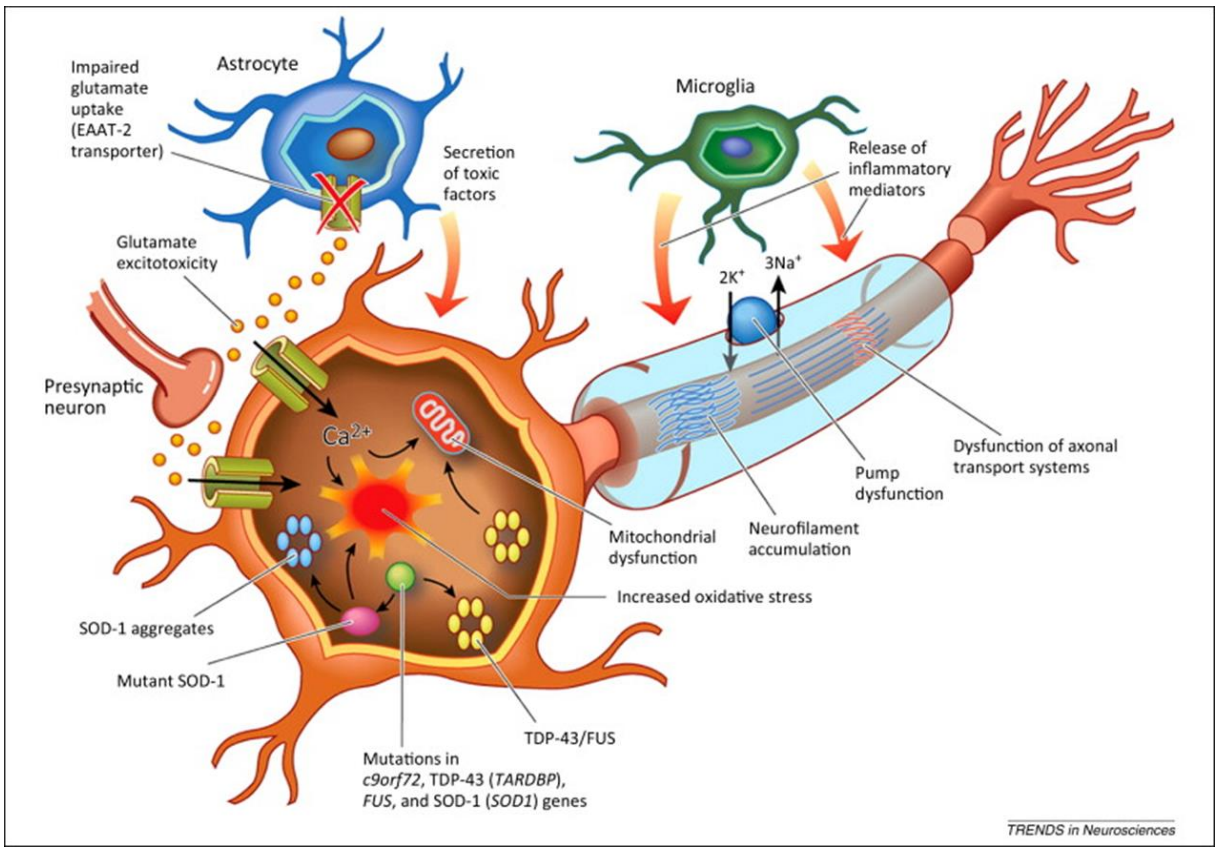

Figure 1.2 Molecular mechanisms underlying motor neuron degeneration in ALS (Figure from Vucic et al., 2014).

1.1.4.1 Failure of proteostasis

As with most neurodegenerative conditions, a hallmark feature of ALS is the presence of pathological protein aggregates. This, along with disease-linked mutations in multiple genes involved in protein degradation and maintenance of protein homeostasis, indicates failure of proteostasis as a key pathogenic mechanism.

The aggregation of mutant proteins in ALS is well-documented. Mutant SOD1 has been shown to misfold and adopt a conformation to prevent ubiquitylation-mediated degradation (Niwa et al. 2007). Mutant SOD1 forms toxic oligomers (Urushitani et al. 2002), which further accumulates as aggregates to induce a stress response in cells (Atkin et al. 2006). The oxidation of WT SOD1 also leads to misfolding and aggregation of the protein, similar to mutant SOD1. Aggregation of SOD1 has toxic effects on two major protein degradation pathways, the UPS and autophagy.

Similarly, TDP-43 and FUS have been observed in protein aggregates in ALS as well as other neurodegenerative disorders. Mutant TDP-43 and FUS are recruited into cytoplasmic stress granules upon stress. Stress granules are normally resolved by disaggregases and chaperones; however, it is thought that mutant TDP-43 and mutant FUS aggregates with stress granule components in an irreversible manner to give rise to pathological inclusions. This may be mediated by mislocalisation of the mutant protein and the prion-like domain within the protein structure of TDP-43 and FUS.

A characteristic feature of C9ORF72-linked ALS cases is the presence of neuronal cytoplasmic inclusions in the hippocampus, cerebellum and neocortex that are immunoreactive for p62, an adaptor protein that facilitates clearance of misfolded proteins by autophagy and UPS (Al-Sarraj et al. 2011). Several studies subsequently demonstrated that this unique protein pathology arose from unconventional repeat-associated non-ATG-initiated translation of sense and antisense transcripts of the expanded hexanucleotide repeat (Mori et al. 2013). TDP-43 inclusions are also present and are abundant in the tissues that most commonly undergo neurodegenration (Stewart et al. 2012; Mann et al. 2013)

1.1.4.2 Aberrant RNA metabolism

The first link between alterations in RNA processing and motor neuron degeneration was described more than a decade ago. In experimental models, chronic loss of glutamate transport has been shown to produce motor neuron degeneration and may contribute to disease. The astroglial glutamate transporter EAAT2 (excitatory amino acid transporter 2) protein is severely decreased in the motor cortex and spinal cord of ALS patients (Rothstein et al., 2004). Aberrant *EAAT2* mRNA species, due to intron-retention and exon-skipping, have been shown to occur in SALS and its presence correlated with the selective loss of EAAT2 protein in ALS (Lin et al., 1998). In addition, the expression of a neurofilament transgene was found to affect binding of ribonucleoprotein to the neurofilament mRNA and lead to the degeneration of enteric and motor neurons in

transgenic mice (Canete-Soler et al. 1999). The discovery of disease-linked mutations in multiple RNA binding proteins has since highlighted dysfunctional RNA processing as a major pathogenic pathway in ALS. Studies of pathology, cellular and animal models have provided evidence of abnormalities in multiple steps of RNA processing, including transcription, splicing, translation and decay.

A recent study investigating the mechanism of C9ORF72-mediated toxicity found that the hexanucleotide repeat expansion leads to the formation of stable DNA and RNA quadruplexes (Haeusler et al. 2014). The DNA G-quadruplex affected the ratio of C9ORF72 transcripts, such that longer GGGGCC hexanucleotide repeats produced increasing amounts of truncated transcripts, which caused a concomitant decrease in full-length transcripts (Haeusler et al. 2014). The authors postulated that the change in this ratio is due to the inability of cellular transcription machinery to access the transcript within the quadruplex structure. Cellular studies have shown that the hexanucleotide is transcribed bi-directionally, which generates an antisense transcript containing a CCCCGG-repeat that will also be expanded in patients carrying the mutation (Zu et al. 2013). Furthermore, pathologically expanded sense and antisense transcripts can be retained in neuronal nuclei forming RNA foci in the brains of C9ORF72 expansion-positive patients. Some expanded transcripts are exported and are RAN translated to generate GP, GA, GR, PR and PA dipeptides which form p62-labeled inclusions (Mori et al. 2013).

TDP-43 and FUS mutations have also been shown to affect several RNA processing steps, such as splicing, mRNA transport and translation. Using genome-wide approaches, several studies have shown that TDP-43 and FUS have thousands of RNA targets, and that disease-linked mutations alter the RNA targets bound by these proteins (Hoell et al. 2011; Tollervey et al. 2011; Tollervey et al. 2011; Lagier-Tourenne et al. 2012; Rogelj et al. 2012). These studies also show that both proteins are involved in the maturation of RNA and splicing, as knockdown of TDP-43 and FUS altered the levels and splicing of hundreds of RNAs. In addition, both TDP-43 and FUS are present in cytoplasmic RNA granules, and mutant TDP-43 and mutant FUS have been shown to alter the transport of these granules

(Alami et al. 2014) or affect the translation of RNA present in these granules (Yasuda et al. 2013).

1.1.4.3 Axon failure

Motor neurons are characterised by a unique morphology. These cells are highly polarised, typified by axonal projections that can reach a meter in length in adult humans. This morphology requires active axonal transport of organelles, cytoskeletal, synaptic components, and trophic factors to maintain normal cellular function. Axonal defects have been shown to occur in pre-symptomatic stages of disease in animal models of motor neuron disease, and the selective loss of neuromuscular synapse subtypes are believed to precede motor neuron degeneration (Frey et al. 2000).

Changes in the number of neurofilaments or destruction of neurofilaments along with thinning of the axonal diameter have been reported in SALS cases (Atsumi 1981). In addition, there is accumulation of neurofilaments in spinal cord motor neurons in ALS (Hirano et al. 1984). Early evidence of involvement of neurofilament proteins in motor neuron degeneration came from studies of mice overexpressing neurofilament proteins which impaired the axonal transport of cytoskeletal components and mitochondria, accompanied by the degeneration loss of enteric and motor neurons (Collard et al. 1995; Canete-Soler et al. 1999).

Other components of axonal transport have also been shown to contribute neurodegeneration. In particular, several studies have found a role for microtubule-dependent motors proteins kinesin and dynein in the molecular biology of ALS. Landers et al. (2009) identified a single nucleotide polymorphism within the *KIFAP3* gene. This was associated with reduced expression of the encoded kinesin-associated protein, KIFAP3, and longer survival in sporadic ALS cases (Landers et al. 2009). Tateno et al. (2009) reported the localisation of KIFAP3 in SOD1 aggregates in human ALS cases. This study further demonstrated that the association between KIFAP3 and mutant SOD1 impairs the transport of choline acetyltransferase and release of acetylcholine before the onset of

motor symptoms in transgenic SOD1 mice (Tateno et al. 2009). Finally, a mutation in a subunit of the axonal transport protein, dynactin, was identified in a family with a lower motor neuron disease (Puls et al. 2003). This mutation occurs within a domain involved in microtubule binding and impairs binding of dynactin to microtubules (Puls et al. 2003). These features suggest neurofilament alterations and accumulation impair the transport of vesicles and organelles along microtubules to contribute axonal defects and subsequent motor neuron degeneration.

1.1.4.4 Mitochondrial dysfunction

Evidence for mitochondrial involvement in ALS was first observed in ultrastructural studies of patient tissues. Atsumi (1981) reported changes in mitochondria in the axons of remaining myelinated fibers in ALS muscles, which are considered to show axonal degeneration of motor neurons or a disturbance of the slower components of axonal transport (Atsumi 1981). Similarly, Hirano et al. (1984) reported morphological abnormalities of mitochondria in skeletal muscle, intramuscular nerves and proximal axons of SALS patients (Hirano et al. 1984). In addition, the levels of mitochondrial DNA deletion mutation are increased in the motor cortex and spinal cord of ALS patients, and this was associated with decrease in respiratory chain enzyme activities (Dhaliwal and Grewal 2000; Wiedemann et al. 2002).

Findings from animal and cellular models also implicate mitochondrial dysfunction in ALS. Mutant SOD1 transgenic mice develop motor neuron degeneration and show vacuolisation and swollen mitochondria (Dal Canto and Gurney 1995; Wong et al. 1995). At the end stage, mitochondrial structure was completely unravelled and transformed into a series of membranes (Dal Canto and Gurney 1995). Mitochondrial degeneration was specific to motor neurons, as the majority of mitochondria in non-motor neurons and adjacent non-neuronal cells remained unaffected and indistinguishable from normal mice and transgenic mice expressing WT SOD1 (Wong et al. 1995). Transgenic mice expressing TDP-43 also display mitochondrial abnormalities and develop impaired motor function

(Xu et al. 2010) . They showed that expression of human TDP-43 resulted in aggregation of mitochondria and reduced expression of mitofusin 1, a protein essential for mitochondrial fusion. Mitochondrial fusion is critical for the maintenance of mitochondrial morphology, as inhibition of fusion results in loss of mitochondrial DNA and mitochondrial fragmentation (Rapaport et al., 1998).

Mitochondrial dysfunction is also observed in cellular models of ALS. Neuroblastoma cells expressing mutant SOD1 demonstrate a significant decrease of mitochondrial membrane potential and impaired long-term storage of calcium (Carrì et al. 1997). Mitochondrial impairment has also very recently been recapitulated in patient-derived iPSCs. Kiskinis et al., (2014) showed that human motor neurons generated from patient-specific iPSC with the SOD1 A4V mutation have reduced long-term survival and deranged mitochondria with a vacuolar appearance. SOD1 motor neurons showed differential expression of several mitochondrial proteins, along with mitochondrial transportation deficiencies compared to control motor neurons (Kiskinis et al. 2014). These findings show that mitochondrial dysfunction is an important feature of motor neuron degeneration.

1.1.4.5 Oxidative stress

Oxidative stress occurs in a cell when there is an imbalance between the production of reactive oxygen species (ROS) and the ability of the cell to restore the homeostatic environment and reduce the toxic reactive intermediates. There is evidence of increased oxidative stress in postmortem tissue from ALS patients. Spinal cord samples from FALS and SALS patients contain higher levels of several markers of oxidative damage, such as protein carbonyl levels and 3-nitrotyrosine (Shaw et al. 1995; Ferrante et al. 1997). Elevated levels of lipid oxidation markers and free radicals have been detected in the cerebrospinal fluid of ALS patients in the earlier stages of disease (Ihara et al. 2005).

The same markers of oxidative stress are also found in animal and cellular models of ALS. Elevated levels of protein carbonyl and 3-nitrotyrosine have been reported in the

spinal cord and cortex of mutant SOD1 transgenic mice (Ferrante et al. 1997; Andrus et al. 1998). Furthermore, Liu et al. (1999) showed that mutant SOD1 mice have higher levels of several ROS and oxidation products (Liu et al. 1999). These observations suggest that there is an impairment of detoxification pathways in ALS.

1.1.4.6 Neuroinflammation

Neuroinflammation is another pathological hallmark of ALS. The presence of microglia and infiltrating lymphocytes is often observed at sites of motor neuron loss, such as the motor cortex and spinal cord, as well as regions of mild degeneration (Kawamata et al. 1992; Henkel et al. 2004). Microglial activation, as measured by [11C](R)-PK11195 positron emission tomography, occurs throughout the disease (Turner et al. 2004). These findings suggest that neuroinflammation is an active process during ALS disease progression. It is believed that microglia present two phenotypes, a protective M2 phenotype and the neurotoxic M1 phenotype and it remains unclear whether the inflammation responses protect motor neurons or contribute to neuronal injury (Henkel et al. 2009).

Evidence from mutant SOD1 transgenic mice has shown a protective role of T cells by mediating a beneficial inflammatory response. The infiltration of T cells in the CNS of mutant SOD1 mice has been shown to occur early in the disease and stabilizes disease progression (Beers et al. 2008; Chiu et al. 2008). It is believed that T cells serve a protective role by reducing the pro-inflammatory response and by increasing the release of trophic factors (Beers et al. 2008). The transplantation of T cells can also delay motor neuron loss, improve neurological function and prolong the survival of mutant SOD1 mice (Banerjee et al. 2008).

Conversely, during the later stages of disease, microglia in the mutant SOD1 transgenic mice switch from the protective M2 phenotype to the toxic M1 phenotype. This change is associated with increased expression of reactive oxygen species and pro-inflammatory cytokines, along with accelerated disease progression (Alexianu et al. 2001;

Hensley et al. 2002; Henkel et al. 2004; Beers et al. 2008). Nguyen et al. (2004) further demonstrated a positive correlation between the degree of M1 microglial activation and the severity of the disease (Nguyen et al. 2004). These results indicate non-cell autonomous involvement in ALS pathogenesis.

1.1.4.7 Glutamate excitotoxicity

Finally, there is much evidence that excitotoxicity plays a role in the pathogenesis of ALS. Excitotoxicity occurs when extracellular concentrations of excitatory neurotransmitters lead to excess ion influx, energy depletion and calcium accumulation, resulting in neuronal damage and degeneration. A key argument for a role of excititoxicity in ALS is the fact that gabapentin and riluzole, the sole available drug for ALS, both interfere with excitatory neurotransmission, and have proven neuroprotective effects in patients and animal models.

Abnormalities in glutamate metabolism have been observed in ALS patients. For instance, the concentration of excitatory amino acids are highly elevated in the cerebrospinal fluid of ALS patients (Rothstein et al., 1990), whereas glutamate levels are significantly decreased in the brain and spinal cord of ALS patients (Plaitakis et al., 1988). In addition, there is a selective loss of excitatory amino acid transporter 2 (EAAT2) in the brain and spinal cord of ALS patients (Rothstein et al., 1995). There is also a selective defect in sodium-dependent glutamate transport in the brain and spinal cord of ALS patient, with a dramatic reduction in glutamate uptake (Rothstein et al., 1992).

In addition to these abnormalities, *in vivo* and *in vitro* studies have shown that motor neurons demonstrate a selective vulnerability to glutamate receptor agonists. Selective excitotoxic degeneration has previously been reported in mature cultures of rat spinal neurons. Following addition of kainic acid, a glutamate receptor agonist, distal axonal swellings consistent with excitotoxic injury was observed in mature motor neurons, but not observed in immature motor neurons or cortical neurons (King et al., 2007). Excitotoxicity appears to be mediated by non-*N*-methyl-$_{D}$-aspartate (NMDA)

receptors, as kainic acid-induced excitotoxicity was blocked by the addition of non-NMDA receptor atagonist CNQX (King et al., 2007). Reductions, to a lesser degree, in kainic acid-induced excitotoxicity were also observed following the application of MK801, an NMDA receptor antagonist, suggesting some involvement of NMDA receptors in glutamate excitotoxicity (King et al., 2007).

1.1.5 Treatment

Currently, no curative or disease modifying therapies exist, despite half a century of clinical trials and testing of more than 150 pharmacological agents in models of ALS (Thomsen et al. 2014). The sole available drug, Riluzole, only prolongs patient survival by approximately 2-3 months. Riluzole's mechanism of action is not well understood; however, it is a small molecule that has been shown to suppress glutamate activity (Fumagalli et al. 2008). Other measures are taken to improve the quality of life for ALS patients, such as the use of feeding tubes and respiratory assistance devices.

Several approaches are currently under investigation as potential therapies for ALS. These include small molecules involved in macrophage activation, muscle contractility, neuronal excitability and cellular stress response, stem cell therapies and antisense oligonucleotides (Sreedharan and Brown 2013).

1.2 THE ROLE OF FUS IN ALS

1.2.1 FUS structure

FUS is a member of the FET family of DNA and RNA binding proteins, which includes EWS and TAF15. FUS, TAF15 and EWS share similar domain architecture (Fig. 1.3). FUS is a 526-amino acid protein with a molecular mass of 53 kDa (Crozat et al. 1993). The N-terminal 165 amino acids form a transactivating domain that is enriched for serine, tyrosine, glycine and glutamine. This domain is considered as a low complexity region and is predicted to contribute to exaggerated protein aggregation (Kato et al. 2012). Next to this is an arginine-glycine-glycine domain (RGG) consisting of 102 amino acids. This is

followed by an RNA-recognition motif (RRM), which contains a nuclear export signal (NES) made up of 11 amino acids. The next 130 amino acids contain another two RGG domains and a 31-amino acid zinc finger motif (ZnF).

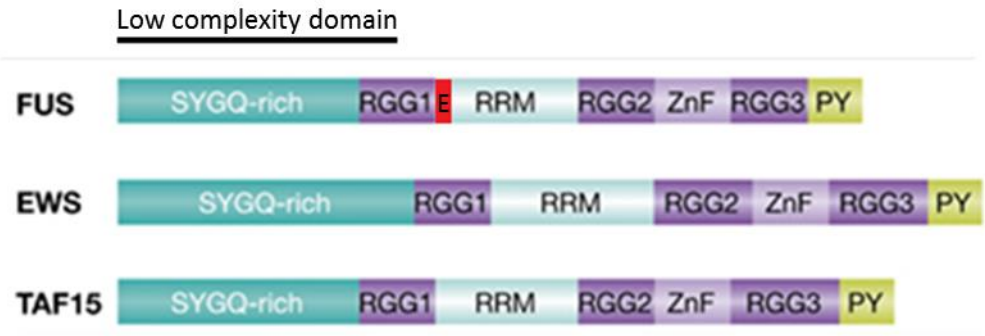

Figure 1.3 Schematic diagram showing the domain architecture of the FET family of proteins. Figure adapted from (Kaneb et al. 2012). SYGQ-rich, serine, tyrosine, glycine, glutamine-rich domain; RGG, arginine-glycine-glycine domain; E, nuclear export signal; RRM, RNA recognition motif; ZnF, zinc finger; PY, proline-tyrosine nuclear localisation signal.

1.2.2 FUS location

In cells, FUS normally displays a clear nuclear localization and a diffuse distribution in the cytoplasm with some localization in nuclear speckles and cytoplasmic granules (Fig. 1.4) (Andersson et al. 2008). The shuttling of FUS between the nucleus and cytoplasm is mediated by transportin-1, a subunit of a receptor complex that targets nuclear proteins to the nucleus (Dormann et al. 2010). Within the nucleus, FUS exists as a nuclear matrix protein and associates with several SR proteins, such as SC35 and SRp75 (Meissner et al. 2003). FUS is involved in spliceosome assembly and the formation of nuclear gems (Hartmuth et al. 2002; Yamazaki et al. 2012). In the cytoplasm, FUS is present in punctate structures known as RNA granules. RNA granules are complexes composed of RNA and other proteins. In neurons, FUS can be found in the postsynaptic

density of synapses (Aoki et al. 2012). Fujii et al. (2005) showed that FUS is specifically recruited to dendritic spines upon neuronal activation.

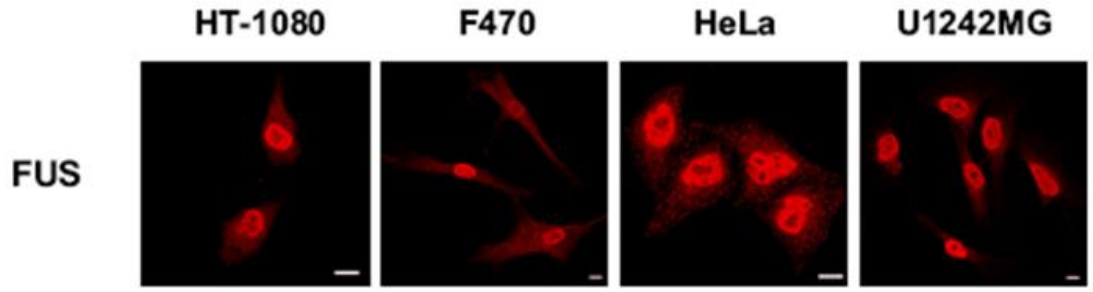

Figure 1.4 FUS localization in cultured human cells (figure adapted from Andersson et al., 2008). HT-1080, fibrosarcoma cells; F470, primary human fibroblasts; HeLa, cervical cancer cells; U1242MG, glioblastoma cells.

1.2.3 FUS functions

FUS is a ubiquitously expressed multifunctional protein that plays a role in numerous biological processes, including transcription regulation, multiple levels of RNA processing, cell proliferation, differentiation and DNA repair.

1.2.3.1 Transcription regulation

FUS was initially identified as a fusion oncogene in myxoid liposarcoma (Crozat et al. 1993). The N-terminus of FUS was shown to function as a transcriptional activation domain to oncogenic fusion proteins (Zinszner et al. 1997). FUS associates with TFIID and RNA polymerase II, key components of the transcriptional pre-initiation complex, which is essential for transcription induction (Bertolotti et al. 1996). The co-expression of FUS and transcription factor NF-κB has been shown to co-activate transcription (Uranishi et al. 2001). Thus, it has been proposed that FUS is involved in the recruitment of general and specific factors for the initiation of transcription and acts as a transcriptional modulator of gene expression (Law et al. 2006).

1.2.3.2 Splicing and maturation of RNA

A number of studies have demonstrated the importance of FUS in splicing and RNA maturation. Splicing removes introns from pre-mRNAs and is mediated by the spliceosome, a complex composed of ribonucleoproteins (RNPs). FUS associates with the spiceosomal complex (Meissner et al. 2003). In particular, specific FUS domains have been shown to interact with spliceosome members, such as SF1 and SR proteins (Yang et al. 1998; Yang et al. 2000). FUS also associates with components of the SMN complex or Gems, a structure involved in the regulation of snRNPs (Yamazaki et al. 2012). In fact, FUS is necessary for the formation of Gems, and a reduction in Gems is observed in ALS patient fibroblasts (Yamazaki et al. 2012).

FUS has thousands of RNA targets and changes in alternative splicing are observed in a minority of these when the levels of FUS are manipulated (Rogelj et al. 2012). Yang et al. (1998) showed that overexpression of FUS alters the accumulation of alternatively spliced mRNAs. Conversely, knockdown of FUS in mouse cortical neurons leads to increases in four-repeat tau isoforms (Orozco et al. 2012). Depletion of FUS in the central nervous system of adult mice leads to changes in hundreds of splicing events (Lagier-Tourenne et al. 2012). This study also showed that FUS binding sites are enriched in alternatively excluded or included exons, supporting the view that FUS mediates splicing of its RNA targets (Lagier-Tourenne et al. 2012).

In addition to this, FUS has been observed in a multi-protein complex with Drosha and DGCR8, two key proteins that mediate the genesis of microRNAs (Gregory et al. 2004; Shiohama et al. 2007). The role of FUS in microRNA biogenesis remains unclear however, and Gregory et al. (2004) suggest that this complex likely mediates preribosomal RNA processing, rather than microRNA processing.

1.2.3.3 RNA transport and translation

It is now established that FUS is a nucleic acid-binding protein (Zinszner et al. 1997; Baechtold et al. 1999). The finding that FUS binds RNA and engages in

nucleocytoplasmic shuttling, led to the idea that FUS may function as a chaperone of RNA and participate in RNA transport (Zinszner et al. 1997). A later study demonstrated that FUS does in fact function in the transport of mRNA transcript in neurons. Fujii and Takumi (2005) found that FUS associates with actin-related mRNA transcripts and facilitates their transport to dendritic spines following neuronal activation.

RNP complexes containing FUS have also been implicated in local translation. A recent study showed the presence of FUS in an RNP complex containing the tumor suppressor protein adenomatous polyposis coli (APC) (Yasuda et al. 2013). It was previously shown that APC targets mRNA transcripts to cell protrusions to form APC-RNPs (Mili et al. 2008). Yasuda et al. (2013) showed that while FUS is not required for the localization of APC-RNPs, nor RNAs, to cell protrusions, it is necessary for efficient translation of the associated RNA transcripts in cell protrusions. Thus, in addition to splicing and RNA maturation, transport and translation are also important features of FUS-containing RNP complexes.

1.2.3.4 DNA repair, cell proliferation and differentiation

A role for FUS in DNA repair was identified by investigating DNA homologous pairing (DHP) activity, a central step in homologous recombination and repair in certain forms of DNA damage. Bertrand et al. (1999) found that FUS is one of two major mammalian nuclear extracts with DHP activity. Kuroda et al. (2000) reported that FUS knockout mice demonstrate meiotic defects and enhanced radiation sensitivity, demonstrating the functional significance of FUS in DNA repair. Recently, FUS was shown to be important for both homologous recombination and non-homologous end joining-mediated DNA repair (Wang et al. 2013). Importantly, this study showed that FUS is recruited to the site of DNA damage at a very early stage of the DNA damage response, and that its localization at the site of DNA damage recruits histone deacetylase 1 (HDAC1), a protein with a prominent role in DNA repair in neurons (Wang et al. 2013).

The DHP activity of FUS also correlates with cell proliferation. Bertrand et al. (1999) showed that immortalizing cells leads to stimulation of FUS DHP activity, and that DHP activity is stimulated in proliferating cells. Alternatively, inducing differentiation resulted in the inhibition of FUS DHP activity, linking FUS DHP activity with cell proliferation (Bertrand et al. 1999). A later study also provided support for a role of FUS in cell differentiation. Andersson et al. (2008) showed that the expression of FUS and related protein TAF15 is down-regulated in differentiating hESCs and neuroblastoma cells.

FUS has also been implicated in the development of other cell types, Disruption of *FUS* in mice results in neonatal lethality and abnormal lymphocyte development (Hicks et al. 2000). In addition, hippocampal neurons from these mice demonstrate abnormal morphology, with irregularly branched dendrites, multiple immature axons and reduced dendritic spines (Fujii et al. 2005). Whether these developmental phenotypes are associated with the DHP activity of FUS remains unknown. Regardless, these data imply a key role for FUS in development.

1.2.4 FUS pathology

Similar to other neurodegenerative conditions, the neuropathology of FUS-associated ALS is characterized by protein inclusions (Fig. 1.5). Within FALS cases with FUS mutations, examinations have revealed a heterogeneous neuropathology. One particular feature that appeared to distinguish early from late-onset cases was the frequency and anatomical distribution of basophilic inclusions (Mackenzie et al. 2011). Basophilic inclusions are sharply defined, single or multiple, round, oval or multilobulated bodies, often similar in size to the neuronal nucleus. In late-onset cases, basophilic inclusions are rarely observed; most brain regions examined contained no more than a single basophilic inclusion. In contrast, basophilic inclusions are a very obvious pathological feature of early-onset cases. Multiple inclusions were found in the spinal cord and motor cortex, as well as several other neuroanatomical regions. In addition, dense basophilic deposits were observed in upper and lower motor neurons.

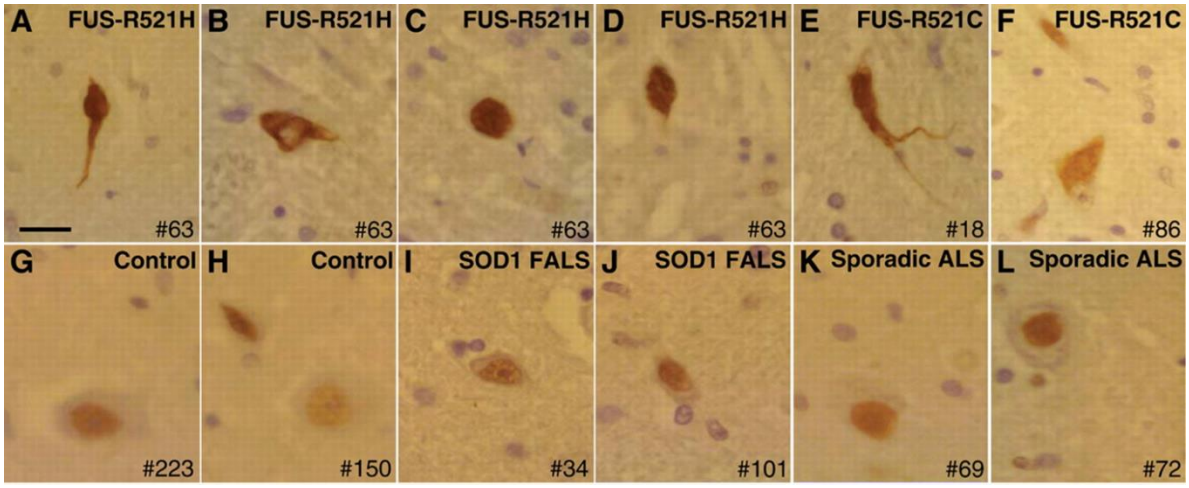

Figure 1.5 Immunostaining of FUS in the anterior horn of the spinal cord in patients with *FUS* mutations (A to F), controls (G and H), patients with *SOD1* mutations (I and J) and SALS patients (K and L) (Figure adapted from Vance et al., 2009).

Another characteristic that differentiated early- from late-onset cases was the frequency, anatomical distribution and appearance of FUS-immunoreactive neuronal cytoplasmic inclusions (NCIs) (Vance et al. 2009). While NCIs were observed in lower motor neurons of all cases, they were more prevalent in early-onset cases. Early-onset cases also exhibited numerous NCIs in the motor cortex and cerebellar dentate nucleus, whereas late-onset cases were characterized by NCIs in the basal ganglia (Mackenzie et al. 2011). The appearance of NCIs also differed between early- and late-onset cases. Late-onset cases displayed NCIs with thick filaments in the perikaryon. This feature was mostly absent in early-onset cases, which typically exhibited compact and round NCIs.

Finally, early- and late-onset cases may be distinguished pathologically by the presence of glial cytoplasmic inclusions (Mackenzie et al. 2011). Inclusions in glia are rarely seen in early-onset cases. In contrast, glial inclusions are numerous in late-onset cases, and correlate well with the anatomical distribution of neuronal cytoplasmic inclusions. The appearance of these inclusions was variable, with round, crescent or flame-shaped bodies.

1.2.5 Mechanisms of mutant FUS-mediated toxicity

Since the discovery of ALS-linked mutations in *FUS,* cellular studies and animal models have been used to determine the mechanism through which these mutations lead to motor neuron degeneration. Findings from these studies have led to the proposal of both toxic gain of function and loss of function models.

1.2.5.1 Loss of function

Several animal models with reduced levels of FUS have demonstrated that a lack of physiological functions of FUS in the nucleus is sufficient to induce abnormal neuronal morphology, locomotive dysfunction and motor neuron degeneration. As mentioned above, hippocampal neurons from FUS knockout mice show abnormal dendritic morphology, with reduced spine density (Fujii et al. 2005). These mice have a perinatal lethal phenotype (Hicks et al. 2000), although another study has reported that surviving knockout mice exhibit male sterility (Kuroda et al. 2000).

Several *Drosophila* models have shown that knockdown of *Cabeza* (*Caz*), the *Drosophila* orthologue of human *FUS*, recapitulates key features of motor neuron disease. Sasayama et al. (2012) showed that knockdown of *Caz* causes reduced mobility, reduced length of synaptic branches of motor neurons and decreased number of synaptic boutons. However, *Caz*-knockdown flies had a life span comparable to WT flies (Sasayama et al. 2012).

Loss of endogenous *fus* in zebrafish also causes a motor phenotype. *Fus* knockdown by antisense morpholino oligonucleotide (ASO) resulted in abnormal motor behavior characterized by a deficient touch-evoked escape response, as well as reduced axonal outgrowth from spinal cord motor neurons (Kabashi et al. 2011). This motor phenotype was rescued by the co-injection of ASO and human WT *FUS* mRNA, but not or only partially rescued mutant *FUS* mRNA, providing strong evidence for a loss of function mechanism.

1.2.5.2 Gain of function

Conversely, several lines of evidence suggest that *FUS* mutations cause ALS by a gain of function effect related to the mislocalisation or aggregation of mutant FUS in the cytoplasm. Murakami et al. (2011) showed that the expression of mutant FUS in *Caenorhabditis elegans* causes cytoplasmic mislocalisation of FUS protein, progressive motor dysfunction and reduced lifespan. Importantly, this animal model demonstrated a correlation between the degree of mislocalisation and the severity of neuronal dysfunction, recapitulating an important feature observed in the human condition. Murakami et al. (2011) also showed that the co-expression of WT-FUS does not rescue the motor dysfunction caused by the expression of mutant FUS. This finding strongly suggests that mutant FUS causes ALS through a gain of function effect.

The overexpression of mutant *FUS* R521H mRNA in zebrafish also causes motor deficit in zebrafish, resulting in deficient touch-evoked escape response and reduced motor neuron axonal outgrowth (Kabashi et al. 2011). This study showed that the overexpression of mutant *FUS* R521C and S57Δ did not lead to the same drastic motor phenotype, suggesting *FUS* mutations contribute to motor neuron degeneration via different mechanisms (Kabashi et al. 2011).

Mice overexpressing human WT FUS show a rapid decline in motor function, characterised by the development of a tremor, progressive hind limb paralysis, and death by 12 weeks (Mitchell et al. 2013). These mice also show pathological hallmarks of ALS-FUS, such as ubiquitin-negative FUS-positive inclusions in spinal cord and brain stem motor neurons, significant loss of motor neurons in the spinal cord and loss of fast-twitch muscle fibres (Mitchell et al. 2013).

Overexpression of mutant FUS also results in progressive paralysis in transgenic rats (Huang et al. 2011). Degenerating axons are observed in the corticospinal tracts of mutant FUS transgenic rats at late stages of the disease, resulting in atrophy of skeletal muscle cells and denervation without a significant loss of motor neurons, but substantial

loss of cortical and hippocampal neurons (Huang et al. 2011). Whereas overexpression of mutant FUS in rats was associated with a motor phenotype, overexpression of WT FUS caused deficits in learning and memory, along with loss of neurons in the frontal cortex and dentate gyrus (Huang et al. 2011).

These results seem to support a toxic gain of function mechanism associated with ALS-FUS. However, the overexpression of human FUS is associated with down-regulation of endogenous Fus in transgenic animals (Mitchell et al. 2013). Thus, it is difficult to dissect the contribution of loss or gain of function mechanisms in transgenic animal models.

1.3 THE NEED FOR NEW CELLULAR MODELS

One of the biggest impediments to our understanding of disease mechanisms in neurological conditions is the inaccessibility of human neural cell types. Studies of animal models have circumvented this issue and enable the study of ALS in an intact organism. Numerous transgenic models have been created, including yeast, *Drosophila,* nematode, zebrafish, mouse and rat models of SOD1, TDP-43, FUS and C9ORF72 pathology. These models have been successful in modelling the degeneration of motor axons and ALS-like motor phenotypes. They have provided some insight into the underlying disease mechanisms. However, preclinical successes in the treatment of existing animal models have not translated well into clinical benefit for patients. This may be due to differences in experimental design between the treatment of existing animal models and the treatment of patients. For instance, mice are often treated at the pre-symptomatic stage, whereas humans are treated at the end stage of disease. Thus, this is an issue that needs to be addressed as improvements are made to current ALS diagnostic tools. Another difference is the issue of compliance. Whereas studies using animal models have high compliance, low or noncompliance in patients may be a significant contributor to the high failure of drugs in clinical trials. Therefore, better attempts at analysing patient compliance during drug testing may also lead to improvements in clinical trials (Czobor and Skolnick, 2011).

Alternatively, this may be due to inherent anatomical and genetic variations between animal and man, or complex genetic and environmental interactions that result in disease, thus limiting the potential of animal models of ALS.

Human cellular models can address some of these issues; however, current cellular models have severe limitations. For years, studies have used techniques to overexpress mutant protein in immortalised cell lines or in non-neuronal cell types to develop a cellular model to study fundamental disease mechanisms and screen for drugs that reverse these processes. Immortalised cell lines are known to acquire genetic abnormalities with prolonged culture. In addition, the ability of these cells to divide continuously and the massive overexpression of human protein do not mirror normal physiological conditions. Thus, there are significant limitations to the use of these cells as a model for ALS.

An attractive alternative has emerged in the past decade with the discovery that human embryonic stem cells (hESCs) and induced pluripotent stem cells can be directed to differentiate into motor neurons. hESCs are pluripotent stem cells derived from human embryos at the blastocyst stage. They have the ability to proliferate indefinitely in culture while maintaining the capacity to differentiate to all cell types. It is possible to study genetic disease conditions in hESCs by using genome-editing tools to introduce disease-causing mutations. An alternative approach is to reprogram adult somatic cells to generate induced pluripotent stem cells.

1.4 INDUCED PLURIPOTENT STEM CELLS

The method of reprogramming adult somatic cells to pluripotent stem cells was reported in 2006 by Takahashi and Yamanaka (Takahashi and Yamanaka 2006). They reported that dermal fibroblasts from adult mice can be reprogrammed into a pluripotent state by retroviral transduction of four transcription factors, *OCT4. KLF4, c-MYC* and *SOX2* (Fig. 1.6). The reprogrammed cells were termed induced pluripotent stem cells (iPSCs). iPSCs are similar to embryonic stem cells (ESCs) in their morphology, proliferation,

surface antigens, gene expression and capacity to differentiate into the cell types of the three germ layers. A year later, Takahashi et al. (2007) applied the same technology to human adult dermal fibroblasts to generate the first human iPSCs (Takahashi et al. 2007).

Since this discovery, many others have shown that it is possible to generate iPSCs from other adult somatic cell types, including blood cells, urine cells, amniotic cells and others (Wang et al. 2013). In addition, a variety of techniques have been developed to deliver the four reprogramming transcription factors. These include non-integrating viral vectors, small molecules, transduction of proteins and microRNAs (Wang et al. 2013). Since the initial discovery, the efficiency of iPSC generation has greatly improved and the technology continues to develop.

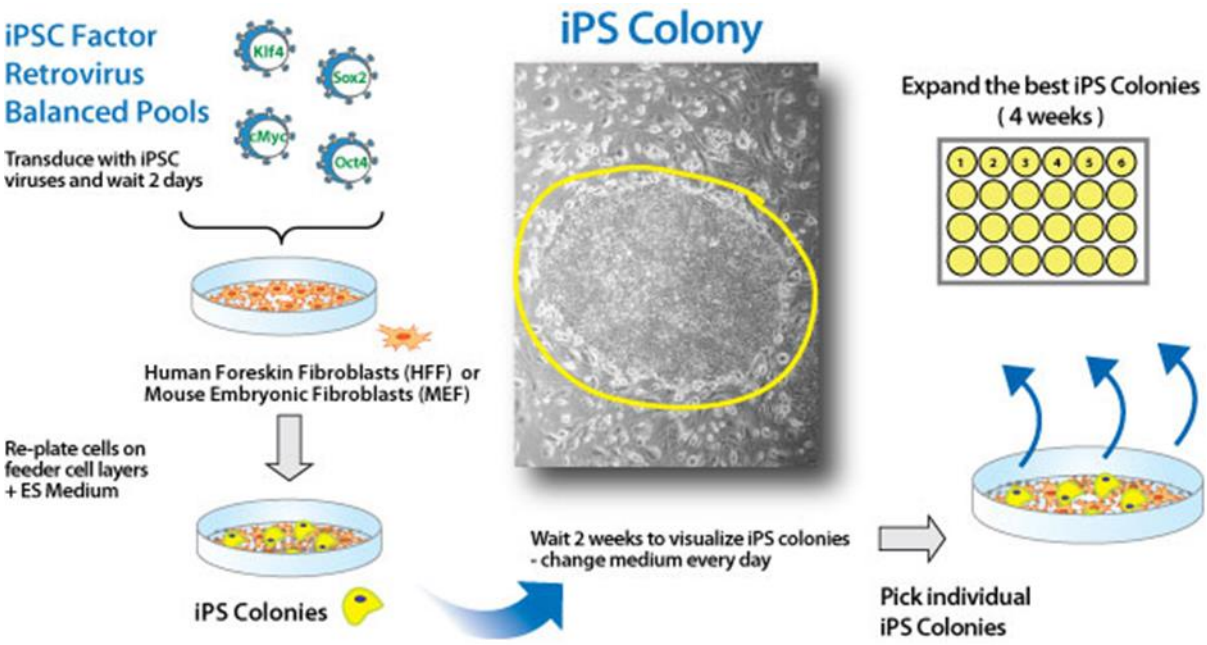

Figure 1.6 Schematic diagram showing the process of iPSC reprogramming and generation (Figure reproduced from System Biosciences).

Yamanaka's seminal studies provided an avenue to generate patient and disease-specific iPSCs and led to his being rewarded the Nobel Prize in Medicine and Physiology in 2012. This discovery, combined with protocols for the directed differentiation of neurons,

enabled access to these cell types without the ethical issues involved with the use of hESCs. Since this discovery, iPSCs have been used to model numerous genetic disorders, including neurodegenerative conditions such as Alzheimer's, Huntington's and Parkinson's disease (Zhang et al. 2010; Nguyen et al. 2011; Israel et al. 2012).

Although iPSCs offer tremendous potential for studies of disease mechanisms and drug discovery, there are also some disadvantages to using these cells as a model system. Compared to other cellular models, such as immortalised cell lines, iPSC cultures are costly to establish and maintain. The generation of iPSCs requires time and the reprogramming occurs at relatively low efficiency. In addition, compared to other cell lines, iPSCs exhibit a high degree of variance, even within subclones from the same individual. Furthermore, iPSCs carry an epigenetic memory, such that they have a bias towards differentiating into the cell type from which they were derived. Therefore, there remains a number of caveats concerning the use of iPSCs as a model system.

1.4.1 iPSC models of ALS

The first application of iPSC technology in the study of ALS was in 2008. Dimos et al. (2008) showed that fibroblasts from an 82-year old ALS patient could be reprogrammed into iPSCs. Furthermore, these patient-specific iPSCs can be directed to differentiate into functional motor neurons (Dimos et al. 2008). For the first time, it became possible to gain access to the cell types affected in ALS, but they did not describe a pathological phenotype. This study was followed by two reports of iPSCs generated from patients with pathogenic TDP-43 mutations (Bilican et al. 2012; Egawa et al. 2012). Both of these studies showed that patient-derived iPSCs recapitulated cellular and biochemical features associated with ALS-TDP and that motor neurons generated from patient-derived iPSCs show selective vulnerability to cell stressors (Bilican et al. 2012; Egawa et al. 2012). Furthermore, Egawa et al. (2012) identified a compound that reversed some of the ALS phenotypes found in mutant motor neurons.

Similarly, Almeida et al. (2013) reported that iPSCs derived from patients carrying the hexanucleotide repeat expansion in C9ORF72 also recapitulated key features of ALS-C9ORF72. This was followed closely by another study of iPSC-derived motor neurons from *C9ORF72* ALS patients that also recapitulated *C9ORF72* pathology, which was reversed by the use of antisense oligonucleotides (Sareen et al. 2013). Very recently, two elegant studies combined iPSC technology, stem cell differentiation approaches and genome editing technology to investigate the pathways perturbed as a result of ALS-linked *SOD1* mutations (Chen et al. 2014; Kiskinis et al. 2014). These studies showed that endogenous levels of mutant protein were sufficient in recapitulating aspects of ALS pathology. Furthermore, they demonstrate the utility of iPSC models for drug screening and provide support for their use in mechanistic studies.

1.5 PROJECT RATIONALE

When this project was initiated, the exploration of FUS iPSCs was entirely novel. There had been only one publication on iPSCs and motor neurons differentiated from an ALS patient, without a description of any pathogenic phenotype. Our recent work on iPSCs derived from a patient with a TDP-43 mutation was the first to recapitulate aspects of ALS pathology (Bilican et al. 2012). We wished to determine whether mutant FUS iPSC lines show a similar propensity to protein mislocalisation and aggregation as was seen in the mutant TDP-43 iPSC lines.

This thesis begins by describing the methods used to characterise iPSC lines derived from a patient carrying the FUS R521C mutation and the directed differentiation of these iPSC lines into neural progenitors and motor neurons. Our prediction was that the FUS R521C mutation would not prevent the functional maturation of motor neurons. The next part of the thesis illustrates the characterisation of FUS-ALS phenotypes: mislocalisation of FUS protein, redistribution into stress granules and cellular toxicity. We predicted that neuralised cells would recapitulate the key features observed in ALS patients carrying *FUS* mutations. The last section describes the investigation of neuronal morphology in neurons

differentiated from patient-derived iPSCs and demonstrates that compromised dendrite and synaptic morphology may represent an underlying pathogenic mechanism. Although our study used multiple lines generated from patient fibroblasts, they represented one pathogenic mutation and may limit the interpretation of results. We therefore sought to investigate the neuronal morphology in a range of ALS-linked *FUS* mutants which had been previously established (Vance et al. 2013). The advantages and limitations of the iPSC model are discussed. Finally, the thesis concludes with an outline of future directions related to this work.

CHAPTER 2

MATERIALS AND METHODS

All chemicals and reagents used were purchased from Life Technologies, unless otherwise stated.

2.1 CELL CULTURE

All cell culture work was carried out in a class II microbiological flow hood under sterile conditions. All incubations were undertaken at 37°C in a humidified 5% CO_2 incubator. Fifteen cell lines were used, 6 human iPSC lines, one hESC line (HUES), 6 neural progenitor cell lines, Human Embryonic Kidney (HEK-293T) and human neuroblastoma (SH-SY5Y) cell lines.

2.1.1 Generation of iPSCs

Procurement of skin tissue for use in reprogramming experiments was obtained via informed consent under a protocol approved by the King's College Hospital, NHS Foundation Trust ethics review committee and the Department of Research and Development. Skin biopsies were taken from a 40-year-old female ALS patient carrying the FUS R521C mutation. The biopsy was cut into pieces and plated in a T12.5 tissue culture flask and grown in human fibroblast derivation media (DMEM, 10% fetal bovine serum (FBS), and 1x penicillin-streptomycin). Outgrowth of cells appeared after 1-2 weeks. Medium was changed every 2-3 days. Cells were passaged 1:3 with 0.25% trypsin-EDTA (TE) upon reaching confluency. Human dermal fibroblasts from a normal male (56 years old, CRL-2465) and a normal female (46 years old; CRL-2524) were obtained from ATCC. All fibroblasts were maintained in alpha-MEM with 10% inactivated fetal calf serum. Fibroblasts were reprogrammed into pluripotent stem cells following transduction by four transcription factors *OCT4, SOX2 KLF4,* and *c-MYC*, as previously described (Takahashi et al., 2007).

Reprogramming was performed by In-Hyun Park in George Daley's laboratory at Harvard. cDNA of *OCT4, SOX2 KLF4,* and *c-MYC* were generated by RT-PCR and inserted into pMIG vector. SV40 large T in the pBABE-puro vector and *hTERT* in the pBABE-hygro vector were obtained from Addgene. HEK-293T cells were plated in 10-cm tissue culture plates and transfected with 2.5 μg of retroviral vector, 0.25 μg of VSV-G vector and 2.25 μg of Gag-Pol vector using FUGENE 6 reagents. The supernatant was collected and filtered through 0.45 μm cellulose acetate filter two days after transfection, then centrifuged at 23,000 RPM for 90 minutes and stored at -80°C until use. 1 x 10^5 control and patient fibroblasts were plated in one well of a six-well plate and infected with the retrovirus and protamine sulphate. Three days post-infection, cells were passaged into plates pre-seeded with mouse embryonic fibroblasts (MEFs). Seven days after infection, medium was changed to human embryonic stem cell (hESC) medium (Dulbecco's Modified Eagle Medium: Nutrient Mixture F-12 (DMEM/F12) containing 20% Knockout Serum Replacement, 10 ng/mL human recombinant basic fibroblast growth factor (bFGF), 1 x non-essential amino acids, 5.5 mM β-Mercaptoethanol (Sigma) and 1 x penicillin-streptomycin), supplemented with 5 μM ROCK inhibitor (Y27632; Calbiochem). 30 days after transduction, hESC-like colonies were picked and expanded. Multiple clonal lines were generated and 6 of the most stable were chosen for subsequent differentiation.

2.1.2 General maintenance of pluripotent stem cells

iPSCs and hESCs were maintained in feeder-free conditions on Matrigel (BD Biosciences). Matrigel was diluted in a 1 in 30 dilution in chilled DMEM/F12 and used to cover the bottom of flasks and plates for pluripotent stem cell culture. Coating was prepared at least one day before passaging of pluripotent stem cells and stored at 4°C, wrapped in parafilm. Matrigel-coated flasks or plates were washed with DMEM/F12 prior to use.

Pluripotent stem cells were maintained in mTESR1 or TeSR-E8 media (STEMCELL Technologies). iPSCs and hESCs were thawed by warming one vial of cells in a 37°C water

bath until an ice drop was seen inside the cryovial (Fisher Scientific). 1 ml of fresh warmed medium was added to the vial and cells were transferred into a conical tube and centrifuged for 4 minutes at 1000 rpm. The supernatant was removed and the cell pellet was resuspended in fresh medium supplemented with 5 μM Y27632 and transferred to a Matrigel-coated T-25 flask.

Medium was changed daily and cells were passaged with Dispase (BD Biosciences) or Gentle Cell Dissociation Reagent (STEMCELL Technologies) once a week, when cell colonies were big, in contact with other colonies, and when a change in colour in the middle of the colony was observed under the microscope in low magnification. To split the cells, old medium was removed and the cells were washed once with DMEM/F12. 1ml of Dispase or Gentle Cell Dissociation Reagent was added to a T-25 flask. Cells were incubated at 37°C until cells at the edge of colonies started to detach. Cells were washed again with DMEM/F12 once and fresh medium was added. Cells were split manually using a sterile fire sharped glass pipette Pasteur. Cells were transferred to a conical tube and centrifuged at 1000 rpm for 4 minutes. The supernatant was removed and the cell pellet was resuspended in fresh media in a 1 in 3 dilution.

To freeze the cells, 5 μM of Rho-associated kinase (ROCK) inhibitor was added to the medium two hours before freezing. The medium was removed and cells were washed once with DMEM/F12. 1ml of Dispase or Gentle Cell Dissociation Reagent was added to a T-25 flask. Cells were incubated at 37°C until cells at the edge of colonies started to detach. Cells were washed again with DMEM/F12 once and Knockout Serum Replacement supplemented with 10% dimethyl sulfoxide (DMSO) was added. Cells were scraped manually using a sterile fire sharped glass pipette Pasteur and transferred to a cryovial. Vials were placed in a Mr. Frosty freezer container (Thermo Scientific) at -80°C overnight. Cells were transferred to liquid nitrogen the next day.

2.1.3 Maintenance of other cell lines

HEK293T cells were maintained in DMEM with 10% fetal bovine serum (FBS) and 1% penicillin-streptomycin. SH-SY5Y cells were maintained in DMEM/F12 with 10% FBS and 1% penicillin-streptomycin. Cells were split upon reaching 80% confluence. To split the cells, old medium was removed and cells were washed with PBS. TE was added to the flask and incubated at 37°C until cells detached. Cells were collected in fresh medium and centrifuged at 1000 rpm for 4 minutes. The supernatant was removed and the cell pellet resuspended in fresh media. An aliquot of this was used in a 1 in 50 dilution in a new flask.

2.1.4 *In vitro* embryoid body differentiation of induced pluripotent stem cells

Embryoid bodies were generated from iPSCs using Aggrewell Plates (StemCell Technologies) according to the manufacturer's instructions. Briefly, cells were grown in suspension culture in Aggrewell Plates in mTeSR1 or TeSR E8 medium for two days. Cell clusters were then collected and cultured on low adherence Poly (2-hydroxyethylmethacrylate) (polyHEMA)-treated tissue culture dishes (Sigma) in differentiation medium consisting of DMEM supplemented with 20% FBS, 0.1 mM β-Mercaptoethanol and 1 mM L-glutamine.

PolyHEMA-treated tissue culture dishes were prepared by dissolving 1.25 grams of polyHEMA in 10 ml of ethanol in a shaker at 37°C overnight. Once completely dissolved the polyHEMA solution was diluted in 100 ml of ethanol and applied to tissue culture dishes and dried on a level, vibration-free surface. PolyHEMA-treated tissue culture dishes were UV-sterilised prior to use.

After 7 days of culture in suspension, embryoid bodies were differentiated for a further 2 weeks in differentiation medium on 0.1% gelatin-coated plates. 0.1% gelatin solution was prepared by dissolving gelatin in endotoxin-free water and sterilisation by autoclaving. Tissue culture plates were coated with gelatin solution at room temperature for 2 hours, aspirated and dried before use.

2.1.5 *In vitro* motor neuron differentiation of induced pluripotent stem cells

Motor neuron differentiation of iPSCs was performed by using an established protocol as described previously (Bilican et al., 2012) (See Figure 2.1 for a schematic for the motor neuron differentiation process). iPSC cultures were differentiated into neuroectoderm by dual-SMAD signaling inhibition in chemically defined medium (CDM) (Table 2.1) with SB431542 (10 µM; Tocris) and dorsomorphin (2.5 µM; Calbiochem) for 5-7 days.

Figure 2.1. Motor neuron differentiation was initiated with dual SMAD inhibition in CDM on days 1-7, followed by the addition of 0.1 µM RA in CDM for 7 days, then 0.1 µM RA and 1 µM purmophamine in neuronal medium for 7 days, and terminally differentiated in 0.1 µM RA, 0.1 µM purmophamine, 10 ng/ml brain-derived neurotrophic factor (BDNF) and glial cell line-derived neurotrophic factor (GDNF) in maturation medium for 3-6 weeks.

Table 2.1. Chemically defined medium

Component	Final concentration
DMEM:F12	up to 250 ml
L-glutamine (10X)	1x
BSA	5mg/ml
Lipid 100x	1x
Monothioglycerol	450 µM
Insulin	7 µg/ml
Transferrin	15 µg/ml

Penicillin-streptomycin	1x

Neurospheres were formed by mechanical dissociation of neuroectoderm. Neurospheres were grown in suspension in poly-HEMA-treated tissue culture dishes and caudalised in CDM with retinoic acid (RA, 0.1 μM; Sigma) for 7-10 days. Caudalised neurospheres were collected and washed with DMEM/F12. They were then resuspended in neuronal medium (Table 2.2) and grown in suspension the same polyHEMA-treated tissue culture dish for 7-9 days to generate motor neuron precursors.

Table 2.2. Neuronal medium

Component	Final concentration
Neurobasal medium	1x
L-glutamine	1x
Retinoic acid	0.1 μM
Purmorphamine	1 μM
N2	1x
B27	1x
Penicillin-streptomycin	1x
Non-essential amino acids	1%
bFGF	5 ng/ml
Heparin	5 ng/ml

Poly-L-ornithine (Sigma), fibronectin (Sigma) and laminin-coated substrate was prepared for plating down and maturation of motor neuron cultures. A coating solution consisting of PBS with 1% poly-L-ornithine, 3.75 μg/ml fibronectin and 10 μg/ml laminin was applied to tissue culture plates or coverslips and incubated at 37°C overnight. The coating solution was removed and the substrate was washed with PBS prior to use.

Motor neuron precursors were collected in a 15 ml falcon tube and washed with PBS. They were dissociated with Accutase by incubating in a 37°C water bath and gentle trituration until most cells had dissociated from the neurosphere clusters. DMEM/F12 was added to the cells and cells were centrifuged at 1 000 rpm for 4 minutes. The supernatant was removed and the cell pellet resuspended maturation medium (Table 2.3) and plated at a seeding density of 0.5 x 10^5/200 mm^2. Medium was changed once or twice a week by removing a half volume of old medium and adding a half volume of fresh maturation medium.

Table 2.3. Maturation medium

Component	Final concentration
Neurobasal medium	1x
L-glutamine	1x
Retinoic acid	0.1 µM
Purmorphamine	0.1 µM
N2	1x
Penicillin-streptomycin	1x
Non-essential amino acids	1%
Ascorbic acid	400 µM
Forskolin	10 µM
BDNF	10 ng/ml
GDNF	10 ng/ml

2.1.6 Neural conversion of induced pluripotent stem cells and neural progenitor cell culture

Neural progenitor cells (NPCs) were maintained on Matrigel. Matrigel was diluted in a 1 in 100 dilution in chilled DMEM: Nutrient Mixture F-12 (DMEM/F12) and used to cover the bottom of flasks and plates for NPC culture. Coating was prepared at least one

day before passaging of NPCs and stored at 4°C, wrapped in parafilm. Matrigel-coated flasks or plates were washed with phosphate buffered saline (PBS) prior to use.

NPCs were generated by differentiating iPSCs into neuroectoderm by dual-SMAD signaling inhibition in CDM with SB431542 (10 μM; Tocris) and dorsomorphin (2.5 μM; Calbiochem) for 5-7 days. Neurospheres were formed by mechanical dissociation of neuroectoderm. Neurospheres were grown in suspension in poly-HEMA-treated tissue culture dishes and caudalised in CDM with RA (0.1 μM; Sigma) for 7-10 days. Caudalised neurospheres were collected and resuspended in expansion media (Table 2.4) and plated on Matrigel.

Table 2.4. Expansion medium

Component	Final concentration
Advanced DMEM/F12	1x
L-glutamine	1x
N2	1x
Penicillin-streptomycin	1x
B27	0.05x
bFGF	10 ng/ml

Several days after plating, radial arrangement of columnar neuroepithelial cells known as neural rosettes emerge, surrounded by "flat" cells (Fig. 2.2). Neural rosettes were selected using the STEMdiff Neural Rosette Selection Reagent (StemCell Technologies) following the manufacturer's protocol. Neural rosette clusters were resuspended in expansion media and plated on fresh Matrigel. After two days, NPCs grow out and form a monolayer form the clusters.

Medium was changed every other day and cells were passaged with Accutase one day after reaching 100% confluence. To split the cells, old medium was removed and cells were washed with PBS. Accutase was added to the flask and incubated at 37°C until cells

detached. Cells were collected in fresh medium and centrifuged at 1 000 rpm for 4 minutes. The supernatant was removed and the cell pellet resuspended in fresh media. An aliquot of this was used in a 1 in 2 dilution in a new flask.

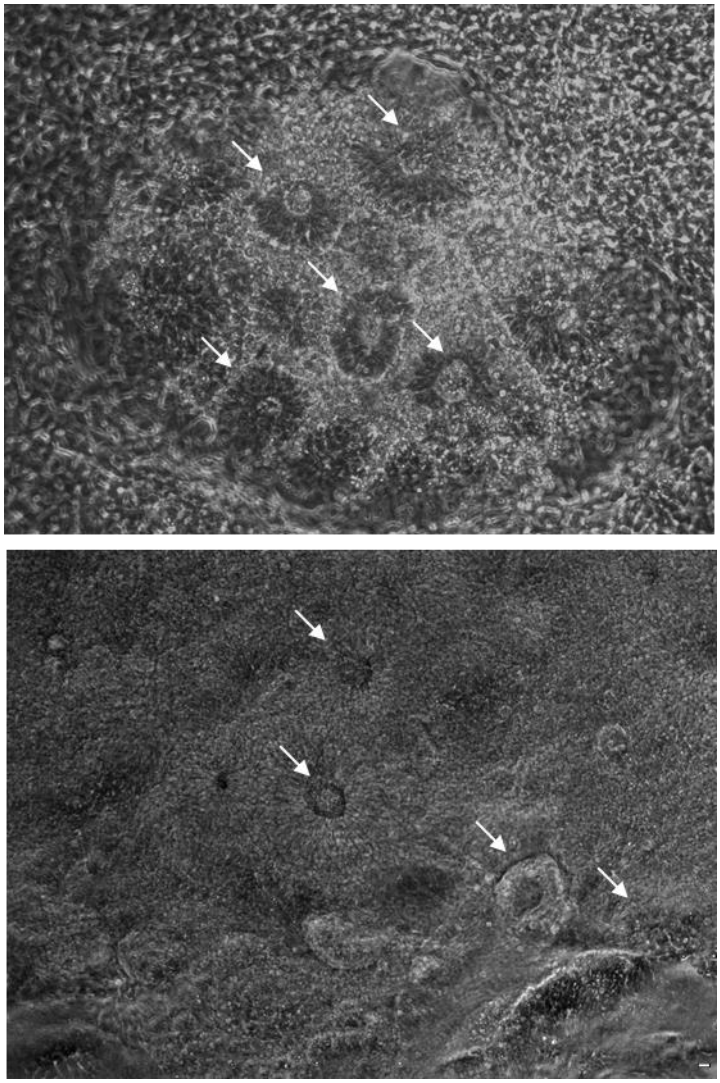

Figure 2.2. Neural rosettes (arrows) formed two days after plating iPSC-derived neurospheres on Matrigel. Neuroepithelial cells derived from (A) FUS1 iPSCs and (B) WT-1 iPSCs. Scale bar = 10 μm.

2.1.7 Differentiation of neural progenitor cells

iPSC-derived NPCs were differentiated into cortical neurons by withdrawal of bFGF. NPCs were plated at a seeding density of 0.3 x 10^5/200 mm^2 on Matrigel in expansion media. The next day, the medium was removed and default medium (Table 2.5)

was added. Medium was changed once or twice a week by removing a half volume of old medium and adding a half volume of fresh default medium. After 7 days in default medium, a half volume of media was removed and a half volume of default maturation medium (Table 2.6) was added.

Table 2.5. Default medium

Component	Final concentration
Advanced DMEM/F12	1x
L-glutamine	1x
N2	0.5x
Penicillin-streptomycin	1x
B27	0.1x
Heparin	2 µg/ml

Table 2.6. Default maturation medium

Component	Final concentration
Advanced DMEM/F12	1x
L-glutamine	1x
N2	0.5x
Penicillin-streptomycin	1x
B27	0.1x
Heparin	2 µg/ml
BDNF	5 ng/ml
GDNF	5 ng/ml

2.1.8 Cell counting

A haemocytometer was used to quantify the number of cells before plating for experiments and for transfection of cells. To do this, a cell suspension of 2 µl of cells and 18 µl of DMEM/F12 was prepared in a polypropylene tube. The cell suspension was added to the chamber and the haemocytometer placed under a microscope. 3 sets of 4 square groups were counted. Only cells that were within the square and positioned on the left hand or bottom boundary lines were counted. Clumps of cells or cells touching the right hand or upper boundary lines were omitted. The total cell count was divided by three and multiplied by 50,000 (dilution factor x 5000) to obtain the number of cells per ml.

2.1.9 Plasmid miniprep

Bacterial cultures were prepared by inoculating frozen glycerol stock in Luria-Bertani (LB) media containing 100 µg/ml of ampicillin and incubating in a shaker overnight at 37°C. Plasmids DNA was isolated from bacterial cultures using the NucleoSpin Plasmid kit (Macherey-Nagel) following the manufacturer's instructions. Plasmid DNA was eluted with 30 µl of nuclease-free water (Ambion), quantified with microvolume spectrophotometer (Nanodrop, Thermo Scientific). Plasmid DNA was stored at -20°C.

2.1.10 Transfection of iPSC-derived neurons

Approximately 2 x 10^4 cells neural progenitors were seeded per well in 24-well plates in 500 µl of media. On the day of transfection, 250 µl of media was removed from each well and kept in sterile polypropylene tubes as conditioned medium. For each transfection, 1 µg of the plasmid construct was mixed and incubated with 1 µl of Lipofectamine 2000 and 50 µl of OPTIMEM for 50 minutes at room temperature to form complexes. The mixture was added to 250 µl of media drop-wise. 24 hours post-transfection, the medium was replaced with a 1:1 mixture of conditioned medium and fresh medium. At 24 hours post-transfection, transfection efficiency was about 10% across experimental replicates. Similar transfection efficiencies were also observed for different

plasmids (ie. GFP-WT vs. GFP-mutant). However, after 7 days of differentiation, transfection efficiency dropped to about 4%.

2.1.11 Treatment of cells

Arsenite treatment was used as a cellular stressor for the induction of stress granules. A 250 mM stock solution was prepared by dissolving the appropriate amount of arsenite in endotoxin-free water and sterilisation by autoclaving. Arsenite was added to cells at a final concentration of 1 mM for 30 minutes.

2.1.12 Mycoplasma test

All cell lines were tested every month for mycoplasma infection. 2 ml of medium were taken from cell cultures and analysed using the MycoAlert™ Mycoplasma Detection Kit (Lonza) following the manufacturer's instructions. The luminescence generated by the presence of mycoplasma was measured by a microplate reader (FLUOstar Omega, BMG LABTECH).

2.2 ANALYSES

2.2.1 Extraction of RNA from cells

Cells were manually scraped or collected by enzymatic dissociation in polypropylene tubes. Cells were centrifuged for 1 minute at 10 000 rpm and cell pellets were kept on ice and washed in PBS three times prior to RNA extraction. Total RNA was isolated from cultures of cell lines with the RNeasy kit (Qiagen) according to manufacturer's instructions. RNA was quantified using a microvolume spectrophotometer (Nanodrop, Thermo Scientific).

2.2.2 Reverse transcription polymerase chain reaction

cDNA was synthesised by using 1 µg of total RNA with the SuperScript® III First-Strand Synthesis System in a 20 µl volume. cDNA was diluted to 5 ng/µl and standard

polymerase chain reactions (PCR) were performed using *Thermophilus aquaticus* (*Taq* DNA polymerase). 25 ng of cDNA of each sample was amplified in a 25 µl reaction containing 0.2 mM dNTP, PCR primers, 1.5 mM $MgCl_2$, 10x PCR buffer and 0.1 µl Taq DNA polymerase. Amplification was performed at 95°C for 30 seconds, 35 cycles of 58°C or 61°C for 30 seconds and 72°C for 30 seconds, followed by extension at 72°C for 10 minutes. PCR products were electrophoresed in 1% agarose gels.

2.2.3 Agarose gel electrophoresis

The agarose gel electrophoresis involved heating the 1% agarose (w/v) with 1x TAE buffer using a microwave oven for a few minutes on high power until dissolved. When the agarose solution had cooled down to about 50°C, ethidium bromide was added, then poured into a levelled gel casting tray. The gel was allowed to set at room temperature for about 30 minutes, then placed into a horizontal electrophoresis unit and finally covered with 1x TAE buffer. 5x loading buffer was added to each PCR product and the resultant mixture loaded onto the gel, along with 2 µl of DNA ladder. Gels were run at 125 V for about 1 hour. Gels were removed and placed into the BioDOC-IT Imaging system, an UV transilluminator (UVP Inc., San Gabriel, U.S.A.), and photographed digitally under UV transillumination. The size of the DNA was determined by a 100 base pair (bp) DNA ladder (New England BioLabs).

2.2.4 Immunofluorescence

Cells were fixed in 4% paraformaldehyde at room temperature for 15 minutes, permeabilised in 0.5% Triton-X in PBS at room temperature for 15 minutes and blocked in 10% donkey serum (Sigma) in PBS at room temperature for 1 hour. Cells were probed with the appropriate primary antibodies diluted in 5% donkey serum overnight at 4°C. AlexaFluor-488, AlexaFluor-550 and AlexaFluor-650-labelled secondary antibodies (ThermoScientific) were diluted 1:400 in PBS and applied for 1 hour at room temperature in the dark. DAPI (Sigma) counterstaining (1.25 µg/ml) was then applied for 5 minutes at

room temperature in the dark. Coverslips were mounted on microscope slides (SuperFrost, VWR) with DAKO mounting medium and dried at 4°C overnight before imaging with a Zeiss Axiovert S100 (HB0100) (Carl Zeiss Ltd.) inverted phase contrast fluorescent microscope or a Leica laser scanning confocal microscope (TCS-SP5).

2.2.5 Quantitative image analysis

MetaMorph Image System 7.5 (v. 7.7, Molecular Devices) and ImageJ (version 1.45e, NIH, Bethesda, USA, http://rsb.info.nih.gov/ij/) software programs were used for quantitative image analysis. For each analysis, 7-12 images were taken with the same exposure times as 16-bit images from each biological replicate. Three biological replicates were performed. All image analysis was performed in an automated fashion, with the exception of the quantification of dendritic protrusions and localization of synaptic proteins, which was counted by eye. Detailed description of different analyses will be provided in the corresponding chapters.

2.2.6 Protein extraction

Cells were manually scraped or collected by enzymatic dissociation in polypropylene tubes. Cells were centrifuged for 1 minute at 10 000 rpm and cell pellets were kept on ice and washed in PBS three times prior to protein extraction. Cells were lysed in Radio Immunoprecipitation assay (RIPA) buffer (Table 2.7) supplemented with 1X Complete protease inhibitor (Roche) and left on ice for 20 minutes. Samples were sonicated for 10 seconds then centrifuged at 4°C for 30 minutes at maximum speed.

Table 2.7 RIPA buffer

Component	Final concentration
Triton X-100	1%
SDS	0.1%

Sodium Deoxycholoate	0.5%
Tris	20 mM, pH 7.4
NaCl	150 mM
EDTA	1 mM
EGTA	1 mM

2.2.7 Protein assay

Protein concentrations were determined using the *DC* Protein Assay Kit II (BioRad) according to the manufacturer's instructions. Briefly, 2 µl of bovine serum albumin (BSA) standards (0 – 1.5 µg/µl) and samples were used in duplicates and pipetted onto a microtiter plate (Corning). 25 µl of a mixture containing 1 mL of Reagent A and 20 µl of Reagent S were added to each well. 200 µl of Reagent B was then added to each well. A clean, dry pipet tip was used to pop any air bubbles. After 15 minutes, absorbance was read with a microplate reader set to 750 nm. Protein concentrations were calculated based on the mean absorbance of sample duplicates.

2.2.8 Western immunoblotting

5 – 10 µg of lysates were denatured by boiling with 2X SDS sample buffer (Table 2.8) for 10 minutes at 100°C. Biological replicates, along with 2 µl of Precision Plus Protein Dual Color Standard (BioRad), were run on separate NuPAGE Novex 10% Bis-Tris Midi gels in 4Morpholinepropanesulfonic acid (MOPS) buffer for 60 minutes at 170 V. The gels were incubated in transfer buffer for 15 minutes and transferred to nitrocellulose membranes using iBlot Transfer Stack and the iBlot Gel Transfer Device for 7.5 minutes. Membranes were incubated with Ponceau Red (Sigma; 0.1% w/v in 5% acetic acid) at room temperature to detect protein bands. Membranes were washed with Tris-buffered saline with 0.1% Tween 20 (TBST; Table 2.9) (Sigma) until Ponceau staining was completely removed. Membranes were then blocked with 5% non-fat milk solution in

TBST for 30 minutes prior to probing with primary antibodies diluted in a 1% milk solution in TBST at 4°C overnight. Membranes were then washed three times with TBST and probed with the relevant IRDye secondary antibodies (Li-Cor) diluted 1:5000 in 1% milk solution in TBST for 1 hour at room temperature in the dark. Membranes were washed three times with TBST and the fluorescent signal was detected with the Odyssey Infrared Imaging System (Li-Cor Biosciences). Blots were quantitated using ImageJ (version 1.45e, NIH, Bethesda, USA, http://rsb.info.nih.gov/ij/).

Table 2.8 2X SDS sample buffer

Component	Final concentration
Tris	0.2 M, pH 6.8
SDS	4%
Glycerol	20%
Bromophenol blue	2 mg/ml
Water	Up to final volume

Table 2.9 10X TBS Buffer

Component	Final concentration
Tris	24.2 g/l
NaCl	80 g/l
Water	1 l, pH 7.6

2.2.9 PE Annexin V Apoptosis detection

Neural progenitor cell viability was monitored by the Annexin V-PE Apoptosis Detection Kit I (BD Bioscience). Apoptosis is characterised by particular morphological features, including the loss of plasma membrane. An early feature of apoptosis is the translocation of membrane phospholipid phosphatidylserine (PS) from the inside of the

plasma membrane to the outside of the plasma membrane. Annexin V is a protein with high affinity for (PS). Thus, Annexin V conjugated to fluorochrome such as Phycoerythrin (PE) may be used to probe for cells that are undergoing apoptosis. 7-AAD is a fluorescent chemical compound with strong affinity for DNA. As 7-AAD cannot pass through intact plasma membranes, it may be used as a marker for late apoptosis, when the plasma membrane has been compromised.

Annexin V and 7-AAD staining of neural progenitors was performed according to the manufacturer's instructions and assessed with a fluorescence activated cell sorting (FACS) Canto flow cytometer (BD Biosciences). 10 000 cells were sorted for each condition in each experiment. Three biological replicates were performed. Data were analysed with FlowJo software.

CHAPTER 3

iPSC CHARACTERISATION

3.1 BACKGROUND

In this study, we used molecular biology approaches to validate the pluripotency of mutant and WT iPSC lines and their capacity to generate functional motor neurons, the cell type affected in Motor Neuron Disease. The seminal papers by Takahashi and Yamanaka (Takahashi and Yamanaka 2006; Takahashi et al. 2007) used several methods to demonstrate that the novel cell types recapitulate key features of ESCs. We have characterised the morphology, karyotype, genotype, expression of ESC markers, and differentiation ability of two iPSC lines generated from a patient carrying the FUS R521C mutation and two control iPSC lines generated from two different control individuals. To confirm that iPSC lines maintained the parental FUS genotype, we have carried out direct sequencing of genomic DNA extracted from these iPSC lines. Finally, we assessed the neural differentiation potential of the iPSC lines by examining the expression of a number of neuronal lineage-specific markers and by electrophysiological characterisation.

3.1.1 Morphology

hESCs isolated from in vitro fertilised human embryos have an undifferentiated morphology consisting of a high ratio of nucleus to cytoplasm, prominent nucleoli, and a colony morphology similar to rhesus monkey ESCs (Fig. 3.1; (Thomson et al. 1995; Thomson et al. 1998). Undifferentiated pluripotent stem cell colonies typically have clear borders and contain small round cells with spaces between them. Any colony with a change from this typical morphology can be considered to be differentiating (Fig. 3.1; (Aasen et al. 2008)). Colonies remain mostly undifferentiated; however, spontaneous differentiation can occur in small areas within colonies. These cells must be removed since they might have undergone mutations that will affect their behaviour on differentiation.

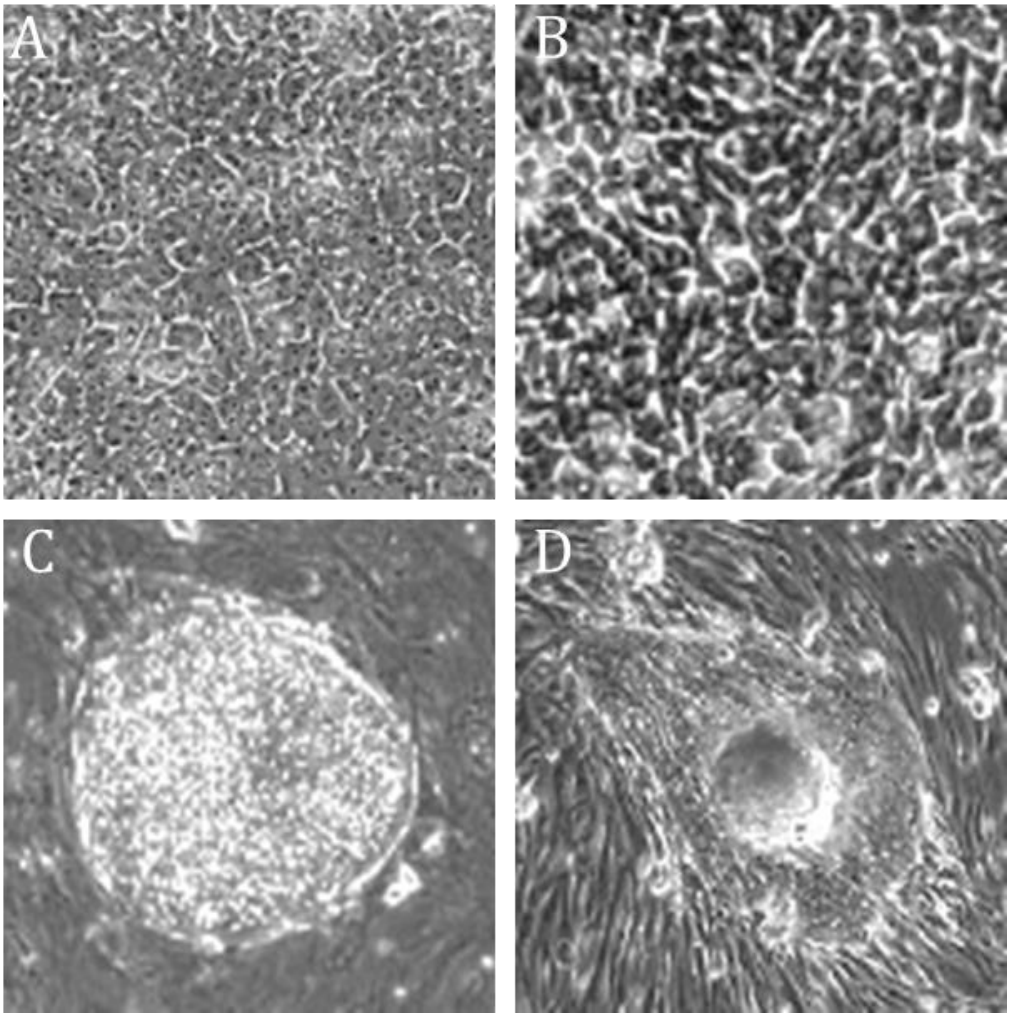

Figure 3.1. Colony morphology of ESCs. A) Undifferentiated rhesus monkey ESCs (R278.5 cell line; Thomson et al., 1995). B) Undifferentiated hESCs (H9 cell line; (Thomson et al. 1998)). C) H9 colony (Thomson et al. 1998). D) An iPSC colony with a cluster of differentiated cells on top (Aasen et al. 2008).

3.1.2 Karyotype analysis

Prolonged culture of pluripotent stem cells has been shown to result in genetic abnormalities (Draper et al. 2004). Karyotype analysis is necessary to show that iPSC lines have maintained genomic integrity. This is done by staining the DNA in cells in the metaphase stage of cell division. Based on cytogenetic characteristics of chromosomes at metaphase, abnormalities can be observed under a microscope.

3.1.3 Direct sequencing

Direct sequencing was performed to confirm that iPSCs are derived from the parent fibroblasts rather than cross contamination. Genomic DNA was obtained from individual cell lines using the Wizard® Genomic DNA Purification Kit (Promega) according to the manufacturer's instructions. Direct sequencing of exon 15 of FUS was performed on all iPSC lines.

3.1.4 Marker gene expression

A standard step to confirm the pluripotency of newly generated cell lines is to use immunocytochemistry and reverse transcriptase- polymerase chain reaction (RT-PCR) to examine the expression of stem cell markers. A panel of molecular markers specific to ESC physiology has been identified that are fundamental to maintaining the undifferentiated state including: nuclear transcription factors OCT4, NANOG, and SOX2, as well as keratin sulphate antigens TRA-1-60 and TRA-1-80. Maintenance of pluripotency depends on a tight regulation of OCT4, NANOG and SOX2, and the expression of all markers is necessary as a definition of pluripotency (Martí et al. 2013).

3.1.5 Embryoid Body formation

After verifying that newly generated cell lines express pluripotency markers, the next step in characterisation is to determine their capacity to differentiate into cells of the three primordial germ layers of the embryo (endoderm, mesoderm and ectoderm). This may be done by an in vitro or in vivo differentiation test. The in vivo test involves injecting newly generated pluripotent cells into severe combined immunodeficient (SCID) mice. Pluripotent cells will proliferate and differentiate in the tissues where they have been injected and form a teratoma containing tissues from the three germ layers. Differentiation may then be confirmed by immunohistochemistry for germ layer markers.

The *in vitro* test involves the differentiation of embryoid bodies (EBs) in culture. Newly generated pluripotent cells are first cultured in suspension to form large aggregates, called EBs. EBs are then allowed to adhere to a cell surface where they can either be guided to differentiate toward a specific cell lineage, or allowed to spontaneously differentiate into the cell types derived from the three germ layers. Again, confirmation of differentiation may be done by immunocytochemistry and RT-PCR for germ layer markers. As the field has evolved fewer laboratories are using an in vivo differentiation test (Nestor and Noggle 2013), and we opted to use an in vitro EB formation test. This method is reliable and demonstrates the ability of our newly generated iPSC lines to differentiate into cells from the three germ layers. Characteristic, tissue-specific markers include: endoderm – *GATA4*, mesoderm – *RUNX1* and *BRACHYURY*, and ectoderm – *PAX6* (Park et al. 2008).

3.1.6 Neural conversion of iPSCs and motor neuron differentiation

Once the pluripotency of the iPSCs is confirmed, the next step is to direct their differentiation into the cell type of interest, for the purpose of this study, motor neurons (MNs). The developmental steps involved in the generation of MNs were identified more than a decade ago (Jessell, 2000). The first step in MN specification requires neural inductive signals to convert primitive ectodermal cells to a rostral neural state. This is followed by the caudalisation of rostral neural cells by signaling molecule retinoic acid (RA) to generate spinal progenitors. Finally, the activation of Sonic hedgehog (Shh) signaling pathway specifies the terminal differentiation of spinal progenitors into MNs.

Using these signaling factors, Wichterle et al. (2002) showed that it was possible to generate MNs from mouse ESCs and that this developmental pathway recapitulated the development of MNs in vivo. The first protocol to direct the differentiation of ESCs into MNs relied on EB formation. This method was not without its limitations, as the differentiation of EBs is often heterogeneous and the yield of neural cells is often very low. A recent method of neural differentiation was developed to address these issues. This

approach used two factors, Noggin and SB431542, to inhibit the SMAD signaling pathway to induce the neural differentiation of monolayer hESCs and hiPSCs (Chambers et al. 2009). Dual SMAD inhibition yielded 82% neuroepithelial cells that express typical neural stem cell markers. Chambers et al. (2009) showed that these cells can be differentiated into MNs after two weeks of exposure to BDNF, RA, Shh and ascorbic acid.

Thus, we chose this approach for the neural conversion of iPSCs and subsequent motor neuron differentiation. The use of Noggin was eventually replaced with a small molecule, Dorsomorphin, which was recently shown to be more effective in the inhibition of the SMAD signaling pathway (Kim et al. 2010). Similarly, we have also used purmorphamine, a small molecule that activates the Shh pathway, in the place of Shh. Purmorphamine has been shown to induce the differentiation of ventral spinal progenitors and motor neurons with similar efficiency to Shh but at a significantly lower cost (Li et al. 2008) .

3.2 METHODS

3.2.1 Microscopy

Initial characterisation of iPSCs was done using light microscopy. Phase contrast images of all iPSC lines were obtained with a Zeiss Axiovert S100 microscope.

3.2.2 Karyotype analysis

Intermediate (passage 40 or earlier) and late (passage 50 or more) passage iPSCs from all iPSC lines were used for karyotype analysis. iPSCs were washed with PBS three times and manually scraped from tissue culture flasks. Samples were centrifuged 1 minute at 10 000 rpm and the supernatant removed. Cells were kept at 4°C and sent for G-banding analysis (TDL Genetics, The Doctors laboratory, London).

3.2.1 Immunocytochemistry

iPSCs were fixed and samples prepared as described in Section 2.2.4. iPSCs were probed with primary antibodies (Table 3.1) diluted in 5% donkey serum overnight at 4°C. Donkey anti-rabbit or mouse AlexaFluor-488 secondary antibodies diluted 1:400 in PBS were then applied for 1 hour at room temperature in the dark. DAPI counterstaining (1.25 μg/ml) was applied and coverslips mounted as described in Section 2.2.4. Images were obtained with a Zeiss Axiovert S100 microscope.

Table 3.1. Primary antibodies

Antibody	Host	Company	Dilution
SSEA4	Mouse monoclonal	Millipore	1:200
Tra-1-60	Mouse monoclonal	Millipore	1:200
Nanog	Rabbit polyclonal	Santa Cruz	1:50
OCT3/4	Mouse monoclonal	Millipore	1:200
SOX1	Mouse monoclonal	BD Pharmingen	1:100
Nestin	Rabbit polyclonal	Millipore	1:500
MAP2	Mouse monoclonal	Abcam	1:500
β3-Tubulin	Mouse monoclonal	Sigma	1:500
HB9	Mouse monoclonal	Hybridoma Bank	1:20
Islet1	Mouse monoclonal	Hybridoma Bank	1:20
Synaptophysin	Rabbit polyclonal	Synaptic Systems	1:100
PSD95	Mouse monoclonal	Synaptic Systems	1:100
ChAT	Sheep polyclonal	Millipore	1:100

3.2.1 RT-PCR

iPSCs were washed with PBS three times and manually scraped from tissue culture flasks (2500 mm2). iPSC-derived neural progenitors were enzymatically dissociated from tissue culture plates with 1 mL of Accutase, then washed with PBS three times. RNA and cDNA were extracted and synthesised as previously described (Sections 2.2.1 and 2.2.2).

PCR reactions were performed as described in Section 2.2.2. The annealing temperature for primers of PAX6, SOX1, HOXB4, NKX6.1, GATA4, RUNX1, AFP and BRACHYURY was 58°C, and for the rest of the primers, 61°C (Table 3.2).

Table 3.2. PCR primers

Gene	Forward primer	Reverse primer
BETA-ACTIN	GTTACAGGAAGTCCCTTGCCATCC	CACCTCCCCTGTGTGGACTTGGG
OCT4	GTACTCCTCGGTCCCTTTCC	CAAAAACCCTGGCACAAACT
NANOG	AATACCTCAGCCTCCAGCAGATG	TGCGTCACACCATTGCTATTCTTC
C-MYC	CAACAACCGAAAATGCACCAGCCCCAG	CGCTCGAGGTTAACGAATT
KLF4	GATGAACTGACCCAGGCACTA	GTGGGTCATATCCACTGTCT
GATA4	CTAGACCGTGGGTTTTGCAT	TGGGTTAAGTGCCCCTGTAG
RUNX1	CCCTAGGGGATGTTCCAGAT	TGAAGCTTTTCCCTCTTCCA
BRACHYURY	ACCCAGTTCATAGCGGTGAC	CAATTGTCATGGGATTGCAG
NESTIN	GGCGCACCTCAAGATGTCC	CTTGGGGTCCTGAAAGCTG
SOX1	GGAAACACAATCGCTGAACC	ATTATTTTGCCCGTTTTCCC
PAX6	ATGTGTGAGTAAAATTCTGGGCA	GCTTACAACTTCTGGAGTCGCTA
NKX6.1	CACACGAGACCCACTTTTTCC	CCCAACGAATAGGCCAAACG
HOXB4	GTGAGCACGGTAAACCCCAAT	CGAGCGGATCTTGGTGTTG

3.3 RESULTS

3.3.1 iPSCs exhibit ESC morphology and growth characteristics

The morphology of all iPSC lines was evaluated by light microscopy to compare with the morphology of ESC line HUES. iPSCs formed tightly packed and flat colonies with clear borders (Fig. 3.2). Individual iPSCs exhibited morphological features similar to ESCs, including a high nucleus to cytoplasm ratio, notable nucleoli, a round shape and spontaneous differentiation in culture. In addition, iPSCs proliferate for more than 80 passages while maintaining these characteristics, with at least 11 months in culture. The

population doubling time of iPSCs were approximately 50 hours. All of the cell lines were successfully cryopreserved and thawed.

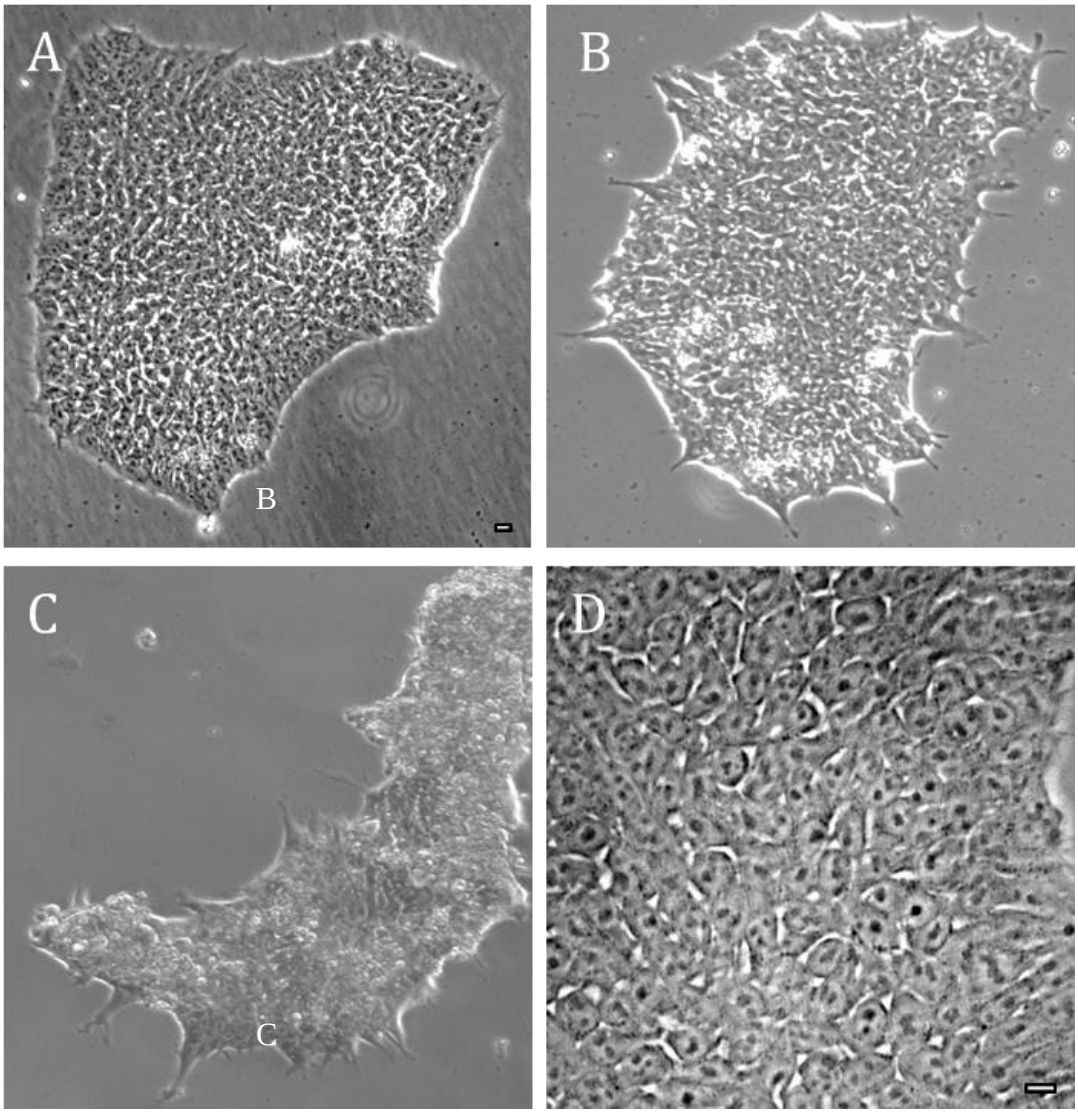

Figure 3.2. Phase contrast images of human pluripotent stem cells. Colonies of iPSCs derived from A) FUS fibroblasts and B) WT fibroblasts and C) colonies of hESCs from HUES cell line. D) Undifferentiated iPSCs. Scale bar = 10 μm.

3.3.2 iPSCs maintain normal karyotypes

Karyotype analysis was undertaken to examine the chromosomal integrity of iPSC lines. All of the iPSC lines generated did not acquire any chromosomal abnormalities following the reprogramming and after more than 40 passages in culture. FUS iPSC lines

had a normal karyotype of 46 XX, WT1 iPSC line had a normal karyotype of 46 XY (Fig. 3.3) and WT2 iPSC line had a normal karyotype of 46 XX (not shown). On one occasion, WT1 iPSCs exhibited an abnormal banding pattern, with alteration in the chromosome 22. This is a common region of normal variation, and this unusual banding pattern may simply reflect a polymorphism. Alternatively, the karyotype alteration may be due to poor maintenance of the iPSC culture, as differentiated might show alterations in the karyotype. We included this line in our analysis as they did not behave any differently from the other subclone or from the other WT iPSC line.

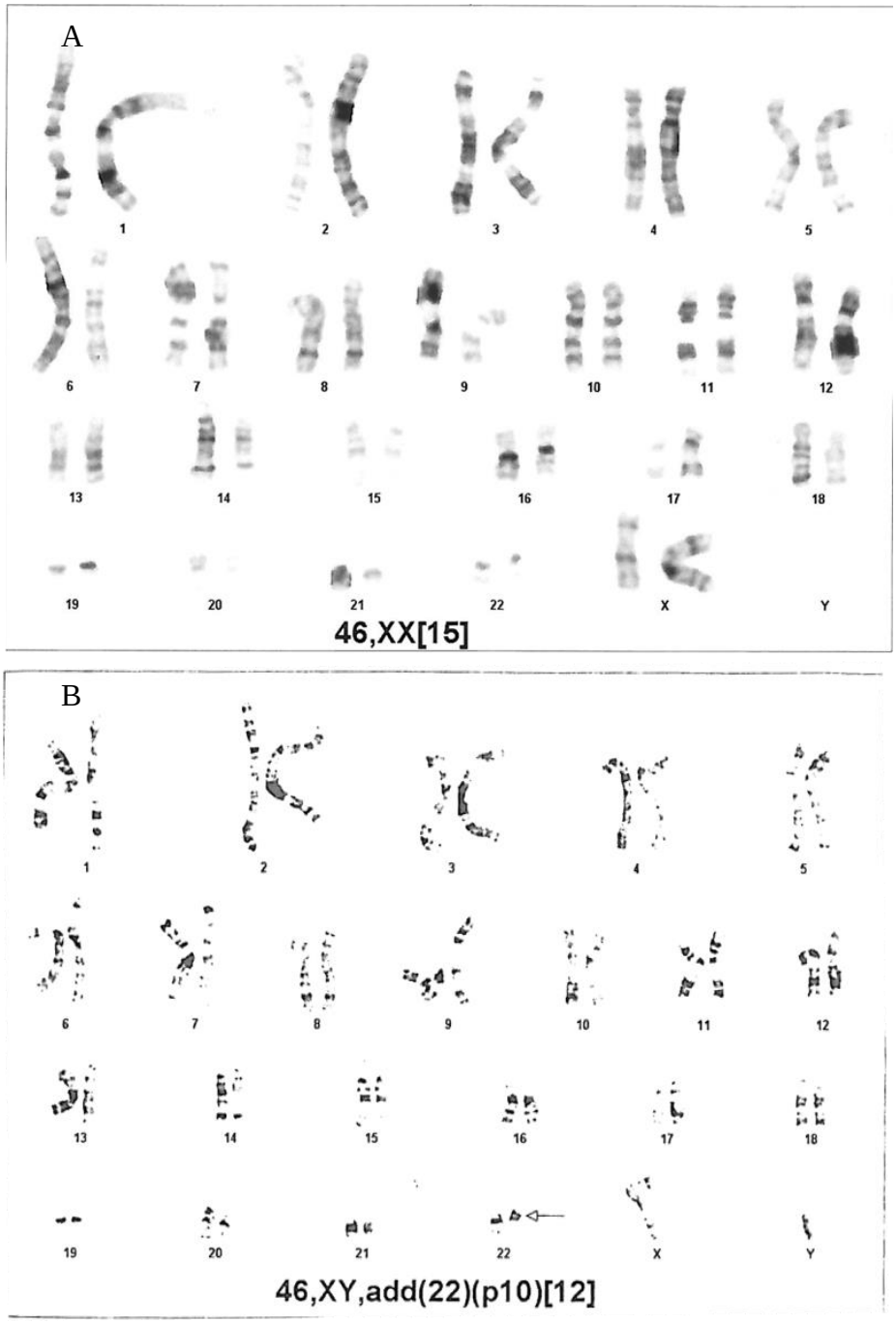

Figure 3.3. Representative karyogram of A) FUS iPSCs at passage 52 and B) WT1 iPSCs at passage 53. Arrow indicates an unusual banding pattern in the short arm of chromosome 22 of WT1 iPSCs.

3.3.3 iPSCs maintain parent genotype

Direct sequencing of exon 15 of *FUS* was performed on all iPSC lines to confirm that patient-derived iPSC lines had retained the genetic mutation of the parental fibroblast

cell line. iPSC lines derived from controls maintained the WT genotype (Fig. 3.4). All iPSC lines derived from patient fibroblasts carried the R521C *FUS* mutation (Fig. 3.4).

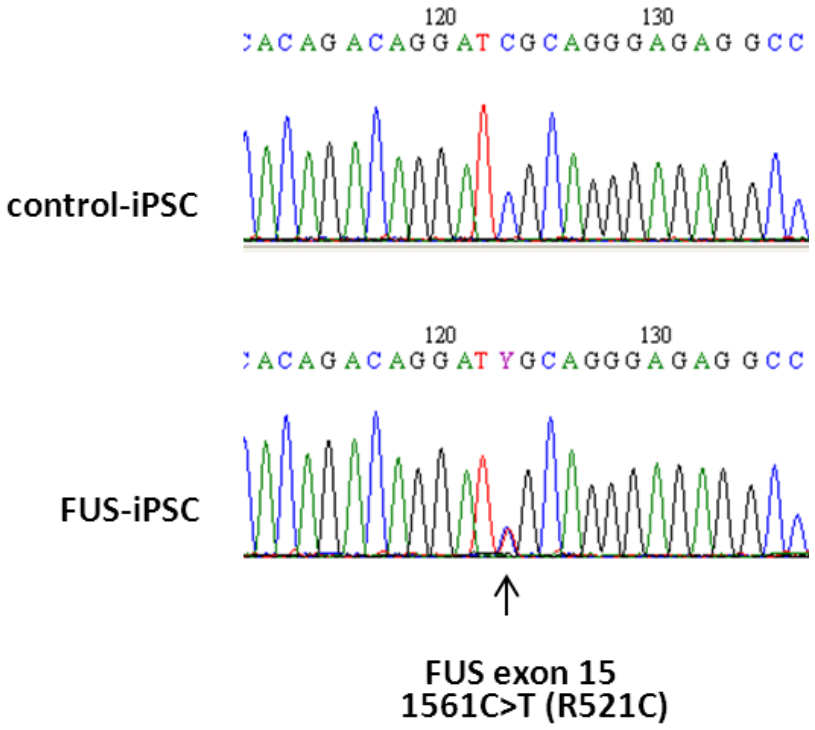

Figure 3.4. Representative chromatogram of direct sequencing of FUS exon 15 in WT and FUS iPSC lines. Arrow indicates the location of the R521C mutation in FUS iPSCs.

3.3.4 Marker gene expression

Colonies from FUS and WT1 iPSC lines showed strong protein expression of pluripotency markers OCT4, SSEA4, TRA-1-60 and NANOG (Fig. 3.5). All iPSC lines expressed *OCT4, NANOG, c-MYC* and *KLF4* by RT-PCR (Fig. 3.6). Relative to hESC lines HUES, iPSC lines expressed higher levels of *C-MYC*. FUS2 iPSCs expressed lower levels of *KLF4* compared to all other pluripotent stem cell lines. The expression of pluripotency markers was also assessed in WT2 iPSC line, which expressed *OCT4, NANOG, c-MYC* and *KLF4* by RT-PCR (data not shown).

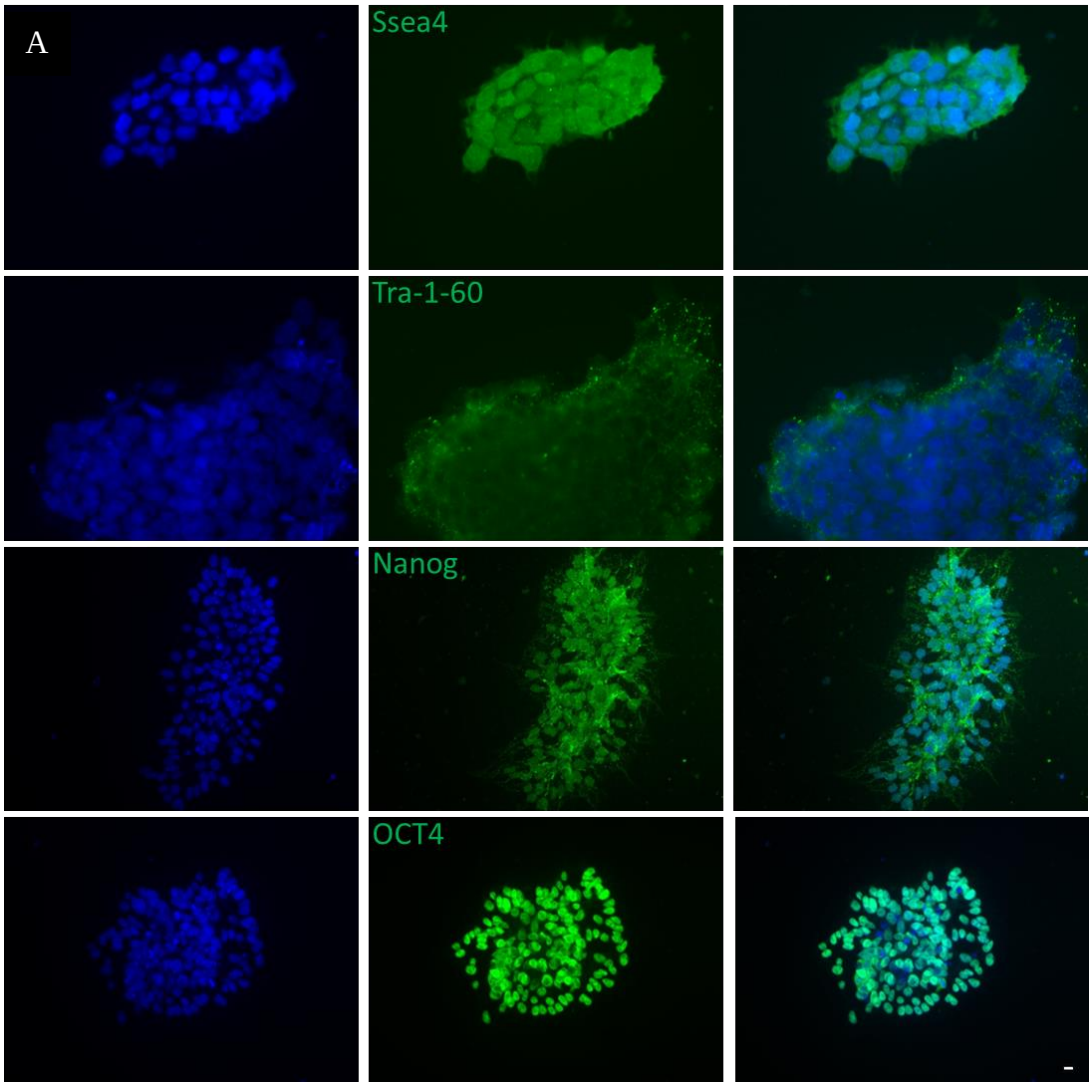
A
Ssea4
Tra-1-60
Nanog
OCT4

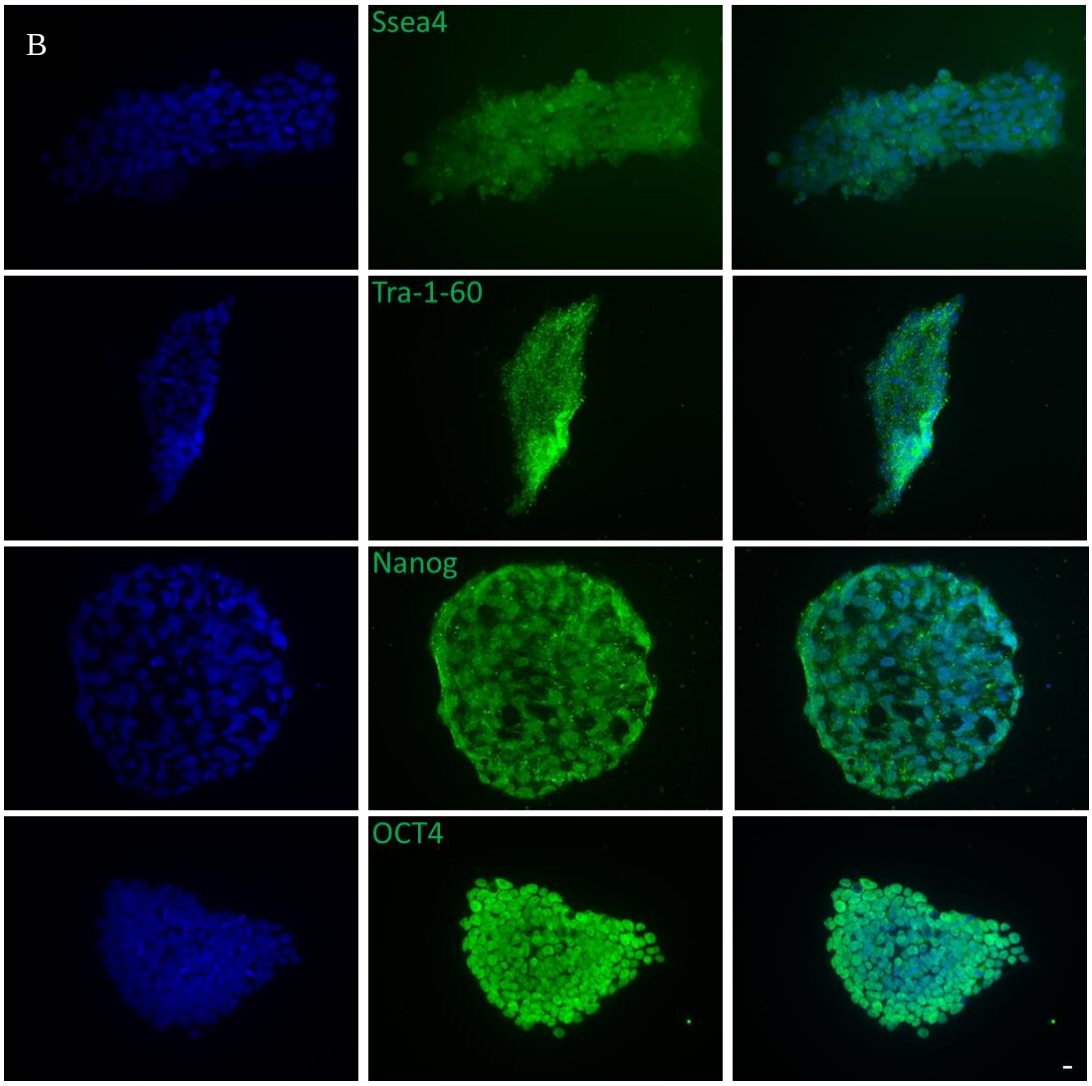

Figure 3.5. Representative images (20x) of A) FUS and B) WT iPSC colonies stained positive for pluripotency markers OCT4, SSEA4, TRA-1-60, and NANOG. Scale bar = 10 μm.

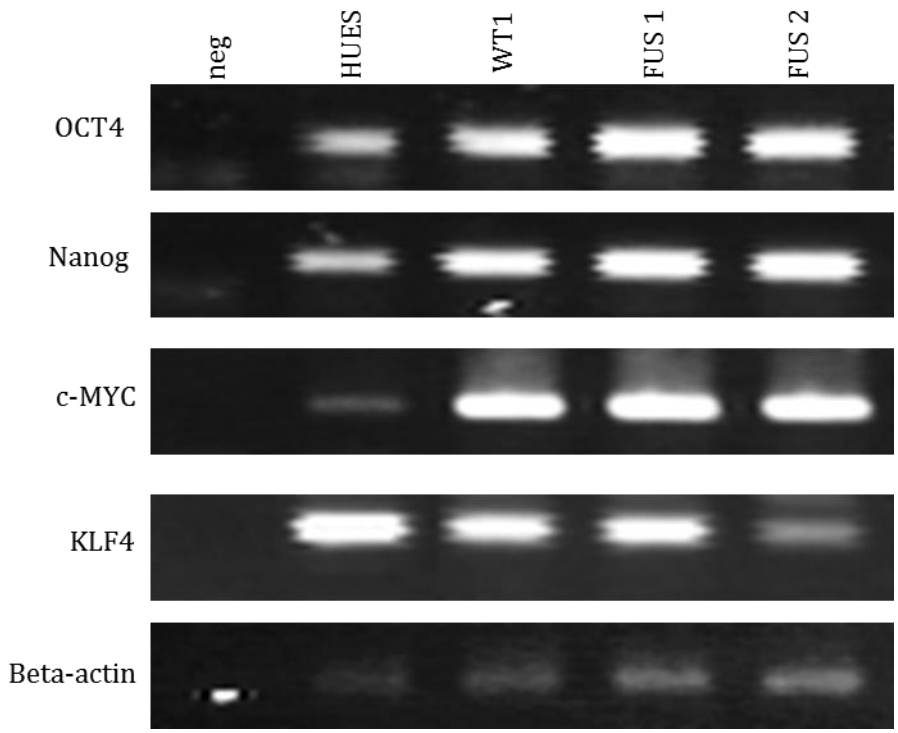

Figure 3.6. WT and FUS iPSCs demonstrate expression of pluripotency markers. RT-PCR was performed on HUES and iPSC cultures. No cDNA is used as a negative control. Beta-actin is shown as a positive amplification and loading control. HUES ESCs, WT1, FUS1 and FUS2 iPSCs all demonstrate expression of pluripotency transcription factors *OCT4, NANOG, C-MYC,* and *KLF4.*

3.3.5 iPSCs can differentiate into EBs

EBs derived from FUS and WT1 iPSCs showed similar gene expression of embryonic germ layers: *GATA4* (endoderm), *RUNX1* and *BRACHYURY* (mesoderm), *PAX6* (ectoderm) (Fig. 3.7). Some embryoid bodies exhibited spontaneous beating, a feature of contractile cardiomyocytes with pacemaker activity (Xu et al. 2002). FUS and WT1 iPSC lines demonstrated a similar capacity to differentiate into the three germ layers. EBs were derived from WT2 iPSCs at a later time point, and also demonstrated gene expression of the embryonic germ layers (data not shown).

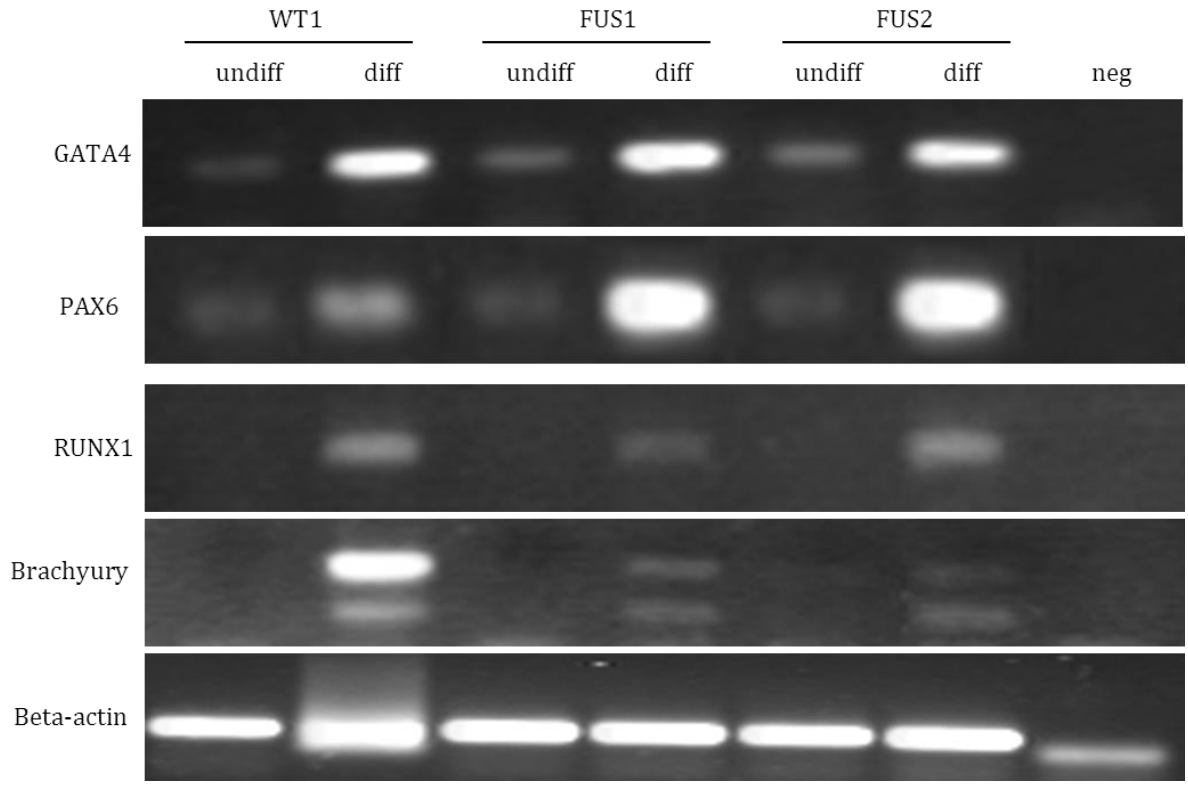

Figure 3.7. In vitro differentiated WT and FUS iPSCs demonstrate gene expression from the three germ layers. Semi-quantitative RT-PCR was performed on undifferentiated (undiff) iPSC cultures and differentiated (diff) EBs. No cDNA is used as a negative control. Beta-actin is shown as a positive amplification and loading control. FUS1, FUS2 and WT1 EBs all demonstrate upregulation of characteristic, tissue-specific markers upon differentiation relative to the corresponding iPSCs from which they were derived. Endoderm – *GATA4*, ectoderm – *PAX6*, mesoderm – *RUNX1*, Brachyury.

3.3.6 Neuronal marker expression

During neural induction there is a down-regulation of OCT4 expression and a corresponding upregulation of nestin expression (Fig. 3.8). FUS and WT1 iPSCs displayed variable rates of neural differentiation. Expression of pluripotency marker OCT4 was dramatically reduced by day 7 of neural differentiation in FUS iPSCs, and completely down-regulated by day 8, WT1 iPSCs still displayed strong expression of OCT4 by day 7 of neural differentiation, and OCT4 expression was still observed in some cells of WT1 iPSC colonies by day 8 of neural differentiation (Fig. 3.9). FUS iPSCs were positive for nestin at

day 5, whereas expression of nestin was induced in day 6 of neural differentiation in WT iPSCs (Fig. 3.10). FUS and WT1 iPSCs differentiated into neuroepithelial cells that expressed neuroectoderm markers SOX1 and nestin (Fig. 3.12). The rate of neural differentiation was similar between WT1 and WT2 iPSCs (data not shown).

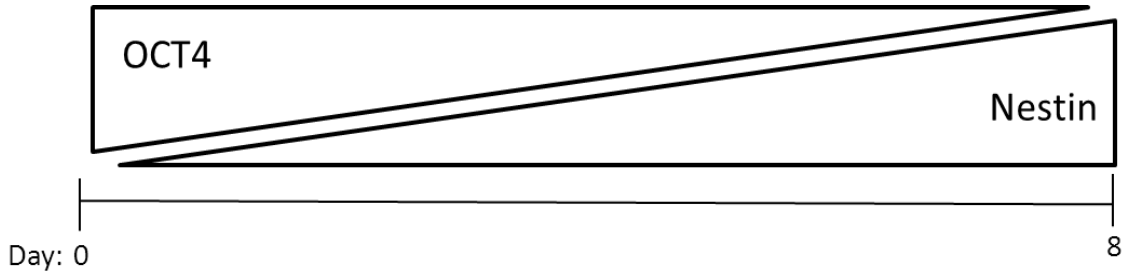

Figure 3.8. Expression of OCT4 is high on D0 of neural induction. OCT4 expression is down-regulated during neural induction. Nestin is not expressed on D0 of neural induction, but nestin expression is up-regulated during neural induction.

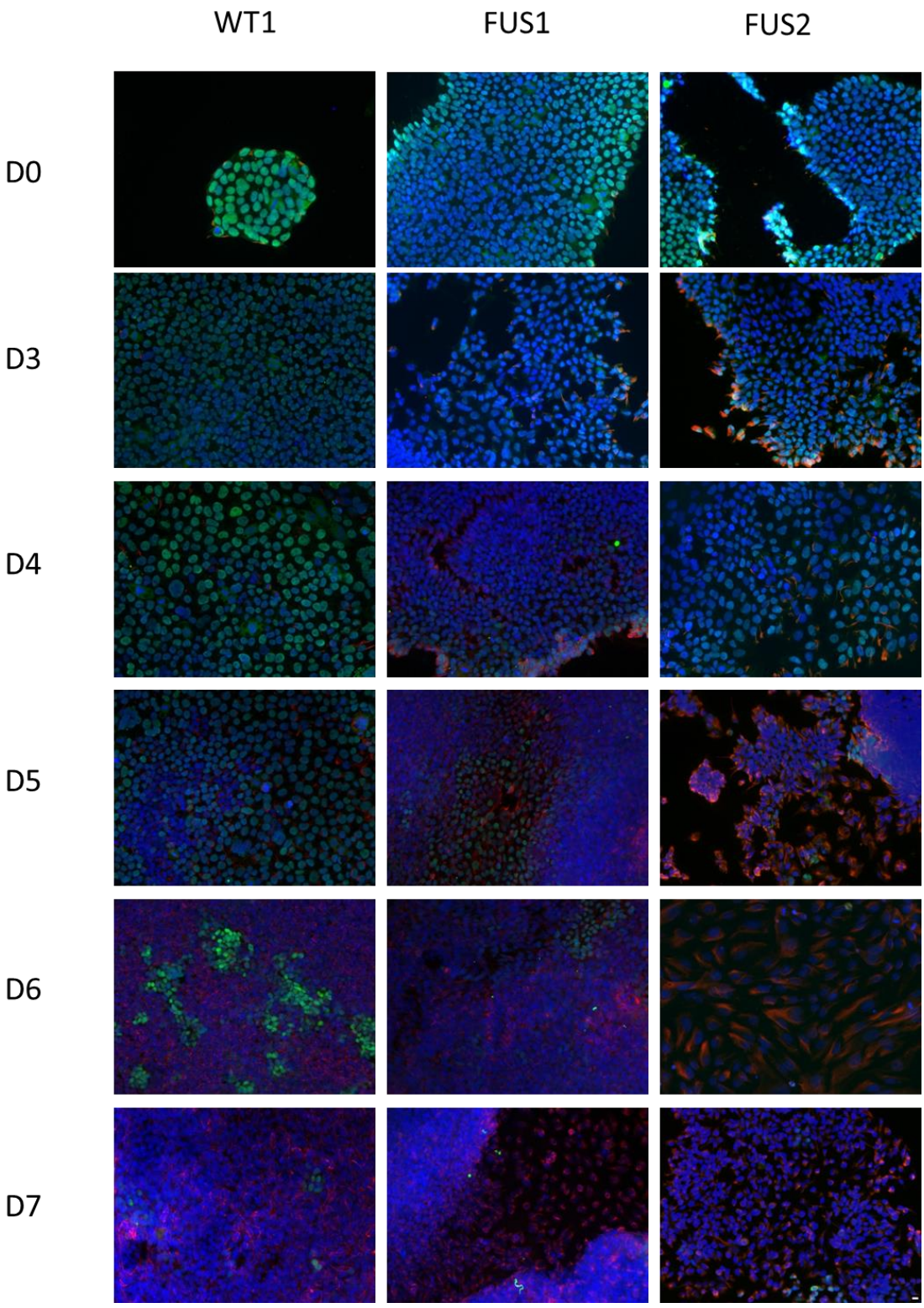

Figure 3.9. Immunocytochemistry of dual SMAD inhibition neuralisation. By day 7 of neural differentiation, OCT4 (green) expression was mostly down-regulated. By day 5 of neural differentiation, nestin expression was up-regulated in FUS iPSC lines. Nestin (red) expression was up-regulated in day 6 of neural differentiation in WT1 iPSC line. Scale bar = 10 μm.

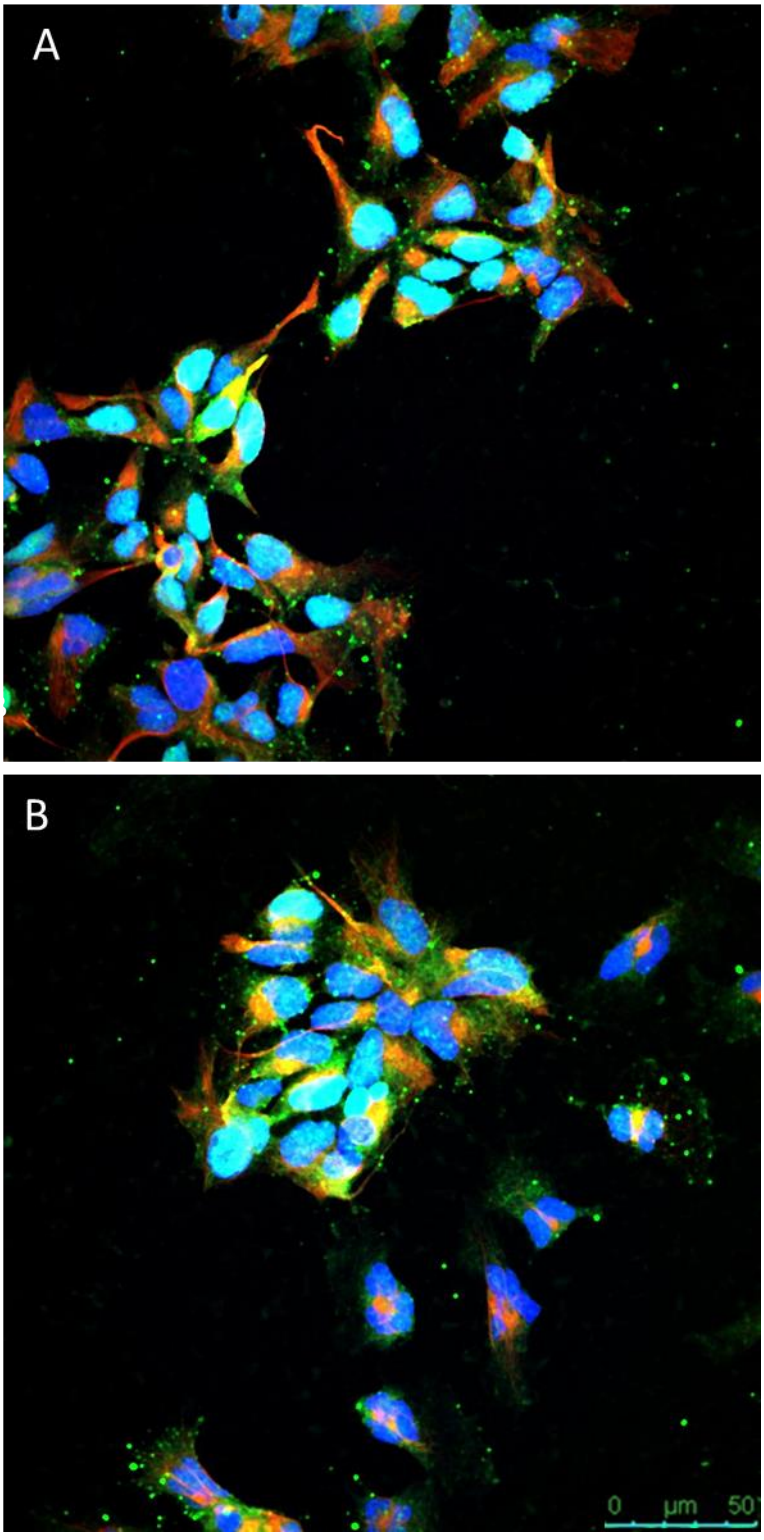

Figure 3.10. Representative images (20x) of a) WT and b) FUS iPSC neural progenitors, following two weeks of differentiation, stained positive for neuroectoderm markers SOX1 (green), nestin (red) and DAPI (blue).

FUS and WT neuroepithelial cells were treated with 0.1 μM retinoic acid and 1 μM purmorphamine to generate NKX6.1- and HOXB4-positive ventral spinal progenitors (See section 2.1.5; Fig. 3.13). By 5 weeks of culture, FUS and WT iPSCs differentiated into neurons displaying strong expression of MAP2 (Fig. 3.14) and β3-tubulin (Fig. 3.15). The presence of MNs in these cultures was confirmed by expression of Islet1 (Fig. 3.16), HB9 (Fig. 3.17) and choline acetyltransferase (ChAT) (Fig. 3.18). Using this differentiated method, FUS and WT iPSCs differentiated into neuronal cultures with a similar proportion of MNs (Fig. 3.17). By 8 weeks of culture, FUS and WT iPSC-derived neurons expressed synaptic markers VGLUT1, synaptophysin and PSD95 (Fig. 3.29).

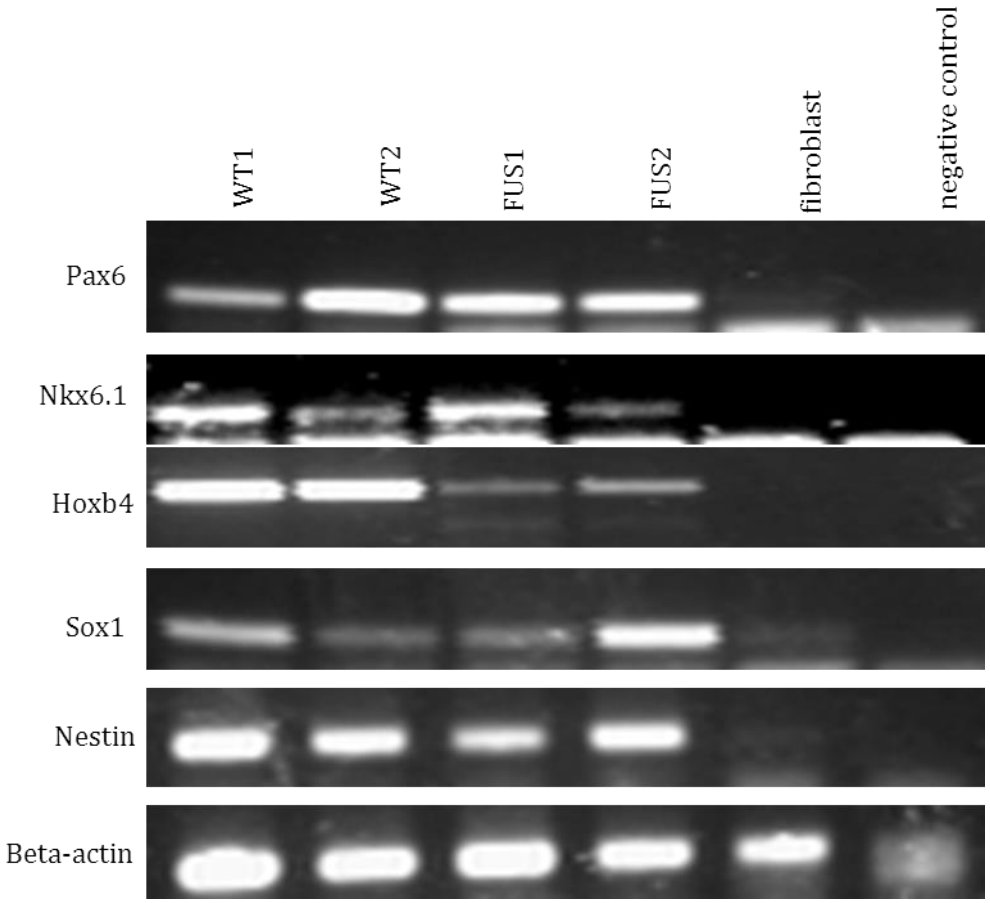

Figure 3.11. In vitro differentiated WT and FUS iPSCs demonstrate gene expression of neuroectoderm and spinal progenitor markers. Semi-quantitative RT-PCR was performed on neural progenitors differentiated for 3 weeks. cDNA from fibroblasts and no cDNA is used as a negative control. Beta-actin is shown as a positive amplification and loading control. WT1, WT2, FUS1 and FUS2 neural progenitors all demonstrate upregulation of characteristic, lineage-specific neural progenitor markers.

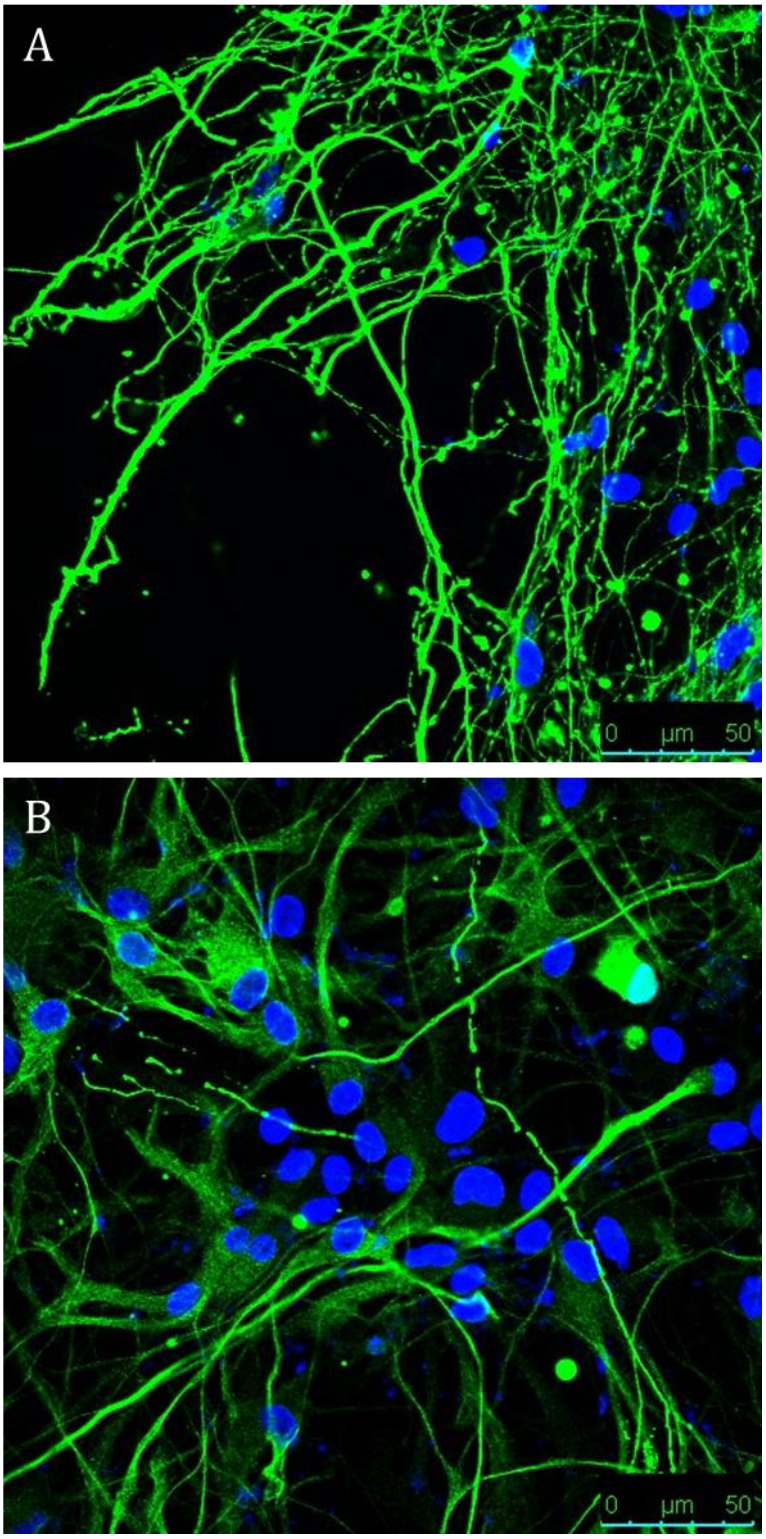

Figure 3.12. Confocal representative images (63x) of a) WT and b) FUS iPSC cortical neurons differentiated for 8 weeks stained positive for neuronal dendrite-specific marker MAP2 (green) and DAPI (blue).

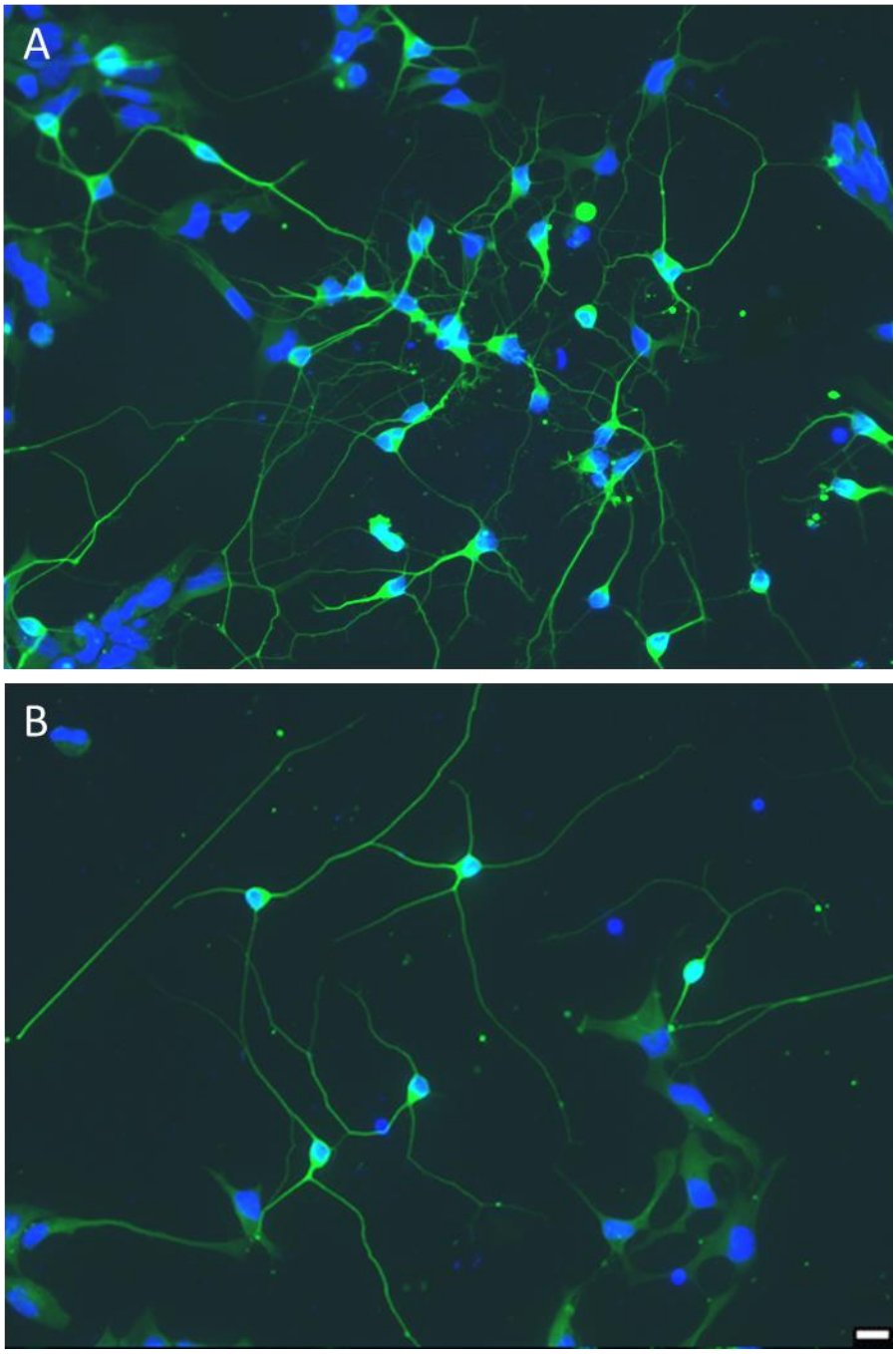

Figure 3.13. Representative images (20x) of a) WT and b) FUS iPSC motor neuron populations differentiated for 5 weeks stained positive for neuron-specific marker β3-tubulin (green) and DAPI (blue). Scale bar = 10 μm.

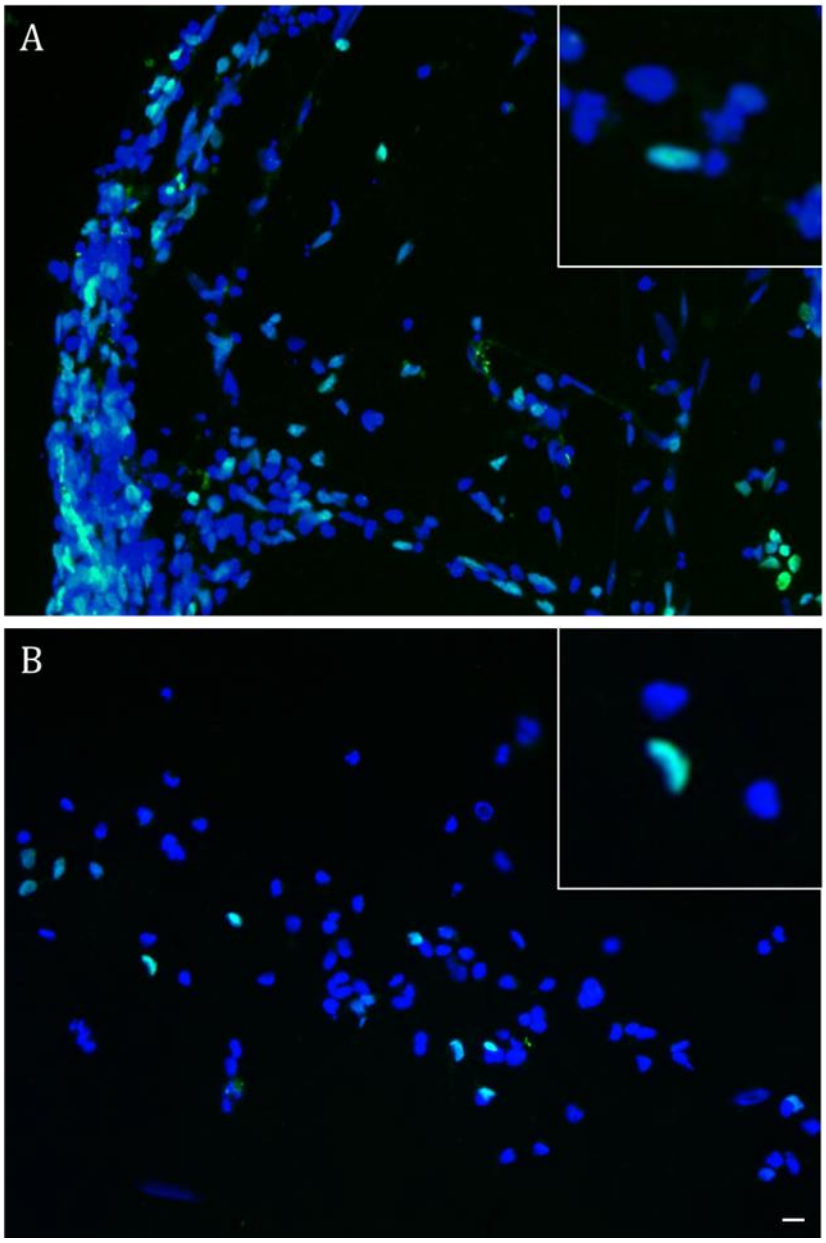

Figure 3.14. Representative images (20x) of a) WT and b) FUS iPSC motor neuron populations differentiated for 8 weeks stained positive for Islet1 (green), a marker of motor neurons and interneurons, and DAPI (blue). Scale bar = 10 μm.

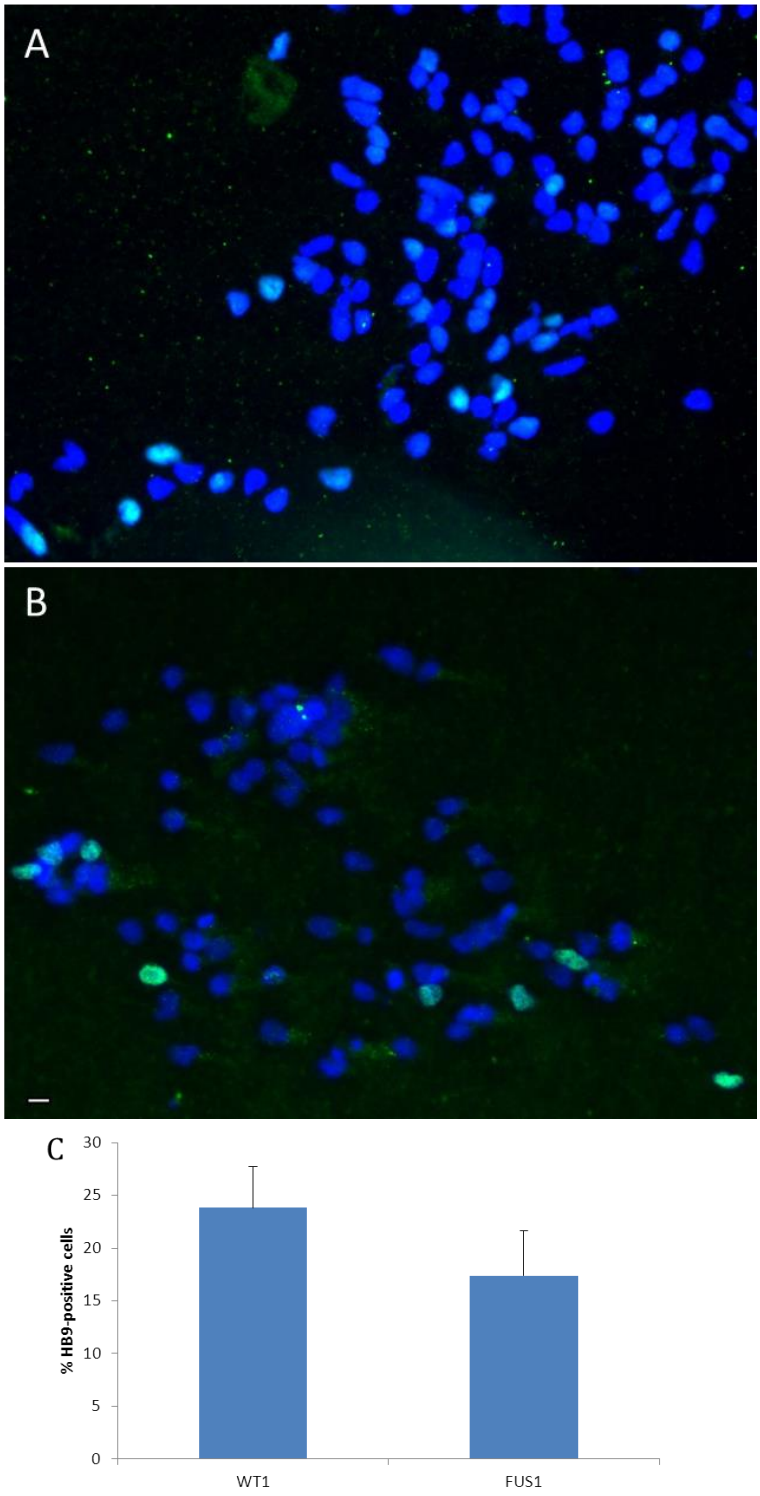

Figure 3.15. Representative images (20x) of a) WT and b) FUS iPSC motor neuron populations differentiated for 8 weeks stained positive for motor neuron-specific marker HB9 (green) and DAPI (blue). c) Percentage of cells expressing the motor neuron marker HB9 differentiated from WT1 and FUS1 iPSC lines. Error bars represent standard error of three technical replicates. Scale bar = 10 μm.

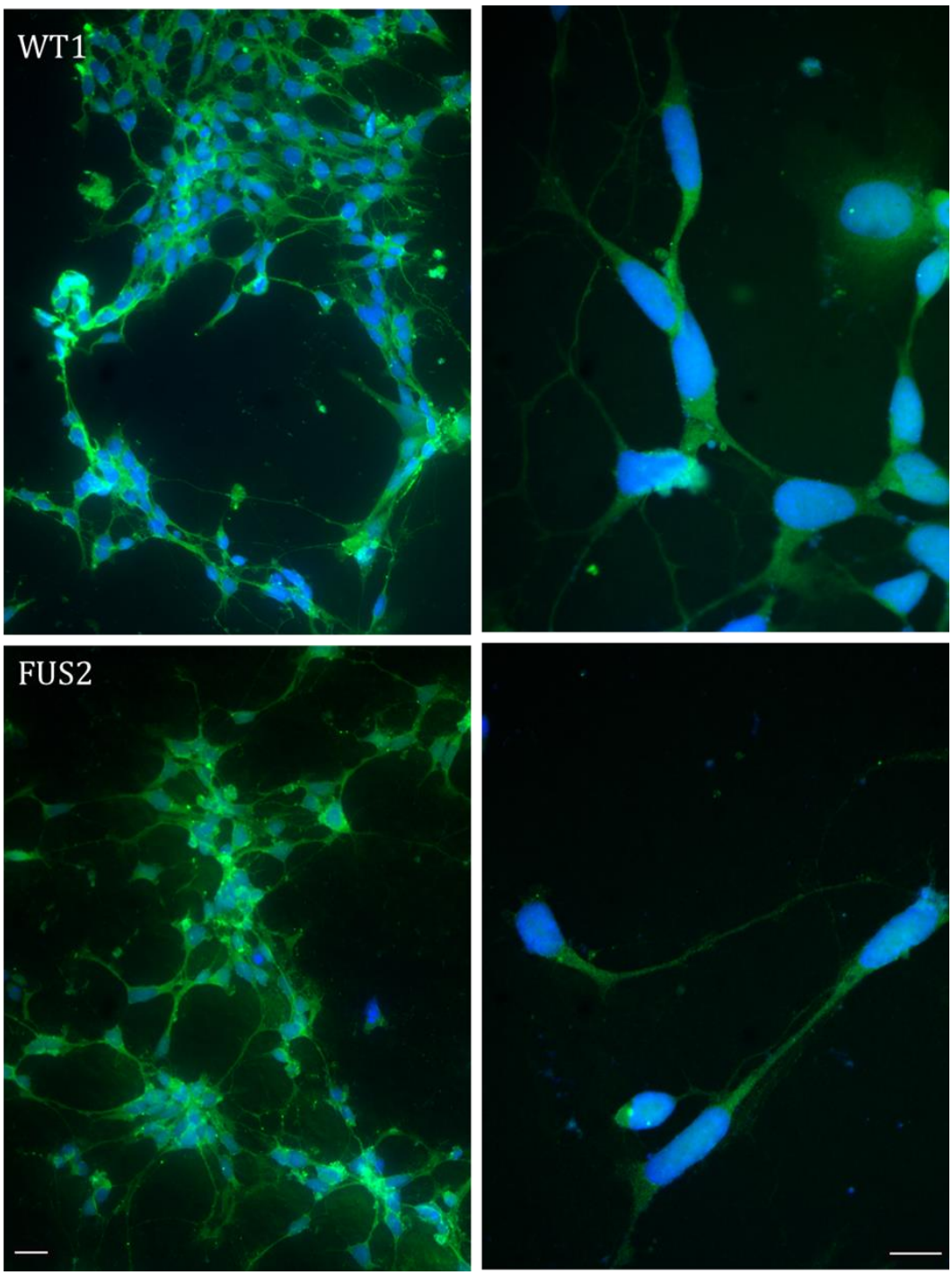

Figure 3.16. Representative images of WT and FUS iPSC motor neuron populations differentiated for 8 weeks stained positive for ChAT (green), the enzyme responsible for biosynthesis of acetylcholine, and DAPI (blue). ChAT is a specific indicator for monitoring the functional state of cholinergic neurons. (Right panels) Higher magnification images of WT and FUS iPSC neurons positive for ChAT (green). Scale bar = 10 μm.

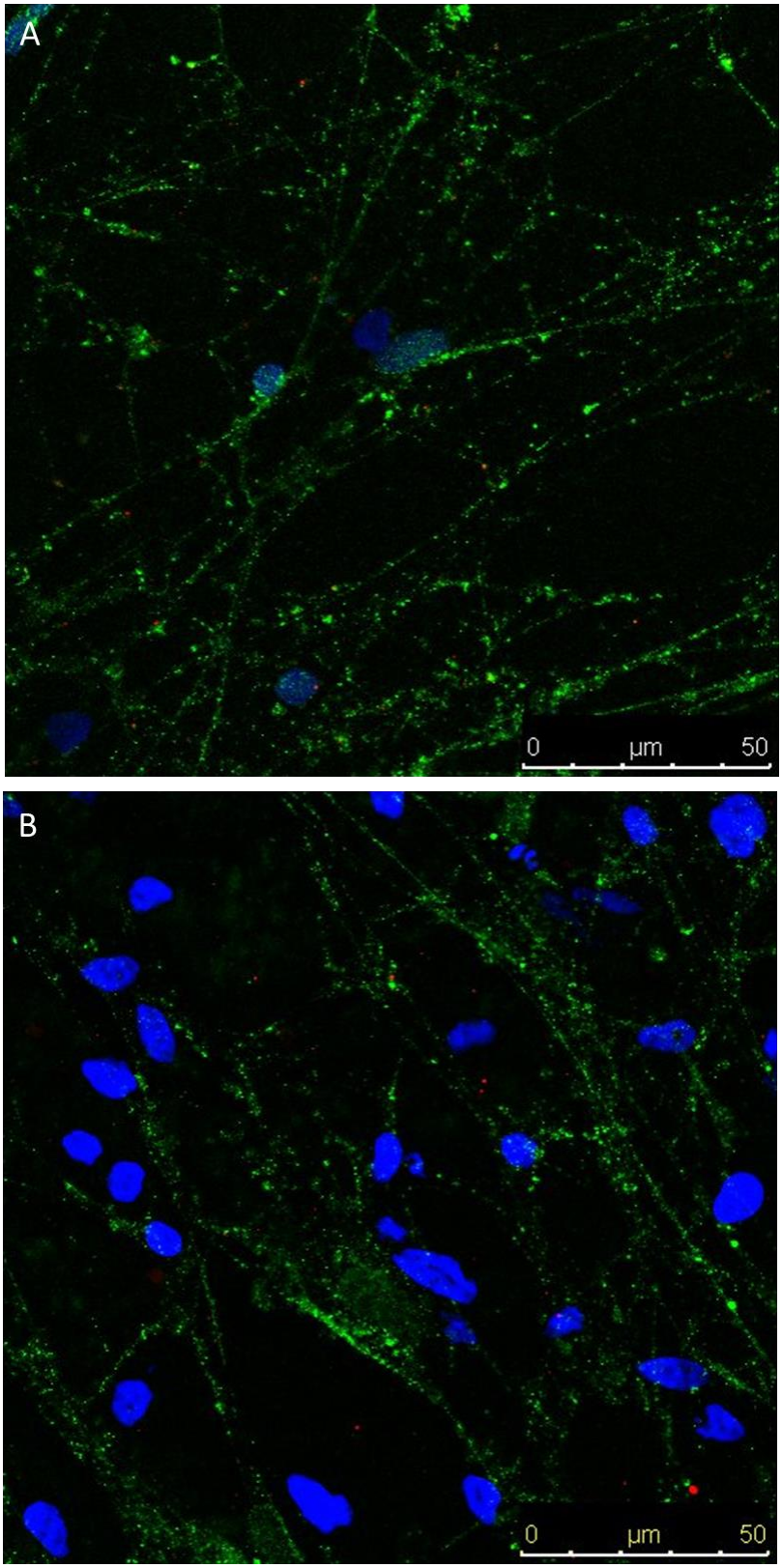

Figure 3.17. Representative images of a) WT and b) FUS iPSC motor neuron populations differentiated for 12 weeks stained positive for pre-synaptic marker piccolo (green), post-synaptic marker PSD95 (red) and DAPI (blue).

3.3.6 Electrophysiology

After more than 12 weeks in culture, FUS and WT iPSCs differentiated into functional neurons that generated single and multiple action potentials following current injections of various amplitudes (Fig. 3.20). FUS and WT iPSC-derived neurons also exhibited spontaneous excitatory postsynaptic currents (results not shown).

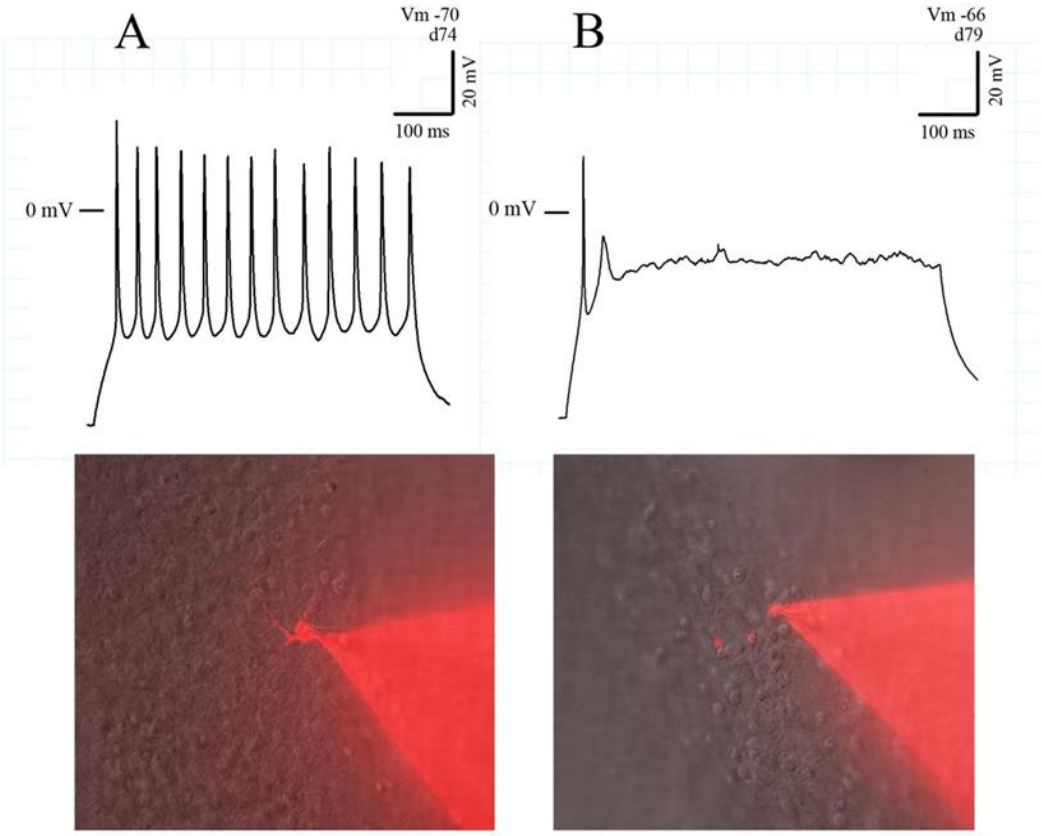

Figure 3.18. Representative action potentials evoked in FUS iPSC motor neuron populations differentiated for 12 weeks under current clamp conditions by current injection. iPSC neurons had a negative resting potential and following injection of current, a) repetitive spiking and b) single spiking were recorded. (Experiments and images performed and generated by Catherine Smith and Gerald Finnerty, unpublished)

3.4 Discussion

In this chapter, it was described the characterisation of iPSC lines that were generated from one ALS patient fibroblast line carrying the FUS R521C mutation and two control fibroblast lines. All iPSC lines exhibited ESC-like morphology, normal karyotypes, and pluripotency gene expression. The lines derived from the patient fibroblasts maintained the FUS R521C mutation, determined by direct sequencing of exon 15 of *FUS.* All iPSC lines demonstrated the ability to differentiate into EBs and the cells express markers of the three germ layers. All iPSCs are capable of differentiating into functional motor neurons *in vitro*. Neurons derived from FUS and WT iPSCs expressed neuronal markers, generated action potentials and exhibited spontaneous excitatory postsynaptic currents.

Although teratoma formation is considered a gold standard of pluripotency, we did not have the facilities required to perform this assay. Teratoma formation requires the use of animals, and may not necessarily accurately predict differentiation potential in culture. Although an *in vivo* test of differentiation is required for the registration of a cell line, its necessity is debated and some argue that *in vitro* test of differentiation is sufficient (Buta et al. 2013). Thus, we opted to use the *in vitro* test to confirm the capacity of our iPSC lines to generate cell types of the three germ layers.

Recently, an alternative approach was developed for assessing the pluripotency in human cells, including iPSCs. This approach, known as the PluriTest, takes advantage of gene expression datasets generated from about 450 genome-wide microarray-based transcriptional profiles from diverse stem cell preparations to generate a much larger dataset from which to both assess pluripotency and to obtain detailed information on features of a sample that deviate from typical pluripotent stem cell lines (Muller et al., 2011). This test is now commonly used as a method of characterising iPSC lines and comparing their features with established human pluripotent stem cell lines.

The WT1 iPSC line exhibited an unusual banding pattern in the short arm of chromosome 22 in this karyotype analysis (see fig. 3.3). Karyotypic changes are common in human embryonic and induced pluripotent stem cells (Taapken et al., 2011), but this

particular abnormality has not been published to date. The appearance of this chromosome is not typical. It is possible that this aberration pattern may be the result of segment duplications. However, this is a common region of normal variation, and this unusual banding pattern may simply reflect a polymorphism. Spectral karyotyping is another technique that improves the resolution of the traditional karyotype analysis, where chromosome-specific DNA sequences are labeled with different fluorophores. The coloured chromosomes are then visualized to detect any genomic changes. This technique is more expensive and has a higher resolution for identification of translocations. Alternatively, array-based analyses of genomic integrity, such as array-comparative genomic hybridization and single nucleotide polymorphism arrays, enable the detection of copy number changes along the genome and allow for much higher resolution, albeit at much higher costs. Finally, whole genome sequencing of iPSCs may be done to examine genomic integrity at the single-base resolution. The cost of this approach is much higher than the other techniques, and unlikely to be used as a routine stem cell integrity analysis currently.

We have assessed the expression of pluripotency markers and embryonic germ layer markers using RT-PCR in this study. The negative control used for both of these experiments was no cDNA. Another negative control that may have been used for assessing the expression of pluripotency markers is cDNA from fibroblasts or other somatic cell types. Alternatively, cDNA from tissue corresponding to each of the three germ layer may have been used as a positive control for assessing the expression of embryonic germ layer markers.

All iPSC lines were successfully differentiated into functional MNs as shown by detailed cell-lineage and electrophysiology studies. iPSC lines from the patient and controls were induced to differentiate into neuroectoderm and spinal progenitor cells, and subsequently into similar proportions of HB9+ cultures. In our cultures, 17-24% of neuronal populations were HB9-positive. However, as HB9 and ISLET1 expression are variable, we rely on ChAT expression to represent mature MNs. All iPSC lines

demonstrated strong expression of ChAT as shown by immunocytochemistry. However, the specificity of the antibody used in this study was not assessed, and may lead to unspecific staining. Problems with antibody specificity may be addressed by using the antibody for immunoblotting of tissue with and without the protein of interest.

Patient iPSC lines showed an earlier neural induction relative to control iPSC lines. It has been reported that human iPSCs differentiate into neuroepithelia with variable rates and efficiency (Hu et al. 2010). Whether this variability is a consequence of the R521C mutation or inherent variability between iPSC lines merits further investigation. It would be of interest to determine whether iPSC lines derived from patients carrying other ALS-associated *FUS* mutations demonstrate a similar propensity to differentiate into neuroepithelia earlier.

In summary, we have carried out extensive characterisation of patient and control-derived iPSC lines to show that all iPSC lines demonstrate the hallmarks of pluripotency. These iPSC lines can be differentiated into functional motor neurons using developmentally relevant signaling factors. Thus, the FUS R521C mutation does not prevent differentiation and functional maturation of motor neurons. In the next chapter, I describe the characterisation of FUS-associated ALS phenotypes in neural cells derived from these iPSC lines.

CHAPTER 4

CHARACTERISATION OF FUS-ASSOCIATED ALS PHENOTYPES

4.1 BACKGROUND

In this study, we used molecular and cellular biology techniques to determine whether neural populations derived from FUS iPSCs recapitulate the key pathological features of FUS-associated ALS. Several studies have reported that ALS patient-derived iPSCs can be differentiated into neural populations that reveal mutation-specific phenotypes. MN cultures derived from mutant TDP-43 iPSCs have elevated levels of insoluble TDP-43 protein, perturbed RNA metabolism, abnormal morphology and decreased survival (Bilican et al. 2012; Egawa et al. 2012). Neurons derived from iPSC lines containing the hexanucleotide repeat in *C9ORF72* have RNA foci containing the GGGGCC repeat, repeat-associated non-ATG (RAN) translation products, elevated p62 levels and increased sensitivity to cellular stress (Almeida et al. 2013). We therefore sought to assess three well-defined phenotypes specific to *FUS* mutations, the mislocalisation of mutant FUS protein, the redistribution of mutant FUS in stress granules and cell death and increased vulnerability to cellular stress as have been reported in cell line transfection studies (Vance et al. 2009; Bosco et al. 2010; Dormann et al. 2010; Vance et al. 2013).

4.1.1 Mislocalisation of FUS protein

In cultured human cells, FUS protein displays a diffuse nuclear localisation with infrequent nuclear granules, and a diffuse distribution in the cytoplasm, with some localisation in small cytoplasmic granules (Andersson et al. 2008). An assessment of the distribution of FUS protein in post-mortem tissue of patients with FUS mutations revealed occasional very large FUS immunoreactive inclusions in the cytoplasm in lower MNs (Kwiatkowski et al. 2009; Vance et al. 2009).

Functional studies have shown that ALS-associated *FUS* mutations result in an increase in the cytoplasmic localisation of FUS protein compared to the WT protein

(Kwiatkowski et al. 2009; Vance et al. 2009). It was subsequently revealed that the majority of ALS-associated *FUS* mutations occur within a non-classical proline-tyrosine (PY) nuclear localisation signal which is necessary for Transportin-mediated nuclear import of FUS protein (Dormann et al. 2010). Interference with this transport pathway resulted in the redistribution of FUS to the cytoplasm and reduction of nuclear levels of FUS.

4.1.2 Redistribution of mutant FUS in stress granules

Protein aggregates are a key pathological hallmark of ALS. In the initial reports of *FUS* mutations in FALS patients, neuropathological exams of individuals with *FUS* mutations revealed large globular and elongated cytoplasmic inclusions labelled positively by FUS antibodies in spinal cord MNs and dystrophic neurites (Fig. 4.1; (Kwiatkowski et al. 2009; Vance et al. 2009). A detailed analysis of six ALS-FUS cases later showed that FUS-immunoreactive neuronal and glial inclusions are a consistent feature in multiple neuroanatomical regions (Mackenzie et al. 2011).

Figure 4.1. Immunostaining of FUS in dystrophic neurites from the basal ganglia in a patient with *FUS* R514G mutation (Image generated by Andrew King, unpublished).

Subsequently, several independent groups reported that ALS-linked FUS mutants are redistributed into cytoplasmic stress granules under conditions of cellular stress, such as strong inhibition of transportin-dependent import, oxidative stress or heat shock cellular insults (Bosco et al. 2010; Dormann et al. 2010; Vance et al. 2013). Dormann et al. (2010) also showed that pathological inclusions in ALS-FUS patients label positively for stress granule marker proteins such as poly(A)-binding protein 1 (PABP-1) and eIF4G. As its name suggests, PABP-1 binds the poly(A) tail of mRNA and regulates mRNA translation and stability by functioning in miRNA-mediated gene expression regulation and nonsense-mediated decay. PABP-1 is a central component of stress granules, and are recruited to stress granules during stress granule assembly and disassembly (Kedersha et al., 2001). These findings suggest that stress granule formation may be involved in the formation of protein aggregates observed in ALS-FUS.

4.1.3 Neuronal susceptibility

ALS is a neurodegenerative disorder characterised by the progressive loss of upper and lower motor neurons. It is believed that various initiating triggers, such as gene mutations, protein damage by oxidation or protein seeding, lead to the aggregation of specific proteins that results in neuronal toxicity. Animal models of FUS-related proteinopathy have demonstrated that expression of wild type or mutant human FUS protein leads to the formation of FUS aggregates and progressive neurodegeneration such as axonal loss and loss of neurons in the brain (Lanson Jr and Pandey 2012).

Several iPSC models of ALS have also revealed selective cellular vulnerability in ALS. ALS neurons with pathogenic TDP-43 mutations and C9ORF72 hexanucleotide repeat expansion show increased spontaneous cell death in long term cell culture and greater sensitivity to a variety of cell stressors (Bilican et al. 2012; Almeida et al. 2013). Several cellular models of ALS indicate that cells expressing mutant proteins (SOD1, TDP-43 and the G4C2 expansion in C9ORF72) are likely to die by apoptosis, a process of programmed cell death. However, a very recent study provided evidence of necroptosis, a programmed form of necrotic cell death, mediated by ALS-derived human astrocytes (Re et al. 2014).

4.2 METHODS

4.2.1 Immunofluorescence

iPSC-derived neural progenitors and neurons were cultured, fixed processed for immunocytochemistry as described in Section 2.2.4. iPSC-derived neural progenitors and neurons were probed with primary antibodies (Table 4.1) diluted in 5% donkey serum overnight at 4°C. Donkey anti-rabbit or mouse AlexaFluor-488 secondary antibodies diluted 1:400 in PBS were then applied for 1 hour at room temperature in the dark. DAPI counterstaining (1.25 μg/ml) was applied and coverslips mounted as described in Section 2.2.4. Images were obtained with a Zeiss Axiovert S100 microscope and a Leica TCS-SP5 laser scanning confocal microscope.

Table 4.1. Primary antibodies

Antibody	Host	Company	Dilution
FUS	Rabbit polyclonal	Novus Biologicals	1:400
PABP1	Mouse monoclonal	Millipore	1:500

4.2.2 Quantitative image analysis - Metamorph

To assess the subcellular distribution of FUS protein in iPSC-derived neurons, quantitative image analysis was performed using MetaMorph Microscopy Automation & Image Analysis Software 7.5 (Molecular Devices). Fields based on uniform DAPI staining were selected and imaged in two channels. 7-12 images of each cell line were obtained with the Zeiss Axiovert S100 microscope. The exposure time for capturing the images was maintained and all images were taken on the same day.

Images were first converted to grayscale and the DAPI and FUS channels were used to define the thresholds. The number of cells in each image was determined using the "Count nuclei" app and the DAPI images. Nuclear FUS was also determined using the "Count nuclei" app, but using FUS images; the integrated intensity of each image was divided by the number of cells in that image to determine the amount of nuclear FUS per cell. To quantify cytoplasmic FUS, the DAPI image was first used to mask the nucleus of the corresponding FUS image. The integrated intensity of each image was then obtained and divided by the number of cells in that image to determine the amount of cytoplasmic FUS per cell. Total FUS per cell was calculated by adding the integrated intensity of nuclear and cytoplasmic FUS.

4.2.3 Quantitative image analysis - ImageJ

To quantify the colocalisation of FUS protein with stress granule marker PABP1 in iPSC-derived neural progenitors, quantitative image analysis was performed using Image J (version 1.48p). Fields based on uniform DAPI staining were selected and imaged in two channels. 7-12 images of each cell line were obtained with the Leica TCS-SP5 laser

scanning confocal microscope. The exposure time for capturing the images was maintained and all images were taken on the same day.

Images were first converted to greyscale and the FUS and PABP1 channels were used to define the thresholds. The number of cells in each image was quantified with the ImageJ plug-in "analyse particles" using DAPI images. The ImageJ plug-in "analyse particles" was used to filter the granule size (0-50 pixels^2) and to quantify the number of FUS and PABP1 granules. The total number of FUS or PABP1 granules was divided by the number of cells in that image to determine the average number of granules per cell. The ImageJ plug-in "colocalisation" was used to determine colocalised particles in corresponding FUS and PABP1 images. The "analyse particles" plug-in was then used to quantify the number of colocalised particles. The total number of colocalised particles was divided by the number of cells in that image to determine the average number of colocalised granules per cell. Data were normalised to the mean number of FUS, PABP1 and colocalised granules in control WT1 neural progenitors.

4.2.4 PE Annexin V and 7AAD profiling

Apoptotic cell death in iPSC-derived neural progenitors was assessed by fluorescence activated cytometric sorting (FACS) analysis of Annexin V and 7AAD staining. Neural progenitors were chosen as more mature neurons have complex processes and were not suitable for FACS anslysis. iPSC-derived neural progenitors were plated on Matrigel-coated 6-well tissue culture plates at a density of 200,000 cells per well. One day before FACS analysis, one well was treated with 1 μM staurosporine (Cell Signaling Technology) to induce apoptosis as a positive control. Unstained cells were used as a negative control. On the day of FACS analysis, culture medium was collected into separate conical tubes for each sample. Neural progenitors were enzymatically dissociated from tissue culture plate with Accutase (1.5 ml per 25 cm^2). Cells were transferred to the corresponding conical tube and centrifuged at 1000 rpm for 4 minutes. The supernatant

was removed and cells were stained with Annexin V and 7-AAD as described in Section 2.2.9.

4.3 RESULTS

4.3.1 R521C neurons have increased cytoplasmic FUS protein levels

To determine whether FUS neurons recapitulate the mislocalisation of FUS protein observed in post-mortem tissue in patients carrying *FUS* mutations, the subcellular distribution of FUS protein was analysed in neurons differentiated for 6 weeks by quantitative image analysis (Fig. 4.2). MN-containing neural populations derived from two independent FUS iPSC clones had significantly higher levels of cytoplasmic FUS than WT1 MN-containing neural populations following identical differentiation protocols (Fig. 4.3). Some clonal variation was observed between the FUS lines, but a 1.3 fold or more of cytoplasmic FUS expression was consistently found in FUS neurons than in WT neurons (levels of cytoplasmic FUS normalised to WT1: FUS1 = 1.33 ± 0.1; FUS2 = 1.61 ± 0.1; FUS1 vs WT1, $P < 0.05$; FUS2 vs WT1, $P < 0.001$; FUS1 vs FUS2, not significant).

FUS2 motor neuron-containing neural populations had significantly lower levels of nuclear FUS than WT1 motor neuron-containing neural populations (Fig. 4.3; FUS2 normalised to WT1 = 0.80 ± 0.05, FUS2 vs WT1, $P < 0.05$). FUS1 motor neuron-containing neural populations also had lower levels of nuclear FUS than WT motor neuron-containing neural populations; however, this did not quite reach statistical significance (FUS1 normalised to WT1 = 0.90 ± 0.05; FUS1 vs WT1, not significant; FUS1 vs FUS2, not significant). FUS and WT neurons had similar levels of total FUS (Fig. 4.3; levels of total FUS normalised to WT1: FUS1 = 1.03 ± 0.06; FUS2 = 0.92 ± 0.05; FUS1 vs WT1, not significant; FUS2 vs WT1, not significant; FUS1 vs FUS2, not significant).

Quantification of the subcellular distribution of FUS was also performed in WT2 motor neuron-containing neural populations in an independent set of experiments (data not shown). Data from WT2 motor neuron-containing neural populations were similar to WT1.

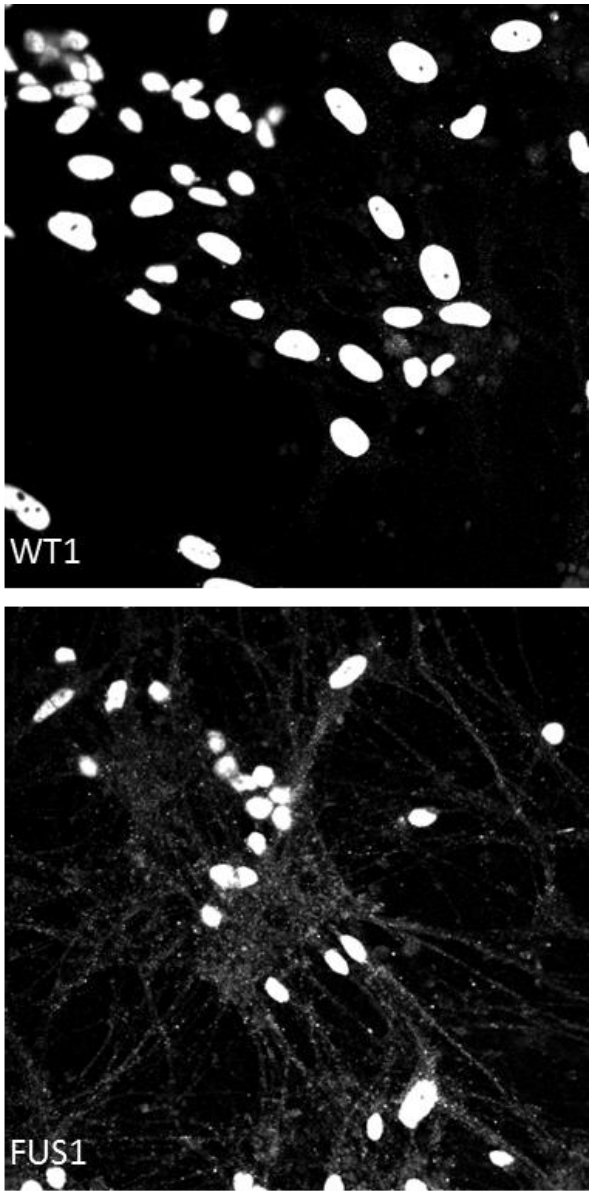

Figure 4.2. Representative images (20x) of a) WT and b) R521C iPSC neurons stained for FUS.

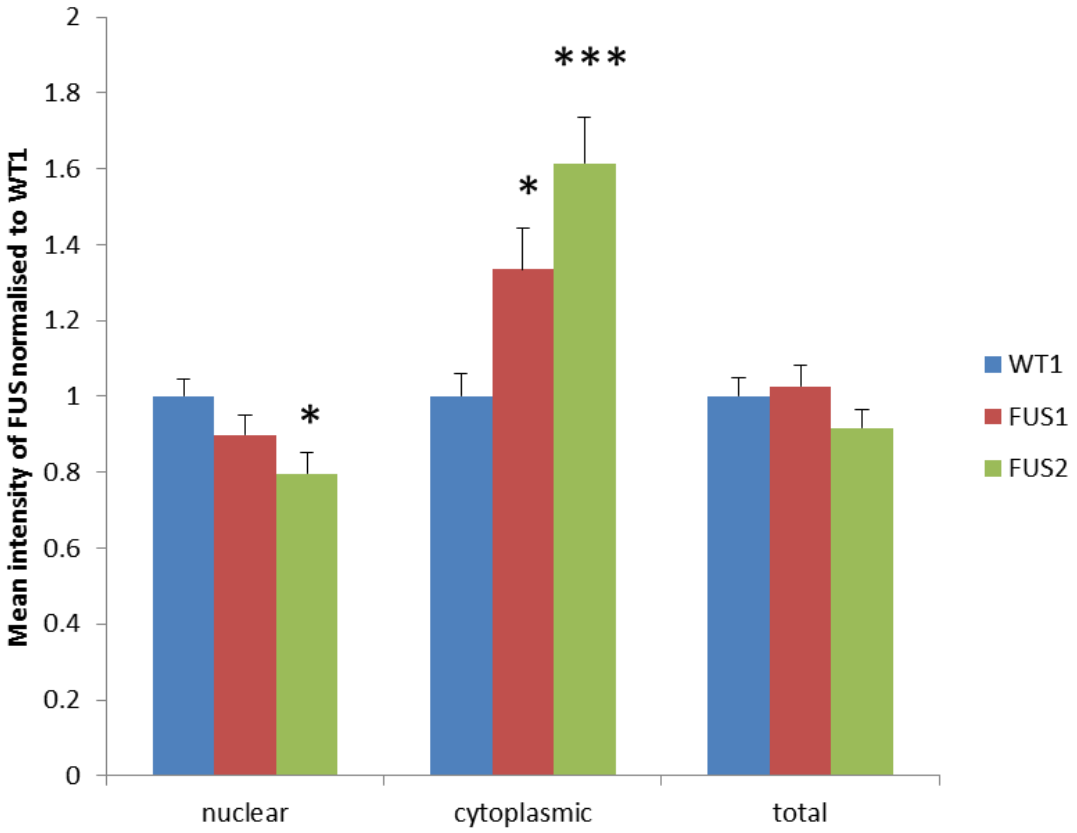

Figure 4.3. Quantitative image analysis of subcellular distribution of FUS in WT1, FUS1 and FUS2 iPSC neurons. Mean intensity of FUS staining in samples were normalised to mean intensity of FUS staining in WT1 neurons. Data represent means ± SEM. Significance levels were determined by one-way ANOVA and post-hoc Tukey test. Significance of difference between iPSC lines (* $P < 0.05$; *** $P < 0.001$; n = 2000+ cells per line from 3 independent experiments).

4.3.2 R521C FUS protein is redistributed into cytoplasmic stress granules

A second feature of *FUS*-associated ALS is the redistribution of mutant *FUS* protein into cytoplasmic stress granules. This experiment was initially attempted on iPSC-derived neurons; however, due to problems with adherence of iPSC-derived neurons on coverslips following treatment with arsenite, we opted to use iPSC-derived neural progenitors. To assess whether FUS neural progenitors recapitulate this feature, iPSC-derived neural progenitors were treated with 1 mM arsenite for 30 minutes, and colocalisation of FUS and stress granule marker PABP1 was determined with quantitative image analysis(Fig. 4.4

and 4.5). FUS neural progenitors exhibited FUS-positive, PABP1-positive granules after treatment with 1 mM arsenite (Fig. 4.5). WT neural progenitors also exhibited PABP1-positive granules after treatment with 1 mM arsenite, but they did not colocalise with FUS (Fig. 4.5).

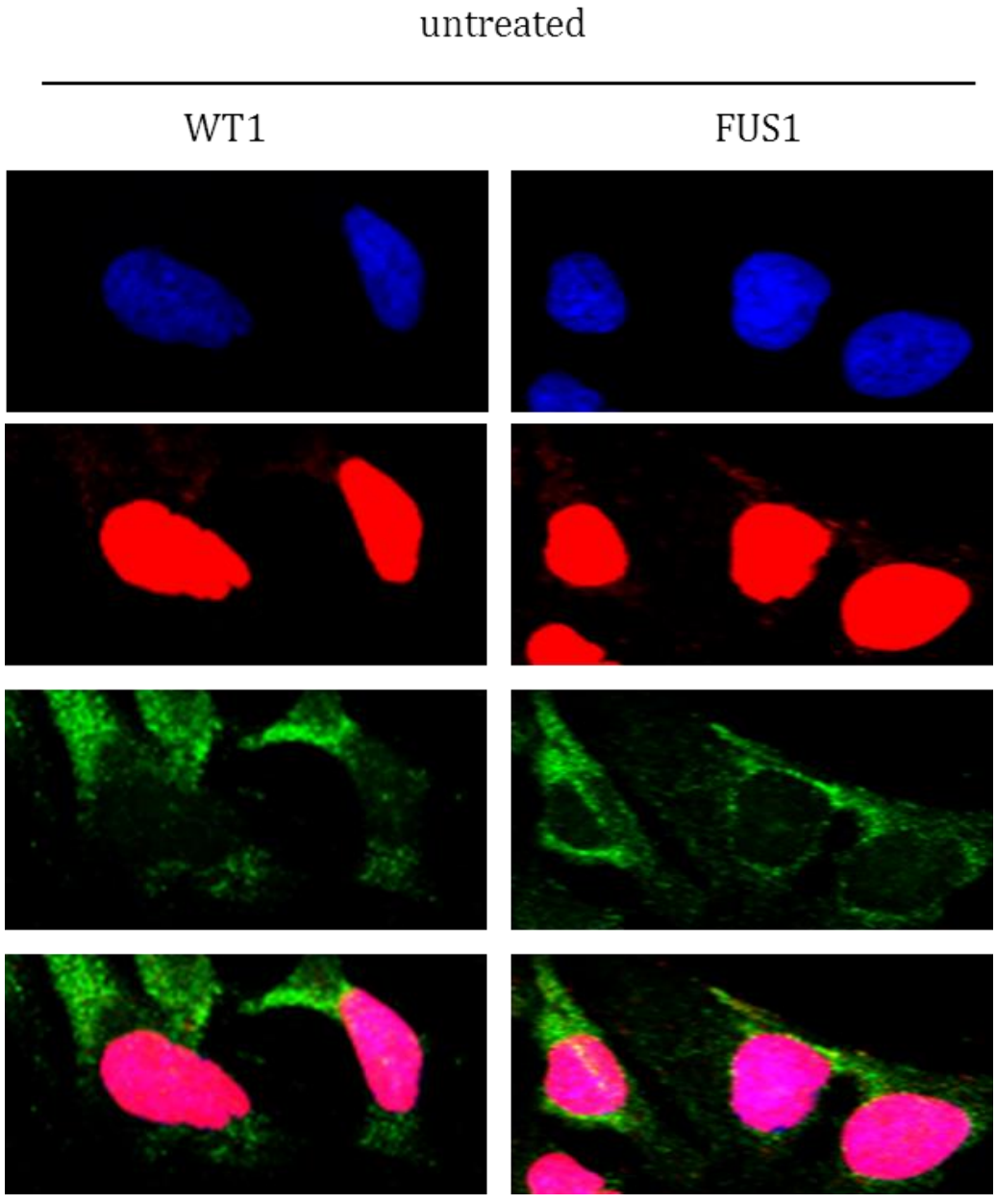

Figure 4.4. Representative images (40x) of untreated WT and FUS iPSC neural progenitors stained for FUS (red), PABP1 (green) and DAPI (blue).

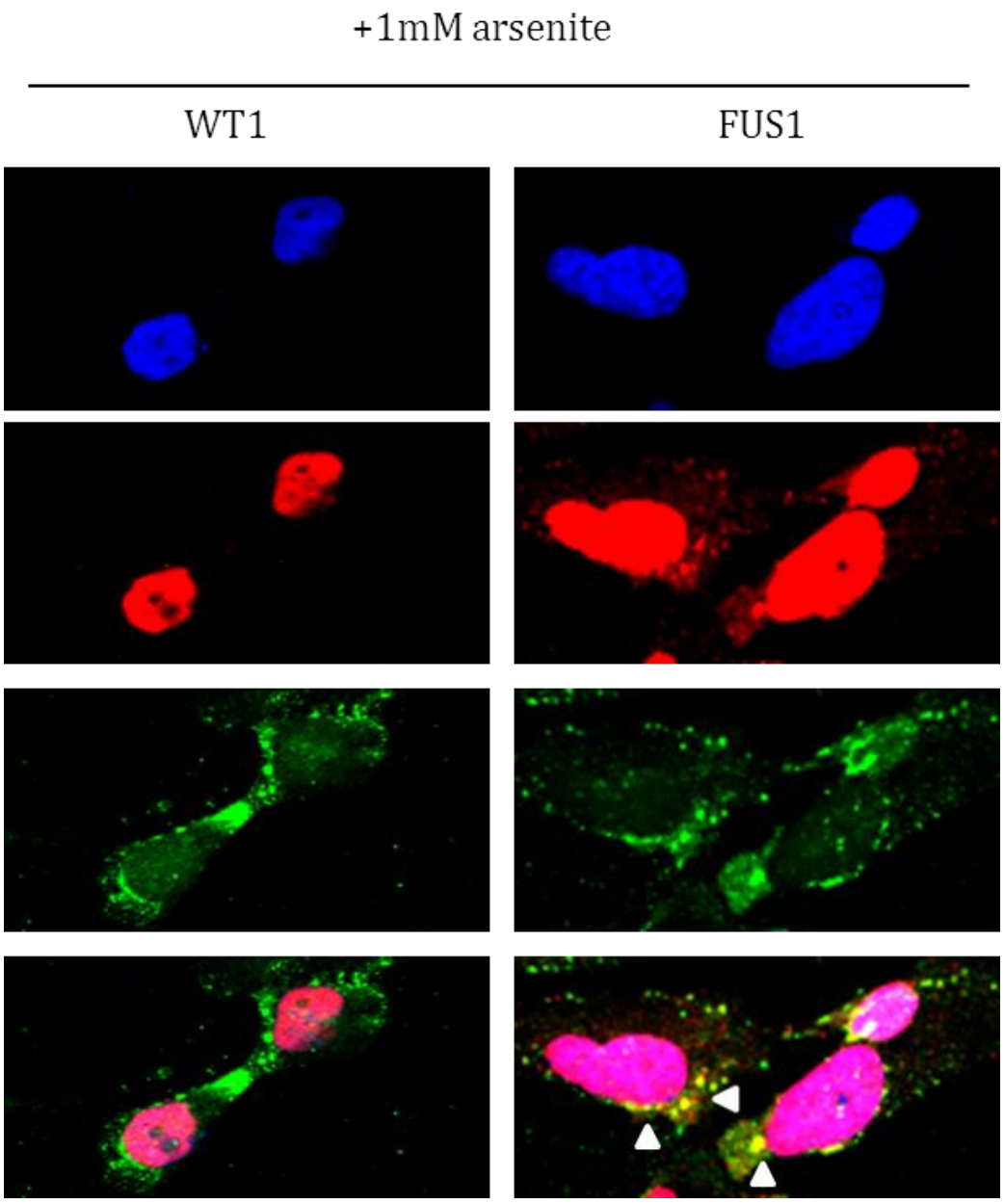

Figure 4.5. Representative images (40x) of WT and FUS iPSC neural progenitors treated with 1mM arsenite for 30 minutes, stained for FUS (red), PABP1 (green) and DAPI (blue). Colocalisation of FUS and PABP1 is indicated by arrowheads.

FUS neural progenitors had more FUS-positive granules per cell than WT neural progenitors (Fig. 4.7). Some clonal variability was observed between FUS and WT lines, but FUS neural progenitors consistently had 4-fold (or more) FUS-positive granules in each cell than WT neural progenitors (Fig. 4.6; WT1 = 0.79 ± 0.10; WT2 = 1.30 ± 0.23; FUS1 = 5.56 ± 1.07; FUS2 = 5.02 ± 0.77. WT1 vs WT2, not significant; FUS1 vs WT1, $P <$

0.001; FUS2 vs WT1, $P < 0.001$; FUS1 vs WT2, $P < 0.001$; FUS2 vs WT2, $P < 0.001$; FUS1 vs FUS2, not significant).

FUS neural progenitors also had significantly more stress granules per cell than WT neural progenitors (Fig. 4.8). Again, clonal variability was observed between both FUS and WT lines, but FUS neural progenitors consistently had approximately double the number of stress granules per cell than WT neural progenitors (Fig. 4.6; WT1 = 4.50 ± 0.51; WT2 = 4.07 ± 0.38; FUS1 = 10.3 ± 1.69; FUS2 = 8.59 ± 1.33. WT1 vs WT2, not significant; FUS1 vs WT1, $P = 0.006$; FUS2 vs WT1, $P = 0.04$; FUS1 vs WT2, $P < 0.001$; FUS2 vs WT2, $P = 0.002$; FUS1 vs FUS2, not significant).

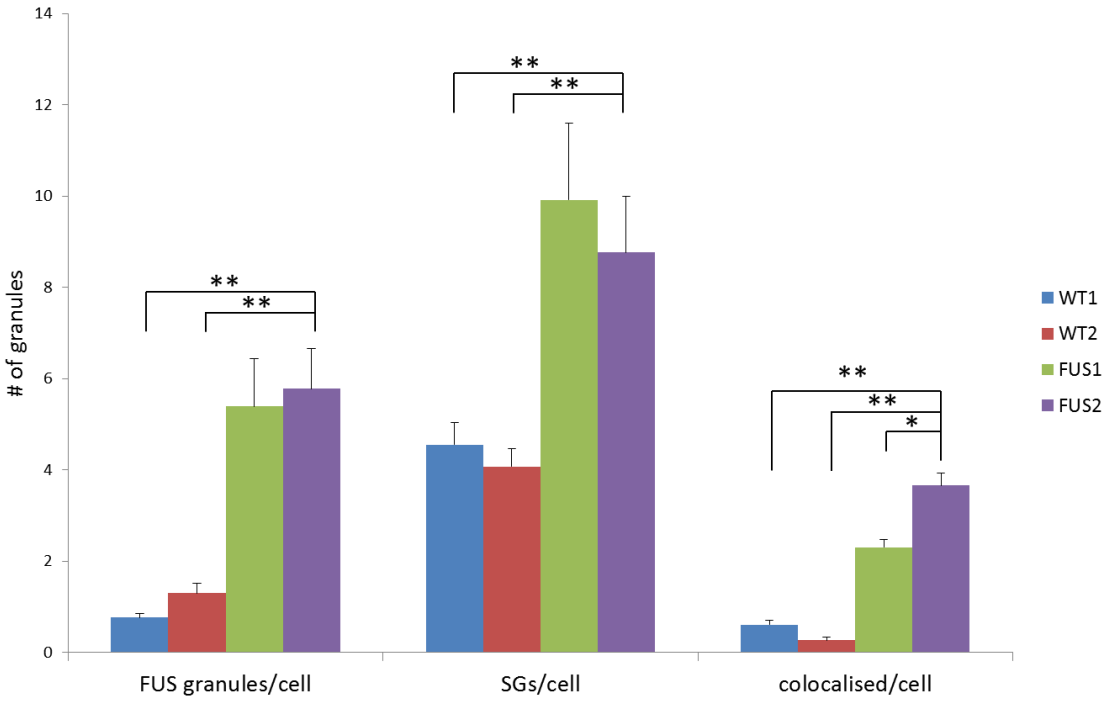

Figure 4.6. Quantitative image analysis of FUS-, PABP1-positive and colocalised particles in WT1, WT2, FUS1 and FUS2 neural progenitors following treatment with 1mM arsenite. Data represent means ± SEM. Significance levels were determined by one-way ANOVA and post-hoc Tukey test. Significance of difference between iPSC lines (* P<0.05; ** P<0.005; *n* = 400+ cells per line from 3 independent experiments).

There was variability in the number of FUS particles that colocalised with PABP1 particles between the lines, but FUS neural progenitors had at least 3.7-fold (or more) colocalised particles in each cell compared to WT neural progenitors (Fig. 4.6; WT1 = 0.47 ± 0.07; WT2 = 0.27 ± 0.06; FUS1 = 2.41 ± 0.15; FUS2 = 3.06 ± 0.14. WT1 vs WT2, not significant; FUS1 vs WT1, $P < 0.001$; FUS2 vs WT1, $P < 0.001$; FUS1 vs WT2, $P < 0.001$; FUS2 vs WT2, $P < 0.001$). FUS2 neural progenitors also had significantly more colocalised particles than FUS1 neural progenitors (Fig. 4.6; FUS1 vs FUS2, $P = 0.007$).

4.3.3 FUS neural progenitors have increased apoptotic cell death

Finally, to determine whether the R521C mutation confers a selective cellular vulnerability, we performed Annexin V and 7-AAD profiling using flow cytometry. We decided against the use of iPSC-derived neurons for this experiment due to the nature of the experimental protocol. Enzymatic dissociation is required to collect cells for flow cytometry and FACS analysis. In a mature neuronal culture, enzymatic dissociation may damage cells and induce apoptosis. Therefore, we opted to perform this analysis on iPSC-derived neural progenitors. iPSC-derived neural progenitors in untreated culture or treated with 1 mM arsenite for 30 minutes were stained for PE Annexin V and 7-AAD (Fig. 4.9). FACS analysis showed that in untreated cultures, FUS neural progenitors have significantly greater percentages of PE Annexin V-positive cells (Fig. 4.10; WT1 = 6.39 ± 2.01; FUS1 = 13.7 ± 1.56; FUS2 = 13.8 ± 1.12; FUS1 vs WT1, $P = 0.04$; FUS2 vs WT2, $P = 0.03$; FUS1 vs FUS2, not significant). In untreated cultures, FUS neural progenitors also have significantly greater percentages of 7-AAD-positive cells (Fig. 4.11; WT1 = 5.9 ± 0.35; FUS1 = 14.4 ± 0.13; FUS2 = 10.02 ± 2.12; FUS1 vs WT1, $P = 0.01$; FUS2 vs WT1, $P < 0.005$; FUS1 vs FUS2, not significant).

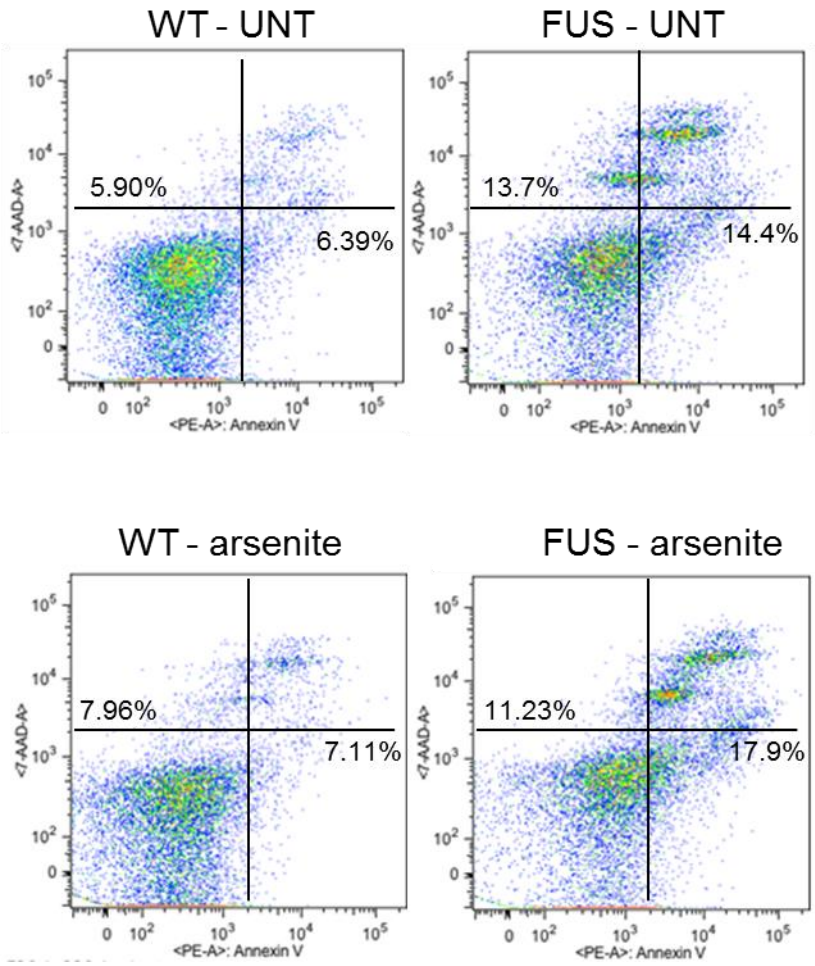

Figure 4.9. Representative dot plots of PE Annexin V and 7AAD of WT and FUS neural progenitors in untreated cultures (top) and of WT and FUS neural progenitors treated with 1mM arsenite for 30 minutes (bottom).

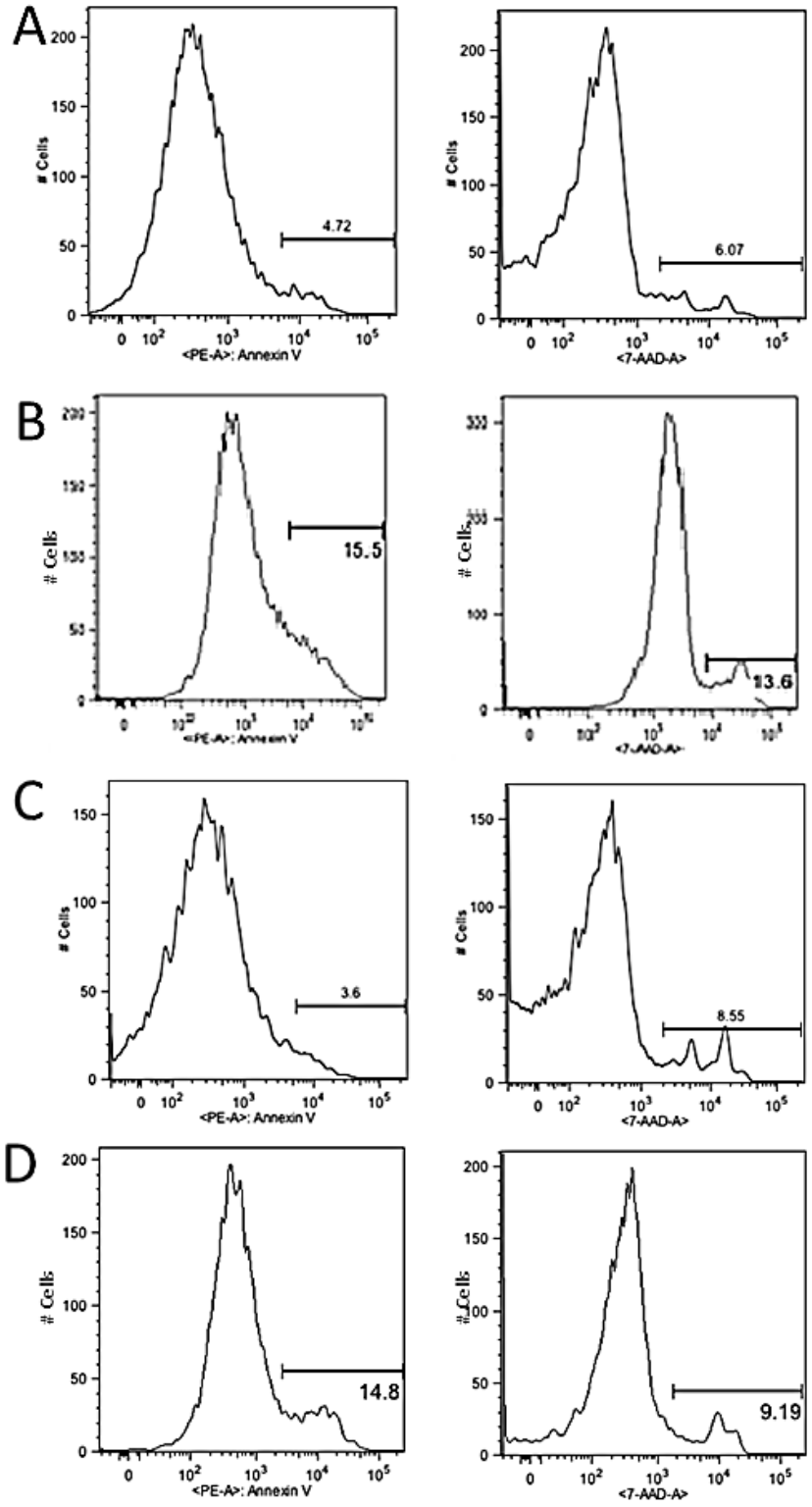

Figure 4.10. Representative gate of PE Annexin V (left) and 7AAD (right) of A) WT and B) FUS neural progenitors in untreated cultures and of C) WT and D) FUS neural progenitors treated with 1mM arsenite for 30 minutes. Gating was performed manually to avoid bleed-through staining of PE Annexin V in 7AAD channel and to ensure that only cells positive for PE Annexin V and 7AAD were included in the analyses.

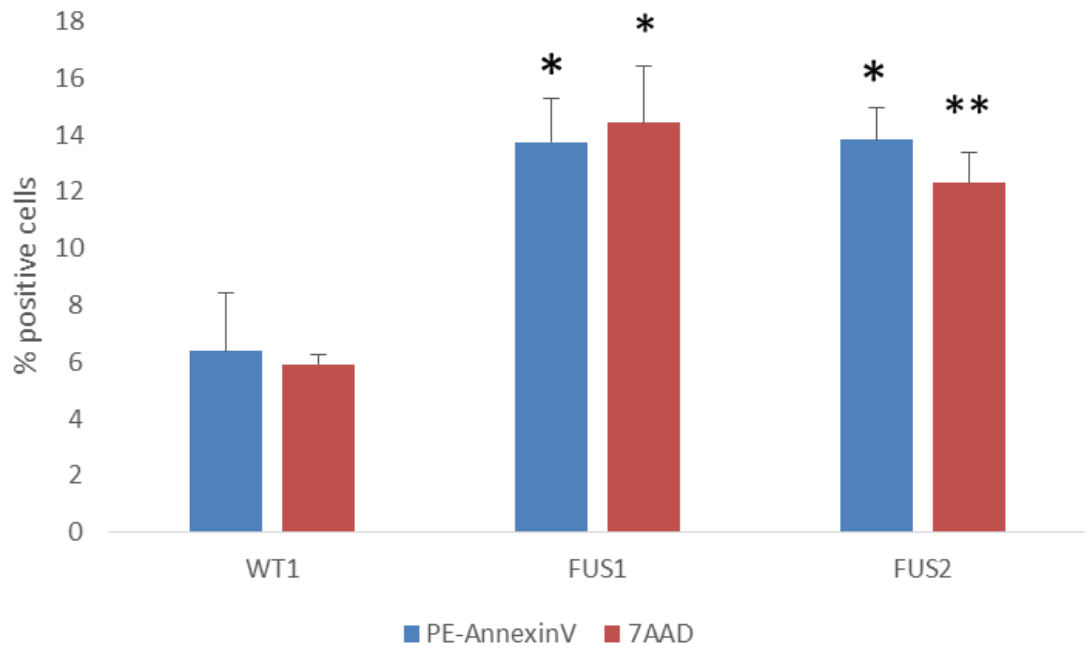

Figure 4.11. FACS analysis of PE Annexin V and 7-AAD in untreated WT1, FUS1 and FUS2 neural progenitors. Data represent means ± SEM. Significance levels were determined by one-way ANOVA and post-hoc Tukey test between lines in the same treatment condition. Significance of difference between iPSC lines (*P<0.05; **P<0.005; *n* = 30,000 cells per line from 3 independent experiments).

FACS analysis also showed that in cultures treated with 1 mM arsenite for 30 minutes, FUS neural progenitors have greater percentages of PE Annexin V-positive cells (Fig. 4.12; WT1 = 7.11 ± 2.96; FUS1 = 17.9 ± 1.82; FUS2 = 16.2 ± 1.61). However, FUS neural progenitors showed clonal variability, as only FUS1 neural progenitors had significantly higher percentages of PE Annexin V-positive cells than WT1 neural progenitors (FUS1 vs WT1, $P = 0.03$; FUS2 vs WT2, $P = 0.054$; FUS1 vs FUS2, not significant). Arsenite-treated FUS neural progenitors also have greater percentages of 7-AAD-positive cells (Fig. 4.13; WT1 = 7.96 ± 1.49; FUS1 = 11.23 ± 1.65; FUS2 = 10.24 ± 2.55), but this difference was not significant.

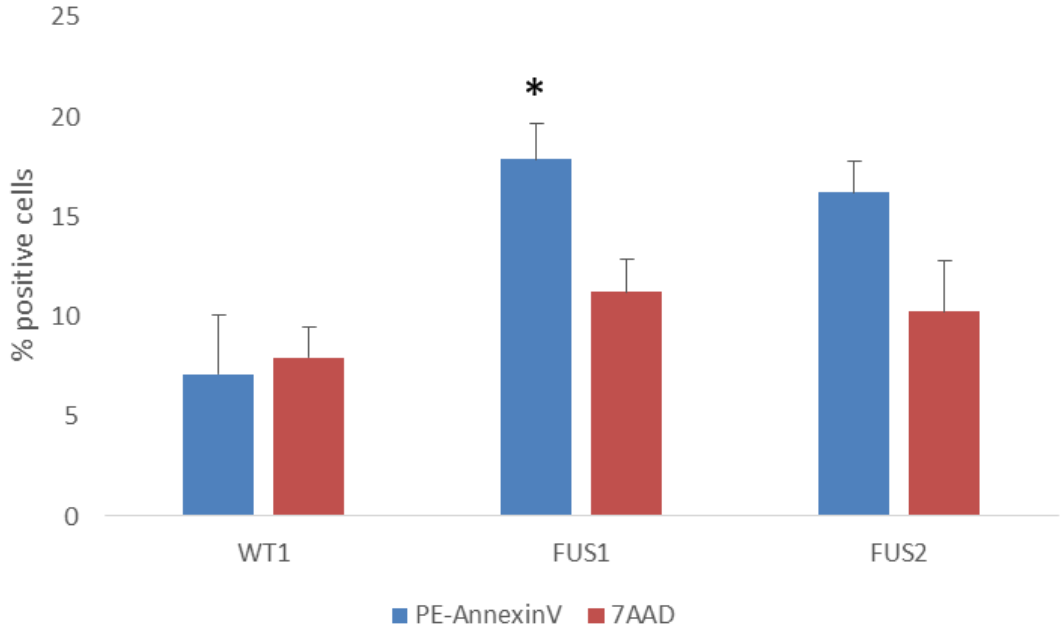

Figure 4.12. FACS analysis of PE Annexin V and 7-AAD in WT1, FUS1 and FUS2 neural progenitors treated with 1 mM arsenite for 30 minutes. Data represent means ± SEM. Significance levels were determined by one-way ANOVA and post-hoc Tukey test between lines in the same treatment condition. Significance of difference between iPSC lines (*P<0.05; *n* = 30,000 cells per line from 3 independent experiments).

4.4 Discussion

In this chapter, I explored three ALS-associated phenotypes in neural progenitors and neurons derived from FUS mutant ALS patient and WT iPSC lines, including cytoplasmic mislocalisation of FUS protein, recruitment of FUS protein in stress granules and spontaneous apoptotic cell death and vulnerability to cellular stress.

FUS neurons show a significant increase in FUS protein levels in the cytoplasm and decreased levels in the nucleus compared to WT neurons. Although FUS protein levels in WT and FUS lines were largely similar, some variability in the subcellular distribution of FUS protein was observed between neurons derived from the two FUS iPSC lines. While both lines showed a decrease in the levels of FUS protein in the nucleus, only FUS2 reached statistical significance. FUS2 also had higher levels of FUS protein in the

cytoplasm, relative to FUS1, although this difference did not reach significance. Line to line variation in transcript and protein abundance is common in iPSCs, even those derived from the same individual, and could arise from the reprogramming of clonal selection. It may be useful to use subcellular fractionation and immunoblotting to quantify any differences. Because of low cell numbers and mixed cell populations, we elected to use quantitative image analysis as very large numbers of neurons are required to obtain enough protein for immunoblotting and information on cell specificity is lost.

Following acute treatment with the oxidative stressor arsenite, cytoplasmic stress granules were observed in both WT and mutant FUS neural progenitors. Relative to mutant FUS neurons, mutant FUS neural progenitors only showed modest staining of FUS in the cytosol in the untreated condition. This may be attributed to alterations in gene expression levels in different cell types. FET proteins have been reported to demonstrate some differences in localization in cultured cells (Andersson et al., 2008). Different cell types may also have variable rates of mRNA translation and protein degradation, which could contribute to the decreased levels of cytosolic FUS observed in mutant FUS neural progenitors.

Quantitative image analysis revealed that cytoplasmic FUS protein was recruited to stress granules in neural progenitors from both FUS mutant lines, but not WT. Neural progenitors from both lines expressing the R521C mutant had a >3.7-fold increase in the number of PABP1 and FUS-positive stress granules per cell compared to WT neural progenitors. Interestingly, neural progenitors derived from the FUS2 line have a greater number of FUS-positive stress granules per cell than those derived from the FUS1 line. Dormann et al. (2010) had shown that the *FUS* mutations associated with the most severe nuclear import defect and the greatest levels of mislocalised cytoplasmic FUS (P525L and R522G) were most readily recruited into stress granules upon heat shock. Similarly, Bosco et al. (2010) also showed that mutant FUS assembled into stress granules in proportion to their cytoplasmic expression levels. The increase in cytoplasmic FUS may affect the assembly or dynamics of stress granules to result in differences in their composition.

The dramatic increase in the number of FUS-positive granules in mutant lines is consistent with previous reports from our laboratory in mutant FUS patient fibroblasts following oxidative stress (Vance et al. 2013). FUS neural progenitors also have approximately double the number of stress granules per cell compared to WT neural progenitors. This finding is consistent with a previous report showing that expression of mutant FUS is associated with increased stress granule size and number in HEK 293 cells (Baron et al. 2013).

Neural progenitors from both lines expressing the R521C mutations showed an increase in spontaneous apoptotic cell death compared to WT1 neural progenitors, as demonstrated by a greater portion of PE Annexin V- and 7AAD-positive cells. Following acute treatment with arsenite, all neural progenitors showed a modest increase in the expression of Annexin V and 7AAD, however, a statistical difference between mutant and controls was only detected in neural progenitors from the FUS1 line. The FUS2 neural progenitors also showed an increase in PE Annexin V-positive cells, but this did not reach significance. Interestingly, differences in levels of late-apoptotic cell death marker 7-AAD were more striking in the untreated mutant FUS lines than following arsenite treatment. These results suggest that the R521C mutation is associated with higher levels of spontaneous and acute oxidative stress induced apoptotic cell death. It would be interesting to assess cell death in the neural progenitors following a period of recovery from acute arsenite treatment or low dose arsenite over a longer period to determine whether mutant FUS progenitors have an increased sensitivity to chronic oxidative stress.

The expression of mutant FUS that is resistant to proteasome-dependent degradation has been shown to induce apoptosis (Perrotti et al., 2000). It is not known whether the FUS R521C mutation is resistant to proteasome-dependent degradation. However, the presence of pathological FUS protein aggregates in disease tissue and the increased insolubility associated with mutant FUS protein suggests that mutant FUS protein may be resistant to proteasomal degradation. Alternatively, the expression of mutant FUS has been shown to induce endoplasmic reticulum stress (Farg et al., 2012).

One downstream pathway triggered by ER stress is the induction of cell death. It would be of interest to investigate the turnover of FUS protein and endoplasmic reticulum homeostasis in iPSC-derived neural progenitors to determine its possible association with apoptotic cell death.

In summary, we have attempted to quantify three relevant phenotypes to determine whether neural populations derived from mutant FUS iPSCs recapitulate key features of FUS-associated ALS. Neural populations derived from mutant FUS iPSCs demonstrated greater mislocalisation of FUS protein to the cytoplasm, recruitment into stress granules and spontaneous and oxidative stress induced apoptotic cell death. The fact that these results were consistent in two independently-derived human stem cell lines from an ALS patient suggest that these events are due to the presence of the R521C mutant protein which is expressed at physiological levels. They provide an important validation of data derived from transfected cell lines (Bosco et al. 2010; Dormann et al. 2010), human fibroblasts (Vance et al. 2013) and transgenic zebrafish (Armstrong and Drapeau 2013), which is consistent with the findings of human pathology (Mackenzie et al. 2011). In the next chapter, I describe the investigation of neuronal morphology in iPSC-derived neurons.

CHAPTER 5

INVESTIGATING NEURONAL MORPHOLOGY AND SYNAPSES IN iPSCs

5.1 BACKGROUND

In this study, we used molecular biology approaches and quantitative image analysis to investigate the morphology and synapses of neurons derived from control WT and FUS mutant patient iPSC lines. Studies have previously shown that pathological changes in motor neuron axons and synapses occur prior to motor neuron degeneration in SOD1 mouse models (Frey et al. 2000; Pun et al. 2006). In support of these findings, recent cellular and animal models have provided evidence that FUS may play a role in determining peripheral neuronal structure and function, particularly at the synapse. We therefore sought to explore any differences in neuronal architecture and subcellular structures in neurons derived from mutant FUS and control iPSC lines by measuring: neurite outgrowth, density of dendritic protrusions and the expression and location of selected synaptic proteins.

5.1.1 Neurite outgrowth

Neurons are the most polarized cells in the body and motor neurons are the largest with an axo-dendritic volume that is 1 million times greater than the cell body. Outgrowth of axons and dendrites occurs rapidly during early neuronal differentiation and continues until adulthood, but remodeling of axons and dendrites occurs throughout life. As axons grow outward, they make contact with the dendritic spines of thousands of neurons, close contacts with astroglia and oligodendroglia and form synapses with neurons centrally and with peripheral target cells such as myocytes and sensory receptors. The axo-dendritic tree is the outcome of a complex, multi-stage process that involves multiple molecular components to achieve an optimal structure and function. A complex and dynamic network of synapses must be made to connect the billions of neurons in the human brain for the nervous system to function properly. Dendritic and synaptic loss and distal axonal degeneration are early and consistent features of all

neurodegenerative disorders, affecting predominantly, but not exclusively, the motor neurons in ALS. In several animal models of ALS, progressive denervation and reinnervation of motor endplates occurs through a process of motor neuron axonal dieback and leads to progressive muscular paralysis (Schaefer et al. 2005).

FUS appears to play a role in the regulation of neuronal morphology. Fujii et al. (2005) showed that in hippocampal neurons from FUS-deficient mice have irregularly branched dendrites and abnormal axonal processes. Similarly, the knockdown of FUS in hippocampal neurons results in reduced axon length and abnormal growth cone morphology (Orozco et al. 2012). The expression of ALS-associated FUS mutations in primary mouse cortical neurons has also been shown to alter axonal morphology, resulting in reduced axon length, decreased axon branches and the area of the growth cone (Groen et al. 2013). These findings suggest that FUS has an important role in cytoskeletal organisation, in axons and dendrites.

5.1.2 Dendritic spine morphology

Dendritic spines are small protrusions that receive synaptic input from axons and dendrites. Changes in dendritic spine morphology and function are associated with synaptic plasticity (Engert and Bonhoeffer 1999) and may be an early feature of neurodegeneration. Neurons from FUS knockout mice have abnormal dendritic spine morphology. WT hippocampal neurons have spines with a mushroom-like shape, whereas FUS-deficient hippocampal neurons have reduced spine density, or spines that were transformed into abnormally thin filopodia-like protrusions (Fujii et al. 2005). This study implies that FUS regulates the stability of dendritic spines, possibly by transporting RNA transcripts and translocating to spines upon glutamate activation (Fujii et al. 2005). Thus, FUS may regulate dendritic spine morphology by transporting transcripts for local translation in dendrites.

5.1.3 Alterations in synaptic proteins

As mentioned, pathological changes at the NMJ are thought to precede degeneration of the motor neuron cell body, a dying back axonopathy. Animal and cellular models of ALS demonstrate several features of synaptic abnormalities prior to onset of motor symptoms, including increased excitability, reduced NMJ synaptic fidelity and susceptibility to excitotoxicity (Kuo et al. 2004; Armstrong and Drapeau 2013). Recently, iPSC-derived motor neurons from ALS patients with *SOD1, C9orf72* and *FUS* mutations were shown to recapitulate the hyperexcitability detected in ALS patients and that a pharmacological agent that reduces excitability increases survival of MNs (Wainger et al. 2014).

Alterations in motor neuron excitability may reflect changes in the compartmentalisation or expression of synaptic proteins. Interestingly, FUS binds to, or regulates mRNA that encodes multiple components of the synapse, including receptors, channel subunits and neurofilaments (Lagier-Tourenne et al. 2012; Rogelj et al. 2012). Furthermore, FUS is associated with adenomatous polyposis coli ribonucleoprotein complexes (APC-RNPs), a type of granule that targets RNAs to cell protrusions. Yasuda et al. (2013) showed that transcripts within APC-RNPs are translated and that the expression of FUS mutants preferentially recruits APC-RNPs. These findings prompted us to investigate whether neurons derived from patient iPSCs carrying mutant FUS display altered abundance and density of selected synaptic proteins.

We chose four different synaptic proteins for this analysis: postsynaptic density protein 95 (PSD 95), piccolo, vesicular glutamate transporter 1 (VGLUT1) and synapsin I. These proteins were selected based on their key location and functions. PSD95 is a membrane associated guanylate kinase scaffolding protein within the postsynaptic density. It is a component of a scaffold for the clustering of receptors, ion channels and associated signaling proteins. Piccolo is a multidomain scaffold protein that has a role in the clustering of synaptic vesicles in nerve terminals at the presynaptic active zone (Mukherjee et al. 2010). VGLUT1 mediates the uptake of glutamate into synaptic vesicles

at the presynaptic terminal of glutamatergic neurons. Synapsin I is a phosphoprotein in the coating of synaptic vesicles that functions to accelerate synaptic vesicle traffic to contribute to short-term synaptic plasticity (Rosahl et al. 1995). Although our analysis is limited to only four synaptic proteins, our selection covers the presynaptic and the postsynaptic compartments with roles in axo-dendritic transport and neurotransmitter signaling, and enables a preliminary investigation of four different functional processes at the synapse.

5.2 METHODS

5.2.1 Transfection

Frozen glycerol stocks of hemagglutinin (HA)-tagged FUS WT or FUS mutants (Q519E, R514G, K510X and R521G) and EGFP-transformed cells generated previously (Vance et al. 2013; Scotter et al. 2014) were cultured in Luria-Bertani (LB) media containing 100 μg/ml of ampicillin, then incubated on an orbital shaker overnight at 37°C. Extraction of plasmid DNA from bacteria was prepared using plasmid DNA purification kit (Machery-Nagel) following the manufacturer's instructions. Plasmid DNA were eluted using nuclease-free water (Ambion), quantified using a microvolume spectrophotometer (Nanodrop, Thermo Scientific), then stored at -20°C. iPSC-derived neural progenitors or neurons were transfected with plasmids as described in Section 2.1.9.

5.2.2 Immunofluorescence

iPSC-derived neurons were fixed and samples prepared as described in Section 2.2.4. iPSC-derived neurons were probed with primary antibodies (Table 5.1) diluted in 5% donkey serum overnight at 4°C. Donkey anti-rabbit or mouse AlexaFluor-488/550/650 secondary antibodies (1:400) were then applied for 1 hour at room temperature in the dark. DAPI counterstaining (1.25 μg/ml) was applied and coverslips mounted as described in Section 2.2.4. Images were obtained with a Zeiss Axiovert S100 microscope or Leica TCS-SP5 laser scanning confocal microscope.

Table 5.1. Primary antibodies

Antibody	Host	Company	Dilution
VGLUT1	Rabbit polyclonal	Synaptic Systems	1:100
Piccolo	Rabbit polyclonal	Synaptic Systems	1:100
PSD95	Mouse monoclonal	Synaptic Systems	1:100
Synapsin	Rabbit polyclonal	Millipore	1:500
Map2	Mouse monoclonal	Abcam	1:500
Map2	Rabbit polyclonal	Abcam	1:500
HA-tag	Rabbit monoclonal	Cell Signaling	1:1000

5.2.3 Quantitative image analysis of dendrite outgrowth - Metamorph

Motor neuron-containing populations were differentiated for 5 weeks, then prepared for immunofluorescence as described above. Cortical neurons were differentiated from iPSC-derived neural progenitors for 7 days, then prepared for immunofluorescence as described above. To quantify dendrite outgrowth in iPSC-derived MNs, quantitative image analysis was performed using MetaMorph Microscopy Automation & Image Analysis Software 7.5 (Molecular Devices). Fields based on uniform DAPI staining or EGFP-positive cells were selected and imaged in two or three channels. 7-12 images of each cell line were obtained with the Zeiss Axiovert S100 microscope. The exposure time for capturing the images was maintained and all images were taken on the same day.

Images were first converted to grayscale and the DAPI, MAP2 and EGFP channels were used to define the thresholds. The number of cells in each image was determined using the "Count nuclei" app and the DAPI images, or in the case of transfected cells, the "Count nuclei" app and the HA images. Dendrite outgrowth was determined using the "Neurite Outgrowth" app, using MAP2 or EGFP images. The outgrowth, processes and

branches of iPSC-derived neurons were analysed (Fig. 5.1). These measurements are defined by the MetaMorph Application Module as follows:

- Cells – number of cells in a field
- Total outgrowth – total length of skeletonised outgrowth in μm (corrected for diagonal lengths)
- Mean outgrowth – average skeletonised outgrowth in μm corrected for diagonal length divided by the number of cells
- Total processes – number of outgrowths that connect to the cell body
- Total branches – number of branching junctions
- Mean processes – number of processes divided by number of cells
- Mean branches – number of branching junctions divided by number of cells

For dendrite outgrowth analysis of iPSC lines, data were obtained from three independent differentiation experiments and at least 500 cells from MN-containing populations in each line. For neurite outgrowth analysis of iPSC cortical neurons transfected with FUS mutants, data were obtained from two independent differentiation experiments and 30-50 cortical neurons differentiated from iPSC-derived neural progenitor cells for each mutation.

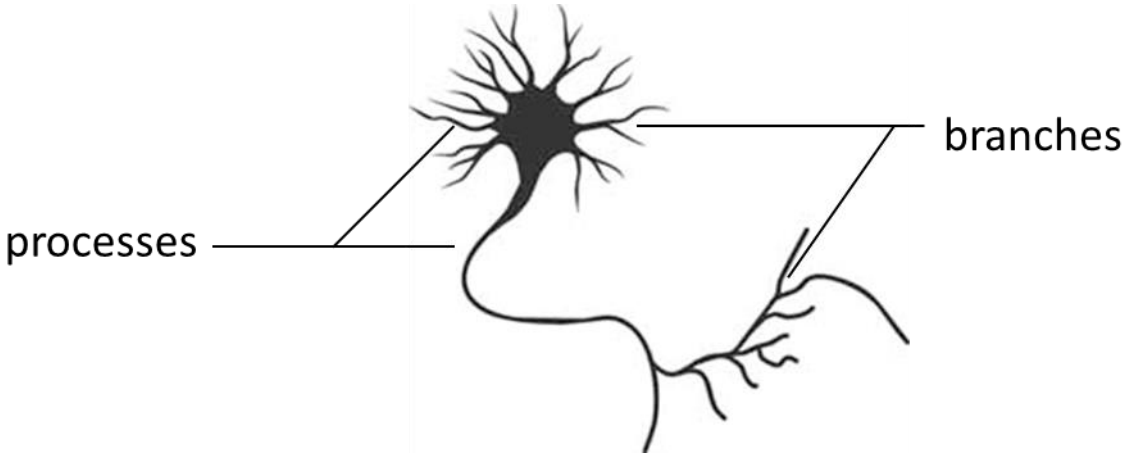

Figure 5.1. Illustration of processes and branches in a neuron (Image from adapted from Medgadget).

5.2.4 Quantitative image analysis of dendritic protrusions - ImageJ

To quantify dendritic protrusions, FUS and WT motor neurons were differentiated for 8 weeks then prepared for immunofluorescence as described in Section 5.2.2. Quantitative image analysis was performed using ImageJ plug-in NeuronJ (Meijering et al. 2004). Fields based on uniform MAP2 staining were selected and imaged in two channels. 7-12 images of each cell line were obtained with the Zeiss Axiovert S100 microscope. The exposure time for capturing the images was maintained and all images were taken on the same day.

Images were first converted to grayscale 8-bit. Dendrites were manually traced and the length of dendrites was measured using MAP2 images. The density of dendritic protrusions was measured by manually counting the number of clearly evident dendritic protrusions on primary dendrites. Dendritic protrusions between 0.5 and 8 μm were included in this analysis.

5.2.5 Quantitative image analysis of synaptic puncta - ImageJ

Synaptic puncta were quantified as described previously, with slight modifications (Marchetto et al. 2010).To quantify pre- and post-synaptic markers, quantitative image analysis was performed using Image J (version 1.48p). Fields based on uniform MAP2 staining were selected and imaged in four channels. 5-7 z-series of each cell line with 0.5-μm increments were obtained with a 63x objective on the Leica TCS-SP5 laser scanning confocal microscope. The exposure time for capturing the images was maintained and all images of the same marker were taken on the same day. A collapsed maximum Z projection of images was generated for each channel within a z-series. For pre- and post-synaptic puncta, maximum projections were converted to grayscale and individual marker channels were used to define the thresholds. The thresholded images were then combined with the MAP2 channel to quantify the density of puncta. To quantify the length of a dendrite, maximum projections of the MAP2 channel were converted to 8-bit images.

NeuronJ was used to add tracings for each Z projection. Data were obtained from two independent differentiation experiments and 30-40 dendrites of 10-12 cells from each line.

5.3 RESULTS

5.3.1 FUS neurons have reduced dendrite outgrowth

To assess neuronal morphology, the dendrite outgrowth of FUS and WT motor neurons was analysed by quantitative image analysis using Metamorph software. MN-containing neural populations derived from two independent R521C mutant FUS iPSC clones had significantly less outgrowths compared to control neural populations (Fig. 5.2). Mutant FUS neurons had ~50% decrease in the mean outgrowth per cell (Fig. 5.3; WT1 = 420.2 ± 14.7; WT2 = 407.9 ± 41.1; FUS1 = 217.98 ± 27.9; FUS2 = 221.5 ±12.7; WT1 vs WT2, not significant; WT1 vs FUS1, $P < 0.001$; WT1 vs FUS2, $P < 0.001$; WT2 vs FUS1, $P < 0.001$; WT2 vs FUS2, $P < 0.001$; FUS1 vs FUS2, not significant).

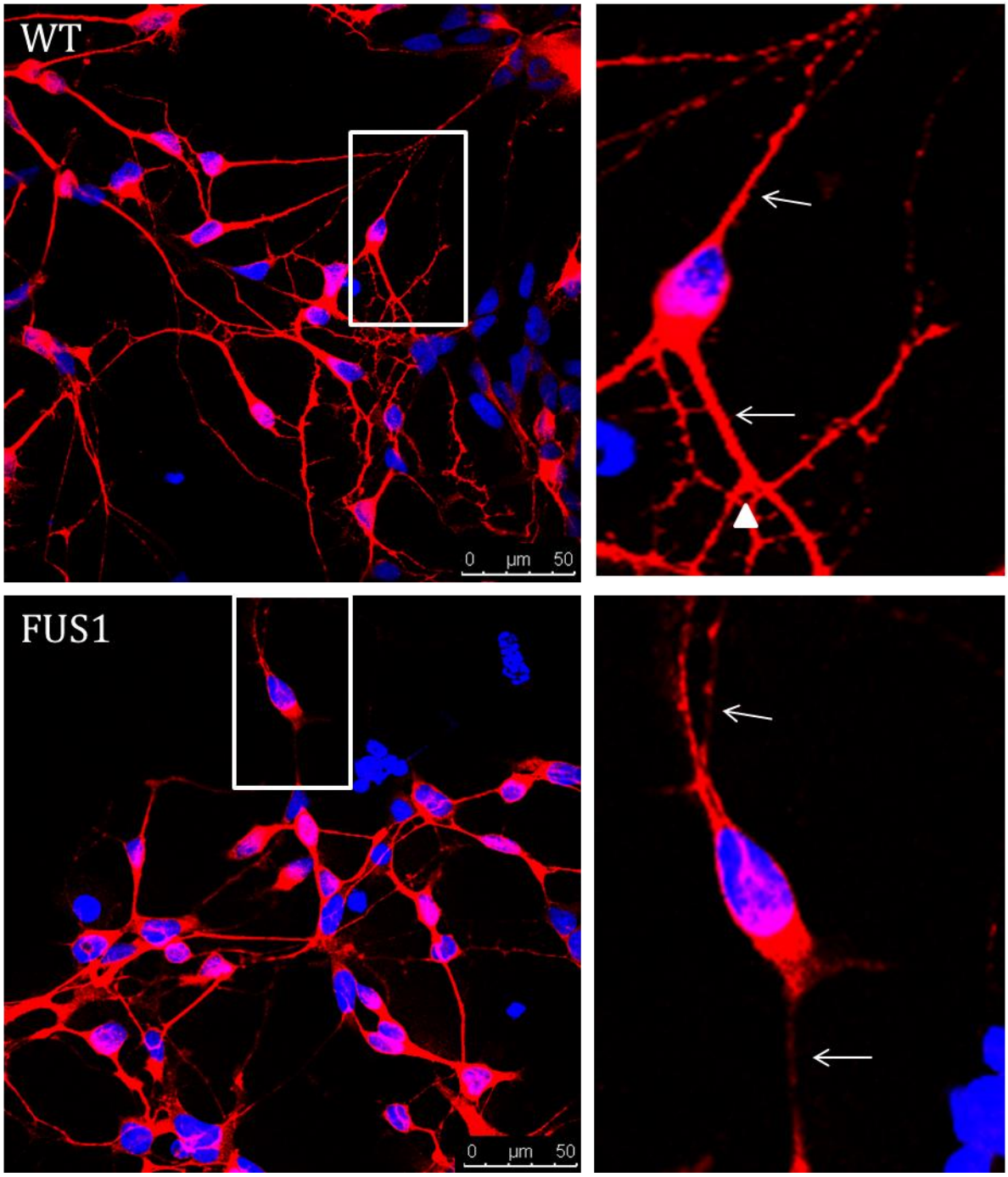

Figure 5.2. Mutant FUS iPSC neurons in motor neuron-containing populations have reduced dendrite outgrowth, processes and branches. Confocal images (40x) of WT and mutant FUS iPSC neurons stained for neuronal dendrite-specific marker, MAP2 (red). (Right panels) Representative images of WT and FUS iPSC neurons. Processes are indicated by arrows. Branches are indicated by arrowheads.

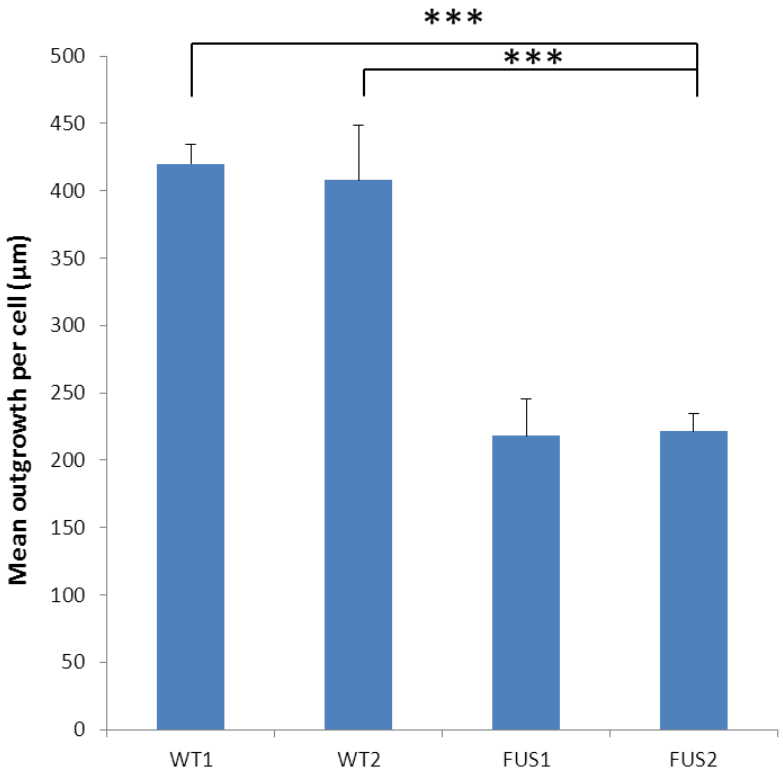

Figure 5.3. Quantitative image analysis of total length of dendrite outgrowth in WT1, WT2, FUS2 and FUS2 motor neurons. Data represent mean outgrowth length per cell ± SEM. Significance levels were determined by one-way ANOVA and post-hoc Tukey test. Significance of difference between iPSC lines (*** $P < 0.001$). n = 400+ cells from 3 independent experiments.

Analysis of the complexity of dendritic arborisation revealed that FUS neurons had a reduction in the number of dendrite processes compared to WT neurons (Fig. 5.4). MN-containing neural populations derived from two independent mutant FUS iPSC clones had significantly less dendritic processes compared to WT MN-containing neural populations (WT1 = 5.44 ± 0.38; WT2 = 6.33 ± 0.56; FUS1 = 3.06 ± 0.28; FUS2 = 3.56 ± 0.30; WT1 vs WT2, not significant; WT1 vs FUS1, $P < 0.001$; WT1 vs FUS2, $P < 0.001$; WT2 vs FUS1, $P < 0.001$; WT2 vs FUS2, $P < 0.001$; FUS1 vs FUS2, not significant).

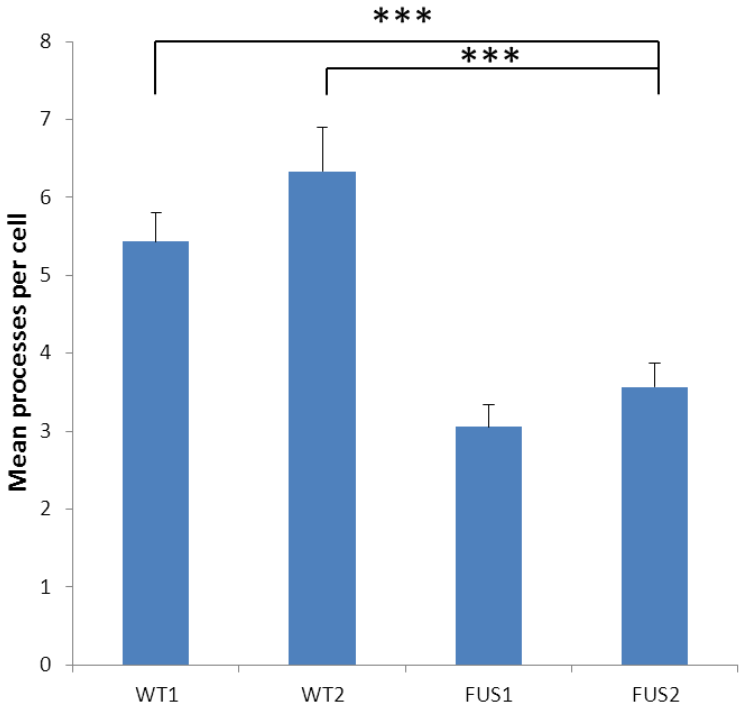

Figure 5.4. Quantitative image analysis of dendritic processes in WT1, WT2, FUS1 and FUS2 neurons. Data represent mean processes per cell ± SEM. Significance levels were determined by one-way ANOVA and post-hoc Tukey test. Significance of difference between iPSC lines (*** $P < 0.001$). n = 400+ cells from 3 independent experiments.

Furthermore, FUS neurons showed reduced branching compared to WT neurons (Fig. 5.5). MN-containing neural populations derived from two independent FUS iPSC clones had significantly fewer dendritic branches compared to WT MN-containing neural populations (WT1 = 2.27 ± 0.21; WT2 = 2.60 ± 0.38; FUS1 = 0.70 ± 0.19; FUS2 = 1.20 ± 0.12 WT1 vs WT2, not significant; WT1 vs FUS1, $P < 0.0001$; WT1 vs FUS2, $P < 0.001$; WT2 vs FUS1, $P < 0.001$; WT2 vs FUS2, $P < 0.001$). FUS1 MN-containing neural populations also had significantly less dendritic branches compared to FUS2 MN-containing neural populations (FUS1 vs FUS2, $P = 0.03$).

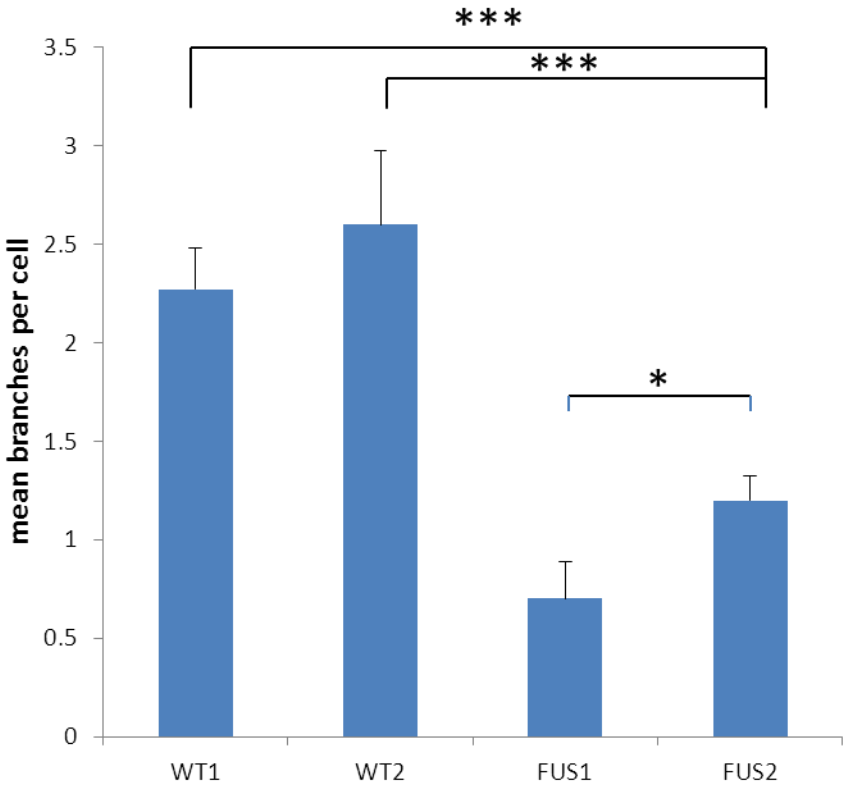

Figure 5.5. Quantitative image analysis of the number of dendritic branches in WT1, WT2, FUS2 and FUS2 neurons. Data represent mean branches per cell ± SEM. Significance levels were determined by one-way ANOVA and post-hoc Tukey test. Significance of difference between iPSC lines (* $P < 0.05$; *** $P < 0.001$). n = 400+ cells from 3 independent experiments.

5.3.2 ALS-associated *FUS* mutations are associated with reduced neurite outgrowth

To determine whether other ALS-linked *FUS* mutations also affect neurite morphology, HA-tagged FUS construct (WT, Q519E, R514G, K510X or R521G) and EGFP construct were expressed in WT2 neural progenitors, which were then differentiated into cortical neurons for 7 days and analysed using MetaMorph software (Fig. 5.6).

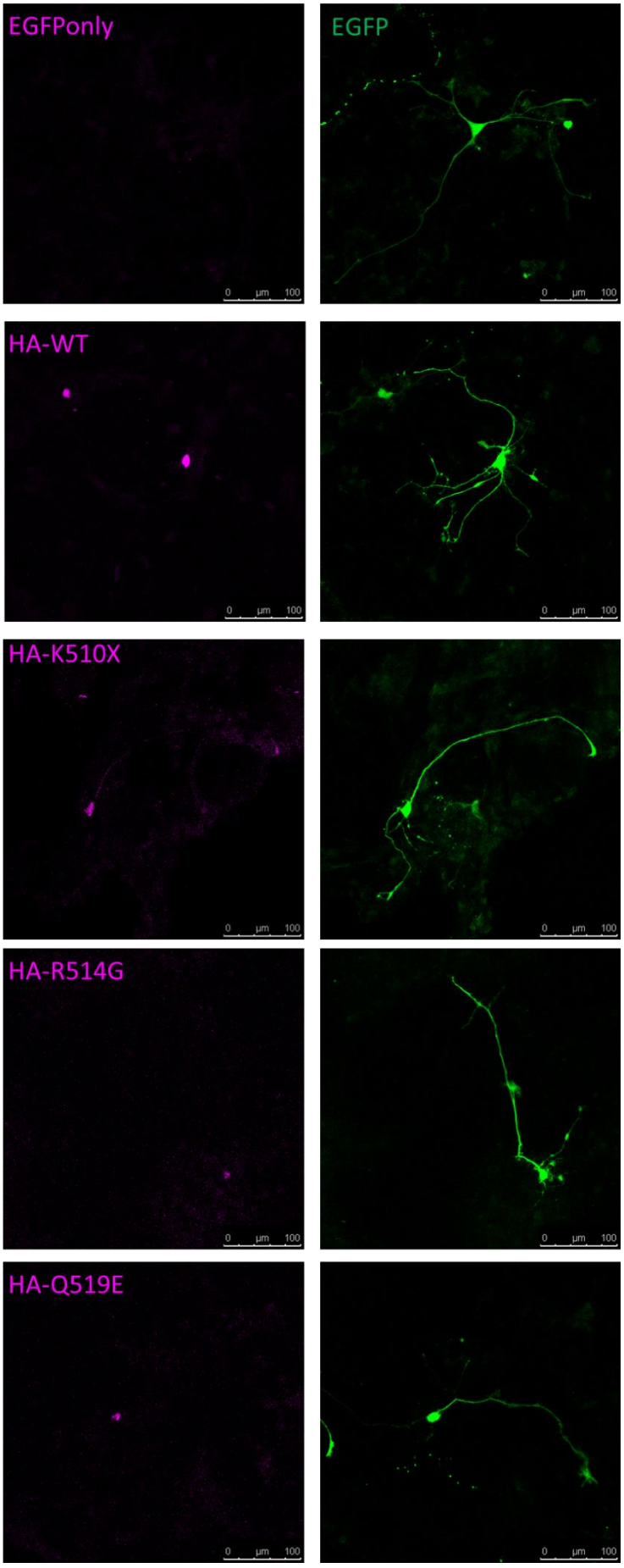
EGFPonly
EGFP
HA-WT
HA-K510X
HA-R514G
HA-Q519E
0 µm 100

Figure 5.6. Confocal representative images of iPSC cortical neurons transfected with EGFP only, HA-FUS-WT and EGFP, HA-FUS-Q519E and EGFP, HA-FUS-R514G and EGFP, and HA-FUS-K510X and EGFP,stained for HA (magenta) and green fluorescence from EGFP.

Neurons expressing Q519E, R514G, K510X and R521G had significantly less neurite outgrowth compared to neurons expressing EGFP only (Fig. 5.7; EGFP only = 598.08 ± 26.7; WT = 533.7 ± 35.6; Q519E = 264.8 ± 18.6; R514G = 268.4 ± 29.0; K510X = 437.8 ± 51.6; R521G = 257.1 ±19.2; EGFP only vs WT, not significant; EGFP only vs Q519E, $P < 0.001$; EGFP only vs R514G, $P < 0.001$; EGFP only vs K510X, $P = 0.006$; EGFP only vs R521G, $P < 0.001$). Compared to neurons expressing WT FUS, neurons expressing Q519E, R514G and R521G had significantly less neurite outgrowth (WT vs Q519E, $P < 0.001$; WT vs R514G, $P < 0.001$; WT vs R521G, $P < 0.001$). Interestingly, the truncation mutant K510X, which shows a greatest degree of cytoplasmic mislocalisation in cell line transfection studies (Vance et al., 2013), showed only a modest reduction in the mean neurite outgrowth and did not reach statistical significance (WT vs K510X, $P = 0.17$).

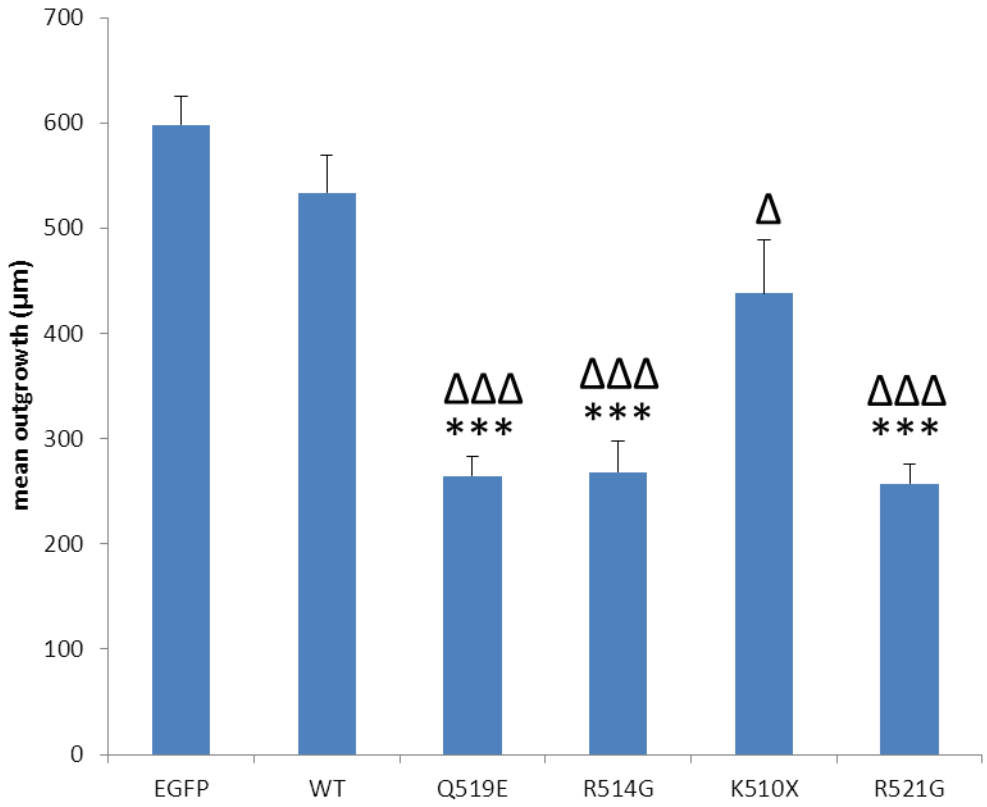

Figure 5.7. Quantitative image analysis of neurite outgrowth in WT cortical neurons transfected with EGFP only, HA-FUS-WT, HA-FUS-Q519E HA-FUS-R514G, HA-FUS-K510X, HA-FUS-R521G All HA-FUS transfected cells were co-transfected with EGFP plasmid. Data represent mean outgrowth per cell ± SEM. Significance levels were determined by one-way ANOVA and post-hoc Tukey test. Significance of difference between EGFPonly and HA-FUS constructs (Δ $P < 0.05$; ΔΔΔ $P < 0.001$). Significance of difference between HA-FUS-WT and HA-FUS mutant constructs (*** $P < 0.001$). n = 40+ cells from 2 independent experiments.

5.3.3 FUS neurons have reduced dendritic protrusions

Dendritic protrusions are filopodia-like processes along dendritic shafts and dendritic growth cones. Protrusions along dendritic shafts appear to initiate synaptogenic contacts with axons and to function in the development and stabilisation of mature dendritic spines (Portera-Cailliau et al., 2003; Ziv and Smith, 1996). Alternatively, protrusions in dendritic growth cones are involved in activity-dependent dendritic growth

and branching (Portera-Cailliau et al., 2003). Dendritic protrusions have also been shown to function as channels for activity-dependent retrograde translocation of postsynaptic molecular complexes to parental dendrites (Kawabata et al., 2011).

In order to evaluate the architecture of dendritic protrusion in motor neurons derived from iPSCs, we analysed the dendritic morphology of each line using ImageJ. Mutant FUS neurons differentiated for 8 weeks showed a reduction in the number of dendritic protrusions compared to WT neurons (Fig. 5.8). MN-containing neural populations derived from two independent FUS iPSC clones had significantly less dendritic protrusions compared to WT MN-containing neural populations (Fig. 5.9; WT1 = 1.46 ± 0.07; WT2 = 1.22 ± 0.06; FUS1 = 0.38 ± 0.04; FUS2 = 0.29 ± 0.04; WT1 vs FUS1, $P < 0.001$; WT1 vs FUS2, $P < 0.001$; WT2 vs FUS1, $P < 0.001$; WT2 vs FUS2, $P < 0.001$; FUS1 vs FUS2, not significant). WT1 MN-containing neural populations also had significantly more protrusions than WT2 MN-containing neural populations (WT1 vs WT2, $P = 0.01$).

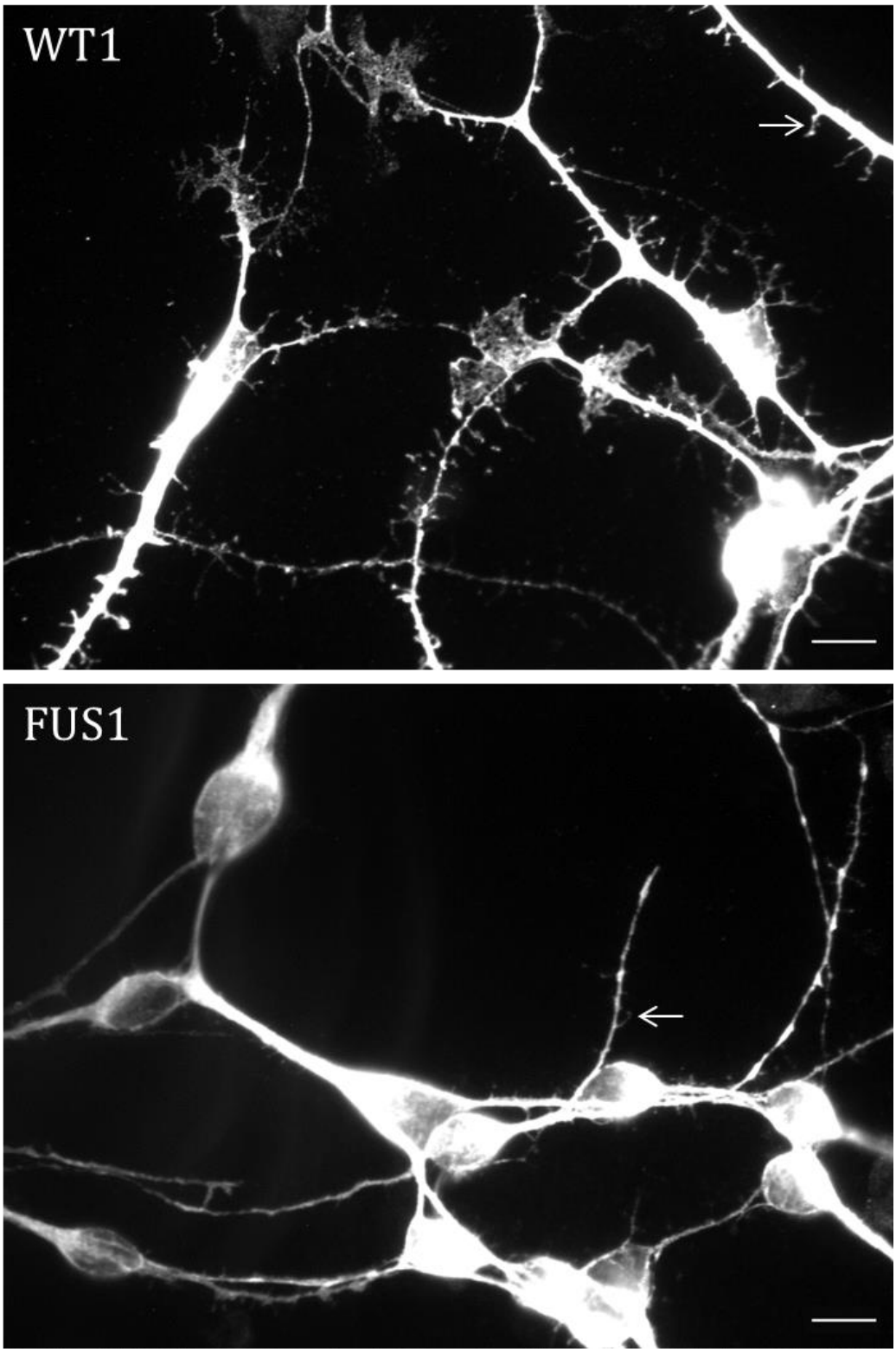

Figure 5.8. Representative images (63x) of a) WT and b) FUS iPSC neurons stained for neuronal dendrite-specific marker, MAP2. Dendritic protrusions are indicated by arrows. Scale bars = 10 μm.

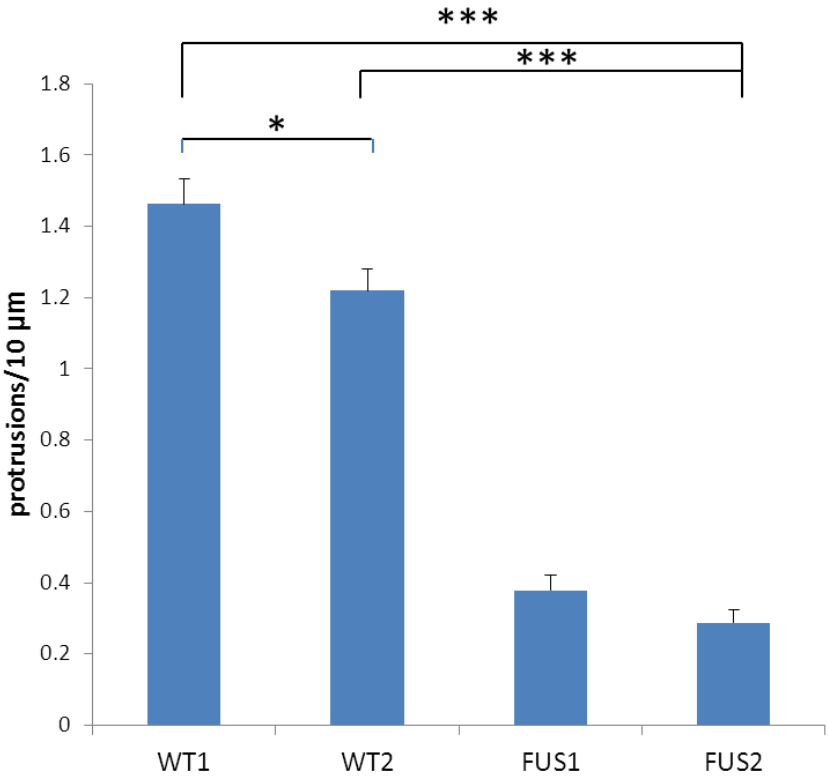

Figure 5.9. Quantitative image analysis of the number of dendritic protrusions in WT1, WT2, FUS2 and FUS2 neurons. Data represent mean number of protrusions per 10 µm length of dendrite ± SEM. Significance levels were determined by one-way ANOVA and post-hoc Tukey test. Significance of difference between iPSC lines (* $P < 0.05$; *** $P < 0.001$). n = 3 neurites per cell from 30+ cells and 2 independent experiments.

5.3.4 Altered synapse number in FUS neurons

In order to determine whether the abnormal dendritic morphology is associated with changes at the synapse, the localisation of synaptic proteins was analysed by quantitative image analysis using ImageJ. The density of piccolo, VGLUT1, synapsin I and PSD 95 puncta within neurites were analysed in cortical neurons differentiated from iPSC-derived neural progenitors for 40+ days.

The expression of piccolo, a component of the presynaptic cytoskeletal matrix, was assessed in FUS and WT neurons (Fig. 5.10). FUS and WT neurons showed comparable density of piccolo puncta (WT1 = 1.05 ± 0.06; WT2 = 0.95 ± 0.05; FUS1 = 0.93 ± 0.08; FUS2 = 0.97 ± 0.06).

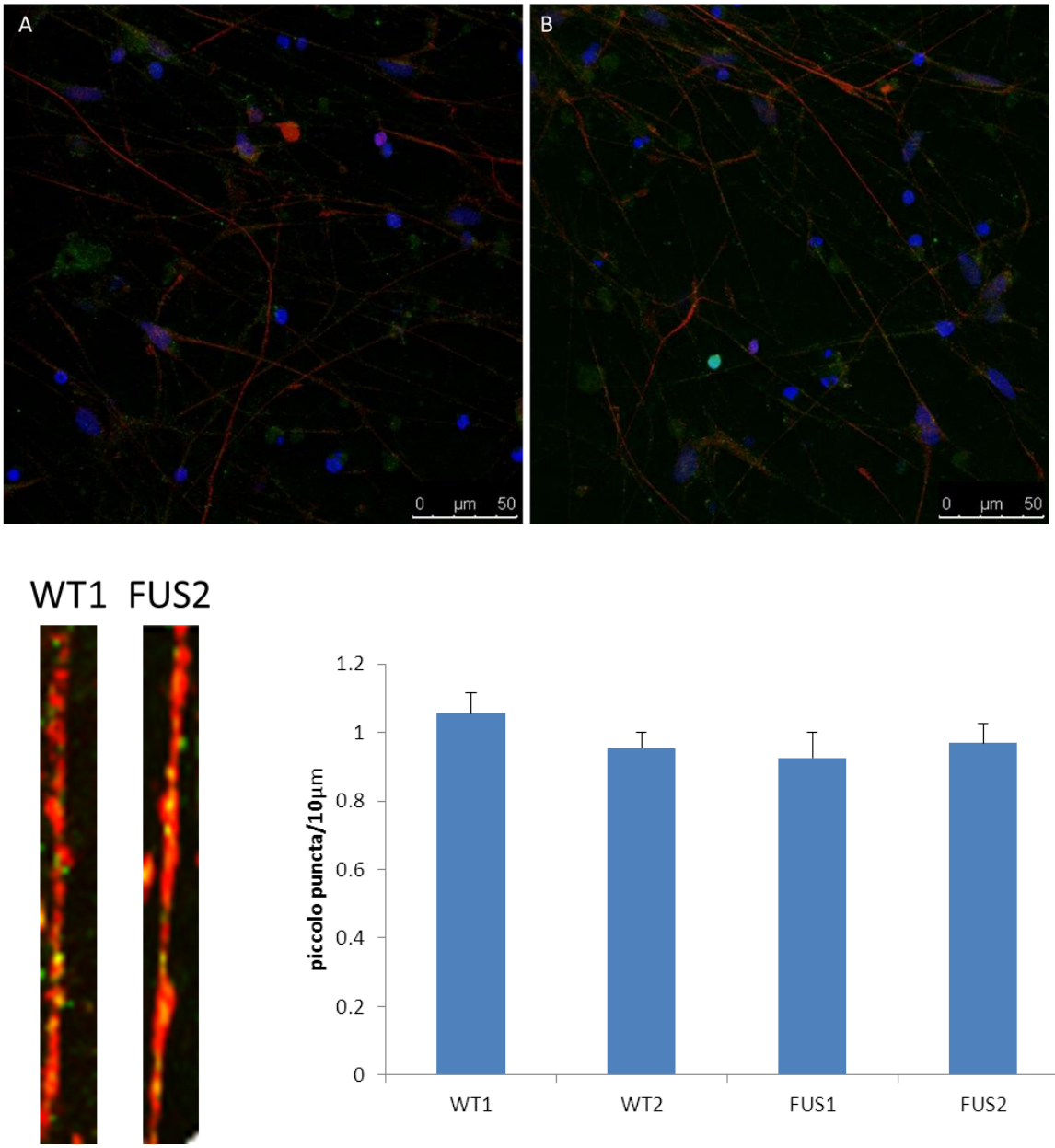

Figure 5.10. Confocal images of A) WT and B) FUS cortical neurons stained for MAP2 (red) and piccolo (green). Quantitative image analysis of piccolo puncta in WT1, WT2, FUS1 and FUS2 neurons. Data represent mean piccolo puncta per 10 µm ± SEM. Significance levels were determined by one-way ANOVA. *n* = 5 neurites per cell from > 10 cells in 2 independent experiments.

In order to verify whether FUS mutant neurons show alterations in the number of glutamatergic synapses, the expression of VGLUT1 was assessed. VGLUT1 is a glutamate transporter in the membrane of synaptic vesicles and a marker of glutamatergic neurons.

FUS and WT neurons displayed comparable density of VGLUT1 puncta (Fig. 5.11). (WT1 = 0.84 ± 0.10; WT2 = 0.89 ± 0.07; FUS1 = 0.72 ± 0.08; FUS2 = 0.82 ± 0.08).

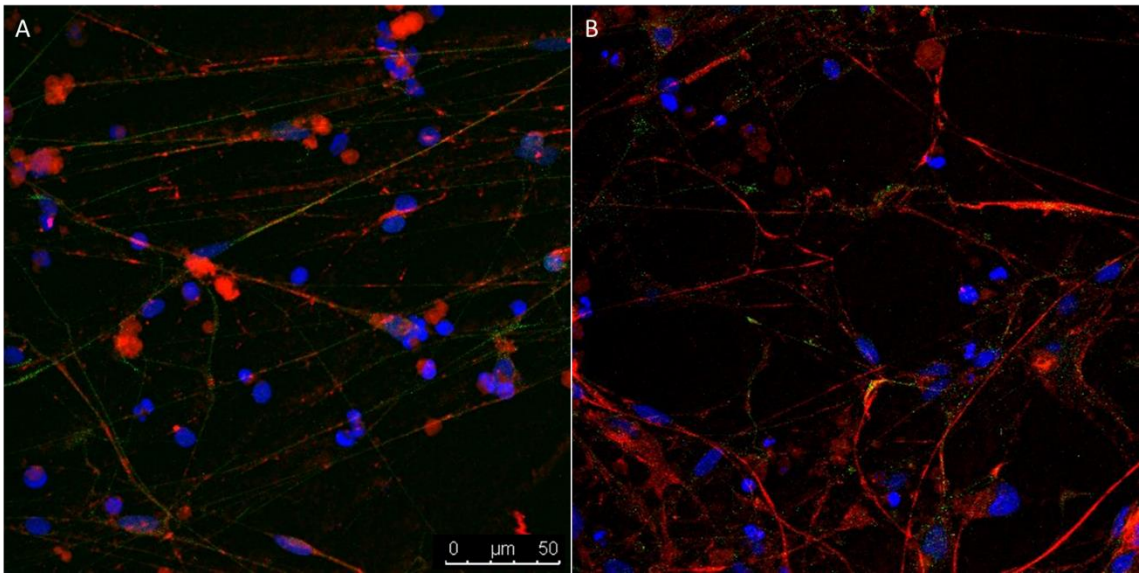

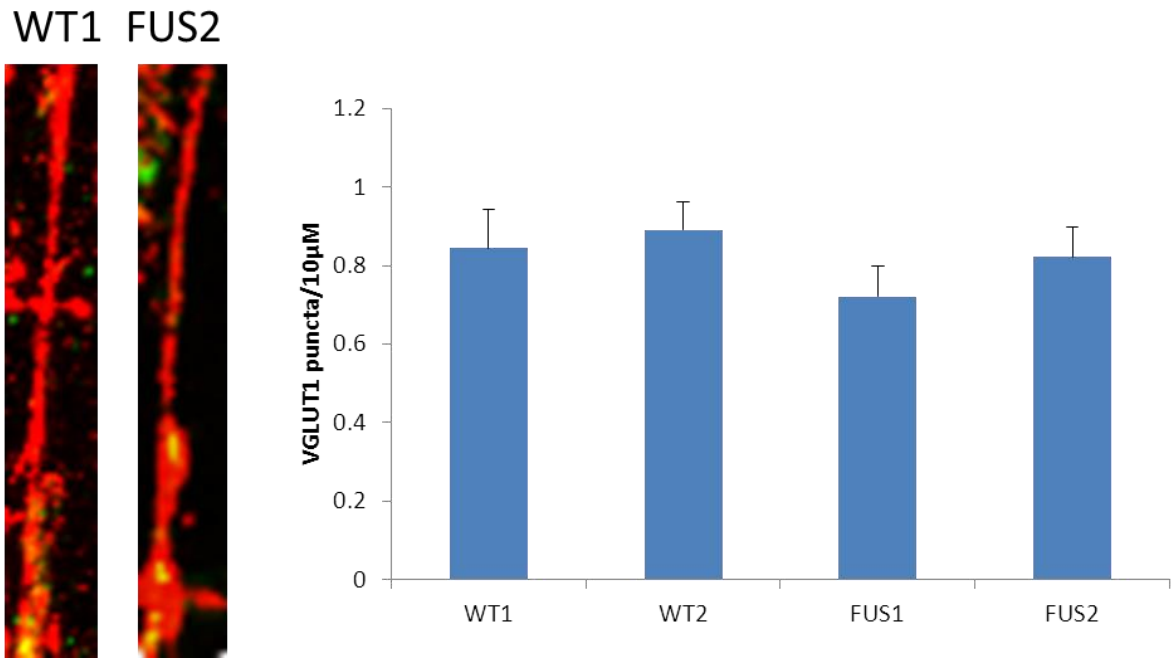

Figure 5.11. Confocal images of A) WT and B) FUS cortical neurons stained for MAP2 (red) and VGLUT1 (green). Quantitative image analysis of VGLUT1 puncta in WT1, WT2, FUS2 and FUS2 neurons. Data represent mean VGLUT1 puncta per 10 µm ± SEM. Significance levels were determined by one-way ANOVA. *n* = 5 neurites per cell from > 10 cells in 2 independent experiments.

The expression of synapsin 1, a phosphoprotein associated with small synaptic vesicles and involved in binding presynaptic vesicles to components of the cytoskeleton, was assessed in mutant FUS and WT neurons (Fig. 5.12). Mutant FUS neurons had an increased density of synapsin puncta when compared to WT neurons (WT1 = 1.35 ± 0.12; WT2 = 1.12 ± 0.10; FUS1 = 2.50 ± 0.16; FUS2 = 3.17 ± 0.21; WT1 vs WT2, not significant; WT1 vs FUS1, $P < 0.001$; WT1 vs FUS2, $P < 0.001$; WT2 vs FUS1, $P < 0.001$; WT2 vs FUS2, $P < 0.001$; FUS1 vs FUS2, $P = 0.02$).

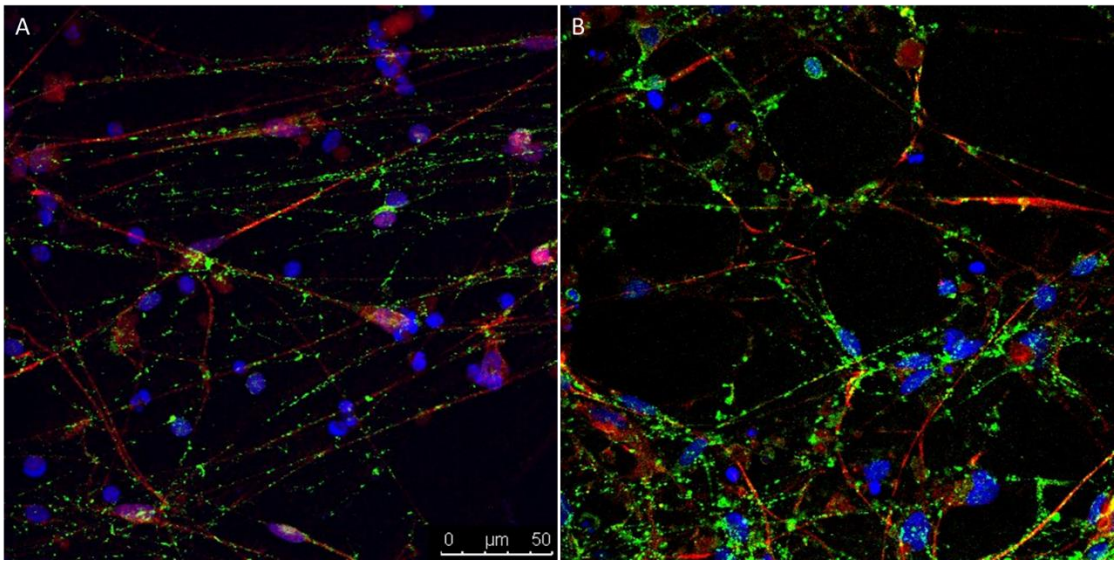

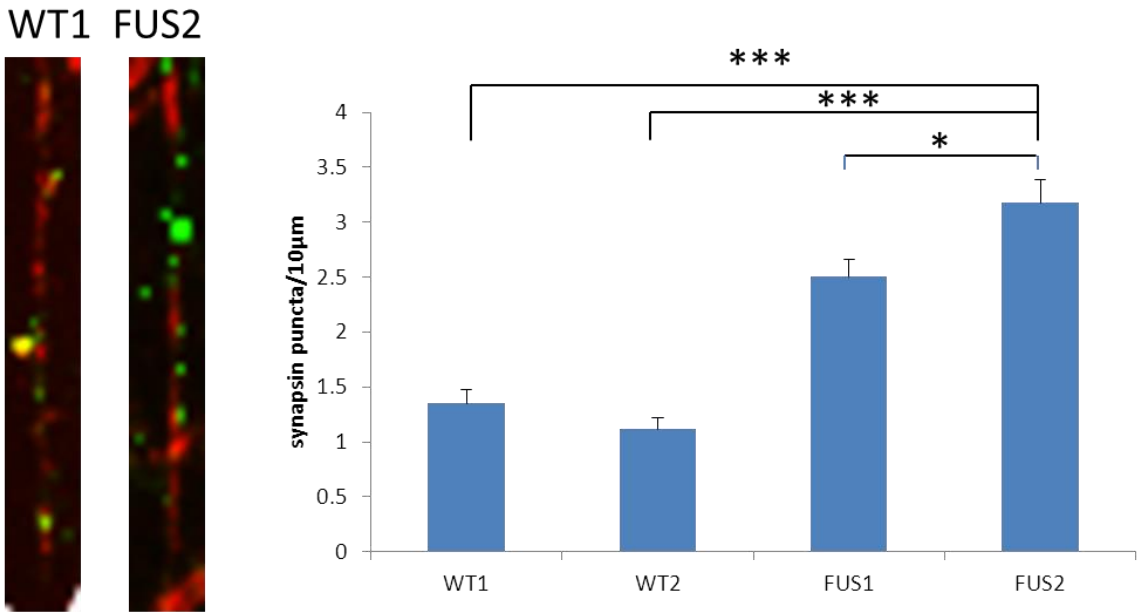

Figure 5.12. Confocal images of A) WT and B) FUS cortical neurons stained for MAP2 (red) and synapsin (green). Quantitative image analysis of synapsin puncta in WT1, WT2, FUS2

and FUS2 cortical neurons. Data represent mean synapsin puncta per 10 µm ± SEM. Significance levels were determined by one-way ANOVA and post-hoc Tukey test. Significance of difference between iPSC lines (* $P < 0.05$; ** $P < 0.0001$). $n = 5$ neurites per cell from > 10 cells in 2 independent experiments.

Finally, the expression of postsynaptic marker PSD95 was also assessed in FUS and WT neurons (Fig. 5.13). FUS neurons had an increased density of PSD95 puncta compared to WT neurons (WT1 = 1.11 ± 0.09; WT2 = 1.44 ± 0.10; FUS1 = 2.10 ± 0.11; FUS2 = 2.11 ± 0.14; WT1 vs FUS1, $P < 0.001$; WT1 vs FUS2, $P < 0.001$; WT2 vs FUS1, $P < 0.001$; WT2 vs FUS2, $P < 0.001$; FUS1 vs FUS2, not significant). WT2 neurons also had an increased density of PSD95 puncta compared to WT1 neurons (WT1 vs WT2, $P = 0.02$).

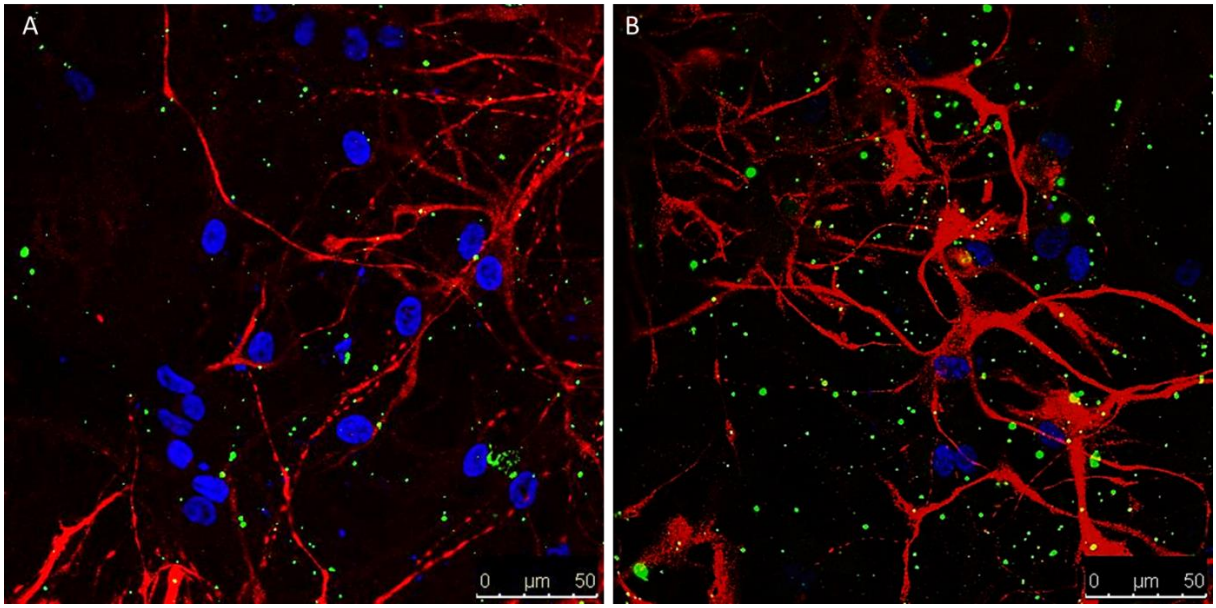

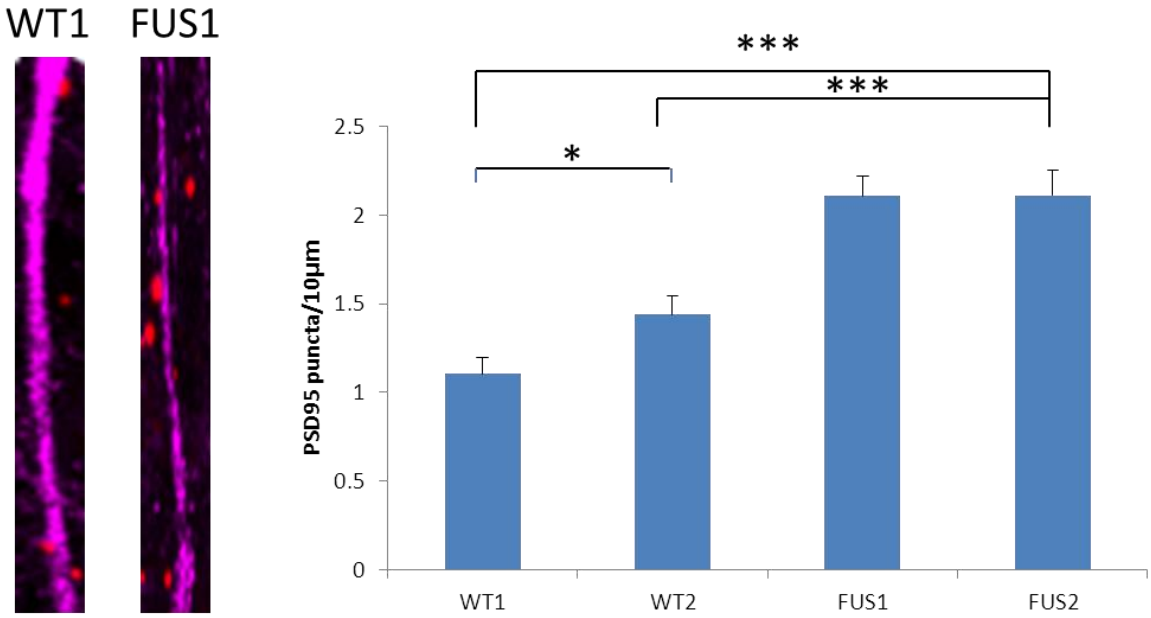

Figure 5.13. Confocal images of Confocal images of A) WT and B) FUS cortical neurons MAP2 (red) and PSD95 (green). Quantitative image analysis of PSD95 puncta in WT1, WT2, FUS2 and FUS2 neurons. Data represent mean PSD95 puncta per 10 µm ± SEM. Significance levels were determined by one-way ANOVA and post-hoc Tukey test. Significance of difference between iPSC lines (* $P < 0.05$; *** $P < 0.001$). $n = 5$ neurites per cell from > 10 cells in 2 independent experiments.

5.4 Discussion

In this chapter, I described the investigation of neurite and synapse morphology in neurons derived from mutant FUS patient and control WT iPSC lines. We first assessed the dendritic morphology in iPSC neurons by analyzing the total length of dendrite outgrowth, the number of processes and their branches, and quantifying the density of dendritic protrusions. In order to validate these findings, we explored the effect of expressing other ALS-associated FUS mutations on neurite outgrowth of transiently transfected WT iPSC-derived neurons. Lastly, we investigated the abundance and distribution of several pre- and post-synaptic proteins.

Mutant FUS neurons demonstrate a reduction in total number and length of dendrites and the complexity of their dendritic arbor compared to WT neurons. FUS

neurons also show a reduction in the number of dendritic protrusions compared to WT neurons. Interestingly, mild variability in the neuronal morphology between the two cell lines derived from both the control and mutant FUS case. WT1 neurons had a greater number of dendritic protrusions compared to WT2 neurons. While both FUS iPSC lines had comparable mean outgrowth and processes, FUS2 neurons had more dendritic branches than FUS1 neurons. As discussed in Chapter 4, the FUS iPSC lines also showed variability in the cytoplasmic distribution of FUS protein. Since FUS regulates neuronal morphology, variation in the levels of FUS protein may lead to changes in dendritic morphology, but in this instance it is impossible to draw a causal connection.

While we have shown that the expression of endogenous mutant FUS protein is associated with abnormal dendrite outgrowth and complexity, it is not known whether axonal morphology is equally affected in our iPSC-derived motor neurons. Previous studies have shown that not all neurite processes in iPSC-derived neurons are MAP2-positive, with some overlap between MAP2 and TuJ1-positive neurites, but also some neurites staining exclusively for MAP2 or TuJ1 (Ricciardi et al., 2012). It would be of interest to carry out a more detailed neurite outgrowth analysis with combined MAP2 and TuJ1 staining, to determine whether expression of endogenous mutant FUS in iPSC-derived motor neurons has a general effect on neuronal cytoskeleton, or whether it is specific to dendritic outgrowth.

The expression of several other ALS-associated FUS mutants (Q519E, R514G and R521G) in neurons derived from the WT2 iPSC line also showed a 50% reduction in the total length of neurites. Interestingly, while the expression of FUS K510X leads to reduced neurite outgrowth compared to the expression of EGFP only, the amount of neurite outgrowth was not significantly different from the amount of neurite outgrowth in neurons expressing FUS WT. The K510X mutation generates truncated FUS protein lacking the nuclear localisation signal and is associated with almost exclusive cytoplasmic localisation (Vance et al. 2013). This observation suggests that the abnormal neuronal morphology associated with mutant FUS may be mediated by the nuclear localisation of

the mutant protein. Intriguingly, a recent genetic study discovered a novel mutation in *CREST*, a gene that encodes a neuronal chromatin remodeling complex component (Chesi et al. 2013). This study showed that *CREST* mutations inhibit activity-dependent neurite outgrowth and that CREST and FUS physically interact in mouse cortical neurons (Chesi et al. 2013). These findings and our observations suggest that mutations in *CREST* or *FUS* may impair interaction with other transcriptional regulators, resulting in transcriptional dysregulation, abnormal neurite outgrowth and subsequent motor neuron degeneration.

It should be noted that there are limitations to studies involving the transient expression of proteins. The constructs used in this thesis have been published previously, and have shown similar levels of expression in primary cortical neurons and cell lines (Vance et al., 2009). We have not used immunoblotting to quantify the levels of transiently expressed wild-type and mutant HA-FUS protein here due to the low transfection efficiency and the large amount of protein required; therefore, we cannot confirm that WT and mutant protein are expressed at the same levels in the iPSC-derived neurons used in this study. Another issue to address is that in the Vance et al. (2009) study, all cells were used for experiments 1-2 days after transfection. As such, it is not known whether WT and mutant proteins have similar levels of stability. Despite these issues, we have observed a similar neurite outgrowth defect in iPSC neurons overexpressing ALS-associated *FUS* mutations. It would be of interest to confirm these data in other iPSC lines derived from patients with these mutations or to use genome editing technology to generate iPSC lines with these mutations, so as to study the effects of endogenous protein.

Both mutant FUS and WT neurons demonstrate strong expression of the four pre- and postsynaptic proteins assessed in this study. This data indicate that iPSC-derived neurons exhibit a clustering of synaptic molecules and imply that these neurons are functionally mature and capable of synaptic activity. FUS and WT neurons show differences in the morphology of specific synaptic markers. The density of piccolo puncta and VGLUT1 puncta were comparable between WT and FUS neurons indicating that the synaptic active zone may be intact and the transport of glutamate vesicles are normal in

both lines. In contrast, FUS neurons have a greater density of synapsin puncta compared to WT neurons. Synapsins are neuron-specific phosphoproteins that interact with synaptic vesicles and cytoskeletal proteins, regulating the neurotransmitter release in presynaptic neurons. Alterations in synapsin function result in abnormal neuronal activity and synaptic transmission (Llinás et al. 1991). Thus, FUS R521C-mediated alterations in the density of synapsin puncta may, in turn lead to aberrant synaptic transmission and contribute to the hyperexcitability observed in ALS patients and in FUS iPSC-derived neurons (Wainger et al. 2014).

Mutant FUS neurons also have a greater density of PSD-95 puncta along their neurites compared to WT neurons. PSD-95 has previously been shown to play a role in regulating dendrite outgrowth and branching, in addition to its role in dendritic spine formation and the anchoring of synaptic signaling molecules. Charych et al. (2006) showed that overexpression of PSD-95 leads to a decrease in the number of secondary dendrites, whereas knockdown of PSD-95 resulted in an increase of primary and secondary dendrites (Charych et al. 2006). Thus, the change in the density of PSD-95 puncta in FUS neurons may be associated with the reduced neurite outgrowth observed in mutant FUS neurons.

Increased immunoreactivity in PSD95 has previously been reported in postmortem brain samples from Alzheimer's disease patients (Leuba et al. 2008). This study showed that the increased expression of PSD95 was specific, as expression of other pre- and postsynaptic proteins were unchanged. The change in PSD95 expression was accompanied by an increase in MAP2 expression (Leuba et al. 2008). Similarly, reductions in several pre- and postsynaptic markers are also observed in brain tissue from dementia patients (Kramer and Schulz-Schaeffer 2007). These results suggest that neurite and synaptic reorganisation may be a common feature of neurodegenerative disorders.

It has previously been shown that in Alzheimer's disease, the widespread loss of synapses is associated with enlargement of synaptic size, suggesting a compensatory response (Scheff et al. 1990). In this study, we have observed an increase in the density of

PSD95 puncta in mutant FUS neurons compared to WT neurons, which may reflect a compensatory response. Since mutant FUS neurons are also characterised by fewer dendritic processes than WT neurons, the few remaining dendrites may express more PSD95 or show increased clustering of PSD95 to compensate for the overall loss of synaptic contacts. A similar compensatory effect has been reported in hippocampal CA3 pyramidal neurons of stressed rats, where increased density of spines were associated with decreased number of dendritic branches (Rao and Raju 1995).

It is also possible that the increased density of synapsin I and PSD95 puncta in FUS neurons may reflect impaired degradation of these proteins. The degradation of PSD95 is mediated by the ubiquitin-proteasome system (UPS) (Colledge et al. 2003). Impairment in this protein degradation system as a result of toxic aggregation of SOD1 has been previously described in a SOD1 mouse model of ALS (Cheroni et al. 2005). It is possible that mutant FUS also impairs UPS function and that increased levels of PSD95 are due to impaired degradation. Synapsin I expression is regulated by fucose-α(1-2)-galactose carbohydrates, as the binding of these carbohydrates to synapsin I inhibits degradation by calcium-dependent protease calpain (Murrey et al. 2006). A role for calpain-dependent cleavage has previously been implicated in several neurodegenerative disorders. Higher levels of calpains are observed in the motor neuron degeneration (mnd) mutant mouse, which exhibits progressive dysfunction of the spinal cord and brain (Li et al. 1998). In addition, calcium influx and the activation of calpain are involved in axonal degeneration (George et al. 1995). Alterations in the calpain system may affect expression levels of synapsin I, alter synaptic activity and could therefore contribute motor neuron degeneration.

In summary, we have investigated the effects of mutant FUS on of neurite outgrowth, arborisation, dendritic protrusion and synapse morphology in neurons derived from patient iPSC lines. iPSC-derived neurons expressing R521C mutant FUS show a reduction in the length and complexity of neurites and dendritic protrusions. This effect was also seen following the expression of several other ALS-associated FUS mutations in

neurons derived from the WT iPSC line which confirms that this phenotype is associated with mutant FUS. In addition, mutant FUS neurons display abnormal synapses and significant alterations in the abundance and localisation of PSD-95 and synapsin. Therefore, the FUS R521C mutation is associated with abnormal neuronal and synaptic morphology which may well have a detrimental effect on neuronal health in motor neurons which have the longest axons and therefore the greatest challenge in maintaining synaptic health.

CHAPTER 6

CONCLUSION

6.1 SUMMARY

The experiments described in this thesis used human stem cells derived from ALS patients to explore the effects of ALS causing FUS mutations on neurons as a model of disease and to investigate the mechanisms underlying disease pathogenesis (Fig. 6.1). I have shown that differentiated motor neurons expressing mutant FUS at physiological levels recapitulate several key features of FUS-associated ALS pathology.

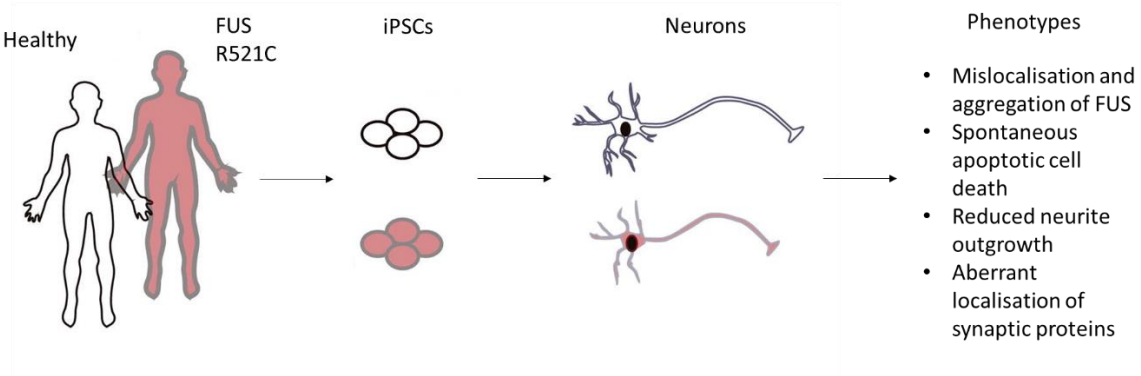

Figure 6.1 Schematic of patient-specific iPS cellular model of FUS-associated ALS (Figure adapted from Kiskinis et al., 2014).

Our initial hypothesis for the project was to determine whether mutant FUS protein in iPSC-derived neurons would show a similar propensity to mislocalise and aggregate as had previously been shown in transfected cell lines and primary neurons (Vance et al. 2013). Neurons and neural progenitors derived from mutant FUS iPSCs show a shift in FUS protein abundance from the nucleus to the cytoplasm and the recruitment of FUS protein into cytoplasmic stress granules following oxidative stress. Neural progenitors derived from mutant FUS iPSCs have an increased propensity to undergo spontaneous apoptotic cell death compared to those derived from WT iPSCs. Furthermore, mature neurons expressing mutant FUS exhibited an abnormal axo-dendritic morphology

and differences in localization of certain synaptic proteins, which may contribute to neurodegeneration in ALS.

6.2 FUS MISLOCALISATION AND AGGREGATION

I have shown that neurons differentiated from mutant FUS iPSC lines show a significant increase in FUS protein levels in the cytoplasm and decreased levels in the nucleus compared to neurons differentiated from control WT iPSC lines. A 1.3 fold or more of cytoplasmic FUS expression was consistently found in mutant FUS neurons than in WT neurons. Mutant FUS neurons also had lower levels of nuclear FUS than WT neurons, although one mutant FUS line did not quite reach statistical significance. I have also shown that mutant FUS protein is redistributed into cytoplasmic stress granule in neural progenitors differentiated from mutant FUS iPSC lines following acute oxidative stress. Mutant FUS neural progenitors had at least 3.7-fold or more FUS particles that colocalised with PABP1 particles compared to WT neural progenitors. In addition, mutant FUS neural progenitors consistently had 4-fold more FUS-positive granules and double the number of stress granules than WT neural progenitors.

These findings are consistent with studies using transfected cell lines, primary neurons and patient fibroblasts (Bosco et al. 2010; Dormann et al. 2010; Vance et al. 2013). These studies demonstrated that ALS-linked *FUS* mutations disrupt the nuclear localizing signal to impair nuclear import, resulting in increased cytoplasmic localization of FUS protein and decreased nuclear FUS. Furthermore, they showed that oxidative stress recruits mutant FUS to cytoplasmic stress granules (Bosco et al. 2010; Dormann et al. 2010; Vance et al. 2013). Pathologic inclusions in ALS patients with *FUS* mutations and FTD-FUS patients also contain marker proteins of stress granules (Dormann et al. 2010), providing support for its relevance to ALS pathology. It is believed that these two pathological hits, nuclear import defects and cellular stress, are involved in the pathogenesis of ALS through the formation of cytoplasmic aggregates, which sequester

FUS, disrupt RNA processing and initiate motor neuron degeneration (Dormann et al. 2010; Vance et al. 2013).

Our findings show that mutant FUS protein in iPSC-derived neurons and neural progenitors also mislocalise and aggregate in a similar manner to transfected cells. We also found that mutant iPSC-derived neural progenitors show differences in the abundance of stress granules compared to WT iPSC-derived neural progenitors following oxidative stress. This observation is in line with a previous report showing that expression of mutant FUS is associated with increased stress granule size and number and a toxic gain of function mechanism of mutant FUS in stress granule dynamics and cellular stress response (Baron et al. 2013)

6.3 Cellular toxicity and vulnerability

I have found that mutant FUS neural progenitors showed an increase in spontaneous and acute oxidative stress induced apoptotic cell death. In untreated cultures, mutant FUS neural progenitors had more than double the percentage of cells undergoing early apoptotic cell death and approximately double the percentage of cells undergoing late apoptotic cell death compared to WT neural progenitors. After acute treatment with arsenite, mutant FUS neural progenitors also had greater percentages of cells undergoing early apoptotic cell death, although only one mutant FUS line reached statistical significance. Mutant FUS neural progenitors also had greater percentages of cells undergoing late apoptotic cell death compared to WT neural progenitors following acute arsenite treatment, but this difference was not significant.

The toxicity of FUS-related neurodegeneration has been reported in a number of animal models. Expression of human FUS in yeast causes the formation of FUS immunoreactive aggregates and cytotoxicity (Fushimi et al. 2011; Sun et al. 2011). Similarly, transgenic models of FUS expression in the fruit fly, nematode, zebrafish, rat and mouse have established that elevated levels of WT and mutant FUS results in motor defects and neurodegeneration (Chen et al. 2011; Huang et al. 2011; Kabashi et al. 2011;

Lanson et al. 2011; Murakami et al. 2011; Mitchell et al. 2013). Although some suggest that the toxic aggregation of FUS protein is necessary to confer toxicity, others have found that knockdown of FUS also leads to neurodegeneration (Kabashi et al. 2011; Wang et al. 2011). Thus, there is evidence for both gain of toxic function and loss of function mechanisms underlying FUS-mediated neurodegeneration.

As shown by FACS analysis, mutant FUS neural progenitors exhibited increased spontaneous and acute oxidative stress induced apoptotic cell death, suggesting selective cellular toxicity of the mutation in neural progenitors. It is not known how physiological levels of mutant FUS leads to cellular toxicity. Apoptosis of neural progenitors is regulated by pro- and anti-apoptotic signaling factors, including an inhibitor of atypical PKCζ, prostate apoptosis response 4 (PAR-4) (Bieberich et al. 2003). Overexpression of FUS has previously been shown to promote growth inhibition and apoptosis of prostate cancer cell by altering the levels of proliferative and anti-proliferative factors (Brooke et al. 2011). Whether this finding translates to neuronal cell types is not known. An understanding of the effect of mutant FUS on pro- and anti-apoptotic signaling factors might be relevant to ALS since cellular models of ALS indicate that cells expressing mutant proteins are likely to die by apoptosis (Lee et al. 2013).

It may also be of interest to investigate the consequences of increased spontaneous cell death in mutant FUS neural progenitors. In human cortical development, neurons are produced temporally by the sequential generation of preplate neurons, deep layer neurons, followed by the superficial layers. In order to generate these diverse neuronal cell types, a pool of cortical progenitors are maintained during development by asymmetric divisions. The spinal cord also consists of diverse neuronal cell types, which differentiate from progenitor cells according to inductive signals (Ericson et al., 1997). Increases in spontaneous cell death may affect the maintenance of the pool of progenitors, subsequently altering the generation of different neuronal subtypes and neural circuits to impact neuronal function and motor behavior.

6.4 NEURITE OUTGROWTH

I have shown that mutant FUS neurons demonstrate a reduction in total length and number of neurites compared to WT neurons. Motor neuron-containing neural populations derived from mutant FUS iPSC lines had ~50% decrease in the mean outgrowth per cell, ~40% decrease in the number of dendritic processes and ~50% decrease in the number of dendritic branches compared to WT motor neuron-containing neural populations. In addition, the expression of several other ALS-associated FUS mutants (Q519E, R514G and R521G) in WT neurons also showed a 50% reduction in the total length of neurites.

An important next step is to understand the role of mutant FUS in mediating these structural differences and the functional consequences of such abnormalities. Defects in neurite outgrowth have previously been reported in several FUS and TDP-43 animal and iPSC models of ALS (Kabashi et al. 2011; Egawa et al. 2012). Reduced axonal outgrowth and branching in zebrafish is associated with a deficient touch-evoked escape response (Kabashi et al. 2011). Thus, reduced neurite outgrowth may impair the strength and stability of connections between neurons in the central nervous system and at the NMJ, which may in turn contribute to ALS.

Neurite outgrowth depends on a complex interplay between extracellular guiding cues and intracellular signaling pathways. Extracellular cues are detected by molecules expressed on the surface of neurons, and transduced to activate cell signaling and gene transcription inside the cell (Hansen et al. 2008). This interplay results in alterations in cytoskeletal dynamics and membrane trafficking that generates neurite outgrowth. There are several ways by which mutant FUS could affect neurite outgrowth. Based on its role in RNA transport and local translation, FUS could alter the normal expression of cell surface molecules or signal transduction components and thereby impair the detection and transduction of extracellular cues. Alternatively, it could reduce the transcription of cytoskeletal molecules to reduce the scaffolding required for neurite outgrowth.

FUS depletion has been shown to down-regulate a number of genes involved in cell surface receptor linked signal transduction, including the cadherins and neuroligins (Lagier-Tourenne et al. 2012). They also showed that FUS binding is enriched for mRNA encoding structural components in neuronal projections, such as neurofilaments and microtubule-associated protein tau (Lagier-Tourenne et al. 2012). Whether ALS-linked FUS mutants impact the expression of these proteins in the same way is unknown. However, Hoell et al. (2011) showed that the RNA binding pattern of FUS reflects its subcellular localization. While mutant FUS proteins maintained their RNA-binding capability and specificity, mutant FUS proteins had an increased interaction with cytoplasmic RNA targets compared to WT FUS (Hoell et al. 2011). These findings suggest that ALS-linked FUS mutants that lead to a decrease in nuclear FUS and an increase in cytoplasmic FUS might alter RNA transcription, editing, trafficking and translation of genes involved in regulating neurite outgrowth. We have not investigated this hypothesis in this thesis due to time limitations; however, it is an important question to address and may explain the specific vulnerability of motor neurons to *FUS* mutations.

Altered neuronal microRNA biogenesis may be another mechanism through which mutant FUS gives rise to abnormal neuronal morphology. MicroRNAs are small non-coding RNAs that function in translational regulation. MicroRNAs are brain-enriched and have a key role in neuronal development and neurodegeneration (Nelson et al. 2008). FUS was recently shown to participate in the biogenesis of a specific subset of neuronal microRNAs (Morlando et al. 2012). The reduction of FUS in the nucleus would inhibit the association of FUS and target microRNAs, as well as the association of FUS and Drosha, a protein necessary for the processing of microRNAs (Morlando et al. 2012). Reduced nuclear FUS, due to mutations affecting the nuclear localisation signal, could affect the processing of microRNAs, leading to translational dysregulation and abnormal neurite outgrowth.

It must also be noted that other ALS-linked mutants have been implicated in neuronal morphology. Mutations in the neuronal chromatin remodeling complex component CREST, which inhibits activity-dependent neurite outgrowth, were recently

identified in ALS patients, (Chesi et al. 2013). Similarly, mutant TDP-43 iPSC-derived motor neurons show reduced neurite outgrowth and a decrease in expression of genes encoding components of cytoskeletal intermediate filaments and neurofilaments (Egawa et al. 2012). Both TDP-43 and CREST are known to interact with FUS. Taken together, these studies suggest a link between reduced neurite outgrowth and ALS-linked genetic mutations. Alterations in the cytoskeleton may have a tremendous impact on a cell such as the motor neuron, due to its highly polarised morphology and vast axonal length. Therefore, an important avenue to explore is the impact of genetic mutations on the factors that regulate neurite outgrowth, in order to find the mechanistic basis responsible for this abnormal neuronal morphology.

In this study, we have found that neurons derived from mutant FUS iPSCs show reduction in the number and length of neurites, and that the expression of other ALS-associated FUS mutants in WT neurons also leads to a reduction in the length of neurites. These abnormalities might be expected to impair the strength and stability of connections between neurons in the central nervous system and at the NMJ. Several lines of evidence provide support for a role of FUS in the regulation of neuronal morphology. Hippocampal neurons from FUS-deficient mice have irregularly branched dendrites and abnormal axonal processes (Fujii et al. 2005). Similarly, knockdown of FUS in hippocampal neurons also results in reduced axon length and abnormal growth cone morphology (Orozco et al. 2012). Defects in neurite outgrowth have previously been reported in several FUS and TDP-43 animal and iPSC models of ALS, as well as primary mouse cortical neurons (Kabashi et al. 2011; Egawa et al. 2012; Groen et al. 2013). Since motor neurons are the most polarized cells in the body, with some axons reaching a meter in length, abnormal neuronal morphology might be especially relevant to ALS.

6.5 SYNAPTIC MORPHOLOGY AND TRANSMISSION

Another observation I made was that neurons differentiated from mutant FUS iPSC lines exhibited abnormal synaptic spine abundance and morphology. Mature neurons

derived from mutant FUS iPSC lines showed a decrease in the density of dendritic protrusions compared to mature neurons derived from WT iPSC lines. They also show an alteration in the abundance of two of the synaptic proteins investigated in this study. In particular, mature neurons derived from mutant FUS iPSC lines showed a greater density of synapsin and PSD95 puncta along dendrites compared to mature neurons derived from WT iPSC lines. Such alterations are likely to affect synaptic transmission For instance, an increase in numbers of synaptic puncta is observed in late phase long-term potentiation, a strengthening of synaptic efficacy is believed to be an important cellular mechanism for memory formation (Bozdagi et al. 2000).

There is strong evidence for disturbances in synaptic physiology in ALS. Fasciculations, which are spontaneous involuntary muscle fibre contractions are a key diagnostic sign of lower motor neuron dysfunction in ALS and indicate that there are major disturbances in membrane excitability. Ultrastructural examination of muscle biopsies from ALS patients shows increased calcium and increased numbers of synaptic vesicles (Siklos et al. 1996). Aggregated synaptic vesicles are also observed in the motor cortex of ALS patients (Sasaki and Iwata 1996). These significant synaptic changes occur throughout the motor system and imply major synaptic dysfunction in the central and peripheral nervous system.

There is further evidence from animal models that disturbed physiology plays an important part in the disease process. Slice preparations from transgenic SOD1 mice exhibit motor neuron hyperexcitability, enhanced spontaneous excitatory and inhibitory transmission (van Zundert et al. 2008). Hyperexcitability, along with reduced synaptic fidelity has also been shown in transgenic TDP-43 zebrafish (Armstrong and Drapeau 2013). Similarly, transgenic FUS zebrafish exhibit a motor phenotype with reduced synaptic fidelity and reduced NMJ transmission (Armstrong and Drapeau 2013). These data have recently been recapitulated in iPSC models of ALS. Wainger et al. (2014) reported that motor neurons from iPSC lines derived from patients with *SOD1, FUS* and *C9ORF72* mutations exhibit hyperexcitability, possibly due to altered ratios of ion

channels. Patient-specific iPSC-derived neurons could provide an important opportunity to investigate how defects in synaptic transmission may contribute to motor neuron degeneration.

One way by which mutant FUS could contribute to alterations in the density of PSD95 and synapsin puncta is by impairing transport and localised translation of mRNA. FUS has previously been implicated in the activity-dependent transport of mRNA to dendritic spines, which are the major sites of synaptic transmission. Upon glutamatergic activation, there is an increase in the dendritic localisation of the ND1-L mRNA transcript, which encodes an actin-stabilising protein (Fujii and Takumi 2005). FUS-deficient hippocampal neurons show a reduction in the ND1-L transcript the dendrites following glutamatergic activation, and may regulate neuronal actin cytoskeleton by supplying Nd1-L mRNA to the local translational machinery in dendrites (Fujii and Takumi 2005).

It is not known whether this activity-dependent transport is transcript-specific or a general mechanism for local translation. Since FUS has been shown to bind to thousands of mRNA species, it may be that FUS participates in the general transport of synaptic mRNA to dendritic spines. An important question to address is whether *FUS* mutations may affect the transport of transcripts critical for synaptic function. It has recently been shown that ALS-linked *TARDBP* mutations lead to impaired transport of RNA granules in motor neuron axons (Alami et al. 2014). It is therefore possible, that *FUS* mutations also impact the transport of RNA granules in motor neuron dendrites to alter local translation of synaptic components.

Another way that mutant FUS could contribute to alterations in the density of synaptic puncta is by promoting the translation of their transcript. Components of the translation machinery are located in dendritic spines, and local protein synthesis in dendrites is required for the rapid enhancement of synaptic transmission induced by exposure to the growth factor BDNF (Santos et al. 2010). FUS is localized in APC-RNP granules in cellular protrusions (Yasuda et al. 2013). These granules target RNA to cell protrusions for the translation of associated transcripts. The expression of *FUS* mutations

facilitated the formation of granules, which were also the sites for local translation (Yasuda et al. 2013). Another question to address is the effect of FUS mutations in a neuronal context, whether the local translation of transcripts is impaired in neurite protrusions of ALS motor neurons.

In this study, we have found that mature neurons derived from mutant FUS iPSCs show alterations in the density of synapsin and PSD95 puncta. These abnormalities might be expected to perturb synaptic physiology and neuronal transmission. Wainger et al. (2014) recently reported that motor neurons derived from mutant FUS iPSCs, as well as mutant SOD1 and C9ORF72 iPSC lines, were hyperexcitable compared to motor neurons derived from WT iPSCs. They further described sensitivity to potassium channel agonists across these mutant iPSC lines (Wainger et al. 2014). It is not known how these different genetic mutations converge to give rise to hyperexcitability. However, this phenotype appears to be broadly relevant to familial ALS, and may also relate to the major disturbances in membrane excitability found in ALS patients.

6.6 iPSCs AS A TOOL FOR DISEASE MODELLING

This study used human stem cells derived from an ALS patient and age-matched control individuals to explore the effects of ALS causing FUS mutations on neuronal populations as a model of disease and to explore underlying disease mechanisms. I have shown that differentiated motor neurons and neural progenitors expressing mutant FUS at physiological levels recapitulated several key features of FUS-associated ALS pathology. Neurons and neural progenitors derived from mutant FUS iPSCs show a shift in FUS protein abundance from the nucleus to the cytoplasm and the recruitment of FUS protein into cytoplasmic stress granules following oxidative stress. Neural progenitors derived from mutant FUS iPSCs have an increased propensity to undergo spontaneous and oxidative stress induced apoptotic cell death compared to those derived from WT iPSCs. Furthermore, neurons expressing mutant FUS exhibited a reduction in total number and length of neurite outgrowth and dendritic protrusions. Mature neurons derived from

mutant FUS iPSCs also show abnormal synaptic morphology, with alterations in the density of PSD95 and synapsin puncta along dendrites.

Since the initiation of this project, several studies have described iPSC models of ALS, using fibroblasts from patients with mutations in *TARDBP*, *C9ORF72* and *SOD1*. We have previously shown that motor neurons derived from an ALS patient carrying a TDP-43 mutation recapitulated several cellular and molecular abnormalities associated with ALS pathology, including mislocalisation from the nucleus to the cytoplasm, protein fragmentation, the formation of insoluble TDP-43 aggregates and spontaneous cell death in prolonged culture (Bilican et al. 2012). Subsequently, Egawa et al. (2012) reported the same cellular phenotypes in iPSC lines derived from multiple patients with TDP-43 mutations and identified a compound that rescued the abnormal ALS phenotype.

Almeida et al. (2013) was the first to report an iPSC model of C9ORF72 ALS and showed that perturbation in autophagy may contribute to pathogenesis. Another study quickly followed and reported abnormal electrophysiology in motor neurons differentiated from C9ORF72 iPSCs and the use of antisense oligonucleotides to rescue the motor neuron phenotype (Sareen et al. 2013).

Recently, two independent groups combined iPSC technology with genome editing to study SOD1 iPSCs and determine the pathogenicity of the mutation. Chen et al. (2014) identified abnormal dysregulation of neurofilament and neurite degeneration due to SOD1 mutations; whereas Kiskinis et al. (2014) found mitochondrial defects, along with induction of ER stress and unfolded protein response pathways. Importantly, both showed the prevention of these phenotypes by the genetic correction of the SOD1 mutation (Chen et al. 2014; Kiskinis et al. 2014). For the first time, this enabled the demonstration of causal connections between mutations and functional phenotypes.

To our knowledge, this study is the first to describe an iPSC model of ALS using fibroblasts from a patient with *FUS* mutation. Similar to the aforementioned studies, our iPSC model of FUS ALS also recapitulated several cellular abnormalities associated with ALS pathology, namely mislocalisation and aggregation of FUS protein and spontaneous

apoptotic cell death. Our finding that mature neurons derived from mutant FUS iPSCs exhibited abnormal axo-dendritic and synaptic morphology suggests that *FUS* mutations may contribute to pathogenesis through perturbations in neuronal cytoskeleton and neurophysiology.

6.7 LIMITATIONS

The current study was limited by the cellular resource as we had access to two iPSC lines derived from a single patient carrying the FUS R521C mutation and two iPSC lines from unrelated age-matched control individuals. All lines were generated from fibroblasts and reprogrammed in the same laboratory at the same time using an identical methodology. Despite these limitations, we were able to identify FUS-specific disease phenotypes in the FUS R521C lines and undertake an early exploration of pathogenic mechanisms. We have now generated three subclones of another iPSC line from a patient with the FUS R514G mutation and have recently begun to carry out cell-lineage and functional studies, as well as characterizing ALS-associated phenotypes in these lines. Unfortunately time constraints do not permit the generation of sufficient replicated data to be included in this thesis.

Another limitation of this project is phenotypic variability arising from *in vitro* differentiation. We and others working in the field consistently observe heterogeneity of cellular populations through all stages of differentiation. It is possible that subtle differences in the percentage of cells at different stages of maturation could result in non-cell autonomous effects that are not accounted for. When this study began, we used an established protocol for differentiation of iPSCs to motor neurons that eliminated the use of stromal feeders or embryoid bodies (Bilican et al. 2012). In all of our experiments, we observed that HB9-positive motor neurons comprised 20-30% of the population after differentiation. One way to enrich for motor neurons is to transfect or transduce neuronal cultures with a reporter containing a fluorescent protein under the control of a motor neuron-specific promoter (such as HB9), then using FACS to purify motor neurons. We

decided against this strategy due to the time, costs and small number of surviving cells left to conduct experiments. Alternatively, a recent study reported a highly efficient motor neuron differentiation of iPSCs, which uses three small molecule inhibitors of BMP type I receptors ALK2 and ALK3, ALK5, ALK4, ALK7 and GSK-3, to differentiate pluripotent stem cells to neuroepithelia, which were then treated with retinoic acid and purmorphamine to generate a population of differentiated cells in which ~90% were post-mitotic motor neurons (Chen et al. 2014). Thus, recent advances in motor neuron differentiation will enable the derivation of more homogenous cultures and may further reduce the source of variability.

It must be mentioned that this study aimed to model a neurodegenerative disorder with an average age of onset of 50 years. Clearly, the few months of cell culture do not compare to 50 years of aging in the adult nervous system. A potential strategy to address this limitation is to promote premature aging in cell culture. Hutchinson-Gilford progeria syndrome (HGPS) is a human premature ageing disease that is caused by a single point mutation in the lamin A gene (*LMNA*) (Eriksson et al. 2003). Mutations in *LMNA* result in the production of a shorter transcript known as progerin. Miller et al. (2013) showed that the overexpression of progerin RNA induces multiple aging-related processes and characteristics in iPSC-derived neurons. Furthermore, this study reported multiple progerin-induced neurodegenerative phenotypes in Parkinson's disease patient iPSC-derived neurons that were not observed otherwise (Miller et al. 2013). In a similar manner, overexpression of progerin RNA in mutant FUS iPSC-derived neurons could be used to accentuate ageing-related processes and provide a model of FUS-ALS with premature ageing. This would allow us to interrogate the contributions of mutant FUS and age-related processes to neurodegeneration and provide additional insights into the molecular mechanisms underlying ALS.

6.8 FUTURE DIRECTIONS

The cellular model presented in this thesis provides a novel tool to study the pathogenesis of ALS that is associated with *FUS* mutation. An important and obvious application of this resource is in its use for therapeutic discovery and drug toxicity studies. The identification of disease-specific phenotypes in neurons derived from FUS R521C iPSC lines could be used for compound screening assays for the reversal of ALS phenotypes such as cytoplasmic mislocalisation and FUS aggregation. These could be used in parallel with neurons derived from other mutant iPSC lines and from SALS patients to enable the identification of compounds that could be effective across a spectrum of ALS pathologies. In addition to the discovery of drugs that will reverse disease phenotypes, it is also important to evaluate the toxicity of potential compounds. This may be addressed by combining patient-specific iPSC lines with methods of directed differentiation of iPSCs to cardiomyocytes and hepatocytes, which are clinically important cell types for studies of drug toxicity (Dick et al. 2010). Failures in clinical trials as a result of imperfect models, such as the animal models which differ genetically and anatomically from humans, would be avoided. These efforts would reduce the time and costs of clinical trials.

Another avenue that merits further investigation is the electrophysiological properties of neurons derived from mutant FUS iPSC lines. In this thesis, we have described several synaptic morphological differences between neurons derived from mutant FUS and WT iPSC lines, namely increased density of PSD95 and synapsin puncta. We were unable to analyse the functional consequences, if any, of these differences due to time constraints. Neurophysiological recordings would enable the evaluation of a number of basic physiological characteristics of FUS mutant expressing neurons, such as action potential firing rate and spike morphology. Whole-cell patch clamp recordings would allow for a more in-depth investigation of electrophysiological properties and health, such as membrane potential, action potential threshold, as well as specific currents which determine neuronal membrane excitability. In addition, calcium imaging may also be used as a measure of neuronal electrical activity. Changes in neuronal calcium concentrations may reflect changes in a number of ion channels and neurotransmitter receptors. These

measures may then be combined with molecular biology techniques to verify whether particular channels or receptors are differentially expressed in mutant and WT neurons to contribute to perturbed synaptic morphology.

An interesting observation is the increase in the number of stress granules following arsenite treatment in FUS R521C neural progenitors. Mutant FUS has been shown to affect the dynamics of stress granules, such as the time required for assembly and resolution, the number and size of granules, and the binding affinity of stress granule proteins TIA1 and G3BP (Baron et al. 2013). The formation of stress granules is triggered by environmental stressors. These foci are composed of a number of ribonucleoproteins, including initiation factors, RNA-binding proteins, transcription factors and other molecules. Thus, another direction that warrants attention is the properties of stress granules in FUS R521C and WT neurons. It could be useful to assess the size of stress granules and to study the assembly and disassembly of stress granules in FUS R521C and WT neural progenitors. Differences in these properties may reflect changes in the binding affinity of mutant FUS for stress granule components. A comparison of stress granule-associated proteins, especially those implicated in ALS and other neurodegenerative disorders, in FUS R521C and WT neural progenitors could provide insight into how *FUS* mutations contribute to neurodegeneration by altering the dynamics of the stress granules.

FUS R521C iPSC lines may also be of value in the study of neurodegenerative conditions with FUS pathology, including FTD, Huntington's disease and spinocerebellar ataxia. The differentiation of these iPSC lines into the neuronal cell types affected in these conditions may allow us to gain insight into the cellular processes underlying these disorders. Comparisons of cortical neurons and motor neurons differentiated from these lines may also shed light on the link between FTD and ALS and how FUS contributes to the degeneration of different neuronal subtypes.

6.9 CONCLUSIONS

In this thesis we have shown that mutant FUS iPSCs recapitulate key aspects of FUS-ALS pathology, including mislocalisation of FUS protein, redistribution of FUS protein into stress granules and a propensity to undergo apoptotic cell death. Furthermore, neurons differentiated from mutant FUS iPSCs exhibit abnormal neuronal and synaptic morphology, such as reduced neurite outgrowth and altered density of selective synaptic molecules. We acknowledge the limitations of studying one mutation in iPSCs derived from a single patient and similar studies in iPSCs from patients with other FUS mutations combined with genome editing technology to reverse the genomic mutation would provide further support for the pathogenicity of these mutations. The study of the factors that regulate neurite outgrowth and synaptic transmission in neurons differentiated from patient-derived iPSCs could help to elucidate the exact role that they have in the pathogenesis of ALS. This model may also be used for drug screening and the discovery of potential therapeutic compounds.

REFERENCES

Aasen, T., A. Raya, M. J. Barrero, E. Garreta, A. Consiglio, F. Gonzalez, R. Vassena, J. Bilic, V. Pekarik, G. Tiscornia, M. Edel, S. Boue and J. C. I. Belmonte (2008). "Efficient and rapid generation of induced pluripotent stem cells from human keratinocytes." Nat Biotech **26**(11): 1276-1284.

Abalkhail, H., J. Mitchell, J. Habgood, R. Orrell and J. de Belleroche (2003). "A New Familial Amyotrophic Lateral Sclerosis Locus on Chromosome 16q12.1-16q12.2." The American Journal of Human Genetics **73**(2): 383-389.

Abel, O., J. F. Powell, P. M. Andersen and A. Al-Chalabi (2012). "ALSoD: A user-friendly online bioinformatics tool for amyotrophic lateral sclerosis genetics." Human Mutation **33**(9): 1345-1351.

Al-Saif, A., F. Al-Mohanna and S. Bohlega (2011). "A mutation in sigma-1 receptor causes juvenile amyotrophic lateral sclerosis." Ann Neurol **70**(6): 913-9.

Al-Sarraj, S., A. King, C. Troakes, B. Smith, S. Maekawa, I. Bodi, B. Rogelj, A. Al-Chalabi, T. Hortobágyi and C. E. Shaw (2011). "p62 positive, TDP-43 negative, neuronal cytoplasmic and intranuclear inclusions in the cerebellum and hippocampus define the pathology of C9orf72-linked FTLD and MND/ALS." Acta Neuropathologica **122**(6): 691-702.

Alami, Nael H., Rebecca B. Smith, Monica A. Carrasco, Luis A. Williams, Christina S. Winborn, Steve S. W. Han, E. Kiskinis, B. Winborn, Brian D. Freibaum, A. Kanagaraj, Alison J. Clare, Nisha M. Badders, B. Bilican, E. Chaum, S. Chandran, Christopher E. Shaw, Kevin C. Eggan, T. Maniatis and J. P. Taylor (2014). "Axonal Transport of TDP-43 mRNA Granules Is Impaired by ALS-Causing Mutations." Neuron **81**(3): 536-543.

Alexianu, M. E., M. Kozovska and S. H. Appel (2001). "Immune reactivity in a mouse model of familial ALS correlates with disease progression." Neurology **57**(7): 1282-1289.

Almeida, S., E. Gascon, H. Tran, H. J. Chou, T. F. Gendron, S. DeGroot, A. R. Tapper, C. Sellier, N. Charlet-Berguerand, A. Karydas, W. W. Seeley, A. L. Boxer, L. Petrucelli, B. L. Miller and F.-B. Gao (2013). "Modeling key pathological features of frontotemporal dementia with C9ORF72 repeat expansion in iPSC-derived human neurons." Acta Neuropathologica **126**(3): 385-399.

Andersen, P. M., Forsgren, L., Binzer, M., Nilsson, P., Ala-Hurula, V., Keränen, M.-L., Bergmark, L., Saarinen, A., Haltia, T., Tarvainen, I., Kinnunen, E., Udd, B. and S. L. Marklund (1996). "Autosomal recessive adult-onset amyotrophic lateral sclerosis associated with homozygosity for Asp90Ala CuZn-superoxide dismutase mutation:A clinical and genealogical study of 36 patients." Brain **119**(4): 1153-1172.

Andersson, M. K., A. Ståhlberg, Y. Arvidsson, A. Olofsson, H. Semb, G. Stenman, O. Nilsson and P. Åman (2008). "The multifunctional FUS, EWS and TAF15 proto-oncoproteins show cell type-specific expression patterns and involvement in cell spreading and stress response." BMC cell biology **9**(1): 37.

Andrus, P. K., T. J. Fleck, M. E. Gurney and E. D. Hall (1998). "Protein Oxidative Damage in a Transgenic Mouse Model of Familial Amyotrophic Lateral Sclerosis." Journal of Neurochemistry **71**(5): 2041-2048.

Aoki, N., S. Higashi, I. Kawakami, Z. Kobayashi, M. Hosokawa, O. Katsuse, T. Togo, Y. Hirayasu and H. Akiyama (2012). "Localization of fused in sarcoma (FUS) protein to the post-synaptic density in the brain." Acta Neuropathologica **124**(3): 383-394.

Armstrong, G. A. and P. Drapeau (2013). "Calcium channel agonists protect against neuromuscular dysfunction in a genetic model of TDP-43 mutation in ALS." The Journal of Neuroscience **33**(4): 1741-1752.

Armstrong, G. A. B. and P. Drapeau (2013). "Loss and gain of FUS function impair neuromuscular synaptic transmission in a genetic model of ALS." Human Molecular Genetics **22**(21): 4282-4292.

Arnold, E. S., S.-C. Ling, S. C. Huelga, C. Lagier-Tourenne, M. Polymenidou, D. Ditsworth, H. B. Kordasiewicz, M. McAlonis-Downes, O. Platoshyn, P. A. Parone, S. Da Cruz, K. M. Clutario, D. Swing, L. Tessarollo, M. Marsala, C. E. Shaw, G. W. Yeo and D. W. Cleveland (2013). "ALS-linked TDP-43 mutations produce aberrant RNA splicing and adult-onset motor neuron disease without aggregation or loss of nuclear TDP-43." Proceedings of the National Academy of Sciences **110**(8): E736-E745.

Ash, Peter E. A., Kevin F. Bieniek, Tania F. Gendron, T. Caulfield, W.-L. Lin, M. DeJesus-Hernandez, Marka M. van Blitterswijk, K. Jansen-West, Joseph W. Paul Iii, R. Rademakers, Kevin B. Boylan, Dennis W. Dickson and L. Petrucelli (2013). "Unconventional Translation of C9ORF72 GGGGCC Expansion Generates Insoluble Polypeptides Specific to c9FTD/ALS." Neuron **77**(4): 639-646.

Ash, P. E. A., Y.-J. Zhang, C. M. Roberts, T. Saldi, H. Hutter, E. Buratti, L. Petrucelli and C. D. Link (2010). "Neurotoxic effects of TDP-43 overexpression in C. elegans." Human Molecular Genetics **19**(16): 3206-3218.

Atkin, J. D., M. A. Farg, B. J. Turner, D. Tomas, J. A. Lysaght, J. Nunan, A. Rembach, P. Nagley, P. M. Beart, S. S. Cheema and M. K. Horne (2006). "Induction of the Unfolded Protein Response in Familial Amyotrophic Lateral Sclerosis and

Association of Protein-disulfide Isomerase with Superoxide Dismutase 1." Journal of Biological Chemistry **281**(40): 30152-30165.

Atsumi, T. (1981). "The ultrastructure of intramuscular nerves in amyotrophic lateral sclerosis." Acta Neuropathologica **55**(3): 193-198.

Ayala, Y. M., P. Zago, A. D'Ambrogio, Y.-F. Xu, L. Petrucelli, E. Buratti and F. E. Baralle (2008). "Structural determinants of the cellular localization and shuttling of TDP-43." Journal of Cell Science **121**(22): 3778-3785.

Baba, M., S. Nakajo, P.-H. Tu, T. Tomita, K. Nakaya, V. Lee, J. Q. Trojanowski and T. Iwatsubo (1998). "Aggregation of alpha-synuclein in Lewy bodies of sporadic Parkinson's disease and dementia with Lewy bodies." The American journal of pathology **152**(4): 879.

Baechtold, H., M. Kuroda, J. Sok, D. Ron, B. S. Lopez and A. T. Akhmedov (1999). "Human 75-kDa DNA-pairing Protein Is Identical to the Pro-oncoprotein TLS/FUS and Is Able to Promote D-loop Formation." Journal of Biological Chemistry **274**(48): 34337-34342.

Banerjee, R., R. L. Mosley, A. D. Reynolds, A. Dhar, V. Jackson-Lewis, P. H. Gordon, S. Przedborski and H. E. Gendelman (2008). "Adaptive Immune Neuroprotection in G93A-SOD1 Amyotrophic Lateral Sclerosis Mice." PLoS One **3**(7): e2740.

Baron, D. M., L. J. Kaushansky, C. L. Ward, R. R. K. Sama, R.-J. Chian, K. J. Boggio, A. Quaresma, J. A. Nickerson and D. A. Bosco (2013). "Amyotrophic lateral sclerosis-linked FUS/TLS alters stress granule assembly and dynamics." Mol. Neurodegener **8**: 30.

Beers, D. R., J. S. Henkel, W. Zhao, J. Wang and S. H. Appel (2008). "CD4+ T cells support glial neuroprotection, slow disease progression, and modify glial

morphology in an animal model of inherited ALS." Proceedings of the National Academy of Sciences **105**(40): 15558-15563.

Bertolotti, A., Y. Lutz, D. J. Heard, P. Chambon and L. Tora (1996). "hTAF (II) 68, a novel RNA/ssDNA-binding protein with homology to the pro-oncoproteins TLS/FUS and EWS is associated with both TFIID and RNA polymerase II." The EMBO Journal **15**(18): 5022.

Bertrand, P., A. T. Akhmedov, F. Delacote, A. Durrbach and B. S. Lopez (1999). "Human POMp75 is identified as the pro-oncoprotein TLS/FUS: both POMp75 and POMp100 DNA homologous pairing activities are associated to cell proliferation." Oncogene **18**(31): 4515-4521.

Bieberich, E., S. MacKinnon, J. Silva, S. Noggle and B. G. Condie (2003). "Regulation of cell death in mitotic neural progenitor cells by asymmetric distribution of prostate apoptosis response 4 (PAR-4) and simultaneous elevation of endogenous ceramide." The Journal of Cell Biology **162**(3): 469-479.

Bilican, B., A. Serio, S. J. Barmada, A. L. Nishimura, G. J. Sullivan, M. Carrasco, H. P. Phatnani, C. A. Puddifoot, D. Story, J. Fletcher, I.-H. Park, B. A. Friedman, G. Q. Daley, D. J. A. Wyllie, G. E. Hardingham, I. Wilmut, S. Finkbeiner, T. Maniatis, C. E. Shaw and S. Chandran (2012). "Mutant induced pluripotent stem cell lines recapitulate aspects of TDP-43 proteinopathies and reveal cell-specific vulnerability." Proceedings of the National Academy of Sciences **109**(15): 5803-5808.

Blair, I. P., K. L. Williams, S. T. Warraich, J. C. Durnall, A. D. Thoeng, J. Manavis, P. C. Blumbergs, S. Vucic, M. C. Kiernan and G. A. Nicholson (2010). "FUS mutations in amyotrophic lateral sclerosis: clinical, pathological, neurophysiological and genetic analysis." Journal of Neurology, Neurosurgery & Psychiatry **81**(6): 639-645.

Bosco, D. A., N. Lemay, H. K. Ko, H. Zhou, C. Burke, T. J. Kwiatkowski, P. Sapp, D. McKenna-Yasek, R. H. Brown and L. J. Hayward (2010). "Mutant FUS proteins that cause amyotrophic lateral sclerosis incorporate into stress granules." Human Molecular Genetics **19**(21): 4160-4175.

Bosco, D. A., G. Morfini, N. M. Karabacak, Y. Song, F. Gros-Louis, P. Pasinelli, H. Goolsby, B. A. Fontaine, N. Lemay, D. McKenna-Yasek, M. P. Frosch, J. N. Agar, J.-P. Julien, S. T. Brady and R. H. Brown (2010). "Wild-type and mutant SOD1 share an aberrant conformation and a common pathogenic pathway in ALS." Nat Neurosci **13**(11): 1396-1403.

Bozdagi, O., W. Shan, H. Tanaka, D. L. Benson and G. W. Huntley (2000). "Increasing Numbers of Synaptic Puncta during Late-Phase LTP: N-Cadherin Is Synthesized, Recruited to Synaptic Sites, and Required for Potentiation." Neuron **28**(1): 245-259.

Brooke, G. N., R. L. Culley, D. A. Dart, D. J. Mann, L. Gaughan, S. R. McCracken, C. N. Robson, B. Spencer-Dene, S. C. Gamble, S. M. Powell, R. Wait, J. Waxman, M. M. Walker and C. L. Bevan (2011). "FUS/TLS Is a Novel Mediator of Androgen-Dependent Cell-Cycle Progression and Prostate Cancer Growth." Cancer Research **71**(3): 914-924.

Brooks, B. R., R. G. Miller, M. Swash and T. L. Munsat (2000). "El Escorial revisited: revised criteria for the diagnosis of amyotrophic lateral sclerosis." Amyotrophic Lateral Sclerosis **1**(5): 293-299.

Buta, C., R. David, R. Dressel, M. Emgård, C. Fuchs, U. Gross, L. Healy, J. Hescheler, R. Kolar, U. Martin, H. Mikkers, F.-J. Müller, R. K. Schneider, A. E. M. Seiler, H. Spielmann and G. Weitzer (2013). "Reconsidering pluripotency tests: Do we still need teratoma assays?" Stem Cell Research **11**(1): 552-562.

Byrne, S., C. Walsh, C. Lynch, P. Bede, M. Elamin, K. Kenna, R. McLaughlin and O. Hardiman (2011). "Rate of familial amyotrophic lateral sclerosis: a systematic review and meta-analysis." Journal of Neurology, Neurosurgery & Psychiatry **82**(6): 623-627.

Canete-Soler, R., D. G. Silberg, M. D. Gershon and W. W. Schlaepfer (1999). "Mutation in neurofilament transgene implicates RNA processing in the pathogenesis of neurodegenerative disease." J Neurosci **19**(4): 1273-83.

Carrì, M. T., A. Ferri, A. Battistoni, L. Famhy, R. Gabbianelli, F. Poccia and G. Rotilio (1997). "Expression of a Cu,Zn superoxide dismutase typical of familial amyotrophic lateral sclerosis induces mitochondrial alteration and increase of cytosolic Ca2+ concentration in transfected neuroblastoma SH-SY5Y cells." FEBS Letters **414**(2): 365-368.

Chambers, S. M., C. A. Fasano, E. P. Papapetrou, M. Tomishima, M. Sadelain and L. Studer (2009). "Highly efficient neural conversion of human ES and iPS cells by dual inhibition of SMAD signaling." Nat Biotech **27**(3): 275-280.

Charych, E. I., B. F. Akum, J. S. Goldberg, R. J. Jörnsten, C. Rongo, J. Q. Zheng and B. L. Firestein (2006). "Activity-independent regulation of dendrite patterning by postsynaptic density protein PSD-95." The Journal of Neuroscience **26**(40): 10164-10176.

Chen, H., K. Qian, Z. Du, J. Cao, A. Petersen, H. Liu, L. W. t. Blackbourn, C. L. Huang, A. Errigo, Y. Yin, J. Lu, M. Ayala and S. C. Zhang (2014). "Modeling ALS with iPSCs Reveals that Mutant SOD1 Misregulates Neurofilament Balance in Motor Neurons." Cell Stem Cell.

Chen, Y.-Z., C. L. Bennett, H. M. Huynh, I. P. Blair, I. Puls, J. Irobi, I. Dierick, A. Abel, M. L. Kennerson, B. A. Rabin, G. A. Nicholson, M. Auer-Grumbach, K. Wagner, P. De Jonghe, J. W. Griffin, K. H. Fischbeck, V. Timmerman, D. R. Cornblath and

P. F. Chance (2004). "DNA/RNA Helicase Gene Mutations in a Form of Juvenile Amyotrophic Lateral Sclerosis (ALS4)." The American Journal of Human Genetics **74**(6): 1128-1135.

Chen, Y., M. Yang, J. Deng, X. Chen, Y. Ye, L. Zhu, J. Liu, H. Ye, Y. Shen, Y. Li, E. J. Rao, K. Fushimi, X. Zhou, E. H. Bigio, M. Mesulam, Q. Xu and J. Y. Wu (2011). "Expression of human FUS protein in Drosophila leads to progressive neurodegeneration." Protein & Cell **2**(6): 477-486.

Cheroni, C., M. Peviani, P. Cascio, S. DeBiasi, C. Monti and C. Bendotti (2005). "Accumulation of human SOD1 and ubiquitinated deposits in the spinal cord of SOD1G93A mice during motor neuron disease progression correlates with a decrease of proteasome." Neurobiology of disease **18**(3): 509-522.

Chesi, A., B. T. Staahl, A. Jovicic, J. Couthouis, M. Fasolino, A. R. Raphael, T. Yamazaki, L. Elias, M. Polak, C. Kelly, K. L. Williams, J. A. Fifita, N. J. Maragakis, G. A. Nicholson, O. D. King, R. Reed, G. R. Crabtree, I. P. Blair, J. D. Glass and A. D. Gitler (2013). "Exome sequencing to identify de novo mutations in sporadic ALS trios." Nature neuroscience **16**(7): 851-855.

Chiò, A., G. Logroscino, B. J. Traynor, J. Collins, J. C. Simeone, L. A. Goldstein and L. A. White (2013). "Global Epidemiology of Amyotrophic Lateral Sclerosis: A Systematic Review of the Published Literature." Neuroepidemiology **41**(2): 118-130.

Chiu, I. M., A. Chen, Y. Zheng, B. Kosaras, S. A. Tsiftsoglou, T. K. Vartanian, R. H. Brown and M. C. Carroll (2008). "T lymphocytes potentiate endogenous neuroprotective inflammation in a mouse model of ALS." Proceedings of the National Academy of Sciences **105**(46): 17913-17918.

Chow, C. Y., J. E. Landers, S. K. Bergren, P. C. Sapp, A. E. Grant, J. M. Jones, L. Everett, G. M. Lenk, D. M. McKenna-Yasek, L. S. Weisman, D. Figlewicz, R. H. Brown

and M. H. Meisler (2009). "Deleterious Variants of FIG4, a Phosphoinositide Phosphatase, in Patients with ALS." The American Journal of Human Genetics **84**(1): 85-88.

Chow, C. Y., Y. Zhang, J. J. Dowling, N. Jin, M. Adamska, K. Shiga, K. Szigeti, M. E. Shy, J. Li, X. Zhang, J. R. Lupski, L. S. Weisman and M. H. Meisler (2007). "Mutation of FIG4 causes neurodegeneration in the pale tremor mouse and patients with CMT4J." Nature **448**(7149): 68-72.

Collard, J.-F., F. Côté and J.-P. Julien (1995). "Defective axonal transport in a transgenic mouse model of amyotrophic lateral sclerosis." Nature **375**(6526): 61-64.

Colledge, M., E. M. Snyder, R. A. Crozier, J. A. Soderling, Y. Jin, L. K. Langeberg, H. Lu, M. F. Bear and J. D. Scott (2003). "Ubiquitination Regulates PSD-95 Degradation and AMPA Receptor Surface Expression." Neuron **40**(3): 595-607.

Conte, A., S. Lattante, M. Zollino, G. Marangi, M. Luigetti, A. Del Grande, S. Servidei, F. Trombetta and M. Sabatelli (2012). "P525L FUS mutation is consistently associated with a severe form of juvenile Amyotrophic Lateral Sclerosis." Neuromuscular Disorders **22**(1): 73-75.

Cooper-Knock, J., C. Hewitt, J. R. Highley, A. Brockington, A. Milano, S. Man, J. Martindale, J. Hartley, T. Walsh, C. Gelsthorpe, L. Baxter, G. Forster, M. Fox, J. Bury, K. Mok, C. J. McDermott, B. J. Traynor, J. Kirby, S. B. Wharton, P. G. Ince, J. Hardy and P. J. Shaw (2012). "Clinico-pathological features in amyotrophic lateral sclerosis with expansions in C9ORF72." Brain **135**(3): 751-764.

Corcia, P., P. Valdmanis, S. Millecamps, C. Lionnet, H. Blasco, K. Mouzat, H. Daoud, V. Belzil, R. Morales, N. Pageot, V. Danel-Brunaud, N. Vandenberghe, P. F. Pradat, P. Couratier, F. Salachas, S. Lumbroso, R. G. A, V. Meininger and W.

Camu (2012). "Phenotype and genotype analysis in amyotrophic lateral sclerosis with TARDBP gene mutations." Neurology **78**(19): 1519-1526.

Corrado, L., Bo, R. B., Castellotti, B., Ratti, A., Cereda, C., Penco, S., Soraru, G., Carlomagno, Y., Ghezzi, S., Pensato, V., Colombrita, C., Gagliardi, S., Cozzi, L., Orsetti, V., Mancuso, M., Siciliano, G., Mazzini, L., Comi, G. P., Gellera, C., Ceroni, M., D'Alfonso, S. and V. Silani (2010). "Mutations of *FUS* gene in sporadic amyotrophic lateral sclerosis." Journal of Medical Genetics **47**:190-194.

Couthouis, J., M. P. Hart, J. Shorter, M. DeJesus-Hernandez, R. Erion, R. Oristano, A. X. Liu, D. Ramos, N. Jethava, D. Hosangadi, J. Epstein, A. Chiang, Z. Diaz, T. Nakaya, F. Ibrahim, H.-J. Kim, J. A. Solski, K. L. Williams, J. Mojsilovic-Petrovic, C. Ingre, K. Boylan, N. R. Graff-Radford, D. W. Dickson, D. Clay-Falcone, L. Elman, L. McCluskey, R. Greene, R. G. Kalb, V. M.-Y. Lee, J. Q. Trojanowski, A. Ludolph, W. Robberecht, P. M. Andersen, G. A. Nicholson, I. P. Blair, O. D. King, N. M. Bonini, V. Van Deerlin, R. Rademakers, Z. Mourelatos and A. D. Gitler (2011). "A yeast functional screen predicts new candidate ALS disease genes." Proceedings of the National Academy of Sciences **108**(52): 20881-20890.

Cox, L. E., L. Ferraiuolo, E. F. Goodall, P. R. Heath, A. Higginbottom, H. Mortiboys, H. C. Hollinger, J. A. Hartley, A. Brockington, C. E. Burness, K. E. Morrison, S. B. Wharton, A. J. Grierson, P. G. Ince, J. Kirby and P. J. Shaw (2010). "Mutations in CHMP2B in lower motor neuron predominant amyotrophic lateral sclerosis (ALS)." PLoS One **5**(3): e9872.

Crozat, A., P. Aman, N. Mandahl and D. Ron (1993). "Fusion of CHOP to a novel RNA-binding protein in human myxoid liposarcoma." Nature **363**(6430): 640-644.

Cudkowicz, M. E., D. McKenna-Yasek, P. E. Sapp, W. Chin, B. Geller, D. L. Hayden, D. A. Schoenfeld, B. A. Hosler, H. R. Horvitz and R. H. Brown (1997). "Epidemiology of mutations in superoxide dismutase in amyotrophic lateral sclerosis." Annals of Neurology **41**(2): 210-221.

D'Ambrogio, A., E. Buratti, C. Stuani, C. Guarnaccia, M. Romano, Y. M. Ayala and F. E. Baralle (2009). "Functional mapping of the interaction between TDP-43 and hnRNP A2 in vivo." Nucleic Acids Research **37**(12): 4116-4126.

Dal Canto, M. C. and M. E. Gurney (1995). "Neuropathological changes in two lines of mice carrying a transgene for mutant human Cu, Zn SOD, and in mice overexpressing wild type human SOD: a model of familial amyotrophic lateral sclerosis (FALS)." Brain research **676**(1): 25-40.

Daoud, H. and G. A. Rouleau (2011). "Motor neuron disease: a role for ubiquilin 2 mutations in neurodegeneration." Nature Reviews Neurology **7**(11): 599-600.

Daoud, H., S. Zhou, A. Noreau, M. Sabbagh, V. Belzil, A. Dionne-Laporte, C. Tranchant, P. Dion and G. A. Rouleau (2012). "Exome sequencing reveals SPG11 mutations causing juvenile ALS." Neurobiology of Aging **33**(4): 839.e5-839.e9.

DeJesus-Hernandez, M., Ian R. Mackenzie, Bradley F. Boeve, Adam L. Boxer, M. Baker, Nicola J. Rutherford, Alexandra M. Nicholson, Nicole A. Finch, H. Flynn, J. Adamson, N. Kouri, A. Wojtas, P. Sengdy, G.-Yuek R. Hsiung, A. Karydas, William W. Seeley, Keith A. Josephs, G. Coppola, Daniel H. Geschwind, Zbigniew K. Wszolek, H. Feldman, David S. Knopman, Ronald C. Petersen, Bruce L. Miller, Dennis W. Dickson, Kevin B. Boylan, Neill R. Graff-Radford and R. Rademakers (2011). "Expanded GGGGCC Hexanucleotide

Repeat in Noncoding Region of C9ORF72 Causes Chromosome 9p-Linked FTD and ALS." Neuron **72**(2): 245-256.

Del Bo, R., C. Tiloca, V. Pensato, L. Corrado, A. Ratti, N. Ticozzi, S. Corti, B. Castellotti, L. Mazzini, G. Sorarù, C. Cereda, S. D'Alfonso, C. Gellera, G. P. Comi, V. Silani and T. S. Consortium (2011). "Novel optineurin mutations in patients with familial and sporadic amyotrophic lateral sclerosis." Journal of Neurology, Neurosurgery & Psychiatry **82**(11): 1239-1243.

Deng, H. X., W. Chen, S. T. Hong, K. M. Boycott, G. H. Gorrie, N. Siddique, Y. Yang, F. Fecto, Y. Shi, H. Zhai, H. Jiang, M. Hirano, E. Rampersaud, G. H. Jansen, S. Donkervoort, E. H. Bigio, B. R. Brooks, K. Ajroud, R. L. Sufit, J. L. Haines, E. Mugnaini, M. A. Pericak-Vance and T. Siddique (2011). "Mutations in UBQLN2 cause dominant X-linked juvenile and adult-onset ALS and ALS/dementia." Nature **477**(7363): 211-5.

Dhaliwal, G. K. and R. P. Grewal (2000). "Mitochondrial DNA deletion mutation levels are elevated in ALS brains." NeuroReport **11**(11): 2507-2509.

Dick, E., D. Rajamohan, J. Ronksley and C. Denning (2010). "Evaluating the utility of cardiomyocytes from human pluripotent stem cells for drug screening." Biochemical Society Transactions **38**(4): 1037.

Dimos, J. T., K. T. Rodolfa, K. K. Niakan, L. M. Weisenthal, H. Mitsumoto, W. Chung, G. F. Croft, G. Saphier, R. Leibel, R. Goland, H. Wichterle, C. E. Henderson and K. Eggan (2008). "Induced Pluripotent Stem Cells Generated from Patients with ALS Can Be Differentiated into Motor Neurons." Science **321**(5893): 1218-1221.

Dormann, D., R. Rodde, D. Edbauer, E. Bentmann, I. Fischer, A. Hruscha, M. E. Than, I. R. A. Mackenzie, A. Capell, B. Schmid, M. Neumann and C. Haass (2010).

"ALS-associated fused in sarcoma (FUS) mutations disrupt Transportin-mediated nuclear import." The EMBO Journal **29**(16): 2841-2857.

Draper, J. S., H. D. Moore, L. N. Ruban, P. J. Gokhale and P. W. Andrews (2004). "Culture and characterization of human embryonic stem cells." Stem cells and development **13**(4): 325-336.

Egawa, N., S. Kitaoka, K. Tsukita, M. Naitoh, K. Takahashi, T. Yamamoto, F. Adachi, T. Kondo, K. Okita, I. Asaka, T. Aoi, A. Watanabe, Y. Yamada, A. Morizane, J. Takahashi, T. Ayaki, H. Ito, K. Yoshikawa, S. Yamawaki, S. Suzuki, D. Watanabe, H. Hioki, T. Kaneko, K. Makioka, K. Okamoto, H. Takuma, A. Tamaoka, K. Hasegawa, T. Nonaka, M. Hasegawa, A. Kawata, M. Yoshida, T. Nakahata, R. Takahashi, M. C. N. Marchetto, F. H. Gage, S. Yamanaka and H. Inoue (2012). "Drug Screening for ALS Using Patient-Specific Induced Pluripotent Stem Cells." Science Translational Medicine **4**(145): 145ra104.

Elden, A. C., H. J. Kim, M. P. Hart, A. S. Chen-Plotkin, B. S. Johnson, X. Fang, M. Armakola, F. Geser, R. Greene, M. M. Lu, A. Padmanabhan, D. Clay-Falcone, L. McCluskey, L. Elman, D. Juhr, P. J. Gruber, U. Rub, G. Auburger, J. Q. Trojanowski, V. M. Lee, V. M. Van Deerlin, N. M. Bonini and A. D. Gitler (2010). "Ataxin-2 intermediate-length polyglutamine expansions are associated with increased risk for ALS." Nature **466**(7310): 1069-75.

Engert, F. and T. Bonhoeffer (1999). "Dendritic spine changes associated with hippocampal long-term synaptic plasticity." Nature **399**(6731): 66-70.

Eriksson, M., W. T. Brown, L. B. Gordon, M. W. Glynn, J. Singer, L. Scott, M. R. Erdos, C. M. Robbins, T. Y. Moses, P. Berglund, A. Dutra, E. Pak, S. Durkin, A. B. Csoka, M. Boehnke, T. W. Glover and F. S. Collins (2003). "Recurrent de novo point mutations in lamin A cause Hutchinson-Gilford progeria syndrome." Nature **423**(6937): 293-298.

Fecto, F., J. Yan, S. P. Vemula, E. Liu, Y. Yang, W. Chen, J. G. Zheng, Y. Shi, N. Siddique, H. Arrat, S. Donkervoort, S. Ajroud-Driss, R. L. Sufit, S. L. Heller, H.-X. Deng and T. Siddique (2011). "SQSTM1 mutations in familial and sporadic amyotrophic lateral sclerosis." Archives of Neurology **68**(11): 1440-1446.

Ferrante, R. J., S. E. Browne, L. A. Shinobu, A. C. Bowling, M. J. Baik, U. MacGarvey, N. W. Kowall, R. H. Brown Jr and M. F. Beal (1997). "Evidence of increased oxidative damage in both sporadic and familial amyotrophic lateral sclerosis." Journal of Neurochemistry **69**(5): 2064-2074.

Ferrante, R. J., L. A. Shinobu, J. B. Schulz, R. T. Matthews, C. E. Thomas, N. W. Kowall, M. E. Gurney and M. F. Beal (1997). "Increased 3-nitrotyrosine and oxidative damage in mice with a human copper/zinc superoxide dismutase mutation." Annals of Neurology **42**(3): 326-334.

Figlewicz, D. A., A. Krizus, M. G. Martinoli, V. Meininger, M. Dib, G. A. Rouleau and J. P. Julien (1994). "Variants of the heavy neurofilament subunit are associated with the development of amyotrophic lateral sclerosis." Hum Mol Genet **3**(10): 1757-61.

Fratta, P., M. Poulter, T. Lashley, J. D. Rohrer, J. M. Polke, J. Beck, N. Ryan, D. Hensman, S. Mizielinska, A. J. Waite, M.-C. Lai, T. F. Gendron, L. Petrucelli, E. M. C. Fisher, T. Revesz, J. D. Warren, J. Collinge, A. M. Isaacs and S. Mead (2013). "Homozygosity for the C9orf72 GGGGCC repeat expansion in frontotemporal dementia." Acta Neuropathologica **126**(3): 401-409.

Frey, D., C. Schneider, L. Xu, J. Borg, W. Spooren and P. Caroni (2000). "Early and Selective Loss of Neuromuscular Synapse Subtypes with Low Sprouting Competence in Motoneuron Diseases." The Journal of Neuroscience **20**(7): 2534-2542.

Fujii, R., S. Okabe, T. Urushido, K. Inoue, A. Yoshimura, T. Tachibana, T. Nishikawa, G. G. Hicks and T. Takumi (2005). "The RNA Binding Protein TLS Is Translocated to Dendritic Spines by mGluR5 Activation and Regulates Spine Morphology." Current Biology **15**(6): 587-593.

Fujii, R. and T. Takumi (2005). "TLS facilitates transport of mRNA encoding an actin-stabilizing protein to dendritic spines." Journal of Cell Science **118**(24): 5755-5765.

Fumagalli, E., M. Funicello, T. Rauen, M. Gobbi and T. Mennini (2008). "Riluzole enhances the activity of glutamate transporters GLAST, GLT1 and EAAC1." European Journal of Pharmacology **578**(2â€“3): 171-176.

Fushimi, K., C. Long, N. Jayaram, X. Chen, L. Li and J. Y. Wu (2011). "Expression of human FUS/TLS in yeast leads to protein aggregation and cytotoxicity, recapitulating key features of FUS proteinopathy." Protein & Cell **2**(2): 141-149.

Gellera, C., C. Tiloca, R. Del Bo, L. Corrado, V. Pensato, J. Agostini, C. Cereda, A. Ratti, B. Castellotti, S. Corti, A. Bagarotti, A. Cagnin, P. Milani, C. Gabelli, G. Riboldi, L. Mazzini, G. SorarÃ[1], S. D'Alfonso, F. Taroni, G. P. Comi, N. Ticozzi, V. Silani and T. S. Consortium (2013). "Ubiquilin 2 mutations in Italian patients with amyotrophic lateral sclerosis and frontotemporal dementia." Journal of Neurology, Neurosurgery & Psychiatry **84**(2): 183-187.

George, E. B., J. D. Glass and J. W. Griffin (1995). "Axotomy-induced axonal degeneration is mediated by calcium influx through ion-specific channels." The Journal of Neuroscience **15**(10): 6445-6452.

Gitcho, M. A., R. H. Baloh, S. Chakraverty, K. Mayo, J. B. Norton, D. Levitch, K. J. Hatanpaa, C. L. White, E. H. Bigio, R. Caselli, M. Baker, M. T. Al-Lozi, J. C. Morris, A. Pestronk, R. Rademakers, A. M. Goate and N. J. Cairns (2008).

"TDP-43 A315T mutation in familial motor neuron disease." Annals of Neurology **63**(4): 535-538.

Greenway, M. J., M. D. Alexander, S. Ennis, B. J. Traynor, B. Corr, E. Frost, A. Green and O. Hardiman (2004). "A novel candidate region for ALS on chromosome 14q11.2." Neurology **63**(10): 1936-8.

Gregory, R. I., K.-p. Yan, G. Amuthan, T. Chendrimada, B. Doratotaj, N. Cooch and R. Shiekhattar (2004). "The Microprocessor complex mediates the genesis of microRNAs." Nature **432**(7014): 235-240.

Groen, E. J. N., K. Fumoto, A. M. Blokhuis, J. Engelen-Lee, Y. Zhou, D. M. A. van den Heuvel, M. Koppers, F. van Diggelen, J. van Heest, J. A. A. Demmers, J. Kirby, P. J. Shaw, E. Aronica, W. G. M. Spliet, J. H. Veldink, L. H. van den Berg and R. J. Pasterkamp (2013). "ALS-associated mutations in FUS disrupt the axonal distribution and function of SMN." Human Molecular Genetics **22**(18): 3690-3704.

Hadano, S., C. K. Hand, H. Osuga, Y. Yanagisawa, A. Otomo, R. S. Devon, N. Miyamoto, J. Showguchi-Miyata, Y. Okada, R. Singaraja, D. A. Figlewicz, T. Kwiatkowski, B. A. Hosler, T. Sagie, J. Skaug, J. Nasir, R. H. Brown, Jr., S. W. Scherer, G. A. Rouleau, M. R. Hayden and J. E. Ikeda (2001). "A gene encoding a putative GTPase regulator is mutated in familial amyotrophic lateral sclerosis 2." Nat Genet **29**(2): 166-73.

Haeusler, A. R., C. J. Donnelly, G. Periz, E. A. J. Simko, P. G. Shaw, M.-S. Kim, N. J. Maragakis, J. C. Troncoso, A. Pandey, R. Sattler, J. D. Rothstein and J. Wang (2014). "C9orf72 nucleotide repeat structures initiate molecular cascades of disease." Nature **507**(7491): 195-200.

Hanby, M. F., Scott, K. M., Scotton, W., Wijesekera, L., Mole, T., Ellis, C. E., Leigh, P. N., Shaw, C. E. and A. Al-Chalabi (2011). "The risk to relatives of patients with sporadic amyotrophic lateral sclerosis." Brain **134**(12): 3451-3454.

Hansen, S. M., V. Berezin and E. Bock (2008). "Signaling mechanisms of neurite outgrowth induced by the cell adhesion molecules NCAM and N-Cadherin." Cellular and Molecular Life Sciences **65**(23): 3809-3821.

Hartmuth, K., H. Urlaub, H.-P. Vornlocher, C. L. Will, M. Gentzel, M. Wilm and R. Lührmann (2002). "Protein composition of human prespliceosomes isolated by a tobramycin affinity-selection method." Proceedings of the National Academy of Sciences **99**(26): 16719-16724.

Henkel, J. S., D. R. Beers, W. Zhao and S. H. Appel (2009). "Microglia in ALS: The Good, The Bad, and The Resting." Journal of Neuroimmune Pharmacology **4**(4): 389-398.

Henkel, J. S., J. I. Engelhardt, L. Siklós, E. P. Simpson, S. H. Kim, T. Pan, J. C. Goodman, T. Siddique, D. R. Beers and S. H. Appel (2004). "Presence of dendritic cells, MCP-1, and activated microglia/macrophages in amyotrophic lateral sclerosis spinal cord tissue." Annals of Neurology **55**(2): 221-235.

Hensley, K., R. A. Floyd, B. Gordon, S. Mou, Q. N. Pye, C. Stewart, M. West and K. Williamson (2002). "Temporal patterns of cytokine and apoptosis-related gene expression in spinal cords of the G93A-SOD1 mouse model of amyotrophic lateral sclerosis." Journal of Neurochemistry **82**(2): 365-374.

Hicks, G. G., N. Singh, A. Nashabi, S. Mai, G. Bozek, L. Klewes, D. Arapovic, E. K. White, M. J. Koury, E. M. Oltz, L. Van Kaer and H. E. Ruley (2000). "Fus deficiency in mice results in defective B-lymphocyte development and activation, high levels of chromosomal instability and perinatal death." Nat Genet **24**(2): 175-179.

Hirano, A., H. Donnenfeld, S. Sasaki and I. Nakano (1984). "Fine structural observations of neurofilamentous changes in amyotrophic lateral sclerosis." Journal of Neuropathology & Experimental Neurology **43**(5): 461-470.

Hoell, J. I., E. Larsson, S. Runge, J. D. Nusbaum, S. Duggimpudi, T. A. Farazi, M. Hafner, A. Borkhardt, C. Sander and T. Tuschl (2011). "RNA targets of wild-type and mutant FET family proteins." Nature structural & molecular biology **18**(12): 1428-1431.

Hu, B.-Y., J. P. Weick, J. Yu, L.-X. Ma, X.-Q. Zhang, J. A. Thomson and S.-C. Zhang (2010). "Neural differentiation of human induced pluripotent stem cells follows developmental principles but with variable potency." Proceedings of the National Academy of Sciences **107**(9): 4335-4340.

Huang, C., H. Zhou, J. Tong, H. Chen, Y.-J. Liu, D. Wang, X. Wei and X.-G. Xia (2011). "FUS Transgenic Rats Develop the Phenotypes of Amyotrophic Lateral Sclerosis and Frontotemporal Lobar Degeneration." PLoS Genet **7**(3): e1002011.

Igaz, L. M., L. K. Kwong, E. B. Lee, A. Chen-Plotkin, E. Swanson, T. Unger, J. Malunda, Y. Xu, M. J. Winton, J. Q. Trojanowski and V. M. Y. Lee (2011). "Dysregulation of the ALS-associated gene TDP-43 leads to neuronal death and degeneration in mice." The Journal of Clinical Investigation **121**(2): 726-738.

Iguchi, Y., M. Katsuno, J.-i. Niwa, S. Takagi, S. Ishigaki, K. Ikenaka, K. Kawai, H. Watanabe, K. Yamanaka, R. Takahashi, H. Misawa, S. Sasaki, F. Tanaka and G. Sobue (2013). "Loss of TDP-43 causes age-dependent progressive motor neuron degeneration." Brain **136**(5): 1371-1382.

Ihara, Y., K. Nobukuni, H. Takata and T. Hayabara (2005). "Oxidative stress and metal content in blood and cerebrospinal fluid of amyotrophic lateral

sclerosis patients with and without a Cu, Zn-superoxide dismutase mutation." Neurological research **27**(1): 105-108.

Israel, M. A., S. H. Yuan, C. Bardy, S. M. Reyna, Y. Mu, C. Herrera, M. P. Hefferan, S. Van Gorp, K. L. Nazor, F. S. Boscolo, C. T. Carson, L. C. Laurent, M. Marsala, F. H. Gage, A. M. Remes, E. H. Koo and L. S. B. Goldstein (2012). "Probing sporadic and familial Alzheimer/'s disease using induced pluripotent stem cells." Nature **482**(7384): 216-220.

Johnson, J. O., J. Mandrioli, M. Benatar, Y. Abramzon, V. M. Van Deerlin, J. Q. Trojanowski, J. R. Gibbs, M. Brunetti, S. Gronka, J. Wuu, J. Ding, L. McCluskey, M. Martinez-Lage, D. Falcone, D. G. Hernandez, S. Arepalli, S. Chong, J. C. Schymick, J. Rothstein, F. Landi, Y.-D. Wang, A. Calvo, G. Mora, M. Sabatelli, M. R. Monsurrò, S. Battistini, F. Salvi, R. Spataro, P. Sola, G. Borghero, G. Galassi, S. W. Scholz, J. P. Taylor, G. Restagno, A. Chiò and B. J. Traynor (2010). "Exome Sequencing Reveals VCP Mutations as a Cause of Familial ALS." Neuron **68**(5): 857-864.

Johnson, J. O., E. P. Pioro, A. Boehringer, R. Chia, H. Feit, A. E. Renton, H. A. Pliner, Y. Abramzon, G. Marangi, B. J. Winborn, J. R. Gibbs, M. A. Nalls, S. Morgan, M. Shoai, J. Hardy, A. Pittman, R. W. Orrell, A. Malaspina, K. C. Sidle, P. Fratta, M. B. Harms, R. H. Baloh, A. Pestronk, C. C. Weihl, E. Rogaeva, L. Zinman, V. E. Drory, G. Borghero, G. Mora, A. Calvo, J. D. Rothstein, C. Drepper, M. Sendtner, A. B. Singleton, J. P. Taylor, M. R. Cookson, G. Restagno, M. Sabatelli, R. Bowser, A. Chio and B. J. Traynor (2014). "Mutations in the Matrin 3 gene cause familial amyotrophic lateral sclerosis." Nat Neurosci **17**(5): 664-6.

Kabashi, E., V. Bercier, A. Lissouba, M. Liao, E. Brustein, G. A. Rouleau and P. Drapeau (2011). "*FUS* and *TARDBP* but Not *SOD1* Interact in Genetic Models of Amyotrophic Lateral Sclerosis." PLoS Genet **7**(8): e1002214.

Kabashi, E., L. Lin, M. L. Tradewell, P. A. Dion, V. r. Bercier, P. Bourgouin, D. Rochefort, S. Bel Hadj, H. D. Durham, C. V. Velde, G. A. Rouleau and P. Drapeau (2010). "Gain and loss of function of ALS-related mutations of TARDBP (TDP-43) cause motor deficits in vivo." Human Molecular Genetics **19**(4): 671-683.

Kabashi, E., P. N. Valdmanis, P. Dion, D. Spiegelman, B. J. McConkey, C. V. Velde, J.-P. Bouchard, L. Lacomblez, K. Pochigaeva, F. Salachas, P.-F. Pradat, W. Camu, V. Meininger, N. Dupre and G. A. Rouleau (2008). "TARDBP mutations in individuals with sporadic and familial amyotrophic lateral sclerosis." Nature genetics **40**(5): 572-574.

Kaneb, H. M., P. A. Dion and G. A. Rouleau (2012). "The FUS about arginine methylation in ALS and FTLD." The EMBO Journal **31**: 4249-4251.

Kato, M., Tina W. Han, S. Xie, K. Shi, X. Du, Leeju C. Wu, H. Mirzaei, Elizabeth J. Goldsmith, J. Longgood, J. Pei, Nick V. Grishin, Douglas E. Frantz, Jay W. Schneider, S. Chen, L. Li, Michael R. Sawaya, D. Eisenberg, R. Tycko and Steven L. McKnight (2012). "Cell-free Formation of RNA Granules: Low Complexity Sequence Domains Form Dynamic Fibers within Hydrogels." Cell **149**(4): 753-767.

Kawamata, T., H. Akiyama, T. Yamada and P. McGeer (1992). "Immunologic reactions in amyotrophic lateral sclerosis brain and spinal cord tissue." The American journal of pathology **140**(3): 691.

Kim, D.-S., J. S. Lee, J. W. Leem, Y. J. Huh, J. Y. Kim, H.-S. Kim, I.-H. Park, G. Q. Daley, D.-Y. Hwang and D.-W. Kim (2010). "Robust Enhancement of Neural

Differentiation from Human ES and iPS Cells Regardless of their Innate Difference in Differentiation Propensity." Stem Cell Reviews and Reports **6**(2): 270-281.

Kim, H. J., N. C. Kim, Y. D. Wang, E. A. Scarborough, J. Moore, Z. Diaz, K. S. MacLea, B. Freibaum, S. Li, A. Molliex, A. P. Kanagaraj, R. Carter, K. B. Boylan, A. M. Wojtas, R. Rademakers, J. L. Pinkus, S. A. Greenberg, J. Q. Trojanowski, B. J. Traynor, B. N. Smith, S. Topp, A. S. Gkazi, J. Miller, C. E. Shaw, M. Kottlors, J. Kirschner, A. Pestronk, Y. R. Li, A. F. Ford, A. D. Gitler, M. Benatar, O. D. King, V. E. Kimonis, E. D. Ross, C. C. Weihl, J. Shorter and J. P. Taylor (2013). "Mutations in prion-like domains in hnRNPA2B1 and hnRNPA1 cause multisystem proteinopathy and ALS." Nature **495**(7442): 467-73.

Kiskinis, E., J. Sandoe, L. A. Williams, G. L. Boulting, R. Moccia, B. J. Wainger, S. Han, T. Peng, S. Thams, S. Mikkilineni, C. Mellin, F. T. Merkle, B. N. Davis-Dusenbery, M. Ziller, D. Oakley, J. Ichida, S. Di Costanzo, N. Atwater, M. L. Maeder, M. J. Goodwin, J. Nemesh, R. E. Handsaker, D. Paull, S. Noggle, S. A. McCarroll, J. K. Joung, C. J. Woolf, R. H. Brown and K. Eggan (2014). "Pathways Disrupted in Human ALS Motor Neurons Identified through Genetic Correction of Mutant SOD1." Cell Stem Cell.

Kon, T., F. Mori, K. Tanji, Y. Miki, Y. Toyoshima, M. Yoshida, H. Sasaki, A. Kakita, H. Takahashi and K. Wakabayashi (2014). "ALS-associated protein FIG4 is localized in Pick and Lewy bodies, and also neuronal nuclear inclusions, in polyglutamine and intranuclear inclusion body diseases." Neuropathology **34**(1): 19-26.

Koppers, M., M. M. van Blitterswijk, L. Vlam, P. A. Rowicka, P. W. J. van Vught, E. J. N. Groen, W. G. M. Spliet, J. Engelen-Lee, H. J. Schelhaas, M. de Visser, A. J. van der Kooi, W. L. van der Pol, R. J. Pasterkamp, J. H. Veldink and L. H. van den

Berg (2012). "VCP mutations in familial and sporadic amyotrophic lateral sclerosis." Neurobiology of Aging **33**(4): 837.e7-837.e13.

Kraemer, B. C., T. Schuck, J. M. Wheeler, L. C. Robinson, J. Q. Trojanowski, V. M. Y. Lee and G. D. Schellenberg (2010). "Loss of murine TDP-43 disrupts motor function and plays an essential role in embryogenesis." Acta Neuropathologica **119**(4): 409-419.

Kramer, M. L. and W. J. Schulz-Schaeffer (2007). "Presynaptic α-synuclein aggregates, not Lewy bodies, cause neurodegeneration in dementia with Lewy bodies." The Journal of Neuroscience **27**(6): 1405-1410.

Kuo, J. J., M. Schonewille, T. Siddique, A. N. A. Schults, R. Fu, P. R. Bar, R. Anelli, C. J. Heckman and A. B. A. Kroese (2004). "Hyperexcitability of Cultured Spinal Motoneurons From Presymptomatic ALS Mice." Journal of Neurophysiology **91**(1): 571-575.

Kuo, J. J., T. Siddique, R. Fu and C. J. Heckman (2005). "Increased persistent Na+ current and its effect on excitability in motoneurones cultured from mutant SOD1 mice." The Journal of Physiology **563**(3): 843-854.

Kuroda, M., J. Sok, L. Webb, H. Baechtold, F. Urano, Y. Yin, P. Chung, D. G. de Rooij, A. Akhmedov, T. Ashley and D. Ron (2000). "Male sterility and enhanced radiation sensitivity in TLS−/− mice." The EMBO Journal **19**(3): 453-462.

Kwiatkowski, T. J., D. A. Bosco, A. L. LeClerc, E. Tamrazian, C. R. Vanderburg, C. Russ, A. Davis, J. Gilchrist, E. J. Kasarskis, T. Munsat, P. Valdmanis, G. A. Rouleau, B. A. Hosler, P. Cortelli, P. J. de Jong, Y. Yoshinaga, J. L. Haines, M. A. Pericak-Vance, J. Yan, N. Ticozzi, T. Siddique, D. McKenna-Yasek, P. C. Sapp, H. R. Horvitz, J. E. Landers and R. H. Brown (2009). "Mutations in the FUS/TLS Gene on Chromosome 16 Cause Familial Amyotrophic Lateral Sclerosis." Science **323**(5918): 1205-1208.

Lagier-Tourenne, C. and D. W. Cleveland (2009). "Rethinking ALS: The FUS about TDP-43." Cell **136**(6): 1001-1004.

Lagier-Tourenne, C., M. Polymenidou and D. W. Cleveland (2010). "TDP-43 and FUS/TLS: emerging roles in RNA processing and neurodegeneration." Human Molecular Genetics **19**(R1): R46-R64.

Lagier-Tourenne, C., M. Polymenidou, K. R. Hutt, A. Q. Vu, M. Baughn, S. C. Huelga, K. M. Clutario, S.-C. Ling, T. Y. Liang, C. Mazur, E. Wancewicz, A. S. Kim, A. Watt, S. Freier, G. G. Hicks, J. P. Donohue, L. Shiue, C. F. Bennett, J. Ravits, D. W. Cleveland and G. W. Yeo (2012). "Divergent roles of ALS-linked proteins FUS/TLS and TDP-43 intersect in processing long pre-mRNAs." Nature neuroscience **15**(11): 1488-1497.

Landers, J., A. Leclerc, L. Shi, A. Virkud, T. Cho, M. Maxwell, A. Henry, M. Polak, J. Glass, T. Kwiatkowski, A. Al-Chalabi, C. E. Shaw, P. N. Leigh, I. Rodriguez-leyza, D. McKenna-Yasek, P. C. Sapp and R. H. Brown Jr (2008). "New VAPB deletion variant and exclusion of VAPB mutations in familial ALS." Neurology **70**(14): 1179-1185.

Landers, J. E., J. Melki, V. Meininger, J. D. Glass, L. H. van den Berg, M. A. van Es, P. C. Sapp, P. W. J. van Vught, D. M. McKenna-Yasek, H. M. Blauw, T.-J. Cho, M. Polak, L. Shi, A.-M. Wills, W. J. Broom, N. Ticozzi, V. Silani, A. Ozoguz, I. Rodriguez-Leyva, J. H. Veldink, A. J. Ivinson, C. G. J. Saris, B. A. Hosler, A. Barnes-Nessa, N. Couture, J. H. J. Wokke, T. J. Kwiatkowski, R. A. Ophoff, S. Cronin, O. Hardiman, F. P. Diekstra, P. N. Leigh, C. E. Shaw, C. L. Simpson, V. K. Hansen, J. F. Powell, P. Corcia, F. Salachas, S. Heath, P. Galan, F. Georges, H. R. Horvitz, M. Lathrop, S. Purcell, A. Al-Chalabi and R. H. Brown (2009). "Reduced expression of the Kinesin-Associated Protein 3 (KIFAP3) gene

increases survival in sporadic amyotrophic lateral sclerosis." Proceedings of the National Academy of Sciences **106**(22): 9004-9009.

Lanson Jr, N. A. and U. B. Pandey (2012). "FUS-related proteinopathies: Lessons from animal models." Brain research **1462**(0): 44-60.

Lanson, N. A., A. Maltare, H. King, R. Smith, J. H. Kim, J. P. Taylor, T. E. Lloyd and U. B. Pandey (2011). "A Drosophila model of FUS-related neurodegeneration reveals genetic interaction between FUS and TDP-43." Human Molecular Genetics **20**(13): 2510-2523.

Lattante, S., G. A. Rouleau and E. Kabashi (2013). "TARDBP and FUS Mutations Associated with Amyotrophic Lateral Sclerosis: Summary and Update." Human Mutation **34**(6): 812-826.

Law, W. J., K. L. Cann and G. G. Hicks (2006). "TLS, EWS and TAF15: a model for transcriptional integration of gene expression." Briefings in Functional Genomics & Proteomics **5**(1): 8-14.

Lee, Y.-B., H.-J. Chen, Joao N. Peres, J. Gomez-Deza, J. Attig, M. Stalekar, C. Troakes, Agnes L. Nishimura, Emma L. Scotter, C. Vance, Y. Adachi, V. Sardone, Jack W. Miller, Bradley N. Smith, J.-M. Gallo, J. Ule, F. Hirth, B. Rogelj, C. Houart and Christopher E. Shaw (2013). "Hexanucleotide Repeats in ALS/FTD Form Length-Dependent RNA Foci, Sequester RNA Binding Proteins, and Are Neurotoxic." Cell Reports **5**(5): 1178-1186.

Leuba, G., A. Savioz, A. Vernay, B. Carnal, R. Kraftsik, E. Tardif, I. Riederer and B. M. Riederer (2008). "Differential Changes in Synaptic Proteins in the Alzheimer Frontal Cortex with Marked Increase in PSD-95 Postsynaptic Protein." Journal of Alzheimer's Disease **15**(1): 139-151.

Li, J., R. Nixon, A. Messer, S. Berman and S. Bursztajn (1998). "Altered gene expression for calpain/calpastatin system in motor neuron degeneration

(Mnd) mutant mouse brain and spinal cord." Molecular Brain Research **53**(1-2): 174-186.

Li, X.-J., B.-Y. Hu, S. A. Jones, Y.-S. Zhang, T. LaVaute, Z.-W. Du and S.-C. Zhang (2008). "Directed Differentiation of Ventral Spinal Progenitors and Motor Neurons from Human Embryonic Stem Cells by Small Molecules." STEM CELLS **26**(4): 886-893.

Ling, S.-C., M. Polymenidou and Don W. Cleveland (2013). "Converging Mechanisms in ALS and FTD: Disrupted RNA and Protein Homeostasis." Neuron **79**(3): 416-438.

Liu, D., J. Wen, J. Liu and L. Li (1999). "The roles of free radicals in amyotrophic lateral sclerosis: reactive oxygen species and elevated oxidation of protein, DNA, and membrane phospholipids." The FASEB Journal **13**(15): 2318-2328.

Llinás, R., J. A. Gruner, M. Sugimori, T. L. McGuinness and P. Greengard (1991). "Regulation by synapsin I and Ca(2+)-calmodulin-dependent protein kinase II of the transmitter release in squid giant synapse." The Journal of Physiology **436**(1): 257-282.

Mackenzie, I. A., O. Ansorge, M. Strong, J. Bilbao, L. Zinman, L.-C. Ang, M. Baker, H. Stewart, A. Eisen, R. Rademakers and M. Neumann (2011). "Pathological heterogeneity in amyotrophic lateral sclerosis with FUS mutations: two distinct patterns correlating with disease severity and mutation." Acta Neuropathologica **122**(1): 87-98.

Mackenzie, I. R. A., P. Frick and M. Neumann (2014). "The neuropathology associated with repeat expansions in the C9ORF72 gene." Acta Neuropathologica **127**(3): 347-357.

Mann, D., S. Rollinson, A. Robinson, J. Bennion Callister, J. C. Thompson, J. S. Snowden, T. Gendron, L. Petrucelli, M. Masuda-Suzukake, M. Hasegawa, Y. Davidson and S. Pickering-Brown (2013). "Dipeptide repeat proteins are present in the p62 positive inclusions in patients with frontotemporal lobar degeneration and motor neurone disease associated with expansions in C9ORF72." Acta Neuropathol Commun **1**(1): 68.

Marchetto, M. C. N., C. Carromeu, A. Acab, D. Yu, G. W. Yeo, Y. Mu, G. Chen, F. H. Gage and A. R. Muotri (2010). "A Model for Neural Development and Treatment of Rett Syndrome Using Human Induced Pluripotent Stem Cells." Cell **143**(4): 527-539.

Martí, M., L. Mulero, C. Pardo, C. Morera, M. Carrió, L. Laricchia-Robbio, C. R. Esteban and J. C. I. Belmonte (2013). "Characterization of pluripotent stem cells." Nat. Protocols **8**(2): 223-253.

Maruyama, H., H. Morino, H. Ito, Y. Izumi, H. Kato, Y. Watanabe, Y. Kinoshita, M. Kamada, H. Nodera, H. Suzuki, O. Komure, S. Matsuura, K. Kobatake, N. Morimoto, K. Abe, N. Suzuki, M. Aoki, A. Kawata, T. Hirai, T. Kato, K. Ogasawara, A. Hirano, T. Takumi, H. Kusaka, K. Hagiwara, R. Kaji and H. Kawakami (2010). "Mutations of optineurin in amyotrophic lateral sclerosis." Nature **465**(7295): 223-6.

Meijering, E., M. Jacob, J. C. F. Sarria, P. Steiner, H. Hirling and M. Unser (2004). "Design and validation of a tool for neurite tracing and analysis in fluorescence microscopy images." Cytometry Part A **58A**(2): 167-176.

Meissner, M., S. Lopato, J. Gotzmann, G. Sauermann and A. Barta (2003). "Proto-oncoprotein tls/fus is associated to the nuclear matrix and complexed with splicing factors ptb, srm160, and sr proteins." Experimental Cell Research **283**(2): 184-195.

Merner, N. D., Girard, S. L., Catoire, H., Bourassa, C. V., Belzil, V. V., Riviere, J.-B., Hince, P., Levert, A., Dionne-Laporte, A., Spiegelman, D., Noreau, A., Diab, S., Szuto, A., Fournier, H., Raelson, J., Belouchi, M., Panisset, M., Cossette, P., Dupre, N., Bernard, G., Chouinard, S., Dion, P. A. and G. A. Rouleau (2012). "Exome sequencing identifies *FUS* mutations as a cause of essential tremor." American Journal of Human Genetics **91**(2): 313-319.

Mili, S., K. Moissoglu and I. G. Macara (2008). "Genome-wide screen reveals APC-associated RNAs enriched in cell protrusions." Nature **453**(7191): 115-119.

Miller, Justine D., Yosif M. Ganat, S. Kishinevsky, Robert L. Bowman, B. Liu, Edmund Y. Tu, P. K. Mandal, E. Vera, J.-w. Shim, S. Kriks, T. Taldone, N. Fusaki, Mark J. Tomishima, D. Krainc, Teresa A. Milner, Derrick J. Rossi and L. Studer (2013). "Human iPSC-Based Modeling of Late-Onset Disease via Progerin-Induced Aging." Cell Stem Cell **13**(6): 691-705.

Mitchell, J., P. Paul, H. J. Chen, A. Morris, M. Payling, M. Falchi, J. Habgood, S. Panoutsou, S. Winkler, V. Tisato, A. Hajitou, B. Smith, C. Vance, C. Shaw, N. D. Mazarakis and J. de Belleroche (2010). "Familial amyotrophic lateral sclerosis is associated with a mutation in D-amino acid oxidase." Proc Natl Acad Sci U S A **107**(16): 7556-61.

Mitchell, J. C., P. McGoldrick, C. Vance, T. Hortobagyi, J. Sreedharan, B. Rogelj, E. L. Tudor, B. N. Smith, C. Klasen, C. C. J. Miller, J. D. Cooper, L. Greensmith and C. E. Shaw (2013). "Overexpression of human wild-type FUS causes progressive motor neuron degeneration in an age- and dose-dependent fashion." Acta Neuropathologica **125**(2): 273-288.

Moreira, M.-C., S. Klur, M. Watanabe, A. H. Nemeth, I. L. Ber, J.-C. Moniz, C. Tranchant, P. Aubourg, M. Tazir, L. Schols, M. Pandolfo, J. B. Schulz, J. Pouget, P. Calvas, M. Shizuka-Ikeda, M. Shoji, M. Tanaka, L. Izatt, C. E. Shaw, A.

M'Zahem, E. Dunne, P. Bomont, T. Benhassine, N. Bouslam, G. Stevanin, A. Brice, J. Guimaraes, P. Mendonca, C. Barbot, P. Coutinho, J. Sequeiros, A. Durr, J.-M. Warter and M. Koenig (2004). "Senataxin, the ortholog of a yeast RNA helicase, is mutant in ataxia-ocular apraxia 2." Nat Genet **36**(3): 225-227.

Mori, K., S. Lammich, I. A. Mackenzie, I. Forne, S. Zilow, H. Kretzschmar, D. Edbauer, J. Janssens, G. Kleinberger, M. Cruts, J. Herms, M. Neumann, C. Van Broeckhoven, T. Arzberger and C. Haass (2013). "hnRNP A3 binds to GGGGCC repeats and is a constituent of p62-positive/TDP43-negative inclusions in the hippocampus of patients with C9orf72 mutations." Acta Neuropathologica **125**(3): 413-423.

Mori, K., S.-M. Weng, T. Arzberger, S. May, K. Rentzsch, E. Kremmer, B. Schmid, H. A. Kretzschmar, M. Cruts, C. Van Broeckhoven, C. Haass and D. Edbauer (2013). "The C9orf72 GGGGCC Repeat Is Translated into Aggregating Dipeptide-Repeat Proteins in FTLD/ALS." Science **339**(6125): 1335-1338.

Morlando, M., S. Dini Modigliani, G. Torrelli, A. Rosa, V. Di Carlo, E. Caffarelli and I. Bozzoni (2012). "FUS stimulates microRNA biogenesis by facilitating co-transcriptional Drosha recruitment." The EMBO Journal **31**(24): 4502-4510.

Mukherjee, K., X. Yang, S. H. Gerber, H.-B. Kwon, A. Ho, P. E. Castillo, X. Liu and T. C. Sudhof (2010). "Piccolo and bassoon maintain synaptic vesicle clustering without directly participating in vesicle exocytosis." Proceedings of the National Academy of Sciences **107**(14): 6504-6509.

Münch, C., R. Sedlmeier, T. Meyer, V. Homberg, A. Sperfeld, A. Kurt, J. Prudlo, G. Peraus, C. Hanemann and G. Stumm (2004). "Point mutations of the p150 subunit of dynactin (DCTN1) gene in ALS." Neurology **63**(4): 724-726.

Munoz, D. G., M. Neumann, H. Kusaka, O. Yokota, K. Ishihara, S. Terada, S. Kuroda and I. R. Mackenzie (2009). "FUS pathology in basophilic inclusion body disease." Acta Neuropathologica **118**(5): 617-627.

Murakami, T., S.-P. Yang, L. Xie, T. Kawano, D. Fu, A. Mukai, C. Bohm, F. Chen, J. Robertson, H. Suzuki, G. G. Tartaglia, M. Vendruscolo, G. S. K. Schierle, F. T. S. Chan, A. Moloney, D. Crowther, C. F. Kaminski, M. Zhen and P. St George-Hyslop (2011). "ALS mutations in FUS causes neuronal dysfunction and death in C. elegans by a dominant gain-of-function mechanism." Human Molecular Genetics.

Murrey, H. E., C. I. Gama, S. A. Kalovidouris, W.-I. Luo, E. M. Driggers, B. Porton and L. C. Hsieh-Wilson (2006). "Protein fucosylation regulates synapsin Ia/Ib expression and neuronal morphology in primary hippocampal neurons." Proceedings of the National Academy of Sciences of the United States of America **103**(1): 21-26.

Nelson, P. T., W.-X. Wang and B. W. Rajeev (2008). "MicroRNAs (miRNAs) in Neurodegenerative Diseases." Brain Pathology **18**(1): 130-138.

Nestor, M. W. and S. A. Noggle (2013). "Standardization of human stem cell pluripotency using bioinformatics." Stem Cell Res Ther **4**: 37.

Neumann, M., D. M. Sampathu, L. K. Kwong, A. C. Truax, M. C. Micsenyi, T. T. Chou, J. Bruce, T. Schuck, M. Grossman, C. M. Clark, L. F. McCluskey, B. L. Miller, E. Masliah, I. R. Mackenzie, H. Feldman, W. Feiden, H. A. Kretzschmar, J. Q. Trojanowski and V. M.-Y. Lee (2006). "Ubiquitinated TDP-43 in Frontotemporal Lobar Degeneration and Amyotrophic Lateral Sclerosis." Science **314**(5796): 130-133.

Nguyen, Ha N., B. Byers, B. Cord, A. Shcheglovitov, J. Byrne, P. Gujar, K. Kee, B. Schule, Ricardo E. Dolmetsch, W. Langston, Theo D. Palmer and Renee R.

Pera (2011). "LRRK2 Mutant iPSC-Derived DA Neurons Demonstrate Increased Susceptibility to Oxidative Stress." Cell Stem Cell **8**(3): 267-280.

Nguyen, M. D., T. D'Aigle, G. Gowing, J.-P. Julien and S. Rivest (2004). "Exacerbation of motor neuron disease by chronic stimulation of innate immunity in a mouse model of amyotrophic lateral sclerosis." The Journal of Neuroscience **24**(6): 1340-1349.

Nishimura, A. L., M. Mitne-Neto, H. C. A. Silva, A. Richieri-Costa, S. Middleton, D. Cascio, F. Kok, J. R. M. Oliveira, T. Gillingwater, J. Webb, P. Skehel and M. Zatz (2004). "A Mutation in the Vesicle-Trafficking Protein VAPB Causes Late-Onset Spinal Muscular Atrophy and Amyotrophic Lateral Sclerosis." The American Journal of Human Genetics **75**(5): 822-831.

Niwa, J.-i., S.-i. Yamada, S. Ishigaki, J. Sone, M. Takahashi, M. Katsuno, F. Tanaka, M. Doyu and G. Sobue (2007). "Disulfide Bond Mediates Aggregation, Toxicity, and Ubiquitylation of Familial Amyotrophic Lateral Sclerosis-linked Mutant SOD1." Journal of Biological Chemistry **282**(38): 28087-28095.

Orlacchio, A., C. Babalini, A. Borreca, C. Patrono, R. Massa, S. Basaran, R. P. Munhoz, E. A. Rogaeva, P. H. St George-Hyslop, G. Bernardi and T. Kawarai (2010). "SPATACSIN mutations cause autosomal recessive juvenile amyotrophic lateral sclerosis." Brain **133**(2): 591-598.

Orozco, D., S. Tahirovic, K. Rentzsch, B. M. Schwenk, C. Haass and D. Edbauer (2012). "Loss of fused in sarcoma (FUS) promotes pathological Tau splicing." EMBO reports **13**(8): 759-764.

Otomo, A., S. Hadano, T. Okada, H. Mizumura, R. Kunita, H. Nishijima, J. Showguchi-Miyata, Y. Yanagisawa, E. Kohiki, E. Suga, M. Yasuda, H. Osuga, T. Nishimoto, S. Narumiya and J.-E. Ikeda (2003). "ALS2, a novel guanine nucleotide

exchange factor for the small GTPase Rab5, is implicated in endosomal dynamics." Human Molecular Genetics **12**(14): 1671-1687.

Ou, S. H., F. Wu, D. Harrich, L. F. García-Martínez and R. B. Gaynor (1995). "Cloning and characterization of a novel cellular protein, TDP-43, that binds to human immunodeficiency virus type 1 TAR DNA sequence motifs." Journal of Virology **69**(6): 3584-96.

Park, I.-H., R. Zhao, J. A. West, A. Yabuuchi, H. Huo, T. A. Ince, P. H. Lerou, M. W. Lensch and G. Q. Daley (2008). "Reprogramming of human somatic cells to pluripotency with defined factors." Nature **451**(7175): 141-146.

Parkinson, N., P. G. Ince, M. O. Smith, R. Highley, G. Skibinski, P. M. Andersen, K. E. Morrison, H. S. Pall, O. Hardiman, J. Collinge, P. J. Shaw, E. M. Fisher, M. P. i. A. Study and F. Consortium (2006). "ALS phenotypes with mutations in CHMP2B (charged multivesicular body protein 2B)." Neurology **67**(6): 1074-7.

Puls, I., C. Jonnakuty, B. H. LaMonte, E. L. Holzbaur, M. Tokito, E. Mann, M. K. Floeter, K. Bidus, D. Drayna, S. J. Oh, R. H. Brown Jr, C. L. Ludlow and K. H. Fischbeck (2003). "Mutant dynactin in motor neuron disease." Nature genetics **33**(4): 455-456.

Pulst, S. M., A. Nechiporuk, T. Nechiporuk, S. Gispert, X. N. Chen, I. Lopes-Cendes, S. Pearlman, S. Starkman, G. Orozco-Diaz, A. Lunkes, P. DeJong, G. A. Rouleau, G. Auburger, J. R. Korenberg, C. Figueroa and S. Sahba (1996). "Moderate expansion of a normally biallelic trinucleotide repeat in spinocerebellar ataxia type 2." Nat Genet **14**(3): 269-76.

Pun, S., A. F. Santos, S. Saxena, L. Xu and P. Caroni (2006). "Selective vulnerability and pruning of phasic motoneuron axons in motoneuron disease alleviated by CNTF." Nature neuroscience **9**(3): 408-419.

Rainier, S., M. Bui, E. Mark, D. Thomas, D. Tokarz, L. Ming, C. Delaney, R. J. Richardson, J. W. Albers, N. Matsunami, J. Stevens, H. Coon, M. Leppert and J. K. Fink (2008). "Neuropathy target esterase gene mutations cause motor neuron disease." Am J Hum Genet **82**(3): 780-5.

Rajput, A., A. H. Rajput, M. L. Rajput, M. Encarnacion, C. Q. Bernales, J. P. Ross, M. J. Farrer and C. Vilariño-Güell (2013). "Identification of FUS p.R377W in essential tremor." European Journal of Neurology **21**(2): 361-363.

Rao, M. S. and T. Raju (1995). "Effect of chronic restraint stress on dendritic spines and excrescences of hippocampal CA3 pyramidal neurons - a quantitative study." Brain research **694**(1): 312-317.

Re, Diane B., V. Le Verche, C. Yu, Mackenzie W. Amoroso, Kristin A. Politi, S. Phani, B. Ikiz, L. Hoffmann, M. Koolen, T. Nagata, D. Papadimitriou, P. Nagy, H. Mitsumoto, S. Kariya, H. Wichterle, Christopher E. Henderson and S. Przedborski (2014). "Necroptosis Drives Motor Neuron Death in Models of Both Sporadic and Familial ALS." Neuron **81**(5): 1001-1008.

Renton, A. E., A. Chio and B. J. Traynor (2014). "State of play in amyotrophic lateral sclerosis genetics." Nat Neurosci **17**(1): 17-23.

Renton, Alan E., E. Majounie, A. Waite, J. Simón-Sánchez, S. Rollinson, J. R. Gibbs, Jennifer C. Schymick, H. Laaksovirta, John C. van Swieten, L. Myllykangas, H. Kalimo, A. Paetau, Y. Abramzon, Anne M. Remes, A. Kaganovich, Sonja W. Scholz, J. Duckworth, J. Ding, Daniel W. Harmer, Dena G. Hernandez, Janel O. Johnson, K. Mok, M. Ryten, D. Trabzuni, Rita J. Guerreiro, Richard W. Orrell, J. Neal, A. Murray, J. Pearson, Iris E. Jansen, D. Sondervan, H. Seelaar, D. Blake, K. Young, N. Halliwell, Janis B. Callister, G. Toulson, A. Richardson, A. Gerhard, J. Snowden, D. Mann, D. Neary, Michael A. Nalls, T. Peuralinna, L. Jansson, V.-M. Isoviita, A.-L. Kaivorinne, M. Hölttä-Vuori, E. Ikonen, R.

Sulkava, M. Benatar, J. Wuu, A. Chiò, G. Restagno, G. Borghero, M. Sabatelli, D. Heckerman, E. Rogaeva, L. Zinman, Jeffrey D. Rothstein, M. Sendtner, C. Drepper, Evan E. Eichler, C. Alkan, Z. Abdullaev, Svetlana D. Pack, A. Dutra, E. Pak, J. Hardy, A. Singleton, Nigel M. Williams, P. Heutink, S. Pickering-Brown, Huw R. Morris, Pentti J. Tienari and Bryan J. Traynor (2011). "A Hexanucleotide Repeat Expansion in C9ORF72 Is the Cause of Chromosome 9p21-Linked ALS-FTD." Neuron **72**(2): 257-268.

Rezaie, T., A. Child, R. Hitchings, G. Brice, L. Miller, M. Coca-Prados, E. Heon, T. Krupin, R. Ritch, D. Kreutzer, R. P. Crick and M. Sarfarazi (2002). "Adult-Onset Primary Open-Angle Glaucoma Caused by Mutations in Optineurin." Science **295**(5557): 1077-1079.

Rogelj, B., L. E. Easton, G. K. Bogu, L. W. Stanton, G. Rot, T. Curk, B. Zupan, Y. Sugimoto, M. Modic, N. Haberman, J. Tollervey, R. Fujii, T. Takumi, C. E. Shaw and J. Ule (2012). "Widespread binding of FUS along nascent RNA regulates alternative splicing in the brain." Sci. Rep. **2**.

Rosahl, T. W., D. Spillane, M. Missler, J. Herz, D. K. Selig, J. R. Wolff, R. E. Hammer, R. C. Malenka and T. C. Sudhof (1995). "Essential functions of synapsins I and II in synaptic vesicle regulation." Nature **375**: 488-493.

Rosen, D. R., T. Siddique, D. Patterson, D. A. Figlewicz, P. Sapp, A. Hentati, D. Donaldson, J. Goto, J. P. O'Regan, H.-X. Deng, Z. Rahmani, A. Krizus, D. McKenna-Yasek, A. Cayabyab, S. M. Gaston, R. Berger, R. E. Tanzi, J. J. Halperin, B. Herzfeldt, R. Van den Bergh, W.-Y. Hung, T. Bird, G. Deng, D. W. Mulder, C. Smyth, N. G. Laing, E. Soriano, M. A. Pericak-Vance, J. L. Haines, G. A. Rouleau, J. S. Gusella, H. R. Horvitz and R. H. Brown Jr (1993). "Mutations in Cu/Zn superoxide dismutase gene are associated with familial amyotrophic lateral sclerosis." Nature **362**(6415): 59-62.

Roy, J., S. Minotti, L. Dong, D. A. Figlewicz and H. D. Durham (1998). "Glutamate potentiates the toxicity of mutant Cu/Zn-superoxide dismutase in motor neurons by postsynaptic calcium-dependent mechanisms." The Journal of Neuroscience **18**(23): 9673-9684.

Ruddy, D. M., M. J. Parton, A. Al-Chalabi, C. M. Lewis, C. Vance, B. N. Smith, P. N. Leigh, J. F. Powell, T. Siddique, E. Postumus Meyjes, F. Baas, V. De Jong and C. E. Shaw (2003). "Two Families with Familial Amyotrophic Lateral Sclerosis Are Linked to a Novel Locus on Chromosome 16q." The American Journal of Human Genetics **73**(2): 390-396.

Saccon, R. A., Bunton-Stasyshyn, R. K. A., Fisher, E. M. C. and P. Fratta (2013). "Is SOD1 loss of function involved in amyotrophic lateral sclerosis?" Brain **138**(2): 2342-2358.

Saeed, M., N. Siddique, W. Y. Hung, E. Usacheva, E. Liu, R. L. Sufit, S. L. Heller, J. L. Haines, M. Pericak-Vance and T. Siddique (2006). "Paraoxonase cluster polymorphisms are associated with sporadic ALS." Neurology **67**(5): 771-6.

Santos, A. R., D. Comprido and C. B. Duarte (2010). "Regulation of local translation at the synapse by BDNF." Progress in Neurobiology **92**(4): 505-516.

Sapp, P. C., B. A. Hosler, D. McKenna-Yasek, W. Chin, A. Gann, H. Genise, J. Gorenstein, M. Huang, W. Sailer, M. Scheffler, M. Valesky, J. L. Haines, M. Pericak-Vance, T. Siddique, H. R. Horvitz and R. H. Brown Jr (2003). "Identification of Two Novel Loci for Dominantly Inherited Familial Amyotrophic Lateral Sclerosis." The American Journal of Human Genetics **73**(2): 397-403.

Sareen, D., J. G. O'Rourke, P. Meera, A. K. M. G. Muhammad, S. Grant, M. Simpkinson, S. Bell, S. Carmona, L. Ornelas, A. Sahabian, T. Gendron, L. Petrucelli, M. Baughn, J. Ravits, M. B. Harms, F. Rigo, C. F. Bennett, T. S. Otis, C. N. Svendsen

and R. H. Baloh (2013). "Targeting RNA Foci in iPSC-Derived Motor Neurons from ALS Patients with a C9ORF72 Repeat Expansion." Science Translational Medicine **5**(208): 208ra149.

Sasaki, S. and M. Iwata (1996). "Ultrastructural study of synapses in the anterior horn neurons of patients with amyotrophic lateral sclerosis." Neuroscience Letters **204**(1): 53-56.

Sasayama, H., M. Shimamura, T. Tokuda, Y. Azuma, T. Yoshida, T. Mizuno, M. Nakagawa, N. Fujikake, Y. Nagai and M. Yamaguchi (2012). "Knockdown of the *Drosophila* Fused in Sarcoma (FUS) Homologue Causes Deficient Locomotive Behavior and Shortening of Motoneuron Terminal Branches." PLoS One **7**(6): e39483.

Schaefer, A. M., J. R. Sanes and J. W. Lichtman (2005). "A compensatory subpopulation of motor neurons in a mouse model of amyotrophic lateral sclerosis." The Journal of Comparative Neurology **490**(3): 209-219.

Scheff, S. W., S. T. DeKosky and D. A. Price (1990). "Quantitative assessment of cortical synaptic density in Alzheimer's disease." Neurobiology of Aging **11**(1): 29-37.

Scotter, E. L., C. Vance, A. L. Nishimura, Y.-B. Lee, H.-J. Chen, H. Urwin, V. Sardone, J. C. Mitchell, B. Rogelj, D. C. Rubinsztein and C. E. Shaw (2014). "Differential roles of the ubiquitin proteasome system and autophagy in the clearance of soluble and aggregated TDP-43 species." Journal of Cell Science **127**(6): 1263-1278.

Shaw, C., Z. Enayat, J. Powell, V. Anderson, A. Radunovic, S. Al-Sarraj and P. Leigh (1997). "Familial amyotrophic lateral sclerosis Molecular pathology of a patient with a SOD1 mutation." Neurology **49**(6): 1612-1616.

Shaw, C. E., Z. E. Enayat, B. A. Chioza, A. Al-Chalabi, A. Radunovic, J. F. Powell and P. N. Leigh (1998). "Mutations in all five exons of SOD-1 may cause ALS." Annals of Neurology **43**(3): 390-394.

Shaw, P. J., P. G. Ince, G. Falkous and D. Mantle (1995). "Oxidative damage to protein in sporadic motor neuron disease spinal cord." Annals of Neurology **38**(4): 691-695.

Shiohama, A., T. Sasaki, S. Noda, S. Minoshima and N. Shimizu (2007). "Nucleolar localization of DGCR8 and identification of eleven DGCR8-associated proteins." Experimental Cell Research **313**(20): 4196-4207.

Siklos, L., J. Engelhardt, Y. Harati, R. G. Smith, F. Joo and S. H. Appel (1996). "Ultrastructural evidence for altered calcium in motor nerve terminals in amyotrophic lateral sclerosis." Annals of Neurology **39**(2): 203-216.

Simpson, C. L., R. Lemmens, K. Miskiewicz, W. J. Broom, V. K. Hansen, P. W. van Vught, J. E. Landers, P. Sapp, L. Van Den Bosch, J. Knight, B. M. Neale, M. R. Turner, J. H. Veldink, R. A. Ophoff, V. B. Tripathi, A. Beleza, M. N. Shah, P. Proitsi, A. Van Hoecke, P. Carmeliet, H. R. Horvitz, P. N. Leigh, C. E. Shaw, L. H. van den Berg, P. C. Sham, J. F. Powell, P. Verstreken, R. H. Brown, Jr., W. Robberecht and A. Al-Chalabi (2009). "Variants of the elongator protein 3 (ELP3) gene are associated with motor neuron degeneration." Hum Mol Genet **18**(3): 472-81.

Skibinski, G., N. J. Parkinson, J. M. Brown, L. Chakrabarti, S. L. Lloyd, H. Hummerich, J. E. Nielsen, J. R. Hodges, M. G. Spillantini, T. Thusgaard, S. Brandner, A. Brun, M. N. Rossor, A. Gade, P. Johannsen, S. A. Sorensen, S. Gydesen, E. M. C. Fisher and J. Collinge (2005). "Mutations in the endosomal ESCRTIII-complex subunit CHMP2B in frontotemporal dementia." Nat Genet **37**(8): 806-808.

Slowik, A., B. Tomik, P. P. Wolkow, D. Partyka, W. Turaj, M. T. Malecki, J. Pera, T. Dziedzic, A. Szczudlik and D. A. Figlewicz (2006). "Paraoxonase gene polymorphisms and sporadic ALS." Neurology **67**(5): 766-70.

Smith, B. N., S. Newhouse, A. Shatunov, C. Vance, S. Topp, L. Johnson, J. Miller, Y. Lee, C. Troakes, K. M. Scott, A. Jones, I. Gray, J. Wright, T. Hortobagyi, S. Al-Sarraj, B. Rogelj, J. Powell, M. Lupton, S. Lovestone, P. C. Sapp, M. Weber, P. J. Nestor, H. J. Schelhaas, A. A. L. M. t. Asbroek, V. Silani, C. Gellera, F. Taroni, N. Ticozzi, L. Van den Berg, J. Veldink, P. Van Damme, W. Robberecht, P. J. Shaw, J. Kirby, H. Pall, K. E. Morrison, A. Morris, J. de Belleroche, J. M. B. Vianney de Jong, F. Baas, P. M. Andersen, J. Landers, R. H. Brown, M. E. Weale, A. Al-Chalabi and C. E. Shaw (2013). "The C9ORF72 expansion mutation is a common cause of ALS+/-FTD in Europe and has a single founder." Eur J Hum Genet **21**(1): 102-108.

Sproviero, W., V. La Bella, R. Mazzei, P. Valentino, C. Rodolico, I. L. Simone, G. Logroscino, C. Ungaro, A. Magariello, A. Patitucci, G. Tedeschi, R. Spataro, F. Condino, F. Bono, L. Citrigno, M. R. Monsurrò, M. Muglia, A. Gambardella, A. Quattrone and F. L. Conforti (2012). "FUS mutations in sporadic amyotrophic lateral sclerosis: Clinical and genetic analysis." Neurobiology of Aging **33**(4): 837.e1-837.e5.

Sreedharan, J., I. P. Blair, V. B. Tripathi, X. Hu, C. Vance, B. Rogelj, S. Ackerley, J. C. Durnall, K. L. Williams, E. Buratti, F. Baralle, J. de Belleroche, J. D. Mitchell, P. N. Leigh, A. Al-Chalabi, C. C. Miller, G. Nicholson and C. E. Shaw (2008). "TDP-43 Mutations in Familial and Sporadic Amyotrophic Lateral Sclerosis." Science **319**(5870): 1668-1672.

Sreedharan, J. and R. H. Brown (2013). "Amyotrophic lateral sclerosis: Problems and prospects." Annals of Neurology **74**(3): 309-316.

Stevanin, G., F. M. Santorelli, H. Azzedine, P. Coutinho, J. Chomilier, P. S. Denora, E. Martin, A.-M. Ouvrard-Hernandez, A. Tessa, N. Bouslam, A. Lossos, P. Charles, J. L. Loureiro, N. Elleuch, C. Confavreux, V. T. Cruz, M. Ruberg, E. Leguern, D. Grid, M. Tazir, B. Fontaine, A. Filla, E. Bertini, A. Durr and A. Brice (2007). "Mutations in SPG11, encoding spatacsin, are a major cause of spastic paraplegia with thin corpus callosum." Nat Genet **39**(3): 366-372.

Stewart, H., N. J. Rutherford, H. Briemberg, C. Krieger, N. Cashman, M. Fabros, M. Baker, A. Fok, M. DeJesus-Hernandez, A. Eisen, R. Rademakers and I. R. A. Mackenzie (2012). "Clinical and pathological features of amyotrophic lateral sclerosis caused by mutation in the C9ORF72 gene on chromosome 9p." Acta Neuropathologica **123**(3): 409-417.

Sun, Z., Z. Diaz, X. Fang, M. P. Hart, A. Chesi, J. Shorter and A. D. Gitler (2011). "Molecular Determinants and Genetic Modifiers of Aggregation and Toxicity for the ALS Disease Protein FUS/TLS." PLoS Biol **9**(4): e1000614.

Takahashi, K., K. Tanabe, M. Ohnuki, M. Narita, T. Ichisaka, K. Tomoda and S. Yamanaka (2007). "Induction of Pluripotent Stem Cells from Adult Human Fibroblasts by Defined Factors." Cell **131**(5): 861-872.

Takahashi, K. and S. Yamanaka (2006). "Induction of Pluripotent Stem Cells from Mouse Embryonic and Adult Fibroblast Cultures by Defined Factors." Cell **126**(4): 663-676.

Tateno, M., S. Kato, T. Sakurai, N. Nukina, R. Takahashi and T. Araki (2009). "Mutant SOD1 impairs axonal transport of choline acetyltransferase and acetylcholine release by sequestering KAP3." Human Molecular Genetics **18**(5): 942-955.

Teyssou, E., T. Takeda, V. Lebon, S. Boillée, B. Doukouré, G. Bataillon, V. Sazdovitch, C. Cazeneuve, V. Meininger, E. LeGuern, F. Salachas, D. Seilhean and S.

Millecamps (2013). "Mutations in SQSTM1 encoding p62 in amyotrophic lateral sclerosis: genetics and neuropathology." Acta Neuropathologica **125**(4): 511-522.

Thomsen, G. M., G. Gowing, S. Svendsen and C. N. Svendsen (2014). "The past, present and future of stem cell clinical trials for ALS." Experimental Neurology(0).

Thomson, J. A., J. Itskovitz-Eldor, S. S. Shapiro, M. A. Waknitz, J. J. Swiergiel, V. S. Marshall and J. M. Jones (1998). "Embryonic Stem Cell Lines Derived from Human Blastocysts." Science **282**(5391): 1145-1147.

Thomson, J. A., J. Kalishman, T. G. Golos, M. Durning, C. P. Harris, R. A. Becker and J. P. Hearn (1995). "Isolation of a primate embryonic stem cell line." Proceedings of the National Academy of Sciences **92**(17): 7844-7848.

Ticozzi, N., C. Vance, A. L. LeClerc, P. Keagle, J. D. Glass, D. McKenna-Yasek, P. C. Sapp, V. Silani, D. A. Bosco, C. E. Shaw, R. H. Brown and J. E. Landers (2011). "Mutational analysis reveals the FUS homolog TAF15 as a candidate gene for familial amyotrophic lateral sclerosis." American Journal of Medical Genetics Part B: Neuropsychiatric Genetics **156**(3): 285-290.

Tollervey, J. R., T. Curk, B. Rogelj, M. Briese, M. Cereda, M. Kayikci, J. Konig, T. Hortobagyi, A. L. Nishimura, V. Zupunski, R. Patani, S. Chandran, G. Rot, B. Zupan, C. E. Shaw and J. Ule (2011). "Characterizing the RNA targets and position-dependent splicing regulation by TDP-43." Nat Neurosci **14**(4): 452-458.

Tollervey, J. R., Z. Wang, T. Hortobagyi, J. T. Witten, K. Zarnack, M. Kayikci, T. A. Clark, A. C. Schweitzer, G. Rot, T. Curk, B. Zupan, B. Rogelj, C. E. Shaw and J. Ule (2011). "Analysis of alternative splicing associated with aging and

neurodegeneration in the human brain." Genome Research **21**(10): 1572-1582.

Turner, M. R., J. Barnwell, A. Al-Chalabi and A. Eisen (2012). "Young-onset amyotrophic lateral sclerosis: historical and other observations." Brain **135**(9): 2883-2891.

Turner, M. R., A. Cagnin, F. E. Turkheimer, C. C. J. Miller, C. E. Shaw, D. J. Brooks, P. N. Leigh and R. B. Banati (2004). "Evidence of widespread cerebral microglial activation in amyotrophic lateral sclerosis: an [11C](R)-PK11195 positron emission tomography study." Neurobiology of disease **15**(3): 601-609.

Uranishi, H., T. Tetsuka, M. Yamashita, K. Asamitsu, M. Shimizu, M. Itoh and T. Okamoto (2001). "Involvement of the Pro-oncoprotein TLS (Translocated in Liposarcoma) in Nuclear Factor-κB p65-mediated Transcription as a Coactivator." Journal of Biological Chemistry **276**(16): 13395-13401.

Urushitani, M., J. Kurisu, K. Tsukita and R. Takahashi (2002). "Proteasomal inhibition by misfolded mutant superoxide dismutase 1 induces selective motor neuron death in familial amyotrophic lateral sclerosis." Journal of Neurochemistry **83**(5): 1030-1042.

Urwin, H., K. A. Josephs, J. D. Rohrer, I. R. Mackenzie, M. Neumann, A. Authier, H. Seelaar, J. C. Van Swieten, J. M. Brown, P. Johannsen, J. E. Nielsen, I. E. Holm, D. W. Dickson, R. Rademakers, N. R. Graff-Radford, J. E. Parisi, R. C. Petersen, K. J. Hatanpaa, C. L. White Iii, M. F. Weiner, F. Geser, V. M. Van Deerlin, J. Q. Trojanowski, B. L. Miller, W. Seeley, J. van der Zee, S. Kumar-Singh, S. Engelborghs, P. P. De Deyn, C. Van Broeckhoven, E. H. Bigio, H.-X. Deng, G. M. Halliday, J. J. Kril, D. G. Munoz, D. M. Mann, S. M. Pickering-Brown, V. Doodeman, G. Adamson, S. Ghazi-Noori, E. M. C. Fisher, J. L. Holton, T. Revesz, M. N. Rossor, J. Collinge, S. Mead and A. M. Isaacs (2010). "FUS

pathology defines the majority of tau- and TDP-43-negative frontotemporal lobar degeneration." Acta Neuropathologica **120**(1): 33-41.

Van Deerlin, V. M., J. B. Leverenz, L. M. Bekris, T. D. Bird, W. Yuan, L. B. Elman, D. Clay, E. M. Wood, A. S. Chen-Plotkin, M. Martinez-Lage, E. Steinbart, L. McCluskey, M. Grossman, M. Neumann, I. L. Wu, W.-S. Yang, R. Kalb, D. R. Galasko, T. J. Montine, J. Q. Trojanowski, V. M. Y. Lee, G. D. Schellenberg and C.-E. Yu (2008). "TARDBP mutations in amyotrophic lateral sclerosis with TDP-43 neuropathology: a genetic and histopathological analysis." The Lancet Neurology **7**(5): 409-416.

van Zundert, B., M. H. Peuscher, M. Hynynen, A. Chen, R. L. Neve, R. H. Brown, M. Constantine-Paton and M. C. Bellingham (2008). "Neonatal neuronal circuitry shows hyperexcitable disturbance in a mouse model of the adult-onset neurodegenerative disease amyotrophic lateral sclerosis." The Journal of Neuroscience **28**(43): 10864-10874.

Vance, C., B. Rogelj, T. Hortobágyi, K. J. De Vos, A. L. Nishimura, J. Sreedharan, X. Hu, B. Smith, D. Ruddy, P. Wright, J. Ganesalingam, K. L. Williams, V. Tripathi, S. Al-Saraj, A. Al-Chalabi, P. N. Leigh, I. P. Blair, G. Nicholson, J. de Belleroche, J.-M. Gallo, C. C. Miller and C. E. Shaw (2009). "Mutations in FUS, an RNA Processing Protein, Cause Familial Amyotrophic Lateral Sclerosis Type 6." Science **323**(5918): 1208-1211.

Vance, C., E. L. Scotter, A. L. Nishimura, C. Troakes, J. C. Mitchell, C. Kathe, H. Urwin, C. Manser, C. C. Miller, T. Hortobágyi, M. Dragunow, B. Rogelj and C. E. Shaw (2013). "ALS mutant FUS disrupts nuclear localization and sequesters wild-type FUS within cytoplasmic stress granules." Human Molecular Genetics **22**(13): 2676-2688.

Veldink, J. H., J. H. J. Wokke, G. van der Wal, J. M. B. Vianney de Jong and L. H. van den Berg (2002). "Euthanasia and Physician-Assisted Suicide among Patients with Amyotrophic Lateral Sclerosis in the Netherlands." New England Journal of Medicine **346**(21): 1638-1644.

Wainger, B. J., E. Kiskinis, C. Mellin, O. Wiskow, S. S. Han, J. Sandoe, N. P. Perez, L. A. Williams, S. Lee, G. Boulting, J. D. Berry, R. H. Brown, Jr., M. E. Cudkowicz, B. P. Bean, K. Eggan and C. J. Woolf (2014). "Intrinsic membrane hyperexcitability of amyotrophic lateral sclerosis patient-derived motor neurons." Cell Rep **7**(1): 1-11.

Wang, J.-W., J. R. Brent, A. Tomlinson, N. A. Shneider and B. D. McCabe (2011). "The ALS-associated proteins FUS and TDP-43 function together to affect Drosophila locomotion and life span." The Journal of Clinical Investigation **121**(10): 4118-4126.

Wang, T., S. Warren and P. Jin (2013). "Toward pluripotency by reprogramming: mechanisms and application." Protein & Cell **4**(11): 820-832.

Wang, W.-Y., L. Pan, S. C. Su, E. J. Quinn, M. Sasaki, J. C. Jimenez, I. R. A. Mackenzie, E. J. Huang and L.-H. Tsai (2013). "Interaction of FUS and HDAC1 regulates DNA damage response and repair in neurons." Nat Neurosci **16**(10): 1383-1391.

Watanabe, M., M. Dykes-Hoberg, V. Cizewski Culotta, D. L. Price, P. C. Wong and J. D. Rothstein (2001). "Histological evidence of protein aggregation in mutant SOD1 transgenic mice and in amyotrophic lateral sclerosis neural tissues." Neurobiology of disease **8**(6): 933-941.

Watts, G. D., J. Wymer, M. J. Kovach, S. G. Mehta, S. Mumm, D. Darvish, A. Pestronk, M. P. Whyte and V. E. Kimonis (2004). "Inclusion body myopathy associated

with Paget disease of bone and frontotemporal dementia is caused by mutant valosin-containing protein." Nature genetics **36**(4): 377-381.

Wicks, P., S. Abrahams, B. Papps, A. Al-Chalabi, C. E. Shaw, P. N. Leigh and L. H. Goldstein (2009). "SOD1 and cognitive dysfunction in familial amyotrophic lateral sclerosis." Journal of Neurology **256**(2): 234-241.

Wiedemann, F. R., G. Manfredi, C. Mawrin, M. F. Beal and E. A. Schon (2002). "Mitochondrial DNA and respiratory chain function in spinal cords of ALS patients." Journal of Neurochemistry **80**(4): 616-625.

Williams, K. L., S. T. Warraich, S. Yang, J. A. Solski, R. Fernando, G. A. Rouleau, G. A. Nicholson and I. P. Blair (2012). "UBQLN2/ubiquilin 2 mutation and pathology in familial amyotrophic lateral sclerosis." Neurobiology of Aging **33**(10): 2527.e3-2527.e10.

Wils, H., G. Kleinberger, J. Janssens, S. Pereson, G. Joris, I. Cuijt, V. Smits, C. Ceuterick-de Groote, C. Van Broeckhoven and S. Kumar-Singh (2010). "TDP-43 transgenic mice develop spastic paralysis and neuronal inclusions characteristic of ALS and frontotemporal lobar degeneration." Proceedings of the National Academy of Sciences **107**(8): 3858-3863.

Wong, P. C., C. A. Pardo, D. R. Borchelt, M. K. Lee, N. G. Copeland, N. A. Jenkins, S. S. Sisodia, D. W. Cleveland and D. L. Price (1995). "An adverse property of a familial ALS-linked SOD1 mutation causes motor neuron disease characterized by vacuolar degeneration of mitochondria." Neuron **14**(6): 1105-1116.

Wu, C. H., C. Fallini, N. Ticozzi, P. J. Keagle, P. C. Sapp, K. Piotrowska, P. Lowe, M. Koppers, D. McKenna-Yasek, D. M. Baron, J. E. Kost, P. Gonzalez-Perez, A. D. Fox, J. Adams, F. Taroni, C. Tiloca, A. L. Leclerc, S. C. Chafe, D. Mangroo, M. J. Moore, J. A. Zitzewitz, Z. S. Xu, L. H. van den Berg, J. D. Glass, G. Siciliano, E. T.

Cirulli, D. B. Goldstein, F. Salachas, V. Meininger, W. Rossoll, A. Ratti, C. Gellera, D. A. Bosco, G. J. Bassell, V. Silani, V. E. Drory, R. H. Brown, Jr. and J. E. Landers (2012). "Mutations in the profilin 1 gene cause familial amyotrophic lateral sclerosis." Nature **488**(7412): 499-503.

Xu, C., S. Police, N. Rao and M. K. Carpenter (2002). "Characterization and Enrichment of Cardiomyocytes Derived From Human Embryonic Stem Cells." Circulation Research **91**(6): 501-508.

Xu, Y.-F., T. F. Gendron, Y.-J. Zhang, W.-L. Lin, S. D'Alton, H. Sheng, M. C. Casey, J. Tong, J. Knight, X. Yu, R. Rademakers, K. Boylan, M. Hutton, E. McGowan, D. W. Dickson, J. Lewis and L. Petrucelli (2010). "Wild-type human TDP-43 expression causes TDP-43 phosphorylation, mitochondrial aggregation, motor deficits, and early mortality in transgenic mice." The Journal of Neuroscience **30**(32): 10851-10859.

Xu, Z., M. Poidevin, X. Li, Y. Li, L. Shu, D. L. Nelson, H. Li, C. M. Hales, M. Gearing, T. S. Wingo and P. Jin (2013). "Expanded GGGGCC repeat RNA associated with amyotrophic lateral sclerosis and frontotemporal dementia causes neurodegeneration." Proceedings of the National Academy of Sciences **110**(19): 7778-7783.

Yamazaki, T., S. Chen, Y. Yu, B. Yan, Tyler C. Haertlein, Monica A. Carrasco, Juan C. Tapia, B. Zhai, R. Das, M. Lalancette-Hebert, A. Sharma, S. Chandran, G. Sullivan, Agnes L. Nishimura, Christopher E. Shaw, Steve P. Gygi, Neil A. Shneider, T. Maniatis and R. Reed (2012). "FUS-SMN Protein Interactions Link the Motor Neuron Diseases ALS and SMA." Cell Reports **2**(4): 799-806.

Yang, L., L. J. Embree and D. D. Hickstein (2000). "TLS-ERG Leukemia Fusion Protein Inhibits RNA Splicing Mediated by Serine-Arginine Proteins." Molecular and Cellular Biology **20**(10): 3345-3354.

Yang, L., L. J. Embree, S. Tsai and D. D. Hickstein (1998). "Oncoprotein TLS Interacts with Serine-Arginine Proteins Involved in RNA Splicing." Journal of Biological Chemistry **273**(43): 27761-27764.

Yasuda, K., H. Zhang, D. Loiselle, T. Haystead, I. G. Macara and S. Mili (2013). "The RNA-binding protein Fus directs translation of localized mRNAs in APC-RNP granules." The Journal of Cell Biology **203**(5): 737-746.

Yim, M. B., J. H. Kang, H. S. Yim, H. S. Kwak, P. B. Chock and E. R. Stadtman (1996). "A gain-of-function of an amyotrophic lateral sclerosis-associated Cu,Zn-superoxide dismutase mutant: An enhancement of free radical formation due to a decrease in Km for hydrogen peroxide." Proceedings of the National Academy of Sciences **93**(12): 5709-5714.

Zhang, N., M. C. An, D. Montoro and L. M. Ellerby (2010). "Characterization of human Huntington's disease cell model from induced pluripotent stem cells." PLoS currents **2**.

Zinszner, H., J. Sok, D. Immanuel, Y. Yin and D. Ron (1997). "TLS (FUS) binds RNA in vivo and engages in nucleo-cytoplasmic shuttling." Journal of Cell Science **110**(15): 1741-1750.

Zu, T., Y. Liu, M. Banez-Coronel, T. Reid, O. Pletnikova, J. Lewis, T. M. Miller, M. B. Harms, A. E. Falchook, S. H. Subramony, L. W. Ostrow, J. D. Rothstein, J. C. Troncoso and L. P. W. Ranum (2013). "RAN proteins and RNA foci from antisense transcripts in C9ORF72 ALS and frontotemporal dementia." Proceedings of the National Academy of Sciences **110**(51): E4968-E4977.